Graphene as a sensor material

Dissertation zur Erlangung des Doktorgrades der Naturwissenschaften
(Dr. rer. nat.)

der Fakultät Chemie und Pharmazie
der Universität Regensburg
Deutschland

vorgelegt von

Sven Kochmann

aus Köthen (ST)
im März 2013

Diese Doktorarbeit entstand in der Zeit vom Oktober 2009 bis zum März 2013 am Institut für Analytische Chemie, Chemo- und Biosensorik der Universität Regensburg.

Die Arbeit wurde angeleitet von Prof. Otto S. Wolfbeis.

Promotionsgesuch eingereicht am:	6. März 2013
Kolloquiumstermin:	8. Mai 2013
Vorsitzender:	Prof. Dr. Joachim Wegener
Erstgutachter:	Prof. Dr. Otto S. Wolfbeis
Zweitgutachter:	Prof. Dr. Bernhard Dick
Drittprüfer:	Prof. Dr. Christian Schüller

"*Be especially critical with expected results.*"

Prof. Dr. Reinhard Hoffmann, July 27, 2012
Seminar "*Good scientific practice*", Universität Regensburg

Contents

1 Introduction

1.1 The history of graphene

In 2004, *Andre K. Geim* and *Konstantin S. "Kostya" Novosëlov* published their results from one of their "Friday night experiments"[1,2]. The very first idea was to prepare graphite films as thin as possible to study potential electric field effects and other properties. Their first attempts with a polishing machine to produce thin graphite films were quite unsuccessful. *Oleg Shklyarevskii*, an expert in scanning tunneling microscopy, prompted the use of adhesive tape to access much smaller pieces of graphite. With this technique *Geim* and *Novosëlov* were the first to isolate a single layer flake from graphite by mechanical exfoliation. That was the birth of the famous "Scotch tape method"[3]. In 2010, both received the Nobel prize in physics for their work on graphene.

Although *Geim* and *Novosëlov* are credited with founding this new interesting research area in 2004, some of the pioneering work was done as early as 145 years before. In 1859, Benjamin Brodie examined the reaction of graphite with strong oxidation agents such as chlorates[4]. He described the product in the following way:

> *The substance has the following properties. It is insoluble in water containing acids or salt, but is very slightly soluble in pure water. The crystals, placed upon litmus paper, have a feeble acid reaction. [...] When a solution of sulphide of ammonium or of potassium is poured upon the dry substance, a crackling sound is heard, and a body is ultimately formed possessing the metallic lustre and general appearance of graphite itself.*

Due to these properties he labeled the material *graphitic acid* (not to be confused with *mellitic acid* which is now referred to *graphitic acid*) and calculated a sum formula of $C_{11}H_4O_5$ (C/O ratio: 2.2). Retrospectively, it is clear that Brodie prepared the first

sample of graphene oxide[2].

However, there is a drawback to this approach. As mentioned before, chlorate was used as oxidation agent and therefore large quantities of ClO_2 gas were generated during the reaction. Due to this and in combination with the heating, explosions routinely occurred. An improved method was developed by *L. Staudenmaier* in 1898[5]. His method rendered the heating step obsolete. Simultaneously, he reduced the reaction time by introducing sulfuric acid into the mixture of nitric acid and potassium chlorate used by *Brodie*. Finally, in 1958, *Hummers* and *Offeman* published their famous method on the preparation of *graphitic oxide* without chlorate, using permanganate instead[6]. The procedure continued to evolve today[7–9].

It is interesting to note that typical batches were produced in significantly different quantities at that time, compared to today. For instance, *Staudenmaier* started with 25 g of graphite and added the large quantity of 450 g potassium chlorate. *Hummers* and *Offeman* used 100 g of graphite and 300 g of potassium permanganate. Given that today's batches are of much smaller quantities[7–9]. This indicates that both methods are scalable up to at least this magnitude.

Nearly 90 years after *Brodie's* paper, *Ruess* and *Vogt* published the first evidence that graphene consists of individual plates[10]. They used transmission electron microscopy to examine the deflagration process of graphene oxide and found "thin, flat bodies which resemble creased paper sheets". The work was continued by *Boehm et al.* who also suggested to label this material as "graphene"[11,12]. The term is a combination of *graphite* and the suffix that refers to aromatic hydrocarbons such as *benzene* or *anthracene*[2,12,13]. During this time, first preparations of epitaxial graphene ("graphitic carbon") on metal[14–16] and insulating substrates[17] were reported.

The first single layer flake prepared by *Geim* and *Novosëlov* set off an avalanche of interest and publications on the topic of graphene. Graphene gained popularity due to its large thermal conductivity (3 000 W m^{-1} K^{-1}), exhibiting the quantum Hall effect at room temperature[18], having the highest possible surface-to-volume ratio (2 600 m^2 g^{-1}), its high electron transfer rate (up to 200 000 cm^2 V^{-1} s^{-1})[19], its interesting mechanical properties[20,21], its exceptional thermal stability[22], and the

possibility of high-sensitive detection[23,24]. Given these properties, graphene is an attractive candidate in analytical chemistry, e.g. for biomedical applications[25].

Since 1859, many methods for preparation of graphene have been developed. In addition to mechanical exfoliation[1], graphene materials may be obtained by thermal decomposition on SiC wafers[26], chemical vapor deposition[27], or chemical synthesis[4–6,9,28–32]. The resulting nanomaterials have been characterized by a broad range of optical[33–38], electrical[1,18,19,39], mechanical[8,40,41] and other methods[42–44].

Unfortunately, many of the materials synthesized have not been properly classified. Each preparation method or even a slight modification of one parameter within in the same method results in "graphenes" which differ in terms of chemical structure, shape, size, number of layers and therefore, in their properties. This problem was previously addressed[13], but remains unresolved. It is therefore critical to first classify graphene materials before associating the materials with any application.

1.2 Classification

1.2.1 Definition of graphene

A collective definition of graphenes does not yet exist. Moreover, related terms are often confused, e.g. *graphite oxide* and *graphene oxide*. Let us first have a look at the term "*graphene*". Most authors describe (rather than define) graphene as a material "*which consists of a single atomic sheet of conjugated sp^2 carbon atoms*"[45] or the like[39,46–48]. IUPAC defines graphene as "*a single carbon layer of the graphite structure, describing its nature by analogy to a polycyclic aromatic hydrocarbon of quasi infinite size*"[49]. Recently, *Chen et al.* made another suggestion, that sheets of polyaromatic hydrocarbons exceeding 100 nm in both directions should be called "graphene"[29].

However, these definitions are missing two important features of graphenes. These are (a) its metallic nature (i.e. the lack of a band gap)[1] and (b) the fact that it should consist of carbon and hydrogen only, in the ideal case. The latter is particularly striking

when looking at literature data for the elemental composition of many graphenes. Fractions of up to 30% of oxygen have been reported which is in clear contradiction to the definitions previously cited.

The smallest possible aromatic structure that matches the definitions is a symmetrical flake of 864 C-atoms, with an edge length of 2.9 nm, an area of 22 nm^2 (see Figure 1.1), with effectively no band gap [50,51]. Hence, this structure could be the smallest graphene flake possible but is only a suggestion, of course.

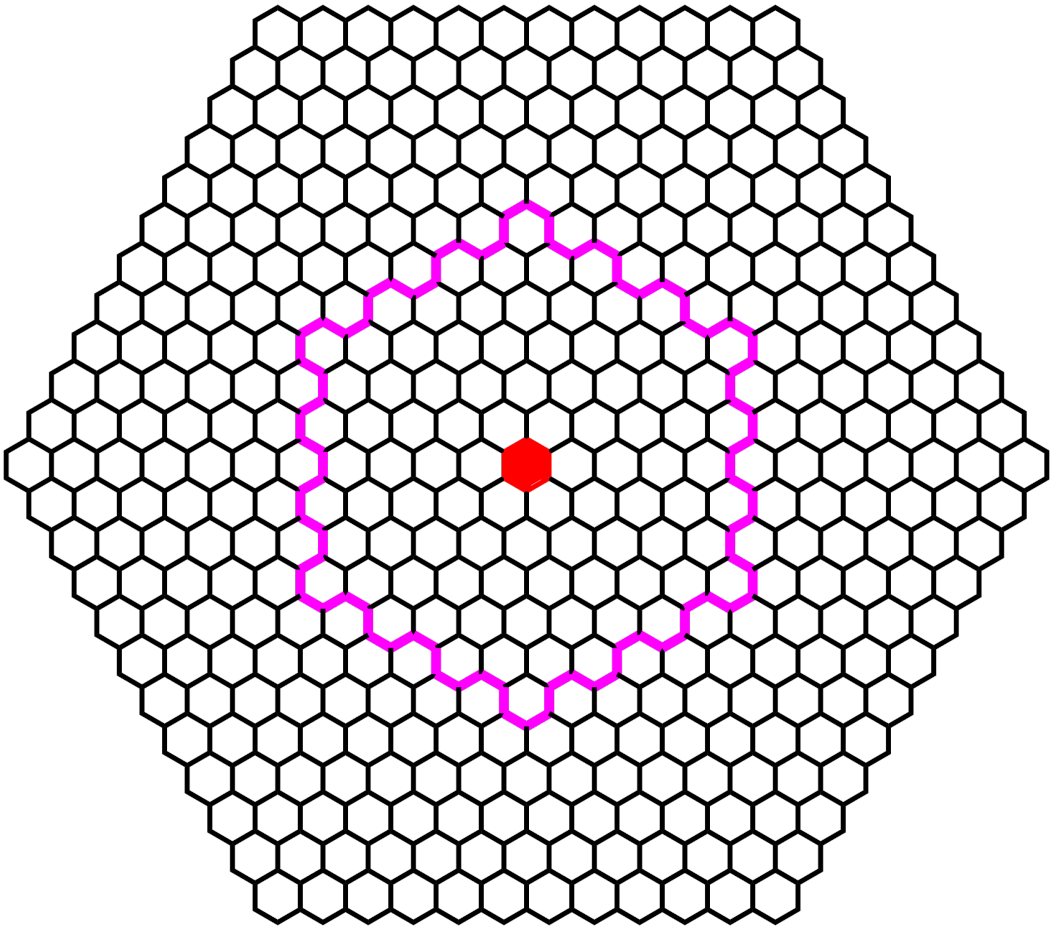

Figure 1.1. Suggested smallest graphene structure: a symmetrical flake of 864 C atoms with an edge length of 2.9 nm and an area of 22 nm^2 with effectively no band gap. There are 11 additional rings around the center benzene ring (red). The purple border marks the dimensions of the famous 222 C atoms graphite sheet prepared at the workgroup of *Klaus Müllen* [52].

1.2.2 The graphene family

Several materials related to graphene are known. They have been obtained in synthesis routes towards graphene. These include graphite oxide, graphene oxide and reduced graphene oxide. This thesis referres to these materials as members of the "graphene-family" that can be best described by the oxidation level of carbon and the number of layers. Other (high-level) properties (e.g. conductivity or photoluminescence) depend on these factors which makes this kind of categorization very useful.

Figure 1.2 illustrates a classification scheme of the graphene-family and the possible routes from one material to another. Even the precursor materials, silicon carbide and methane, fit into this scheme. "Top-down" synthesis routes run from top left to bottom right, i.e. they start with a bulk material such as graphite or graphite oxide. The nanomaterial is obtained by stepwise structural decomposition such as from graphene oxide via reduced graphene oxide to graphene. The mechanical exfoliation route, for example, leads from graphite (left) via layer-by-layer decomposition, resulting in graphene (right). Both materials are placed on the same level on the ordinate, because the oxidation level of carbon does not change during this process. In contrast, the "bottom-up" methods run from bottom right to top left because the materials are assembled layer-by-layer. For example, large areas of graphene can be constructed by chemical vapor deposition of methane which has a lower oxidation level than graphene. It does not possess a layer structure and thus it is shifted to the bottom right relative to graphene.

This classification is also a useful starting point for making definitions because the individual materials can be distinguished by oxidation state and the number of layers. Therefore, this thesis suggests and uses the definitions given in Section 1.2.3. In the following, these definitions are used even if a cited publication itself labels them otherwise.

The exaggerated use of acronyms in the literature, all referring to the same materials, is notable. Examples are CRGO, GO, RGO, GR, G, GNS, EG, GNP, CCG, GE, GP, ERGO, GF, EGO, GS, GN, TRGO, CMG, FG, ERGNO, CRGNO, and the like. This allows for a high risk of confusion (e.g. GO may stand for *graphite oxide* or *graphene*

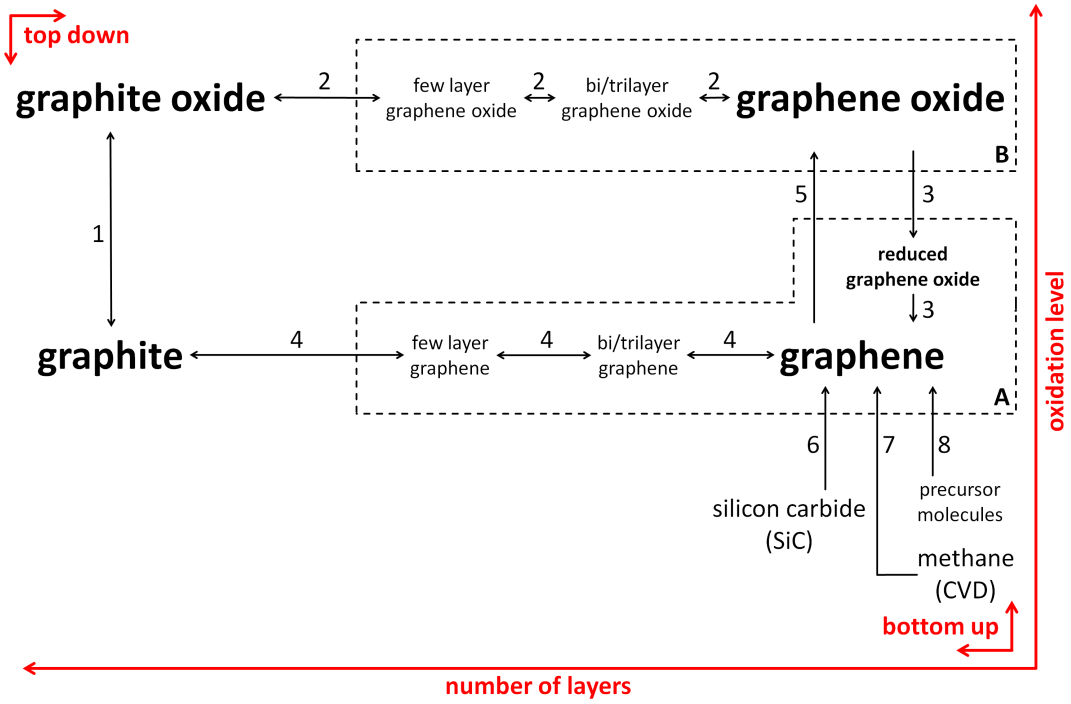

Figure 1.2. Classification of graphene family materials (also see Section 1.2.2). Routes: (1) Oxidation of graphite to graphite oxide according to the Hummers, Staudenmeier or Brodie method [28]. (2) Stepwise exfoliation of graphite oxide to give graphene oxide in aqueous colloidal suspensions by sonication and stirring [28]. (3) Reduction of graphene oxide by chemical reactions [28], thermal annealing [53], flash reduction [54], enzymatic reduction [55] or electrodeposition [32]. (4) Mechanical exfoliation of graphite to give graphene (tape method) [2]. (5) Oxidation of graphene sheets to graphene oxide. (6) Thermal decomposition of a SiC wafer [26]. (7) Growth of graphene films by chemical vapor deposition [27]. (8) Total synthesis routines with precursor molecules [29,52,56,57]. Group A includes graphene materials primarly used for their electronic properties, group B for their optical properties.

oxide). In my opinion the words "graphite" and "graphene" are short enough and do not require an acronym. Hence, in this work confusing acronyms are avoided for graphene materials. All acronyms, abbreviations and terms used in this work are listed in Section 1.4.

1.2.3 Classification of graphene species

Table 1.1 shows definitions of the various graphene family materials as they are used in this thesis. They are based on the suggested defintions and classifications in the previous sections.

Table 1.1. Classification of graphene species as used in this work

Material	Definition
Graphene	Exactly one layer of a polycyclic aromatic hydrocarbon network, with all carbon atoms hexagonally arranged in a planar condensed ring system. It has a metallic character and consists solely of carbon and hydrogen.
Graphene oxide	Exactly one layer of a polycyclic hydrocarbon network, with all carbon atoms hexagonally arranged in a planar condensed ring system. It has various oxygen functional groups (CO, OH, COOH) and is partially aromatic. It possesses a band gap greater than 1.5 eV. The band gap depends on its oxidation level. The C:O ratio is between 2 and 3.
Reduced graphene oxide (rGO)	Exactly one layer of a polycyclic hydrocarbon network, with all carbon atoms hexagonally arranged in a planar condensed ring system. It has an oxygen fraction of around or below 10%. It is mostly aromatic and resembles graphene in terms of electrical, thermal and mechanical properties.
Graphite	"An allotropic form of the element carbon consisting of layers of hexagonally arranged carbon atoms in a planar condensed ring system. The layers are stacked parallel to each other in a three-dimensional crystalline long-range order. There are two allotropic forms with different stacking arrangements, hexagonal and rhombohedral. The chemical bonds within the layers are covalent with sp^2 hybridization and with a C-C distance of 141.7 pm. The weak bonds between the layers are metallic with a strength comparable to van der Waals bonding only." [49]
Graphite oxide	A heterogenous material prepared by the oxidation of graphite. It can be described as an assembly of many layers of graphene oxide.

1.3 Motivation and aim of work

Several proof of principle and analytical concepts do exist (see Chapter 2) which suggest graphene materials being extremely valuable tools for sensor applications. The chemically derived variants, i.e. *(reduced) graphene oxide*, provide additional benefits such as: processing in solutions, higher sensitivies for particular analytes, and attraction and discrimination effects, as compared to pristine graphene (see Section 2.4 for a complete list). As such, this thesis is concerned with *(reduced) graphene oxide* only.

Thus far, the materials themselves and their synthesis were only superficially examined. Although very little detail about the mechanism and structure is known[58], many pictured structure models may imply otherwise. However, "knowing your material" is mandatory for optimal utilization, specific modifications and applications.

Hence, the intention of the thesis is to fill this gap by outlining the benefits of (reduced) graphene oxide, characterizing both materials in detail and extensively investigating the procedure and mechanism of the syntheses.

1.4 Abbreviations, acronyms and terms

GO	Graphene oxide
rGO	Reduced graphene oxide
(r)GO	Both graphene oxide and reduced graphene oxide
AFP	α-fetoprotein
ATP	Adenosine-5'-triphosphate
BRCA1	Breast cancer type 1 susceptibility gene/protein
CEA	Carcinoembryonic antigen
DFT	Density functional theory
DNA	Desoxyribonucleic acid, *ssDNA* single stranded DNA, *dsDNA* double stranded DNA
EGFR	Epidermal growth factor receptor
ELISA	Enzyme-linked immunosorbent assay
FET	Field-effect transistor
ECL	Electrochemiluminescence or electrogenerated chemiluminescence
EDC	1-Ethyl-3-(3-dimethylaminopropyl)carbodiimide
EEM	excitation/emission matrix
GCE	Glassy carbon electrodes
GOx	Glucose oxidase
$H_2O\downarrow$	"unfree" water; water which is immediately absorbed, e.g. by sulfuric acid
HeLa	type of cervical cancer cells; termed after *Henrietta Lacks*
HER2	Human epidermal growth factor receptor 2
HRP	Horseradish peroxidase
ICP-OES	Inductively coupled plasma optical emission spectrometry
ICP-MS	Inductively coupled plasma mass spectrometry
IgG	Immunoglobulin G
ITO	Indium tin oxide (electrode)
LOD	Limit of detection
K562	Type of leukemia cells
MCF-7	Type of breast cancer cells; termed after *Michigan Cancer Foundation*
MDA-231	Type of breast cancer cells; termed after *M.D. Anderson*
NADH	Nicotinamide adenine dinucleotide
NHS	N-Hydroxysuccinimide
NIH-3T3	Type of fibroblast cells; termed after *National Institutes of Health*

FRET	Förster resonance energy transfer
PB	Prussian blue
PET	Poly(ethylene terephthalate)
PSA	Prostate specific antigen
QDs	Quantum dots
SEC	Size exclusion chromatography
SCE	Saturated calomel electrode
SPR	Surface plasmon resonance
SWCNT	Single walled carbon nanotubes
TEM	Transmission electron microscopy
TGA	Thermogravimetric analysis
TMB	Tetramethylbenzidine
TNT	2,4,6-Trinitrotoluene
WHO	World Health Organization
XPS	X-ray photoelectron spectroscopy

1.5 References

[1] K. S. Novosëlov, A. K. Geim, S. V. Morozov, D. Jiang, Y. Zhang, S. V. Dubonos, I. V. Grigorieva, and A. A. Firsov. Electric Field Effect in Atomically Thin Carbon Films. *Science*, 306(5696): 666–669, 2004. doi: 10.1126/science.1102896.

[2] A. K. Geim. Nobel Lecture: Random walk to graphene. *Rev. Mod. Phys.*, 83(3):851–862, August 2011. doi: 10.1103/RevModPhys.83.851.

[3] A. K. Geim. Graphene: Status and Prospects. *Science*, 324(5934):1530–1534, June 2009. doi: 10.1126/science.1158877.

[4] B. C. Brodie. On the Atomic Weight of Graphite. *Philos. Trans. R. Soc. London*, 149:249–259, January 1859. doi: 10.1098/rstl.1859.0013.

[5] L. Staudenmaier. Verfahren zur Darstellung der Graphitsäure. *Ber. Dtsch. Chem. Ges.*, 31(2): 1481–1487, 1898. doi: 10.1002/cber.18980310237.

[6] W. S. Hummers and R. E. Offeman. Preparation of Graphitic Oxide. *J. Am. Chem. Soc.*, 80 (6):1339–1339, March 1958. doi: 10.1021/ja01539a017.

[7] G. Eda, G. Fanchini, and M. Chhowalla. Large-area ultrathin films of reduced graphene oxide as a transparent and flexible electronic material. *Nat. Nano*, 3(5):270–274, May 2008. doi: 10.1038/nnano.2008.83.

[8] D. A. Dikin, S. Stankovich, E. J. Zimney, R. D. Piner, G. H. B. Dommett, G. Evmenenko, S. T. Nguyen, and R. S. Ruoff. Preparation and characterization of graphene oxide paper. *Nature*, 448(7152):457–460, July 2007. doi: 10.1038/nature06016.

[9] S. Stankovich, D. A. Dikin, R. D. Piner, K. A. Kohlhaas, A. Kleinhammes, Y. Jia, Y. Wu, S. T. Nguyen, and R. S. Ruoff. Synthesis of graphene-based nanosheets via chemical reduction of exfoliated graphite oxide. *Carbon*, 45(7):1558–1565, June 2007. doi: 10.1016/j.carbon.2007.02.034.

[10] G. Ruess and F. Vogt. Höchstlamellarer Kohlenstoff aus Graphitoxyhydroxyd. *Monatsh. Chem.*, 78(3):222–242, 1948. doi: 10.1007/BF01141527.

[11] H. P. Boehm, A. Clauss, G. O. Fischer, and U. Hofmann. Das Adsorptionsverhalten sehr dünner Kohlenstoff-Folien. *Z. Anorg. Allg. Chem.*, 316(3-4):119–127, 1962. doi: 10.1002/zaac.19623160303.

[12] H. Boehm, R. Setton, and E. Stumpp. Nomenclature and terminology of graphite intercalation compounds. *Carbon*, 24(2):241–245, 1986. doi: 10.1016/0008-6223(86)90126-0.

[13] D. R. Dreyer, R. S. Ruoff, and C. W. Bielawski. Ein Konzept und seine Umsetzung: Graphen gestern, heute und morgen. *Angew. Chem.*, 122(49):9524–9532, 2010. doi: 10.1002/ange.201003024.

[14] J. Grant and T. Haas. A study of Ru(0001) and Rh(111) surfaces using LEED and Auger electron spectroscopy. *Surf. Sci.*, 21(1):76–85, June 1970. doi: 10.1016/0039-6028(70)90064-6.

[15] J. M. Blakely, J. S. Kim, and H. C. Potter. Segregation of Carbon to the (100) Surface of Nickel. *J. Appl. Phys.*, 41(6):2693–2697, May 1970. doi: 10.1063/1.1659283.

[16] R. Rosei, M. De Crescenzi, F. Sette, C. Quaresima, A. Savoia, and P. Perfetti. Structure of graphitic carbon on Ni(111): A surface extended-energy-loss fine-structure study. *Phys. Rev. B*, 28(2):1161–1164, July 1983. doi: 10.1103/PhysRevB.28.1161.

[17] A. Van Bommel, J. Crombeen, and A. Van Tooren. LEED and Auger electron observations of the SiC(0001) surface. *Surface Science*, 48(2):463–472, March 1975. doi: 10.1016/0039-6028(75)90419-7.

[18] B. Özyilmaz, P. Jarillo-Herrero, D. Efetov, D. A. Abanin, L. S. Levitov, and P. Kim. Electronic Transport and Quantum Hall Effect in Bipolar Graphene p-n-p Junctions. *Phys. Rev. Lett.*, 99 (16):166804, October 2007. doi: 10.1103/PhysRevLett.99.166804.

[19] K. Bolotin, K. Sikes, Z. Jiang, M. Klima, G. Fudenberg, J. Hone, P. Kim, and H. Stormer. Ultrahigh electron mobility in suspended graphene. *Solid State Commun.*, 146(9-10):351–355, June 2008. doi: 10.1016/j.ssc.2008.02.024.

[20] A. R. Ranjbartoreh, B. Wang, X. Shen, and G. Wang. Advanced mechanical properties of graphene paper. *J. Appl. Phys.*, 109(1):014306, January 2011. doi: 10.1063/1.3528213.

[21] I. W. Frank, D. M. Tanenbaum, A. M. van der Zande, and P. L. McEuen. Mechanical properties of suspended graphene sheets. *J. Vac. Sci. Technol. B*, 25(6):2558–2561, November 2007. doi: 10.1116/1.2789446.

[22] M. J. Allen, V. C. Tung, and R. B. Kaner. Honeycomb Carbon: A Review of Graphene. *Chem. Rev.*, 110(1):132–145, 2010. doi: 10.1021/cr900070d.

[23] F. Schedin, A. K. Geim, S. V. Morozov, E. W. Hill, P. Blake, M. I. Katsnelson, and K. S. Novosëlov. Detection of individual gas molecules adsorbed on graphene. *Nat. Mater.*, 6(9): 652–655, 2007. doi: 10.1038/nmat1967.

[24] M. Qazi, T. Vogt, and G. Koley. Trace gas detection using nanostructured graphite layers. *Appl. Phys. Lett.*, 91(23):233101–3, December 2007. doi: 10.1063/1.2820387.

[25] H. Shen, L. Zhang, M. Liu, and Z. Zhang. Biomedical Applications of Graphene. *Theranostics*, 2(3):283–294, 2012. doi: 10.7150/thno.3642.

[26] K. V. Emtsev, A. Bostwick, K. Horn, J. Jobst, G. L. Kellogg, L. Ley, J. L. McChesney, T. Ohta, S. A. Reshanov, J. Rohrl, E. Rotenberg, A. K. Schmid, D. Waldmann, H. B. Weber, and T. Seyller. Towards wafer-size graphene layers by atmospheric pressure graphitization of silicon carbide. *Nat. Mater.*, 8(3):203–207, 2009. doi: 10.1038/NMAT2382.

[27] K. S. Kim, Y. Zhao, H. Jang, S. Y. Lee, J. M. Kim, K. S. Kim, J.-H. Ahn, P. Kim, J.-Y. Choi, and B. H. Hong. Large-scale pattern growth of graphene films for stretchable transparent electrodes. *Nature*, 457(7230):706–710, February 2009. doi: 10.1038/nature07719.

[28] S. Park and R. S. Ruoff. Chemical methods for the production of graphenes. *Nat. Nano.*, 4(4): 217–224, April 2009. doi: 10.1038/nnano.2009.58.

[29] L. Chen, Y. Hernandez, X. Feng, and K. Müllen. From Nanographene and Graphene Nanoribbons to Graphene Sheets: Chemical Synthesis. *Angew. Chem. Int. Ed.*, 51(31):7640–7654, 2012. doi: 10.1002/anie.201201084.

[30] D. Rhinow, N.-E. Weber, and A. Turchanin. Atmospheric Pressure, Temperature-Induced Conversion of Organic Monolayers into Nanocrystalline Graphene. *J. Phys. Chem. C*, 116(22): 12295–12303, May 2012. doi: 10.1021/jp301877p.

[31] H.-L. Guo, X.-F. Wang, Q.-Y. Qian, F.-B. Wang, and X.-H. Xia. A Green Approach to the Synthesis of Graphene Nanosheets. *ACS Nano*, 3(9):2653–2659, August 2009. doi: 10.1021/nn900227d.

[32] M. Hilder, B. Winther-Jensen, D. Li, M. Forsyth, and D. R. MacFarlane. Direct electrodeposition of graphene from aqueous suspensions. *Phys. Chem. Chem. Phys.*, 13(20):9187–9193, 2011. doi: 10.1039/C1CP20173E.

[33] G. Eda, Y.-Y. Lin, C. Mattevi, H. Yamaguchi, H.-A. Chen, I.-S. Chen, C.-W. Chen, and M. Chhowalla. Blue Photoluminescence from Chemically Derived Graphene Oxide. *Adv. Mater.*, 22(4):505–509, 2010. doi: 10.1002/adma.200901996.

[34] A. C. Ferrari, J. C. Meyer, V. Scardaci, C. Casiraghi, M. Lazzeri, F. Mauri, S. Piscanec, D. Jiang, K. S. Novosëlov, S. Roth, and A. K. Geim. Raman Spectrum of Graphene and Graphene Layers. *Phys. Rev. Lett.*, 97(18):187401–, October 2006. doi: 10.1103/PhysRevLett.97.187401.

[35] S. Heydrich, M. Hirmer, C. Preis, T. Korn, J. Eroms, D. Weiss, and C. Schüller. Scanning Raman spectroscopy of graphene antidot lattices: Evidence for systematic p-type doping. *Appl. Phys. Lett.*, 97(4):043113–3, July 2010. doi: 10.1063/1.3474613.

[36] S. Kochmann, T. Hirsch, and O. Wolfbeis. The pH Dependence of the Total Fluorescence of Graphite Oxide. *J. Fluoresc.*, 22(3):849–855, 2012. doi: 10.1007/s10895-011-1019-8.

[37] Z. Luo, P. M. Vora, E. J. Mele, A. T. C. Johnson, and J. M. Kikkawa. Photoluminescence and band gap modulation in graphene oxide. *Appl. Phys. Lett.*, 94(11):111909–3, March 2009. doi: 10.1063/1.3098358.

[38] E. Treossi, M. Melucci, A. Liscio, M. Gazzano, P. Samorì, and V. Palermo. High-Contrast Visualization of Graphene Oxide on Dye-Sensitized Glass, Quartz, and Silicon by Fluorescence Quenching. *J. Am. Chem. Soc.*, 131(43):15576–15577, November 2009. doi: 10.1021/ja9055382.

[39] M. S. Goh and M. Pumera. Single-, Few-, and Multilayer Graphene Not Exhibiting Significant Advantages over Graphite Microparticles in Electroanalysis. *Anal. Chem.*, 82(19):8367–8370, 2010. doi: 10.1021/ac101996m.

[40] H. Chen, M. B. Müller, K. J. Gilmore, G. G. Wallace, and D. Li. Mechanically Strong, Electrically Conductive, and Biocompatible Graphene Paper. *Adv. Mater.*, 20(18):3557–3561, 2008. doi: 10.1002/adma.200800757.

[41] C. L. Wong, M. Annamalai, Z. Q. Wang, and M. Palaniapan. Characterization of nanomechanical graphene drum structures. *J. Micromech. Microeng.*, 20(11):115029, 2010. doi: 10.1088/0960-1317/20/11/115029.

[42] W. Cai, R. D. Piner, F. J. Stadermann, S. Park, M. A. Shaibat, Y. Ishii, D. Yang, A. Velamakanni, S. J. An, M. Stoller, J. An, D. Chen, and R. S. Ruoff. Synthesis and Solid-State NMR Structural Characterization of 13C-Labeled Graphite Oxide. *Science*, 321(5897):1815–1817, 2008. doi: 10.1126/science.1162369.

[43] A. Fasolino, J. H. Los, and M. I. Katsnelson. Intrinsic ripples in graphene. *Nat. Mater.*, 6(11): 858–861, November 2007. doi: 10.1038/nmat2011.

[44] M. B. Müller, J. P. Quirino, P. N. Nesterenko, P. R. Haddad, S. Gambhir, D. Li, and G. G. Wallace. Capillary zone electrophoresis of graphene oxide and chemically converted graphene. *J. Chromatogr., A*, 1217(48):7593–7597, November 2010. doi: 10.1016/j.chroma.2010.09.069.

[45] K. P. Loh, Q. Bao, P. K. Ang, and J. Yang. The chemistry of graphene. *J. Mater. Chem.*, 20 (12):2277–2289, 2010. doi: 10.1039/B920539J.

[46] T. O. Wehling, K. S. Novosëlov, S. V. Morozov, E. E. Vdovin, M. I. Katsnelson, A. K. Geim, and A. I. Lichtenstein. Molecular doping of graphene. *Nano Lett.*, 8(1):173–177, 2008. doi: 10.1021/nL072364w.

[47] Y.-H. Zhang, Y.-B. Chen, K.-G. Zhou, C.-H. Liu, J. Zeng, H.-L. Zhang, and Y. Peng. Improving gas sensing properties of graphene by introducing dopants and defects: a first-principles study. *Nanotechnol.*, 20(18):185504, 2009. doi: 10.1088/0957-4484/20/18/185504.

[48] C. N. R. Rao, A. K. Sood, K. S. Subrahmanyam, and A. Govindaraj. Graphene: The New Two-Dimensional Nanomaterial. *Angew. Chem., Int. Ed.*, 48(42):7752–7777, 2009. doi: 10.1002/anie.200901678.

[49] E. Fitzer, K.-H. Kochling, H. P. Boehm, and H. Marsh. Recommended terminology for the description of carbon as a solid (IUPAC Recommendations 1995). *Pure Appl. Chem.*, 67(3): 473–506, 1995. doi: 10.1351/pac199567030473.

[50] M. D. Watson, A. Fechtenkötter, and K. Müllen. Big Is Beautiful - "Aromaticity" Revisited from the Viewpoint of Macromolecular and Supramolecular Benzene Chemistry. *Chem. Rev.*, 101(5):1267–1300, April 2001. doi: 10.1021/cr990322p.

[51] S. E. Stein and R. L. Brown. .pi.-Electron properties of large condensed polyaromatic hydrocarbons. *J. Am. Chem. Soc.*, 109(12):3721–3729, June 1987. doi: 10.1021/ja00246a033.

[52] C. D. Simpson, J. D. Brand, A. J. Berresheim, L. Przybilla, H. J. Räder, and K. Müllen. Synthesis of a Giant 222 Carbon Graphite Sheet. *Chem.–Eur. J.*, 8(6):1424–1429, 2002. doi: 10.1002/1521-3765(20020315)8:6¡1424::AID-CHEM1424¿3.0.CO;2-Z.

[53] M. J. McAllister, J.-L. Li, D. H. Adamson, H. C. Schniepp, A. A. Abdala, J. Liu, M. Herrera-Alonso, D. L. Milius, R. Car, R. K. Prud'homme, and I. A. Aksay. Single Sheet Functionalized Graphene by Oxidation and Thermal Expansion of Graphite. *Chem. Mater.*, 19(18):4396–4404, May 2007. doi: 10.1021/cm0630800.

[54] L. J. Cote, R. Cruz-Silva, and J. Huang. Flash Reduction and Patterning of Graphite Oxide and Its Polymer Composite. *J. Am. Chem. Soc.*, 131(31):11027–11032, July 2009. doi: 10.1021/ja902348k.

[55] E. C. Salas, Z. Sun, A. Luettge, and J. M. Tour. Reduction of Graphene Oxide via Bacterial Respiration. *ACS Nano*, 4(8):4852–4856, July 2010. doi: 10.1021/nn101081t.

[56] A. Turchanin, A. Beyer, C. T. Nottbohm, X. H. Zhang, R. Stosch, A. Sologubenko, J. Mayer, P. Hinze, T. Weimann, and A. Golzhauser. One Nanometer Thin Carbon Nanosheets with Tunable Conductivity and Stiffness. *Adv. Mater.*, 21(12):1233–+, 2009. doi: 10.1002/adma.200803078.

[57] A. Turchanin, D. Weber, M. Büenfeld, C. Kisielowski, M. V. Fistul, K. B. Efetov, T. Weimann, R. Stosch, J. Mayer, and A. Gölzhäuser. Conversion of Self-Assembled Monolayers into Nanocrystalline Graphene: Structure and Electric Transport. *ACS Nano*, 5(5):3896–3904, 2011. doi: 10.1021/nn200297n.

[58] D. R. Dreyer, S. Park, C. W. Bielawski, and R. S. Ruoff. The chemistry of graphene oxide. *Chem. Soc. Rev.*, 39(1):228–240, 2010. doi: 10.1039/B917103G.

2 Graphenes in chemical sensors and biosensors

Note: All potentials given in this chapter are relative to the standard Ag/AgCl electrode if not stated otherwise.

2.1 Overview

The following chapter gives an insight into the current state of the art of applying graphene materials in chemical sensors and biosensors. A large amount of published work (over 230 references) on this topic is discussed to reveal the individual benefits (and flaws) of the members of the graphene-family.

A statistical evaluation (see Figure 2.1) shows that rGO is the material most commonly used (68% of all publications), probably because of its easy access, scalable synthesis, low cost and simple functionalization. In addition, rGO resembles pristine graphene in terms of electrical, thermal and mechanical properties[1]. However, if one distinguishes between different sensor types, it becomes clear that each material has its own field of application. Pristine graphene is most used in the transistor sector (approximately 60%), but not used at all for luminescence sensors. In the latter application, solubility and quenching (FRET) ability are required, for which the oxide groups are mandatory. This clearly indicates that "graphene" is not one but, in fact, three materials, and that one must select the material which is most suitable for the task.

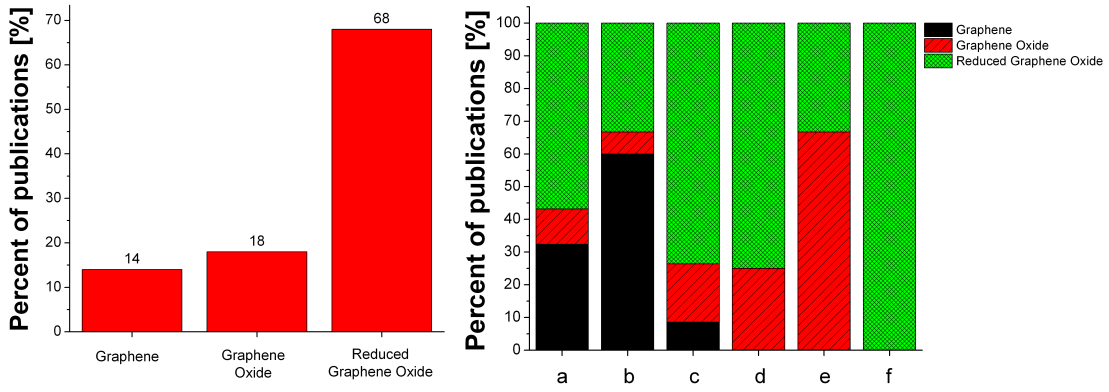

Figure 2.1. Statistical evaluation of the discussed work. Left: 68% of the published work use reduced graphene oxide and only 14% use pristine graphene. Right: If divided into sensor types (a: plain sensors, i.e. non-nanocomposite sensors; b: electro-chemical sensors; c: field effect transistor-based sensors; d: fluorescence-based sensors; e: chemiluminescence-based sensors; f: colorimetric sensors) it becomes clear, that every graphene material has is own application field. For instance, pristine graphene dominates the transistor-based sensors whereas it is not represented at all in optical sensors (block d-f).

2.2 Plain sensors

"Plain sensors" are those where graphene materials have been used without any prior modification. They are primarily used in electrochemical sensors, for example in electrodes due to their excellent conductivity. Typically, they are adsorbed on a glassy carbon electrode to increase the oxidation peak current and decrease of the oxidation overpotential of an analyte[2].

The graphene family is well known for its high adsorption of gases, vapors, ions and even uncharged organic species. *Schedin et al.*[3] claims graphene-based sensors "allow the ultimate sensitivity such that the adsorption of individual gas molecules could be detected". The effect was used to sense gases such as NO_2[4–10], NH_3[8,11,12], CO[6], hydrogen[13], oxygen[6], water vapor (humidity)[4,11,14] and volatile organic compounds such as nonanal, octanoic acid and trimethylamine[11]. The limits of detection (LODs) are in the lower ppm and ppb range if detected by conductivity or amperometry. The low LODs are due to the low electrical noise of graphene devices compared to those based on carbon nanotubes or semiconductor nanowires[11,15]. This is again attributed to the two-dimensional nature of the material. The strong sensing response is attributed to the charge transfer between the material and the adsorbed gases or vapors[8]. A simple and impressive approach was reported by *Dua et al.*[16] who used solutions of (reduced) graphene oxide in an inkjet printer to print it directly

on poly(ethylene terephthalate) (PET). The films can be lifted off the PET surface and then be used directly for conductometric sensing of vapors (Figure 2.2A). With these materials, as low as 500 ppb of NO_2 and of 6-25 ppm of Cl_2 are detectable. The films can be recovered by exposing them to 254 nm UV light. Unfortunately, these sensors are not selective[3] and can only distinguish between electron-withdrawing and electron-donating molecules[16].

Graphene oxide and reduced graphene oxide (rGO) possess functional groups (mainly carboxy and hydroxy groups) on their surfaces which make them both fluorometric[17,18] and voltammetric[19] probes for pH. The pH-dependent fluorescence of graphene oxide in the pH range from 1 to 10 does not depend on the excitation nor the emission wavelength. This makes it a potential probe for sensing pH in extracellular samples[17]. *Lim et al.*[19] discovered that rGO ("anodized graphene") has a high potentiometric pH sensitivity (51.3 mV/pH) that is close to the theoretical maximum of 59.2 mV/pH. Pristine graphene, in contrast, shows a much weaker sensitivity to pH (12.5 mV/pH). The presence of oxide groups relates to the pH-responsivity. The functional groups of (reduced) graphene oxide can also complex metal cations such as Cu^{2+}, Pb^{2+}, and Cd^{2+} which enable their (unselective) detection by anodic stripping voltammetry in the 10-100 pM range[20].

Graphene-modified electrodes are also suitable for the voltammetric and amperometric determination of redox active species such as hydrazine[21–23], hydrogen peroxide[2], dopamine, ascorbic acid and uric acid[24–27], hydroquinone and catechol[28] and β-nicotinamide adenine dinucleotide (NADH)[2,29] at nM to μM levels. *Zhou et al.*[2] have compared the performance of electrodes modified with rGO to those with other carbon materials (graphite and carbon nanotubes). Their study revealed that the former give a higher sensitivity towards hydrogen peroxide in voltammetry. A limit of detection (LOD) of 0.05 μM was found at a low overpotential of -0.20 V. Dopamine, ascorbic acid, uric acid and acetaminophen do not interfere. This high selectivity is claimed to be due to the formation of strong hydrogen bonds between hydrogen peroxide and rGO.

Similar results were obtained by *Chang et al.*[24] who have demonstrated the simultaneous detection of uric acid and ascorbic acid by using screen-printed carbon electrodes

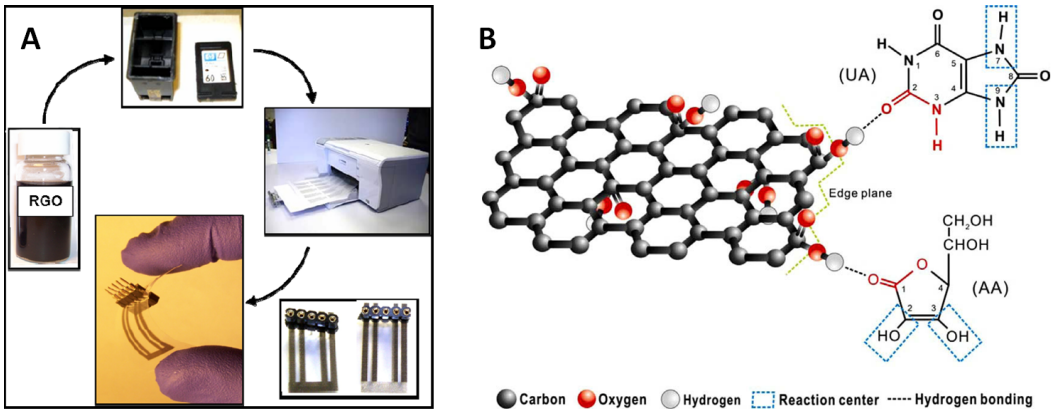

Figure 2.2. (A) Procedure for sensor fabrication according to *Dua et al.*[16]. Inset shows two images of inkjet printed sensors. Adapted with permission from ref. 16. Copyright (2010) Wiley-VCH Verlag GmbH & Co. (B) A schematic diagram illustrating the suggested mechanism causing the improved voltammetric peak separation and sensitivity in a sensor for uric acid and ascorbic acid using reduced graphene oxide. Reprinted with permission from ref. 24. Copyright (2010) Elsevier.

modified with rGO. The improved performance in terms of peak separation and sensitivity was compared to that of plain carbon and graphene oxide modified electrodes. It illustrates that the presence of a nominal amount of functional groups on the surface of the material is mandatory to form hydrogen bonds with the analytes (Figure 2.2B). Both the strength of the bond and the distance of interaction site to the reaction center influence the oxidation step and therefore the peak separation of ascorbic acid (19 mV instead of 0.5 V) and uric acid (0.3 V instead of 0.5 V) with simultaneous doubling of the peak current. Hydroquinone and catechol can also be sensed simultaneously[28] by differential pulse voltammetry. The low LOD (15 and 10 nM, respectively) is attributed to a significantly lower oxidation overpotential, fast electron-transfer kinetics, and a good separation of the oxidation peaks (by about 112 mV) compared to bare carbon electrodes. Interference by common metal ions, uric acid and ascorbic acid is negligible. The same advantages apply to the amperometric determination of hydrazine. A sensing platform based on rGO[21] has an LOD of 1 μM of hydrazine, which is 8-times better than a comparable platform based on using multiwalled carbon nanotubes. The method also was applied to determine acetaminophen (paracetamol)[30,31] (LOD: 32 nM) and 2,4,6-trinitrotoluene (TNT)[32,33] in seawater (LOD: 4 μM).

The simultaneous detection of nucleic bases in DNA is a particular challenge due to the relatively close matching redox potentials and the slow electron transfer rate with most electrode materials[2]. Glassy carbon and graphite electrodes give only two peaks

(at about 0.65 V and 1.0 V) for a solution of all four bases[2,19,34]. An improvement is achieved with the use of a pristine graphene (on SiC substrate) electrode which clearly promotes a third peak that is assigned to cytosine (1.5 V). An even better result is obtained by adding rGO which shows oxidation peaks for all four nucleotides in solution (0.6 V, 0.9 V, 1.25 V, 1.5 V for guanine, adenine, thymine, cytosine, respectively)[19]. Moreover, electrodes with added rGO can detect the bases both in ssDNA and in dsDNA, with an LOD of 0.35 μg mL^{-1} [19,34]. The determination of dsDNA is difficult with most electrode materials without prior hydrolysis and separation, but was accomplished recently by using electron cyclotron resonance nanocarbon film electrodes[2,19]. The feature of separated oxidation peaks was exploited[2] to detect single-nucleotide polymorphism in short oligonucleotides.

2.3 Nanocomposite sensors

2.3.1 Electro-chemical sensors

Assemblies of different materials that form an entity in the nanometer range are often referred to as nanocomposites. They are characterized by a very high surface to volume ratio which explains their superior properties relative to bulk composites. The combination of two or more materials also enables the tailoring of properties such as sensitivity and selectivity.

Calculations predict the enhanced adsorption of gases on graphene sheets decorated with metals. This is due to mutual interactions[35,36]. Graphene nanocomposites were often decorated with metals such as palladium and platinum resulting in sensors for hydrogen[37–44], carbon monoxide[39] and ethanol[45,46] in the gas phase. *Zhang et al.*[13] reported on the use of plain reduced graphene oxide (rGO) for hydrogen sensing with a resistance measurement, but the sensitivity was poor yielding a signal change of only 0.4% R/R_0 for 500 ppm hydrogen. If rGO is combined with an conductive polymer such as polyaniline, the sensitivity is enhanced by a factor of 10 compared to rGO only. The signal change is 3.9% (R/R_0 units) for 600 ppm of hydrogen, and 12.9% (R/R_0) for 0.5% hydrogen. The enhancement effect in the range above 0.5%

hydrogen is attributed to the high porosity of the nanocomposite, while the effect below 0.5% can be assigned to the polyaniline only[37]. A further enhancement in signal response (25 times relative to[13]) is achieved by decorating rGO with palladium nanoparticles (signal change 33% R/R_0 for 0.5% hydrogen). In contrast, this composite reduces the response of plain rGO for NO_2. In fact, a sensor based on the use of rGO with and without palladium nanoparticles can distinguish between hydrogen, NO_2 and humidity[43]. It is interesting to note that a similar approach with graphene as the base material exhibits an enhancement factor of only 11.3 (4.5% R/R_0 for 500 ppm H_2)[44]. This indicates that both the catalytic effect of palladium and the interaction between the two material phases contribute to the sensing ability. *Kumar et al.*[42] used a palladium-platinum alloy on rGO for their resistance measurements to improve response and recovery times of the respective hydrogen sensor. Compared to a similar method reported by *Lange et al.*[43], response times are reduced to 2-20 s, but the signal response is decreased (only 4.3% R/R_0 for 2% H_2). *Kaniyoor et al.*[40,41] have combined multiwalled carbon nanotubes with rGO (1:1 w/w) and decorated this material with platinum nanoparticles. This increases the response to 1-5% hydrogen by a factor of 2 compared to platinum decorated nanotubes. Such sensors work at temperatures up to 160 °C. *Yi et al.*[46] reported on a sensor based on ZnO nanorods and graphene on metal foils for conductive sensing of vapors. Ethanol was determined at low ppm levels at operational temperatures of up to 300 °C and under mechanical deformation with a bending radius of <0.8 cm. *Cuong et al.*[47] used rGO and ZnO nanorods to design a sensor for hydrogen sulfide. This sensor possesses a high resistivity in an oxygen environment, because oxygen is adsorbed on the surface of the nanorods. There oxygen ionic species are formed, capturing electrons from the conduction band. Hydrogen sulfide reacts with the surface oxygen species which decreases the surface concentration of oxygen ions leading to a decrease in the resistance of the sensor. The detection limit is 2 ppm of H_2S in presence of oxygen at room temperature.

rGO was deposited on top of a surface acoustic wave transducer (36° YX $LiTaO_3$) to build a sensor device for hydrogen and carbon monoxide[38,39]. The change in the resonance frequency at room temperature was 5.8 kHz for 1% hydrogen and -8.5 kHz for 0.1% CO. The device can detect as little as 125 ppm of hydrogen and 250 ppm of CO, both at 25 °C and 40 °C. The response and recovery times for hydrogen are 12 s and

less than 1 min for 125 ppm, 5 min and 20 min, respectively, for 250 ppm of CO. The combination of graphene materials with surface acoustic wave technology is promising because the sensors can be operated passively, i.e. with no need of a separate power supply. This overcomes the need for batteries and enables easier miniaturization[48].

rGO and Nafion can be used for anodic stripping voltammetric analysis of cadmium(II)[49–51]. Other work demonstrated the simultaneous detection of Cd^{2+} and Pb^{2+}[50,51]. *Willemse et al.*[51] reported on the determination of Cd^{2+}, Pb^{2+}, Zn^{2+} and Cu^{2+}. The latter approach has LODs of 0.07-0.08 μg mL^{-1} for the individual ions which is comparable to ICP-MS. The high sensitivity is contributed to a combination of enhanced electron conduction of rGO and the cation exchange capacity of Nafion. Nafion also acts as an effective solubilizing agent and antifouling coating[50,51]. However, tests with real water samples revealed two problems. First, organic compounds in the water may form stable complexes with metal ions such as Cu^{2+}, thus making them unavailable for analysis. Secondly, organic compounds can adsorb onto the surface of the working electrode, thus decreasing its surface area which can lead to a reduction of the analytical signal.

Gong et al.[52] have developed a nanocomposite consisting of rGO protected by poly(vinyl pyrrolidone), chitosan and gold nanoparticles for sensing Hg^{2+} by anodic stripping voltammetry. This sensor has a sensitivity of 708.3 μA/ppb, and its detection limit (6 ppt) is far below the guideline value of drinking water set by the WHO (1 ppb). Also, 20 ppb of either Cd^{2+}, Co^{2+}, Cu^{2+}, Fe^{3+}, Zn^{2+} or I^- have negligible effect on the detection of 1.0 ppb of Hg^{2+}. A comparison with a sensor based on the use of carbon nanotubes and the individual components reveals that such properties can be ascribed to the ensemble behavior of the nanostructured material. It was concluded that the surface and structure of rGO greatly improves the interaction with both the deposited gold nanoparticles and the analyte ions, prompting the interfacial electron-transfer process.

Compared to common glassy carbon electrodes (GCEs), electrodes modified with graphene materials already yield enhanced signals or can discriminate between redox-active species due to interactions with surface, catalytic activity, or changed electron transfer kinetics. The determination of hydrochinone, for example, is difficult with

GCEs at low potentials of about 0.0 V by differential pulse voltammetry. In contrast, an electrode modified with rGO shows a well-defined peak at 2 mV. If decorated with platinum nanoparticles, the current density, and therefore the sensitivity (expressed as $\mu A\ M^{-1}\ cm^{-2}$), increased by a factor of 2. *Li et al.*[53] have explained this by the enhanced electron transfer in this system. The charge hopping through the metal and the effective charge migration through the rGO both attribute to this. The effective transport of the electrons to the electrode in the material led to the efficient electrocatalytic oxidation of hydroquinone. By analogy, the detection of catechol can be improved[54,55]. The isomers hydrochinone, catechol and resorcinol can be determined simultaneously with a sensor based on rGO and chitosan[56]. The wide linear ranges (about 1-400 μM each), low detection limits (0.75 μM each) and good sensitivities (about 56-59 $\mu A\ M^{-1}$ for hydrochinone/catechol, and 25 $\mu A\ M^{-1}$ for resorcinol) are a product of high electrocatalytic activities towards the analytes, increased oxidation peak currents, and good peak separations (hydrochinone at 0.0 V, catechol at 0.1 V, resorcinol at 0.5 V).

The electrocatalytic effect of the composites depends on the ratio of the components. *Hong et al.*[57] examined the effects of different ratios of gold nanoparticle and rGO on the peak current of a 5 mM solution of ferricyanide (1 M KCl, 50 $mV\ s^{-1}$). A ratio of 10:1 of gold nanoparticles/rGO showed the highest peak current and therefore the best catalytic activity. This is due to the low conductivity caused by the presence of too many 4-dimethylaminopyridine moieties used as a stabilizer for gold nanoparticles in water on the rGO surface. At ratios >10:1, this composite did not form stable aqueous solutions and precipated after a maximum of 12 h.

The simultaneous determination of ascorbic acid and uric acid was demonstrated by *Chang et al.*[24] using rGO only. *Zhang et al.*[58] used a combination of graphene and multiwall carbon nanotubes in a crosslinked cyclodextrin matrix to sense both dopamine (detection limit: 0.05 μM, range: 0.15-21.65 μM) and ascorbic acid (detection limit: 1.65 μM, range: 5 μM-0.48 mM) by voltammetry. The potential for the oxidation of dopamine (at 0.17 V vs. SCE) and ascorbic acid (at -0.06 V vs. SCE) are well separated. The observed sensitivity for dopamine (23-fold compared to ascorbic acid) is claimed be the result of three effects. First, the host-guest chemical reaction ability of cyclodextrin enhances the oxidation of dopamine by its diffusion through

the cavities of cyclodextrin. Secondly, the easy contact with the dispersed graphene-multiwall carbon nanotubes facilitates the electron transfer. Third, the π-π interaction between the phenyl ring of dopamine and the graphene/carbon nanotubes makes the electron transfer more feasible than that between non-aromatic ring of ascorbic acid and the graphene/carbon nanotubes. Unfortunately, the sensor was not tested for interference by uric acid. A sensor for uric acid in human serum was recently developed which exploits the described discrimination effect[59]. The detection limit and the linear range were suitable (0.3 μM, 0.8-150 μM). 50-fold concentration of dopamine and 500-fold concentration of ascorbic acid did not show any interference.

Comparison with a similar composite consisting of rGO in cyclodextrin by *Tan et al.*[60] reveals that a material composed of graphene and carbon nanotubes has the same effect on discrimination as rGO only. This can be attributed to the similar defect (= border) sites of both materials. However, the latter one has a 10-fold lower detection limit (Zhang: 0.05 μM, Tan: 5.0 nM) with a wider linear range (Zhang: 0.15-21.65 μM, Tan: 9 nM-12.7 μM) for the voltammetric determination of dopamine.

(Reduced) graphene oxide materials were also applied in sensors for the detection of dopamine by fabricating composites with TiO_2[61], ethylenediamine triacetic acid silane[62], layered double hydroxides (Zn/Al)[63] and cupric oxide[64]. The resulting voltammetric sensors share similiar detection limits (10 nM to 2 μM), linear ranges (from 0.1 to 200 μM) and selectivity. There does not appear to be any obvious correlation between the components of the composites and their effects. The choice of the redox peak (0.2 V/0.3 V vs. SCE; 0.272 V vs. Ag/AgCl) and the optimization of other parameters (pH, electron transfer resistance, ratio of materials, etc.). are much more relevant. Still, the simultaneous detection of ascorbic acid, dopamine and uric acid is critical. Different materials promote different redox peaks[65–68]. rGO with platinum particles in a Nafion matrix, for example, provides relatively high peak currents for ascorbic acid (1 mM, 95 μA, 40 mV), dopamine (1 mM, 272 μA, 225 mV) and uric acid (1 mM, 371 μA, 369 mV)[68] in the respective cyclovoltammograms at a scan rate of 50 mV s^{-1}.

The use of an ionic liquid instead of Nafion[67] not only results in a different discrimination of the peaks (e.g. ascorbic acid at 85 mV) but also to a 2-4-fold lower peak

current for all analytes (e.g. 1 mM of dopamine: 87.1 μA; scan rate: 100 mV s^{-1}). The same applies to differential pulse voltammetry. A composite based on graphene oxide and polyaniline was found to further enlarge the distance between the cathodic oxidation peaks (25 mV, 249 mV and 373 mV for ascorbic acid, dopamine and uric acid, respectively)[65]. Here the currents are reduced by another step (scan rate: 50 mV s^{-1}) for ascorbic acid (2 mM: 20 μA), dopamine (1 mM: 40 μA) and uric acid (1 mM: 77 μA). The currents of all composites are greatly enhanced compared to a bare GCE due to the increased surface area and the catalytic activity, which seems best for a combination of rGO and Nafion.

Graphene nanocomposite materials have also served as a basis for constructing enzymatic biosensors[69,70]. Glucose oxidase (GOx) is often chosen as a model enzyme. As previously discussed, plain applied graphene materials are suitable for voltammetric determination of enzymatically generated hydrogen peroxide[2]. *Brownson et al.*[71] report that graphite-based amperometric electrodes (sensitivity: 49.0 μA mM^{-1}) exhibit greatly enhanced electro-catalytic activity over graphene (32.8 μA mM^{-1}) at 400 mV. This is attributed to an increased percentage of edge plane sites. However, after the introduction of Nafion, sensitivities are reversed due to the potential discrimination effect from interferents. Graphene and Nafion (42.2 μA mM^{-1}) are superior over graphite and Nafion (32.0 μA mM^{-1}) due to substantial re-orientation and disorder of graphene (Figure 2.3). This is an indication that (a) composite materials are essential for graphene based amperometric biosensors, and (b) the orientation of the graphene sheets in these composite materials is crucial.

Nafion neither is the only nor the best material to improve the amperometric characteristics of graphene. ZnO nanospheres[72], for example, lead to similiar results with respect to detection limit and sensitivity[73] but provide a wider linear range for hydrogen peroxide detection (1.8 μM to 2.3 mM) at an almost identical potential (about -0.3 V). *Cui et al.*[74] have used a composite consisting of rGO, thionine, gold nanoparticles and horseradish peroxidase for analysis of milk samples. The sensitivity doubled (86 μA mM^{-1}, -0.26 V vs SCE) compared to the graphene/Nafion material described above. The sensor showed a very good detection limit (10 nM) and linear range (10 μM-1.8 mM). Ascorbic acid interferes, but glucose, uric acid, acetic acid, oxalic acid, citric acid and sucrose do not. The addition of gold nanoparticles and

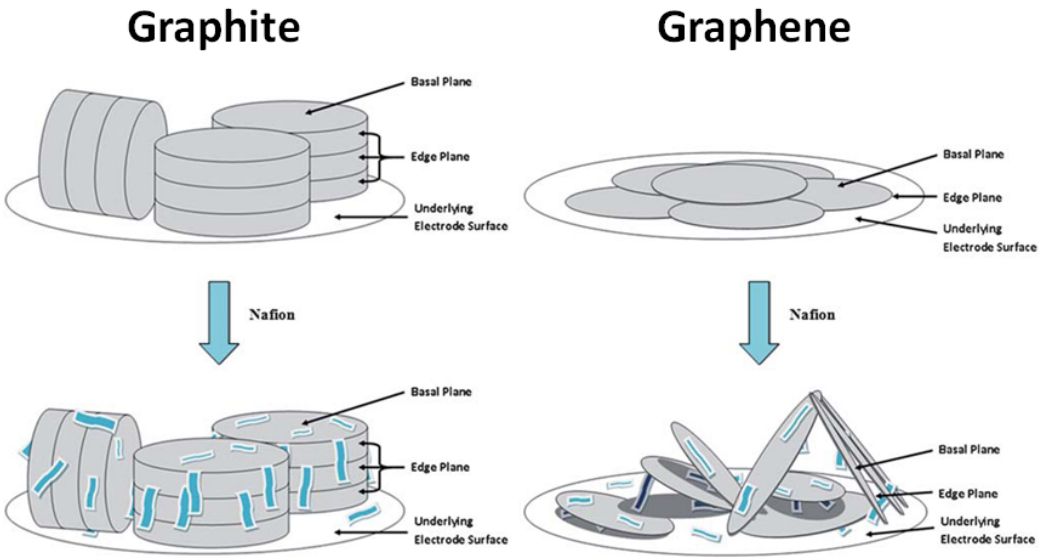

Figure 2.3. Left: Schematic representation of inhibition of edge plane like sites caused by the addition of Nafion to a graphite modified electrode. Right: Schematic representation of the re-orientation of graphene layer cause by the addition of Nafion to a graphene modified electrode. Reproduced by permission on the Royal Society of Chemistry from ref. 71.

thionine doubles sensitivity compared to approaches without these[75,76].

Huang et al.[77] prepared a composite based on rGO, gold nanoparticles and catalase for use in an amperometric sensor for H_2O_2. This approach has similar detection limit (50 nM) and linear range (0.3-600 μM), but sensitivity is low (13.4 μA mM^{-1}, -0.3 V vs SCE). Two other reports confirm that gold nanoparticles improve detection limits and linear ranges[78,79]. Materials incorporating magnetite provide the same enhancements as gold nanoparticles and provide the additional feature of ferromagnetism. This allows easy manipulation of the material (e.g. separation for cleaning processes, immobilizing on electrodes) by application of an external magnetic field[80,81]. Sensors based on all types of graphene materials with silver nanoparticles[82,83], MnO_2[84], DNA[83,85], hemoglobin[86] and microperoxidase-11[87] have been constructed with detection limits in the lower μM range and linear ranges in the upper μM and lower mM range.

Prussian blue (PB, also termed "artificial peroxidase") is known for its excellent performance in sensing H_2O_2[88]. *Cao et al.*[89] synthesized PB nanocubes on top of rGO (Figure 2.4) to construct a sensor for H_2O_2 with an LOD of 45 nM at 0.2 V and a wide linear range (0.05-120 μM). Others have achieved similar results[90,91]. *Guo et*

al.[92] have built a biointerface that consist of multilayers of rGO, PB and the extracellular matrix protein laminin. They were deposited on an indium tin oxide substrate on which human cells were grown. High electrocatalytic activity towards reduction of H_2O_2 was observed at a potential of 0.0 V. Such a low potential prevents anodic and cathodic potential interference. The release of H_2O_2 from the cells in response to different stimuli was explored. It was possible to detect 10^{11} extracellularly released H_2O_2 molecules per cell, which is attributed to the high sensitivity (141 μA mM^{-1}) of this multilayer composite structure.

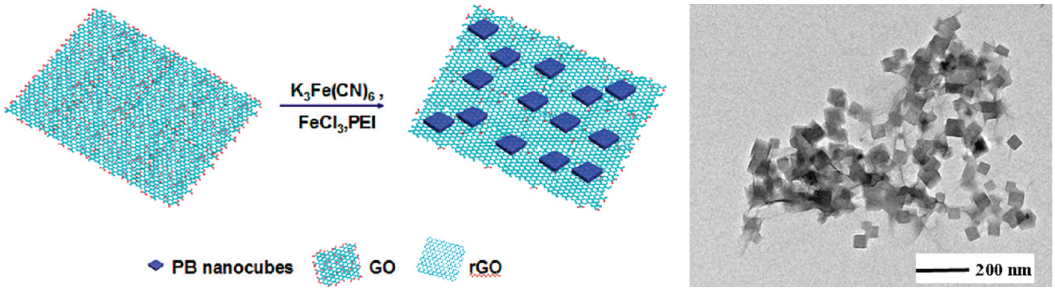

Figure 2.4. Left: Procedure for the fabrication of nanocomposites with Prussian blue nanocubes for sensing hydrogen peroxide. Right: TEM image showing the resulting nanocomposite. Adapted with permission from ref. 89. Copyright (2010) American Chemical Society.

Various attempts have been made to immobilize GOx on rGO in the presence[69,93,94] or absence[95] of a polymer matrix. This resulted in amperometric biosensors for glucose with detection limits (3-20 μM) and linear ranges (0.04-12 mM) that enable glucose to be determined in blood serum (lower mM range). They provide fast response times (5 s) and Michaelis-Menten constants of about 4.5 mM. This indicates that the bound GOx has retained a relatively high enzymatic activity compared to similar materials based on multiwall carbon nanotubes[96]. However, a comparison with GOx-based biosensors modified with gold nanoparticles[96–100], ionic liquids[101,102], platinum particles[103,104] or PB[91] revealed no significant improvements. Modifications with palladium particles[105] or CdS[70] resulted in a reduction of the Michaelis-Menten constant by a factor of 3-4 (to about 1.2-1.6 mM), suggesting that these latter modifications provide a more favorable environment for GOx. *Zhiguo et al.*[106] have developed a multilayer nanocomposite for use in a glucose sensor. rGO decorated with gold nanoparticles was covered with a layer of CdTe-CdS quantum dots, a second layer with gold nanoparticles, and finally with GOx in a chitosan matrix. This sensor displayed remarkable properties in terms of response time (45 ms), detection limit (3 pM),

linear range (10 pM to 10 nM), Michaelis-Menten constant (5.24 pM) and sensitivity (5763 nA nM^{-1} cm^{-2}). Its favorable properties obviously are due to its nanoarchitecture that promotes a "push and pull" effect which accelerates the electron transfer from GOx to rGO. The method was successfully applied to the determination of glucose in diluted saliva.

A nonenzymatic amperometric glucose sensor was constructed[107] from a composite based on rGO and palladium nanoparticles in Nafion. Glucose was determined at a potential of 0.4 V (vs. SCE), and ascorbic acid, uric acid and *p*-acetamidophenol do not interfere. The detection limit (1 μM), sensitivity (2 μA mM^{-1}) and linear range (10 μM to 5 mM) compete with the enzymatic sensors described above. Analysis of serum samples gave good recoveries.

Chang et al.[108] used rGO with gold nanoparticles in a chitosan matrix and observed a remarkable decrease in the oxidation overpotential of NADH (about 220 mV, from 0.58 V to 0.36 V) compared to a bare GCE. This enables amperometric determination of NADH at 0.35 V with good sensitivity (0.318 μA μM^{-1} cm^{-2}), short response time (5 s), low detection limit (1.2 μM) and a wide linear range (1.5-350 μM). The oxidation overpotential is decreased by 440 mV, and sensitivity is improved to 37.43 μA μM^{-1} cm^{-2} if rGO is used along with an ionic liquid in chitosan[109]. They eventually combined the sensor with alcohol dehydrogenase and were then able to measure μM concentrations of ethanol (at 0.45 V). Similar results were reported by *Kumar et al.*[110] who worked at 50 mV (vs SCE). NADH itself can be determined without interference in the presence of a 100-fold excess of dopamine and uric acid, while ascorbic acid causes an increase in signal[110].

The simultaneous detection of all four DNA bases with plain graphene materials also has been described[2,19,34]. The electron transfer rate can be further improved by modifying rGO with gold nanoparticles[111] or ionic liquids[112] which results in higher peak currents. Thus higher sensitivities (13-62 nA μM^{-1} vs. 7-10 nA μM^{-1}) are possible for differential pulse voltammetry[113]. Similar results were reported for graphene composites with TiO_2[114], multi-walled carbon nanotubes[115], polypyrrol[116], Nafion[117] and Fe_3O_4[118].

In order to diagnose pathogenic or genetic diseases[119], a strand of DNA was immobilized on the surface of graphene materials or their composites, and hybridization was detected by impedimetric[120–122] or voltammetric[119,123–126] methods. The method can discriminate between non-target, partial hybridized, and full hybridized dsDNA and enables detection of single nucleotide polymorphism which is, for example, correlated to the development of Alzheimer's disease[120]. The addition of PB further increases the response (current)[127]. Most sensors can detect target ssDNA in the picomolar to nanomolar range. *Du et al.*[128] demonstrated the use of triplex DNA as recognition motif to amplify the detection of DNA. This attempt reduced the detection limit and linear range to the femtomolar range.

Tang et al.[129] used two different ssDNA/graphene oxide complexes to detect target DNA. Both complexes were bound to target DNA (each at a different position) to form large aggregates. The diameter of these aggregates, as determined by dynamic light scattering, is a function of target DNA concentration (Figure 2.5). It was possible to detect target DNA in the 1 pM to 10 nM concentration range with an LOD of 1 pM. Mismatched DNA did not give aggregates under the same conditions. The high specifity was attributed to the synergic and multivalent effects of the DNA/graphene oxide complex formed on hybridization with target DNA.

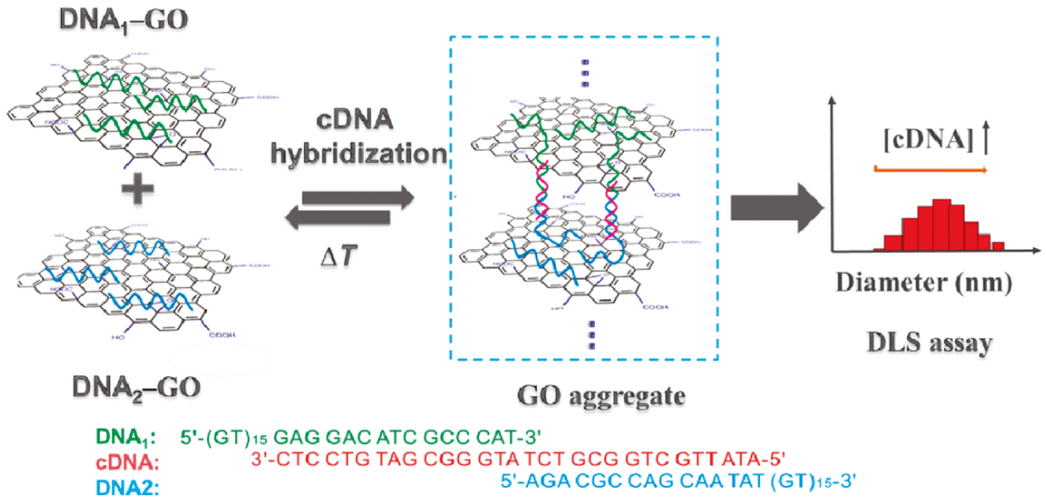

Figure 2.5. Schematic illustration of procedures for DNA-directed self-assembly of graphene oxide and analysis of homogeneous assay of DNA by dynamic light scattering. Adapted with permission from ref. 129. Copyright (2011) American Chemical Society.

DNA sensors using aptamers or DNAzymes as probes allow the sensitive and selective detection of analytes such as L-histidine with an LOD of 0.1 pM[130], dimethylmethylphosphonate (LOD: 0.4 ppm)[131] and thrombin (LOD: 0.45 pM)[132]. *Wang et al.*[133] have combined a selective aptasensor based on rGO for thrombin with the technique of lable-free, regenerative and sensitive surface plasmon resonance (SPR). An SPR gold chip was coated with poly(diallyldimethylammonium chloride) to create a positively charged chip, and immersed into a solution of rGO to assemble the material on the chip. Next, a thrombin aptamer was adsorbed onto the rGO layer through π-π-stacking interactions. The binding between the aptamer and the target molecule greatly disturbed the interaction between the aptamer and rGO causing the release of the aptamer. The chip was regenerated by immersion in aptamer solution. This concept allows for the detection of 0.05 nM of thrombin (linear range: 0.08-200 nM).

All the schemes for signal enhancement also apply to (bio)sensors developed for various other analytes, for example, rutin (detection limit: 0.6-16 nM, linear range: 1 nM-100 μM)[134–136] and indole-3-acetic acid (detection limit: 0.05 μM, linear range: 0.1-7.0 μM)[137]. Explosive nitroaromatic compounds (detection limit: 0.5-4 ppb, sensitivity: 1.75 μA ppb^{-1} cm^{-2}, linear range: 30-1500 ppb) can be detected by stripping voltammetry by exploiting the synergistic adsorptive properties of porphyrin[138] or ionic liquids[139,140], along with the large electroactive surface and fast charge transfer of (reduced) graphene oxide. Sensors have been reported for aloe-emodin[141], 4-aminophenol[142], caffeine[143], carbaryl pesticide[144,145], carbendazim[146], chlorite[147], cholesterol[148], hemoglobin[149], hypoxanthine[150], methyl jasmonate[151], nitromethane[152], nitric oxide[153], organophosphorus agents[154,155], dissolved oxygen[156–158], paracetamol[159], paraoxon[160,161] and other small organic compounds including different benzene derivates and cyclohexane[162]. All are based on the use of (reduced) graphene oxide with its discriminative effect and higher sensitivity through hydrogen bonds as discussed for hydrogen peroxide.

The detection of whole cancer cells was possible[163,164] given that certain types of cancer cells such as HeLa or MCF-7 overexpress folate receptors on their surface. This was exploited by *Song et al.*[164] who used a composite consisting of rGO, folic acid and hemin to detect as little as 1000 cells by photometry. The composite attaches to the folate receptors on the surface of the cells. The hemin on the surface of rGO

catalyzes the chromogenic oxidation of tetramethylbenzidine (Figure 2.6A). The oxidation was monitored via the increase in absorbance at 652 nm. The activity of hemin was significantly enhanced due to the high surface-to-volume ratio of rGO and its high affinity for hydrophobic molecules such as hemin and the used dye. The latter effect increases the local concentration of the substrate, brings the substrate into proximity with the active site of hemin, and thus improves catalytic activity. In addition, the high electrical conductance of rGO facilitates the electron transfer from hemin to the substrate. A label free sensor for cancer cells was developed by *Feng et al.*[163]. A specific aptamer was linked to the surface of rGO, having a high affinity for the nucleolin (a plasma membrane protein) of cancer cells (HeLa, K562, MDA-231, NIH-3T3). The adsorbed cells were quantified (detection limit: 1000 cells) by resistance measurements. If treated with the complementary strand of the aptamer (which releases cells), the sensor can be used again (Figure 2.6B).

Immunoglobulin G (IgG) is often used as a model analyte to demonstrate the operational capability of a new bioanalytical method. *Wang et al.*[165] have assembled reduced graphene oxide (rGO), L-cysteine, gold nanoparticles and anti-IgG antibodies on a glassy carbon electrode (GCE) for detection of human-IgG. The secondary antibodies against anti-IgG were labeled with horseradish peroxidase (HRP) which catalyzes the oxidation of hydrochinone by hydrogen peroxide. Benzoquinone, the product of this reaction, can be detected amperometrically at 0.18 V (vs. SCE). This sensor has a detection limit of 70 ng mL^{-1} and a linear range of 0.2-320 ng mL^{-1} which competes with the standard ELISA. The wide linear range and high sensitivity is attributed to the large surface area of rGO and L-cysteine-induced assembling of the gold nanoparticles. The assembly also enables the transfer of electrons from the enzymatic reaction and thus improves the performance of the immunosensor.

Mao et al.[166] constructed a FET-based sensor for IgG that is based on rGO and gold nanoparticles onto which the probe (anti-IgG) is covalent bounded. The immuno reaction (IgG to anti-IgG) is investigated by direct measurement of the current of the FET (detection limit: 2 ng mL^{-1}, gate voltage: 0 V). The response is non-linear in the range from 2 ng mL^{-1} to 20 µg mL^{-1}. This approach does not require a secondary antibody or a label.

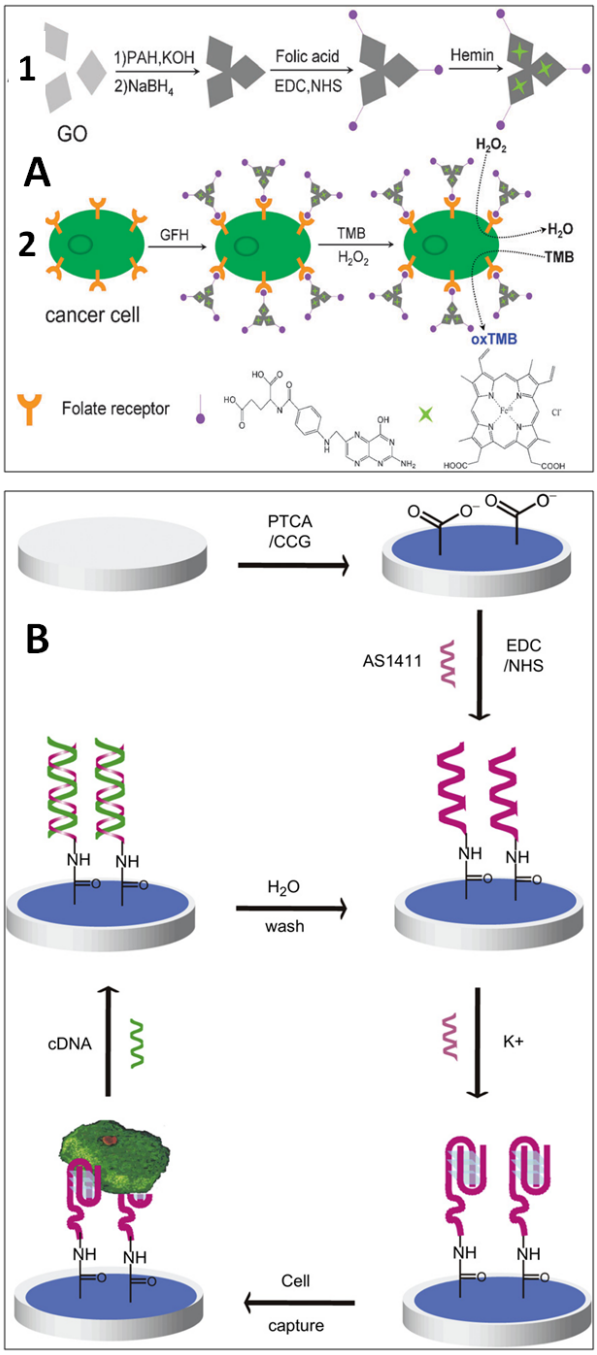

Figure 2.6. Detection of whole cancer cells with an electrode modified with a nanocomposite based on reduced graphene oxide. (A) Schematic representation of (1) preparation of the rGO/hermin composite and (2) cancer cell detection by using a target-directed rGO/hermin composite. Reproduced by permission on the Royal Society of Chemistry from ref. 164. (B) Schematic representation of the reusable aptamer/rGO-based aptasensor. The aptamer and its complementary DNA are used as a nanoscale anchor to capture/release cells. Reprinted with permission from ref. 163. Copyright (2011) Elsevier.

Liu et al.[167] developed a sensor for IgG that is based on a dual amplification strategy (Figure 2.7). rGO and graphene oxide were first functionalized with poly-(diallyldimethyl ammonium chloride) and gold nanoparticles. The rGO composite was deposited on a GCE and then covered with primary antibodies. The graphene oxide composite was covered with secondary antibody labeled with HRP. The peroxidase catalyzes the reaction of o-phenyldiamine and hydrogen peroxide to form 2,3-diaminophenazine. This amperometric approach resulted in an LOD of 0.05 ng mL^{-1} (range: 0.1-200 ng mL^{-1}). This is due to two beneficial effects. First, graphene oxide provides a large number of active sites to increase the amount of the secondary antibody in the enzymatic reaction. Secondly, rGO accelerates the electron transfer on the electrode surface to amplify the electrochemical signal due to its outstanding electric conductivity.

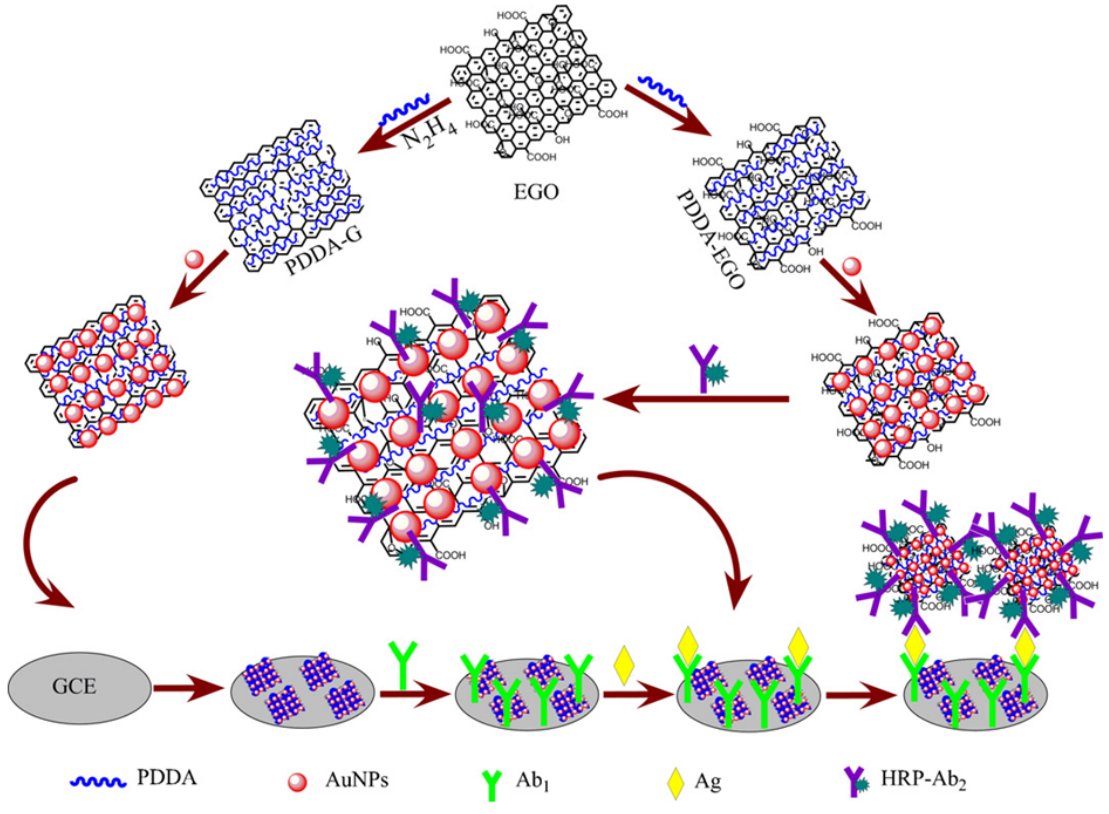

Figure 2.7. Schematic illustration of the preparation of (reduced) graphene oxide-based hybrids and the construction of the sandwich-type electrochemical immunosensor by *Liu et al.*[167]. Reprinted with permission from ref. 167. Copyright (2011) Elsevier.

Liu et al.[168] used graphene oxide on gold electrodes, again to detect IgG. A ferrocene derivative was attached to the primary antibody and eventually adsorbed on graphene oxide. The secondary antibody was labeled with gold nanoflowers which catalyze the reduction of p-nitrophenol to p-aminophenol. The latter is electrochemically oxidized to p-quinone imine by the attached ferrocene at the primary antibody. This process was amperometrically detected by the modified gold electrode. The p-quinone imine can be recycled by adding $NaBH_4$. The detection limit is 0.5 fg mL^{-1} of human IgG (range: 0.5 fg mL^{-1}-10 ng mL^{-1}).

The very low LODs of sensors based on the use of graphene materials can be favorably applied to analytes that occur at very low concentrations, for example tumor markers. Respective sensors have been reported for α-fetoprotein[169–175], prostate specific antigen[176–183], carcinoembryonic antigen[174,184,185], breast cancer susceptibility gene (BRCA1)[176] and the breast cancer markers HER2 and EGFR[186]. The detection limits and linear ranges are comparable and make such sensors suitable for clinical applications.

An immunossensor for prostate specific antigen (PSA)[182], for instance, makes use of a composite made from rGO and chitosan on a GCE. Next, a primary antibody against PSA was deposited on top. In parallel, gold nanorods modified with GOx and a secondary antibody were prepared. After binding of the antigen to the primary antibody (on the electrode), the gold nanorods were introduced which were linked to the antigen on the electrode by the secondary antibody to complete the sandwich. The ECL immunoassay was then conducted at 50 mV in another buffer solution containing luminol and glucose. Human serum samples were analyzed. The detection limit for PSA was 8 pg mL^{-1}. Fetoprotein and carcinoembryonic antigen do not interfere.

A particular approach was made by *Tang et al.*[174] who simultaneously monitored α-fetoprotein (AFP) and carcinoembryonic antigen (CEA). Graphene oxide was coated with magnetic nanobeads made from Fe_3O_4 and then both anti-AFP (AB1) and anti-CEA (AB2) were conjugated onto their surface. This material was immobilized on an indium tin oxide electrode. Two types of multifunctional gold hollow microspheres (GHS) were used as distinguishable signal tags for the corresponding antibodies (GHS-AB1, GHS-AB2). HRP and thionine were encapsulated in GHS-AB2 and ferrocenecar-

boxylic acid in GHS-AB1. The formation of the sandwich occurs in the presence of the analytes. Both α-fetoprotein (at +0.3 V) and carcinoembryonic antigen (at -0.3 V) were determined by differential pulse voltammetry (600 mV to -600 mV). The detection limits (1 pg mL^{-1} for both) and linear ranges (0.01-200 ng mL^{-1} for AFP, 0.01-80 ng mL^{-1} for CEA) revealed very good analytical performance that can compete with other methods and meet the requirements of clinical diagnosis.

Corresponding antibodies allow the construction of immunosensors for a wide range of additional analytes including kanamycin[187], norethisterone[188], salbutamol[189], p53 protein[190], chorionic gonadotropin[191] and even pathogens (rotavirus, bacteria)[192–195]. They all share similar detection limits, linear ranges and selectivity.

2.3.2 Field effect transistor-based sensors

FET-based sensors have the advantage of high sensitivity due to the enhancement of receptor responses (e.g. electron transfer of proteins) at low analyte concentrations. FET-based sensors based on carbon nanotubes have been developed but form Schottky barriers at the interface between the nanotubes and electrodes[196]. Graphene materials, on the other hand, provide extremely high charge mobility and capacity, large detection area, relatively low 1/f noise, tunable ambipolar field-effect characteristics, and biocompatibility[197].

The benefit of using graphenes becomes apparent when looking at the performance of sensors for metal ions. *Sudibya et al.*[197] constructed sensors based on reduced graphene oxide (rGO, Figure 2.8A) and modified one with calmodulin (binds to Ca^{2+}) and another one with metallothionein type II protein (binds to Hg^{2+} and Cd^{2+}) by pre-coated pyrene linkers. At a gate voltage of -0.6 V (p-type region) the detection limit is 1 μM for Ca^{2+} which is consistent with the binding affinity of calmodulin (0.1-1.0 μM). Lower detection limits could be accomplished by using silver hake parvalbumin[197] with its higher affinity for Ca^{2+}. The latter device provided similiar results at the same gate voltage for the detection of Hg^{2+} (detection limit: 1 nM; range: 1-28 nM) and Cd^{2+} (detection limit: 1 nM; range: 1-55 nM). This is again consistent with the binding affinity of the metallothione in type II protein. Both detection limits

strongly depend on the binding affinity and this is attributed to the ability of detecting very low currents in the nanoampere range (e.g. 2 nA response for 1 μM of Ca^{2+}, 0.1 μA for 1 nM of Hg^{2+}). In contrast to FETs based on plain silicon nanowire, this sensor does not respond to Na^+ or K^+, while the FET based on plain rGO does not respond to Ca^{2+}, Hg^{2+} or Cd^{2+} either. The device can be regenerated by washing with acidic buffer to remove bound metal ions, but reusability (3-4 times) is limited due to denaturation of the receptor proteins.

In another attempt, *Zhang et al.*[198] have spin coated a solution of 1-octa-decanethiol on a graphene FET to form a self-assembled monolayer. Thiols form strong Hg-S-bonds enabling the device to sense 10 ppm of Hg^{2+} ions. Unfortunately, detection limits and ranges are not reported. *Sofue et al.*[196] also used graphene, but without modifications, in a FET sensor for sodium ions with a wide dynamic range (1.0 nM to 1.0 mM). As to the underlying mechanism, it was speculated that the hydroxy groups bound to defects on the graphene surfaces can adsorb sodium ions. Interference was not studied. The results also revealed that top-gated devices ("solution gating" / electrolyte gating) have a 100-fold larger transconductance (53 μS instead of 0.50 μS) than backgated devices, probably due to the formation of thin electrical double layers in solutions which act as a thin insulator.

Such double layers were further investigated by *Ang et al.*[199] who observed a potential regime in which the adsorption of OH^- and H_3O^+ dominates the electrochemical double layer of graphene. Hence, such layers are sensitive to pH, but not to ionic strength. If a source-drain voltage of -1 V is applied, the threshold voltage shifts by about 98 mV per pH unit. This sensitivity is higher than the predicted Nernst limit (59.2 mV/pH). This was observed only at negative gate voltages and explained by the interplay between surface potential modulation by ion adsorption and the attached amphoteric OH^- groups (by analogy to carbon nanotubes). The mechanism behind the increase in conductivity or drain current with pH is not clear so far[200]. The results were confirmed by *Ohno et al.*[200,201].

Electrodes modified with plain graphene show almost no sensitivity to hydrogen gas unless decorated or modified with metallic platinum or palladium. *Vedala et al.*[202] report on the preparation of "holey reduced graphene oxide" (hrGO, Figure 2.8B)

which is obtained by horseradish peroxidase catalyzed oxidation of graphene oxide with H_2O_2. This resulted in the formation of holes on its basal plane. Subsequent reduction of the material with hydrazine leads to so-called hrGO which, in contrast to bare rGO, exhibits p-type behavior at room temperature with a Dirac point near $V_g = 0$ V. The hrGO was then decorated with platinum particles by pulsed potentiostatic electrodeposition, and the resulting sensors was used to detect hydrogen in the range from 60 ppm to 40 000 ppm.

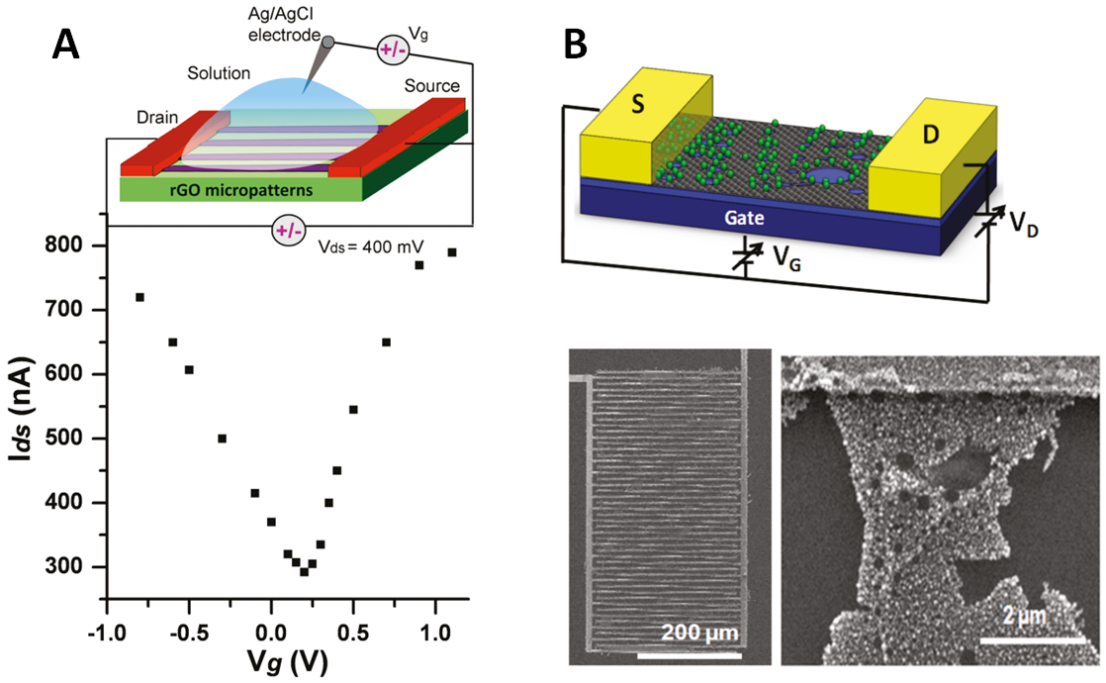

Figure 2.8. Field effect transistor sensors based on graphene materials. (A) Schematic of solution-gated configuration of rGO-FET (top) and ambipolar characteristics of rGO-FET measured in buffer solution (bottom). Adapted with permission from ref. 197. Copyright (2011) American Chemical Society. (B) Illustration of a holey reduced graphene oxide (hrGO) device decorated with metal nanoparticles (top), and two SEM images of prepatterned gold interdigitated microelectrodes consisting of hrGO decorated with gold or platinum nanoparticles (bottom). Adapted with permission from ref. 202. Copyright (2011) American Chemical Society.

Tang et al.[203] compared rGO with platinum nanoparticles in Nafion to an analogous material based on the use of single walled carbon nanotubes (SWCNT) for the amperometric determination of hydrogen peroxide (at +0.5 V). The latter material has higher sensitivity, a larger electrochemical surface area and lower charge transfer resistance (0.992 mA mM^{-1}, 111 m^2/g Pt, 87.2 Ω) than the former one (0.907 mA mM^{-1}, 100 m^2/g Pt, 130.7 Ω) although the content of platinum was lower (10% w/w Pt on SWCNT, 21% Pt on rGO). This was explained by a larger effect of platinum nanopar-

ticles on the 1D single walled carbon nanotube system than on the 2D rGO system, which makes the composite more conductive. Furthermore, the bundle structure of single walled carbon nanotubes leads to a more porous surface structure. This again indicates that the orientation and distribution of graphene materials in the composite are of vital importance.

Graphene FETs are also suitable for biodetection[204]. Respective transistors are gated by the adsorption of charged biomolecules. Recent FETs based on graphene[205,206] and rGO[207] have detection limits in the low nM and high pM range (0.01 nM to 2 nM) for DNA. In addition, it was observed that the position of the minimum of the gate voltage is a function of concentration of target DNA and hybridization state[206]. Mismatched DNA caused no shift at all. This enables detection of single-base mismatch. Graphene modified with gold nanoparticles allows for higher loading of probe DNA. As a result, the upper limit of detection shifts from 10 nM to 500 nM. Proof-of-concept sensors have also been reported for fibronectin[208] based on rGO (LOD: 0.5 nM) and for human immunoglobulin E based on graphene and a specific aptamer (linear range: 0.29 to about 100 nM)[209].

Cui et al.[210] have selectively functionalized graphene using peptides identified from a combinatorial phage display library - a technique enabling identification of peptides that bind to graphene. In combination with another peptide which binds to analytes, such as trinitrotoluene (TNT), bifunctional peptides were synthesized. This enabled the development of a sensor for TNT capable of detection at the ppb level.

2.3.3 Fluorescence sensors

Both reduced graphene oxide (rGO) and graphene oxide are reported to be fluorescence "super-quenchers" with long-range energy transfer properties[211]. There are two types of sensors which exploit this property. In "turn-on" ("signal-on") sensors, a fluorescent label is attached to (reduced) graphene oxide by adsorption. Upon addition of an analyte a reaction such as complexation causes the distance between label and material to increase. This leads to an increase in fluorescence intensity that can be correlated to the concentration of the analyte (Figure 2.9A). "Turn-off" sensors, in contrast, are

making use of fluorescently labeled hybridized probes which are not fully adsorbed by (reduced) graphene oxide, and therefore are not quenched. If analyte DNA is added, the hybridized oligomer is destroyed. The label is adsorbed by (reduced) graphene oxide, and fluorescence quenched. "Turn-off" sensors have lower sensitivity and inferior multiplexing capability compared to "turn-on" sensors[212].

All luminescent sensors reported for heavy metal ions are making use of specific oligonucleotides or DNAzymes due to their high selectivity. In addition, the detection limits and sensitivities can compete with electrochemical sensors and even with ICP-OES[213]. *Wen et al.*[214], for instance, used an Ag^+-specific oligonucleotide as a probe (labeled with fluorescein) that was immobilized on graphene oxide. The resulting "mix-and-detect" method has a detection limit of 5 nM and a linear range of 50-100 nM. A 10-fold excess of other metal ions (Li, Cd, Fe, Hg, Mn, Ni, Co, Cu, Zn, Ca, Mg, Pb) shows negligible interference. Similiar "turn-on" sensors were developed for copper(II) (detection limit: 2 nM, linear range: 0-250 nM)[215], mercury(II) (detection limit: 187 pM, linear range: 0-623 pM)[212] and lead(II) (detection limit: 300 pM, linear range: 1-100 nM)[211]. Respective "turn-off" sensors such as for mercury(II) (detection limit: 2.8 nM, detection range: 10 nM-100 μM)[216] and lead(II) (detection limit: 0.5 nM, dynamic range: 1-100 μM)[217] obviously are less sensitive.

The super-quenching ability of (reduced) graphene oxide was also exploited in DNA sensors[218–221]. These are of the "turn-on" type, with ssDNA tagged with fluorescein. Upon addition of the target sequence, hybridization occurs which weakens the (quenching) interactions with (reduced) graphene oxide[218,222]. This DNA detection scheme based on (reduced) graphene oxide improves the sensitivity by an order of magnitude as compared to methods using molecular beacons. This is attributed to the minimization of background fluorescence due to the super-quenching ability of the (reduced) graphene oxide[218] and leads to rather low dynamic ranges (1-260 nM) and detection limits (0.1-14.3 nM). *Dong et al.*[222] used CdTe quantum dots conjugated to molecular beacons in a "turn-on" probe (Figure 2.9B). Quantum dots possess: a high quantum yield; narrow, symmetric and stable fluorescence; and size-dependent, and tunable absorption and emission.

These approaches have large potential. *Liu et al.*[224] demonstrated the detection of

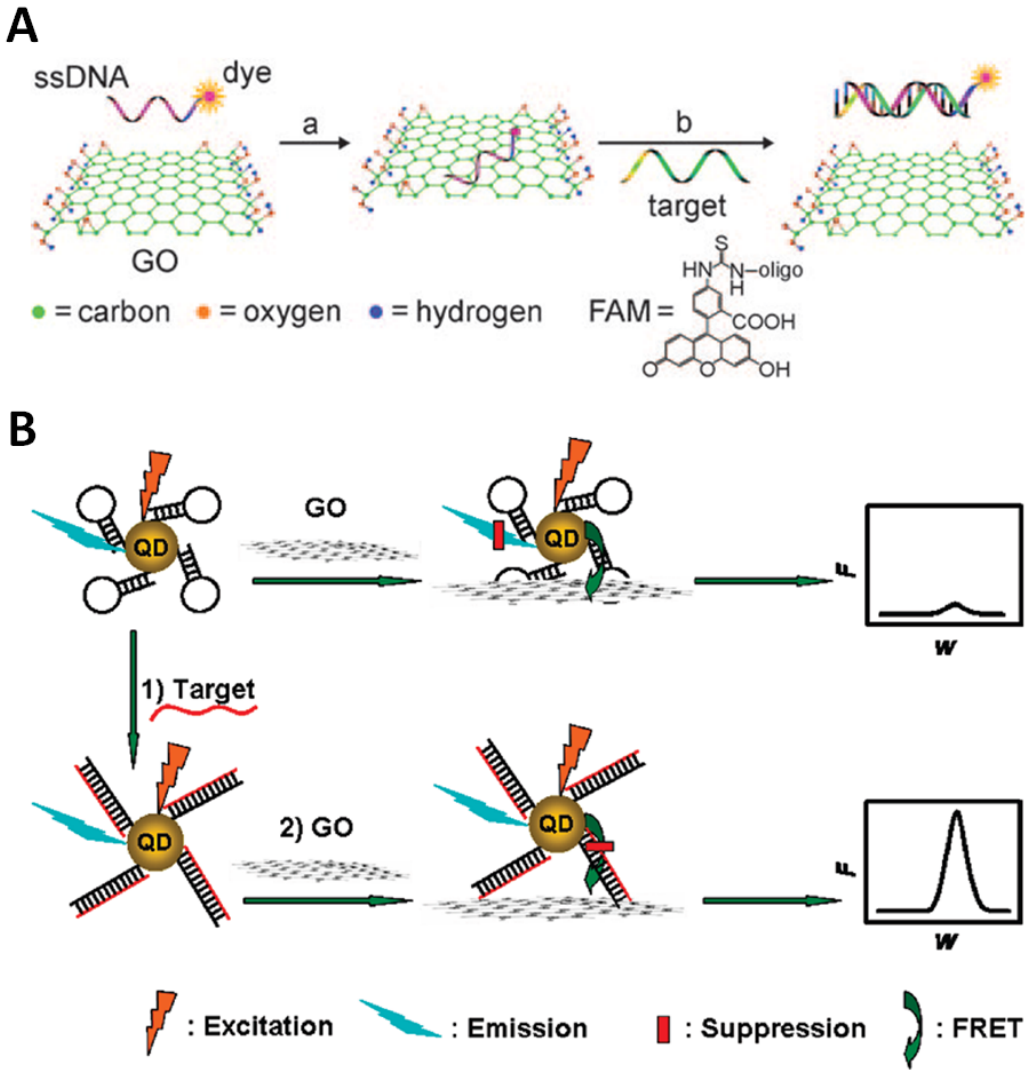

Figure 2.9. (A) Schematic representation of the mechanism of a "turn-on" sensor with fluorescein as dye. Reprinted with permission from ref. 223. Copyright (2009) Wiley-VCH Verlag GmbH & Co. (B) Schematic representation of the mechanism of a "turn-on" sensor with molecular beacon and quantum dots. Reprinted with permission from ref. 222. Copyright (2010) American Chemical Society.

single nucleotide polymorphism based on a DNA ligase reaction and a self-assembled graphene-oligonucleotide complex, without separation steps. Aptamers have also been applied to the sensitive detection of thrombine (detection limit: 31.3 pM, linear range: 62.5-187.5 pM)[223,225], ochratoxin A (detection limit: 1.9 μM, linear range: 2-35 μM)[226] and hemin (detection limit: 50 nM, linear range: 0.31-2.50 μM)[227]. *Wu et al.*[228] designed an assay based on graphene oxide and a fluorescent molecular beacon probe for the analysis of the activity of polynucleotide kinase (LOD: 0.001 units mL^{-1};

working range: 0-0.3 units mL^{-1}). A biosensor for ATP[229] makes use of ssDNA linked to upconversion nanophosphors of the type β-$NaYF_4$:Yb,Er as a probe on graphene oxide. It has a detection limit of 80 nM and a linear range between 0.5 μM to 100 μM. Guanosine triphosphate, cytidine triphosphate and uridine triphosphate, do not generate any fluorescence in this assay.

The activity of protease and the concentration of its inhibitors can be determined by a method reported by *Li et al.*[230]. Quantum dots (QDs) and biotin were coupled to a short peptide sequence which was then immobilized onto the surface of graphene oxide with the help of streptavidin, upon which the fluorescence of the QDs is quenched. Matrix metalloproteinase catalyzes the hydrolysis of peptide bonds and brings the QDs into solution so that luminescence is recovered.

Mei et al.[231] reported on the use of modifed graphene oxide membranes in combination with chemically modified silver nanoparticles to sense glutathione, proteins and DNA. The weak fluorescence of graphene oxide is enhanced through an amine reaction and ring-opening amination at the surface of the material. The emission of the aminated graphene oxide is quenched by the modified silver nanoparticles which carried a recognition element for the corresponding analyte. In the presence of the respective analyte, the silver nanoparticles are desorbed from the surface of the graphene oxide and fluorescence therefore is recovered. The membranes were crafted by a printing process similar to the one reported before[16].

2.3.4 Chemiluminescence sensors

Quantum dots (QDs) on (reduced) graphene oxide also were used to enhance electrochemiluminescence (ECL). *Deng et al.*[232] immobilized QDs on rGO on top of a glassy carbon electrode in order to detect acetylcholine. The ECL at -1.05 V is stronger by a factor of 4 compared to a carbon electrode without rGO. This is attributed to the fast electron transfer and the strong absorbance of intermediate oxygen species. It was also pointed out that the electrochemical reduction of graphene oxide produces a 179-fold enhancement of ECL compared to QDs/graphene oxide. *Wang et al.*[233] used a smiliar approach and the same QDs but with graphene oxide immoblizied on

an indium tin oxide (ITO) electrode in order to detect glutathione. Graphene oxide is claimed be the ideal intermediate between the QDs and the electrode because of the match of the Fermi-levels of graphene oxide (0.9 eV) and QDs (0.7 eV). Furthermore, the band gaps for graphene oxide (1.7-4.1 eV; depending on the oxidation level) and the electrode (3.5 eV) overlap. They also investigated the effects of O_2 and $O_2^{\bullet-}$ on this system and on QD electrode.

One may suspect that the enhancer effect and quencher effect of (reduced) graphene oxide annihilate one another. *Wang et al.*[234] indeed noticed that ECL is completely suppressed at high fractions (30-60%) of graphene oxide in a nanocomposite made from graphene oxide and CdS nanocrystals. However, at fraction of ∼4.6% a 4.3-fold intensity is found compared to a bare film of CdS nanocrystals.

By analogy to the sensors described previously one can differentiate between "turn-on" and "turn-off" ECL sensors. In "turn-off" sensors, the product of the electrochemical reaction quenches ECL, and this effect is related to the concentration of the analyte[232]. Such sensors are simple but have drawbacks[235]. A more complex method to detect thrombin was presented by *Guo et al.*[235] who used a dsDNA with a selective aptamer for thrombin and its complementary oligonucleotide. The hybridization was destroyed in the presence of thrombine and the complementary oligonucleotide could hybridize to another oligonucleotide (labled with CdS particles) bound on the surface of a magnetic microbead. Next, a nicking endonuclease was introduced to cut both strands from the surface, releasing the signal ssDNA and again the complementary oligonucleotide, which could bind again to another oligonucleotide on the microbead. A substantial quantity of ssDNA is generated with only one source of dsDNA. The signal ssDNA is captured onto the surface of a graphene oxide/gold electrode. There the ECL intensity was measured. Luminescence intensity is proportional to the amount of captured CdS-ssDNA which in turn is proportional to the concentration of thrombin. This is obviously a "turn on" sensor. The scheme of this method is shown in Figure 2.10. Thrombin can be detected in the 1.0-100.0 fM range. This high sensitivity is attributed to graphene oxide which is an $O_2^{\bullet-}$ facilitator and has an appropriate band gap corresponding to CdS (i.e. 2.45 eV). This leads to a 463-fold amplified production of signal ssDNA compared to that of the original dsDNA. There is virtually no interference by bovine serum albumin, immunoglobin G, α-fetoprotein, horseradish

peroxidase and lysozyme, even if present in large excess.

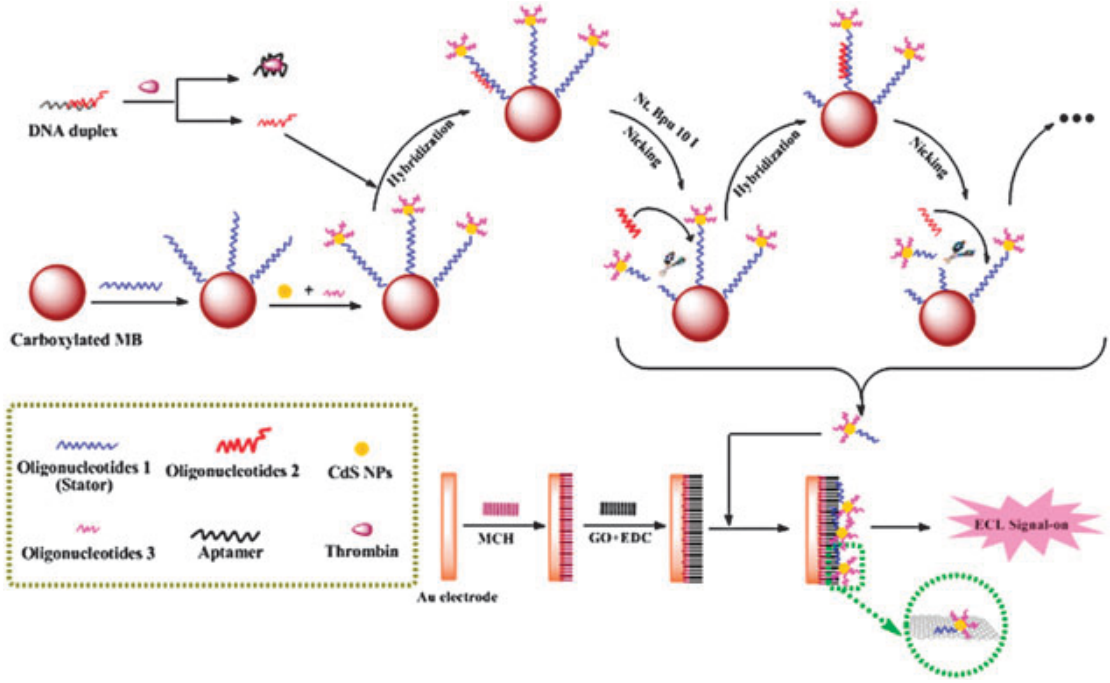

Figure 2.10. Schematic representation of the amplification strategy of *Guo et al.*[235] for their DNA sensor based on graphene oxide. Reproduced by permission on the Royal Society of Chemistry from ref. 235.

Other work for "turn on" sensors for glucose are based on luminol as the luminophore instead of QDs. This resulted in sensors in the 2-100 µM concentration range[236]. A nanocomposite consisting of rGO, nafion and GOx was deposited on a glassy carbon electrode. GOx causes the formation of hydrogen peroxide which enhances the ECL of luminol. The concentration of glucose in human serum is in the mM range, and thus must be diluted before determination. This has two advantages. First, potential interference molecules such as ascorbic acid, uric acid, sucrose, lactose, and maltose are also diluted which reduces their effect. Secondly, less sample is needed.

"Turn-off" sensors possess inferior detection ranges and limits of detection compared to "turn-on" sensors. *Deng et al.*[232] completed their sensor scheme (see beginning of section) by adding choline oxidase (and acetylcholinesterase) to their material to obtain a sensor for (acetyl)choline in the 10-250 µM range and with a detection limit of 4-8 µM. This biosensor is superior to a similar approach based on nanotubes, and to conventional amperometric sensors. *Wang et al.*[233] used a comparable composite with the same QDs but with graphene oxide on ITO for a ECL sensor for glutathione

(linear range of 24-214 μM and a detection limit of 8.3 μM).

2.3.5 Colorimetric sensors

A nanocomposite based on hemin and reduced graphene oxide (rGO) was constructed for a colorimetric detection system [237]. This composite catalyzes a color reaction in the presence of 3,3',5,5'-tetramethylbenzidine and hydrogen peroxide. The color change can be judged by the bare eye and measured by absorptiometry at 652 nm. The composite remains well suspended in the presence of an electrolyte and ssDNA, while coagulation was observed in the presence of dsDNA. Hybridization can be detected by mixing the composite solution with probe and target DNA in the presence of an electrolyte such as NaCl, and then centrifuging the mixture. Hydrogen peroxide and the dye are added to the supernatant and absorbance is measured. Its intensity depends on the concentration of suspended composite in the supernatant which, in turn, depends on the concentration of target DNA (Figure 2.11A). Even a single base mismatch is sufficient to precipate a large amount of the composite, so that the detection of single nucleotide polymorphism becomes possible. Target DNA can be quantified in the 5-100 nM concentration range with an LOD of 2 nM.

A colorimetric platform for visual detection of prostate specific antigen (PSA) was developed by *Qu et al.* [178]. The primary antibody was immobilized on magnetic nanobeads and the secondary antibody on rGO. The sandwich immunocomplex is formed. Next, this magnetic immunocomplex is separated from the non-complexed secondary antibodies with graphene oxide (non-magnetic). (Reduced) graphene oxide possesses an intrinsic peroxide-like activity (similar to horseradish peroxidase) [238]. Therefore, the non-complexed secondary antibodies with graphene oxide can be used to catalyze the reaction of hydroquinone and hydrogen peroxide to 1,4-benzoquinone. This resultes in a color change from light grey to orange (Figure 2.11B). However, graphene oxide is much cheaper and more stable than horseradish peroxidase. The intensity of the final color depends on the amount of antigen bound. If more antigen is bound, the solution is less colored. The concentration of PSA can be estimated with the bare eye. It is possible to distinguish between samples below and above the critical concentration (4 ng mL^{-1}). This makes the method suitable for the homecare diagnosis

of prostate cancer. In addition, the graphene oxide/hydroquinone/H_2O_2 solution can be investigated by squarewave voltammetry. The change of the reduction current of hydroquinone at 0.0 V is proportional to the concentration of PSA.

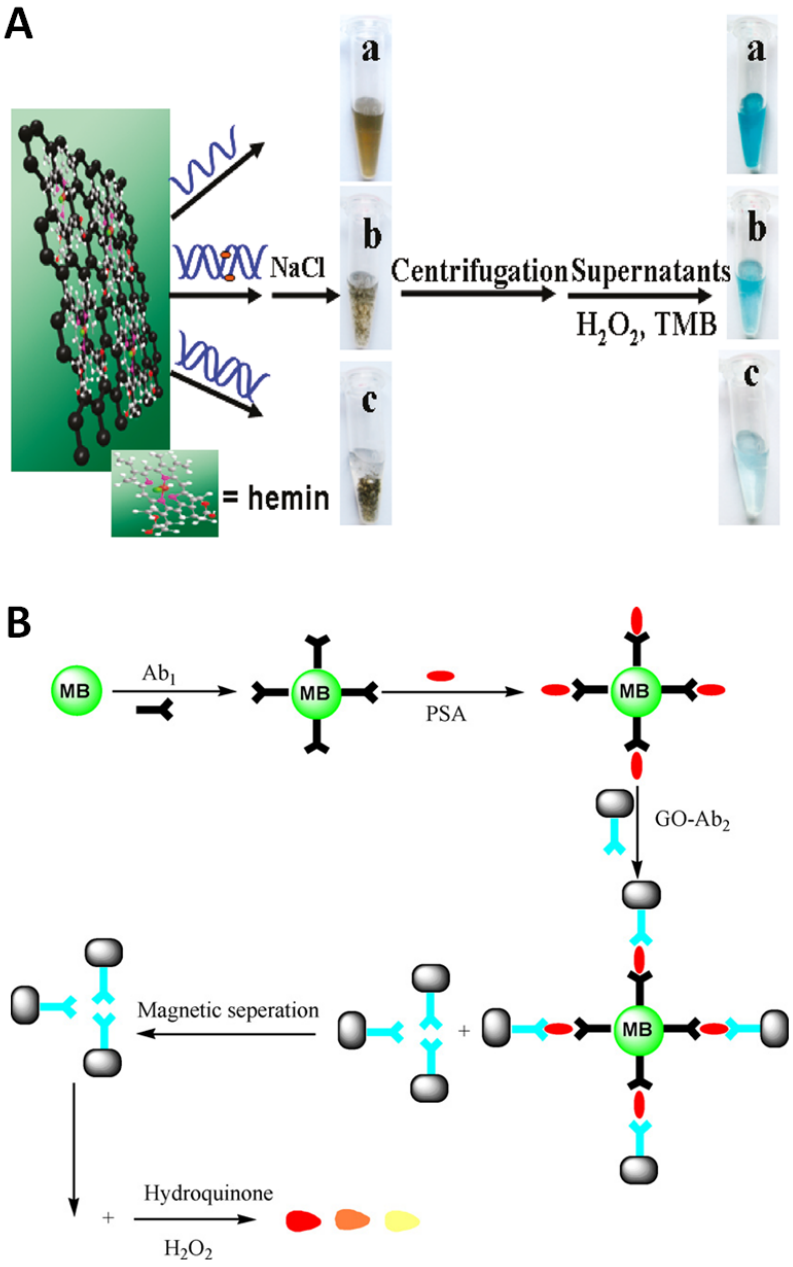

Figure 2.11. (A) Protocol for colorimetric SNP detection. Adapted with permission from ref. 237. Copyright (2011) American Chemical Society. (B) Schematic representation of the immunoassay procedure developed by *Qu et al.*[178]. Reprinted with permission from ref. 178. Copyright (2011) Elsevier.

2.4 Benefits of (reduced) graphene oxide

The huge amount of publications discussed in this chapter make a small résumé necessary to emphasize the benefits and advantages of (reduced) graphene oxide. For this reason, this section provides a short and clear list of them:

Solution processing. Solutions of (r)GO can be used in an inkjet printer to print small sensors on PET foils[16]. These films are sensitive (LOD for NO_2: 500 ppb) and recoverable (with UV-light) but non-selective. Selectivity can be introduced, for instance, by printing a complete nanocomposite of graphene oxide with chemically modified silver nanoparticles to sense small amounts of glutathione (1 nM) and IgG (10 pM)[231].

Interaction effects. The presence of oxygen groups allow the sensitive detection of the pH level of a solution, both fluorometric[17,18] and electrochemical[19]. The lack of dependence on excitation/emission wavelength renders the fluoremetric method extremely suitable in extracellular samples[18]. The electrochemical method provides high sensitivity (51.3 mV/pH) close to the Nerst limit[19]. In contrast, pristine graphene exhibits a much weaker sensitivity to pH (12.5 mV/pH) and no fluorescence.

Additionally, the functional groups of (r)GO complex metal cations (e.g., Cu^{2+}, Pb^{2+}, and Cd^{2+}). This enables their unselective but highly sensitive detection by anodic stripping voltammetry in the picomolar range due to the formation of strong bonds between metal ions and rGO[20]. Strong bonds also promote the highly selective *and* sensitive detection of hydrogen peroxide in voltammetry (LOD: 0.05 µM) in contrast to graphite or carbon nanotubes[2].

Attraction effect. The high surface-to-volume ratio and the high affinity for hydrophobic *and* also hydrophilic molecules increases their local concentration. Due to this, analytes and substrates are brought into proximity with active sites of receptors or catalyzers, which in turn improves their activity[164]. This effect is utilized, for example, in approaches for detection of whole cancer cells[164].

Discrimination effect. (r)GO allows the simultaneous detection of (electrochemically) similar analytes such as uric acid and ascorbic acid[24], hydroquinone and cat-

echol[28], and even nucleic bases (both in solutions and ssDNA/dsDNA)[2,19]. For the discrimination effect, the presence of a nominal amount of functional groups on the surface of the material is mandatory to form hydrogen bonds with the analytes[24]. Both the strength of the bond and the distance of interaction site to the reaction center influence the oxidation step and therefore the peak separation of the analytes.

Conversion effect. GO possesses an intrinsic peroxide-like activity similar to horseradish peroxidase[238]. Therefore, it catalyzes reactions in the same manner. However, GO is much cheaper and more stable than horseradish peroxidase. For instance, this effect is used in a colorimetric glucose sensor[238] to convert TMB (colorless) to its oxidized version (blue).

Luminescence-quencher-paradox. On the one hand, GO and rGO enhance the ECL of quantum dots by a factor of 3-4[232]. This is attributed to the fast electron transfer and strong absorbance of intermediate oxygen species in the case of rGO[232,233]. GO is also a good intermediate between the QDs and the electrode because of the matching Fermi-levels of GO (0.9 eV) and CdTe QDs (0.7 eV), and the overlapping band gaps of GO (1.5-4.1 eV) and the electrode (3.5 eV)[233]. On the other hand, both materials are reported to be fluorescence "super-quenchers" with long-range energy transfer properties[211], which is exploited, for instance, for a sensitive mercury sensor[212].

One may suspect that the enhancer effect and quencher effect annihilate one another. Indeed, high mass fractions (30-60%) of graphene oxide in a nanocomposite made from graphene oxide and CdS nanocrystals completely suppress the ECL[234]. However, at a mass fraction of ∼4.6% a 4.3-fold intensity is found compared to a bare film of CdS nanocrystals. Thus, the mass fraction of the material decides which effect is promoted and which is suppressed.

2.5 References

[1] D. R. Dreyer, S. Park, C. W. Bielawski, and R. S. Ruoff. The chemistry of graphene oxide. *Chem. Soc. Rev.*, 39(1):228–240, 2010. doi: 10.1039/B917103G.

[2] M. Zhou, Y. M. Zhai, and S. J. Dong. Electrochemical Sensing and Biosensing Platform

Based on Chemically Reduced Graphene Oxide. *Anal. Chem.*, 81(14):5603–5613, 2009. doi: 10.1021/ac900136z.

[3] F. Schedin, A. K. Geim, S. V. Morozov, E. W. Hill, P. Blake, M. I. Katsnelson, and K. S. Novosëlov. Detection of individual gas molecules adsorbed on graphene. *Nat. Mater.*, 6(9): 652–655, 2007. doi: 10.1038/nmat1967.

[4] A. Ghosh, D. J. Late, L. S. Panchakarla, A. Govindaraj, and C. N. R. Rao. NO2 and humidity sensing characteristics of few-layer graphenes. *J. Exp. Nanosci.*, 4(4):313–322, 2009. doi: 10.1080/17458080903115379.

[5] H. Y. Jeong, D. S. Lee, H. K. Choi, D. H. Lee, J. E. Kim, J. Y. Lee, W. J. Lee, S. O. Kim, and S. Y. Choi. Flexible room-temperature NO2 gas sensors based on carbon nanotubes/reduced graphene hybrid films. *Appl. Phys. Lett.*, 96(21):213105, 2010. doi: 10.1063/1.3432446.

[6] R. K. Joshi, H. Gomez, F. Alvi, and A. Kumar. Graphene Films and Ribbons for Sensing of O-2, and 100 ppm of CO and NO2 in Practical Conditions. *J. Phys. Chem. C*, 114(14): 6610–6613, 2010. doi: 10.1021/jp100343d.

[7] G. H. Lu, L. E. Ocola, and J. H. Chen. Gas detection using low-temperature reduced graphene oxide sheets. *Appl. Phys. Lett.*, 94(8):083111, 2009. doi: 10.1063/1.3086896.

[8] G. H. Lu, S. Park, K. H. Yu, R. S. Ruoff, L. E. Ocola, D. Rosenmann, and J. H. Chen. Toward Practical Gas Sensing with Highly Reduced Graphene Oxide: A New Signal Processing Method To Circumvent Run-to-Run and Device-to-Device Variations. *ACS Nano*, 5(2):1154–1164, 2011. doi: 10.1021/nn102803q.

[9] M. W. K. Nomani, R. Shishir, M. Qazi, D. Diwan, V. B. Shields, M. G. Spencer, G. S. Tompa, N. M. Sbrockey, and G. Koley. Highly sensitive and selective detection of NO2 using epitaxial graphene on 6H-SiC. *Sens. Actuators, B*, 150(1):301–307, 2010. doi: 10.1016/j.snb.2010.06.069.

[10] R. Pearce, T. Iakimov, M. Andersson, L. Hultman, A. L. Spetz, and R. Yakimova. Epitaxially grown graphene based gas sensors for ultra sensitive NO2 detection. *Sens. Actuators, B*, 155 (2):451–455, 2011. doi: 10.1016/j.snb.2010.12.046.

[11] Y. P. Dan, Y. Lu, N. J. Kybert, Z. T. Luo, and A. T. C. Johnson. Intrinsic Response of Graphene Vapor Sensors. *Nano Lett.*, 9(4):1472–1475, 2009. doi: 10.1021/nl8033637.

[12] B. Huang, Z. Y. Li, Z. R. Liu, G. Zhou, S. G. Hao, J. Wu, B. L. Gu, and W. H. Duan. Adsorption of gas molecules on graphene nanoribbons and its implication for nanoscale molecule sensor. *J. Phys. Chem. C*, 112(35):13442–13446, 2008. doi: 10.1021/jp8021024.

[13] L. S. Zhang, W. D. Wang, X. Q. Liang, W. S. Chu, W. G. Song, W. Wang, and Z. Y. Wu. Characterization of partially reduced graphene oxide as room temperature sensor for H-2. *Nanoscale*, 3(6):2458–2460, 2011. doi: 10.1039/c1nr10187k.

[14] I. Jung, D. Dikin, S. Park, W. Cai, S. L. Mielke, and R. S. Ruoff. Effect of Water Vapor on Electrical Properties of Individual Reduced Graphene Oxide Sheets. *J. Phys. Chem. C*, 112 (51):20264–20268, December 2008. doi: 10.1021/jp807525d.

[15] J. T. Robinson, F. K. Perkins, E. S. Snow, Z. Wei, and P. E. Sheehan. Reduced Graphene Oxide Molecular Sensors. *Nano Lett.*, 8(10):3137–3140, September 2008. doi: 10.1021/nl8013007.

[16] V. Dua, S. P. Surwade, S. Ammu, S. R. Agnihotra, S. Jain, K. E. Roberts, S. Park, R. S. Ruoff, and S. K. Manohar. All-Organic Vapor Sensor Using Inkjet-Printed Reduced Graphene Oxide. *Angew. Chem., Int. Ed.*, 49(12):2154–2157, 2010. doi: 10.1002/anie.200905089.

[17] J. L. Chen and X. P. Yan. Ionic strength and pH reversible response of visible and near-infrared fluorescence of graphene oxide nanosheets for monitoring the extracellular pH. *Chem. Commun.*, 47(11):3135–3137, 2011. doi: 10.1039/c0cc03999c.

[18] S. Kochmann, T. Hirsch, and O. Wolfbeis. The pH Dependence of the Total Fluorescence of Graphite Oxide. *J. Fluoresc.*, 22(3):849–855, 2012. doi: 10.1007/s10895-011-1019-8.

[19] C. X. Lim, H. Y. Hoh, P. K. Ang, and K. P. Loh. Direct Voltammetric Detection of DNA and pH Sensing on Epitaxial Graphene: An Insight into the Role of Oxygenated Defects. *Anal. Chem.*, 82(17):7387–7393, 2010. doi: 10.1021/ac101519v.

[20] B. Wang, Y. H. Chang, and L. J. Zhi. High yield production of graphene and its improved property in detecting heavy metal ions. *New Carbon Mater.*, 26(1):31–35, 2011. doi: 10.1016/S1872-5805(11)60064-4.

[21] C. Wang, L. Zhang, Z. H. Guo, J. G. Xu, H. Y. Wang, K. F. Zhai, and X. Zhuo. A novel hydrazine electrochemical sensor based on the high specific surface area graphene. *Microchim. Acta*, 169(1-2):1–6, 2010. doi: 10.1007/s00604-010-0304-6.

[22] Y. Wang, Y. Wan, and D. Zhang. Reduced graphene sheets modified glassy carbon electrode for electrocatalytic oxidation of hydrazine in alkaline media. *Electrochem. Commun.*, 12(2): 187–190, 2010. doi: 10.1016/j.elecom.2009.11.019.

[23] M. F. Zhu, C. Q. Zeng, and J. S. Ye. Graphene-Modified Carbon Fiber Microelectrode for the Detection of Dopamine in Mice Hippocampus Tissue. *Electroanalysis*, 23(4):907–914, 2011. doi: 10.1002/elan.201000712.

[24] J. L. Chang, K. H. Chang, C. C. Hu, W. L. Cheng, and J. M. Zen. Improved voltammetric peak separation and sensitivity of uric acid and ascorbic acid at nanoplatelets of graphitic oxide. *Electrochem. Commun.*, 12(4):596–599, 2010. doi: 10.1016/j.elecom.2010.02.008.

[25] G. P. Keeley, A. O'Neill, N. McEvoy, N. Peltekis, J. N. Coleman, and G. S. Duesberg. Electrochemical ascorbic acid sensor based on DMF-exfoliated graphene. *J. Mater. Chem.*, 20(36): 7864–7869, 2010. doi: 10.1039/c0jm01527j.

[26] Y. R. Kim, S. Bong, Y. J. Kang, Y. Yang, R. K. Mahajan, J. S. Kim, and H. Kim. Electrochemical detection of dopamine in the presence of ascorbic acid using graphene modified electrodes. *Biosens. Bioelectron.*, 25(10):2366–2369, 2010. doi: 10.1016/j.bios.2010.02.031.

[27] Y. Wang, Y. M. Li, L. H. Tang, J. Lu, and J. H. Li. Application of graphene-modified electrode for selective detection of dopamine. *Electrochem. Commun.*, 11(4):889–892, 2009. doi: 10.1016/j.elecom.2009.02.013.

[28] H. J. Du, J. S. Ye, J. Q. Zhang, X. D. Huang, and C. Z. Yu. A voltammetric sensor based on graphene-modified electrode for simultaneous determination of catechol and hydroquinone. *J. Electroanal. Chem.*, 650(2):209–213, 2011. doi: 10.1016/j.jelechem.2010.10.002.

[29] G. P. Keeley, A. O'Neill, M. Holzinger, S. Cosnier, J. N. Coleman, and G. S. Duesberg. DMF-exfoliated graphene for electrochemical NADH detection. *Phys. Chem. Chem. Phys.*, 13(17): 7747–7750, 2011. doi: 10.1039/c1cp20060g.

[30] X. H. Kang, J. Wang, H. Wu, J. Liu, I. A. Aksay, and Y. H. Lin. A graphene-based electrochemical sensor for sensitive detection of paracetamol. *Talanta*, 81(3):754–759, 2010. doi: 10.1016/j.talanta.2010.01.009.

[31] J. C. Song, J. Yang, J. F. Zeng, J. Tan, and L. Zhang. Graphite oxide film-modified electrode as an electrochemical sensor for acetaminophen. *Sens. Actuators, B*, 155(1):220–225, 2011. doi: 10.1016/j.snb.2010.11.051.

[32] T. W. Chen, Z. H. Sheng, K. Wang, F. B. Wang, and X. H. Xia. Determination of Explosives Using Electrochemically Reduced Graphene. *Chem.–Asian J.*, 6(5):1210–1216, 2011. doi: 10.1002/asia.201000836.

[33] M. S. Goh and M. Pumera. Graphene-based electrochemical sensor for detection of 2,4,6-trinitrotoluene (TNT) in seawater: the comparison of single-, few-, and multilayer graphene nanoribbons and graphite microparticles. *Anal. Bioanal. Chem.*, 399(1):127–131, 2011. doi: 10.1007/s00216-010-4338-8.

[34] Q. X. Wang, M. X. Zheng, J. L. Shi, F. Gao, and F. Gao. Electrochemical Oxidation of Native Double-Stranded DNA on a Graphene-Modified Glassy Carbon Electrode. *Electroanalysis*, 23 (4):915–920, 2011. doi: 10.1002/elan.201000713.

[35] Z. M. Ao, J. Yang, S. Li, and Q. Jiang. Enhancement of CO detection in Al doped graphene. *Chem. Phys. Lett.*, 461(4-6):276–279, 2008. doi: 10.1016/j.cplett.2008.07.039.

[36] X. Qin, Q. Y. Meng, and W. Zhao. Effects of Stone-Wales defect upon adsorption of formaldehyde on graphene sheet with or without Al dopant: A first principle study. *Surf. Sci.*, 605 (9-10):930–933, 2011. doi: 10.1016/j.susc.2011.02.006.

[37] L. Al-Mashat, K. Shin, K. Kalantar-Zadeh, J. D. Plessis, S. H. Han, R. W. Kojima, R. B. Kaner, D. Li, X. L. Gou, S. J. Ippolito, and W. Wlodarski. Graphene/Polyaniline Nanocomposite for Hydrogen Sensing. *J. Phys. Chem. C*, 114(39):16168–16173, 2010. doi: 10.1021/jp103134u.

[38] R. Arsat, M. Breedon, M. Shafiei, K. Kalantar-zadeh, W. Wlodarski, S. Gilje, R. Kaner, and F. Arregui. Graphene-like nano-Sheets/36° LiTaO3 surface acoustic wave hydrogen gas sensor. *Sensors, 2008 IEEE*, pages 188–191, 2008. doi: 10.1109/ICSENS.2008.4716414.

[39] R. Arsat, M. Breedon, M. Shafiei, P. G. Spizziri, S. Gilje, R. B. Kaner, K. Kalantar-Zadeh, and W. Wlodarski. Graphene-like nano-sheets for surface acoustic wave gas sensor applications. *Chem. Phys. Lett.*, 467(4-6):344–347, 2009. doi: 10.1016/j.cplett.2008.11.039.

[40] A. Kaniyoor, R. Imran Jafri, T. Arockiadoss, and S. Ramaprabhu. Nanostructured Pt decorated graphene and multi walled carbon nanotube based room temperature hydrogen gas sensor. *Nanoscale*, 1(3):382–6, 2009. doi: 10.1039/B9NR00015A.

[41] A. Kaniyoor and S. Ramaprabhu. Hybrid carbon nanostructured ensembles as chemiresistive hydrogen gas sensors. *Carbon*, 49(1):227–236, 2011. doi: 10.1016/j.carbon.2010.09.008.

[42] R. Kumar, D. Varandani, B. R. Mehta, V. N. Singh, Z. H. Wen, X. L. Feng, and K. Mullen. Fast response and recovery of hydrogen sensing in Pd-Pt nanoparticle-graphene composite layers. *Nanotechnol.*, 22(27):275719, 2011. doi: 10.1088/0957-4484/22/27/275719.

[43] U. Lange, T. Hirsch, V. M. Mirsky, and O. S. Wolfbeis. Hydrogen sensor based on a graphene - palladium nanocomposite. *Electrochim. Acta*, 56(10):3707–3712, 2011. doi: 10.1016/j.electacta.2010.10.078.

[44] W. Wu, Z. H. Liu, L. A. Jauregui, Q. K. Yu, R. Pillai, H. L. Cao, J. M. Bao, Y. P. Chen, and S. S. Pei. Wafer-scale synthesis of graphene by chemical vapor deposition and its application in hydrogen sensing. *Sens. Actuators, B*, 150(1):296–300, 2010. doi: 10.1016/j.snb.2010.06.070.

[45] Z. X. Jiang, J. J. Wang, L. H. Meng, Y. D. Huang, and L. Liu. A highly efficient chemical sensor material for ethanol: Al2O3/Graphene nanocomposites fabricated from graphene oxide. *Chem. Commun.*, 47(22):6350–6352, 2011. doi: 10.1039/c1cc11711d.

[46] J. Yi, J. M. Lee, and W. Il Park. Vertically aligned ZnO nanorods and graphene hybrid architectures for high-sensitive flexible gas sensors. *Sens. Actuators, B*, 155(1):264–269, 2011. doi: 10.1016/j.snb.2010.12.033.

[47] T. V. Cuong, V. H. Pham, J. S. Chung, E. W. Shin, D. H. Yoo, S. H. Hahn, J. S. Huh, G. H. Rue, E. J. Kim, S. H. Hur, and P. A. Kohl. Solution-processed ZnO-chemically converted graphene gas sensor. *Mater. Lett.*, 64(22):2479–2482, 2010. doi: 10.1016/j.matlet.2010.08.027.

[48] D. Chen, J. Ding, L. Du, G. Liu, and J. He. A Wireless Thin Contact Stress Sensor Based on Surface Acoustic Wave Resonator in ZnO/Si Structure. In J. Ding, L. Du, G. Liu, and J. He, editors, *Instrumentation, Measurement, Computer, Communication and Control, International Conference on*, volume 0, pages 50–53, October 2011. doi: 10.1109/IMCCC.2011.22.

[49] J. Li, S. J. Guo, Y. M. Zhai, and E. K. Wang. Nafion-graphene nanocomposite film as enhanced sensing platform for ultrasensitive determination of cadmium. *Electrochem. Commun.*, 11(5): 1085–1088, 2009. doi: 10.1016/j.elecom.2009.03.025.

[50] J. Li, S. J. Guo, Y. M. Zhai, and E. K. Wang. High-sensitivity determination of lead and cadmium based on the Nafion-graphene composite film. *Anal. Chim. Acta*, 649(2):196–201, 2009. doi: 10.1016/j.aca.2009.07.030.

[51] C. M. Willemse, K. Tlhomelang, N. Jahed, P. G. Baker, and E. I. Iwuoha. Metallo-Graphene Nanocomposite Electrocatalytic Platform for the Determination of Toxic Metal Ions. *Sensors*, 11(4):3970–3987, 2011. doi: 10.3390/s110403970.

[52] J. M. Gong, T. Zhou, D. D. Song, and L. Z. Zhang. Monodispersed Au nanoparticles decorated graphene as an enhanced sensing platform for ultrasensitive stripping voltammetric detection of mercury(II). *Sens. Actuators, B*, 150(2):491–497, 2010. doi: 10.1016/j.snb.2010.09.014.

[53] J. Li, C. Y. Liu, and C. Cheng. Electrochemical detection of hydroquinone by graphene and Pt-graphene hybrid material synthesized through a microwave-assisted chemical reduction process. *Electrochim. Acta*, 56(6):2712–2716, 2011. doi: 10.1016/j.electacta.2010.12.046.

[54] W. Song, D. W. Li, Y. T. Li, Y. Li, and Y. T. Long. Disposable biosensor based on graphene oxide conjugated with tyrosinase assembled gold nanoparticles. *Biosens. Bioelectron.*, 26(7): 3181–3186, 2011. doi: 10.1016/j.bios.2010.12.022.

[55] L. L. Wei, J. Borowiec, L. H. Zhu, and J. D. Zhang. Electrochemical sensor for monitoring the photodegradation of catechol based on DNA-modified graphene oxide. *Microchim. Acta*, 173 (3-4):439–443, 2011. doi: 10.1007/s00604-011-0580-9.

[56] H. S. Yin, Q. M. Zhang, Y. L. Zhou, Q. A. Ma, T. Liu, L. S. Zhu, and S. Y. Ai. Electrochemical behavior of catechol, resorcinol and hydroquinone at graphene-chitosan composite film modified glassy carbon electrode and their simultaneous determination in water samples. *Electrochim. Acta*, 56(6):2748–2753, 2011. doi: 10.1016/j.electacta.2010.12.060.

[57] W. J. Hong, H. Bai, Y. X. Xu, Z. Y. Yao, Z. Z. Gu, and G. Q. Shi. Preparation of Gold Nanoparticle/Graphene Composites with Controlled Weight Contents and Their Application in Biosensors. *J. Phys. Chem. C*, 114(4):1822–1826, 2010. doi: 10.1021/jp9101724.

[58] Y. Zhang, R. Yuan, Y. Q. Chai, W. J. Li, X. Zhong, and H. A. Zhong. Simultaneous voltammetric determination for DA, AA and NO2- based on graphene/polycyclodextrin/MWCNTs nanocomposite platform. *Biosens. Bioelectron.*, 26(9):3977–3980, 2011. doi: 10.1016/j.bios.2011.03.017.

[59] Y. Li, G. Ran, W. Yi, H. Luo, and N. Li. A glassy carbon electrode modified with graphene and poly(acridine red) for sensing uric acid. *Microchim. Acta*, pages 1–7, 2012. doi: 10.1007/s00604-012-0820-7.

[60] L. Tan, K. G. Zhou, Y. H. Zhang, H. X. Wang, X. D. Wang, Y. F. Guo, and H. L. Zhang. Nanomolar detection of dopamine in the presence of ascorbic acid at beta-cyclodextrin/graphene nanocomposite platform. *Electrochem. Commun.*, 12(4):557–560, 2010. doi: 10.1016/j.elecom.2010.01.042.

[61] Y. Fan, H. T. Lu, J. H. Liu, C. P. Yang, Q. S. Jing, Y. X. Zhang, X. K. Yang, and K. J. Huang. Hydrothermal preparation and electrochemical sensing properties of TiO2-graphene nanocomposite. *Colloids Surf., B*, 83(1):78–82, 2011. doi: 10.1016/j.colsurfb.2010.10.048.

[62] S. F. Hou, M. L. Kasner, S. J. Su, K. Patel, and R. Cuellari. Highly Sensitive and Selective Dopamine Biosensor Fabricated with Silanized Graphene. *J. Phys. Chem. C*, 114(35):14915–14921, 2010. doi: 10.1021/jp1020593.

[63] Y. L. Wang, W. Peng, L. Liu, M. Tang, F. Gao, and M. G. Li. Enhanced conductivity of a glassy carbon electrode modified with a graphene-doped film of layered double hydroxides for selectively sensing of dopamine. *Microchim. Acta*, 174(1-2):41–46, 2011. doi: 10.1007/s00604-011-0593-4.

[64] F. Y. Zhang, Y. J. Li, Y. E. Gu, Z. H. Wang, and C. M. Wang. One-pot solvothermal synthesis of a Cu2O/Graphene nanocomposite and its application in an electrochemical sensor for dopamine. *Microchim. Acta*, 173(1-2):103–109, 2011. doi: 10.1007/s00604-010-0535-6.

[65] Y. Bao, J. X. Song, Y. Mao, D. X. Han, F. Yang, L. Niu, and A. Ivaska. Graphene Oxide-Templated Polyaniline Microsheets toward Simultaneous Electrochemical Determination of AA/DA/UA. *Electroanalysis*, 23(4):878–884, 2011. doi: 10.1002/elan.201000607.

[66] D. X. Han, T. T. Han, C. S. Shan, A. Ivaska, and L. Niu. Simultaneous Determination of Ascorbic Acid, Dopamine and Uric Acid with Chitosan-Graphene Modified Electrode. *Electroanalysis*, 22(17-18):2001–2008, 2010. doi: 10.1002/elan.201000094.

[67] F. H. Li, J. Chai, H. F. Yang, D. X. Han, and L. Niu. Synthesis of Pt/ionic liquid/graphene nanocomposite and its simultaneous determination of ascorbic acid and dopamine. *Talanta*, 81 (3):1063–1068, 2010. doi: 10.1016/j.talanta.2010.01.061.

[68] C.-L. Sun, H.-H. Lee, J.-M. Yang, and C.-C. Wu. The simultaneous electrochemical detection of ascorbic acid, dopamine, and uric acid using graphene/size-selected Pt nanocomposites. *Biosens. Bioelectron.*, 26(8):3450–3455, 2011. doi: 10.1016/j.bios.2011.01.023.

[69] S. Alwarappan, C. Liu, A. Kumar, and C. Z. Li. Enzyme-Doped Graphene Nanosheets for Enhanced Glucose Biosensing. *J. Phys. Chem. C*, 114(30):12920–12924, 2010. doi: 10.1021/jp103273z.

[70] K. Wang, Q. A. Liu, Q. M. Guan, J. Wu, H. N. Li, and J. J. Yan. Enhanced direct electrochemistry of glucose oxidase and biosensing for glucose via synergy effect of graphene and CdS nanocrystals. *Biosens. Bioelectron.*, 26(5):2252–2257, 2011. doi: 10.1016/j.bios.2010.09.043.

[71] D. A. C. Brownson and C. E. Banks. Graphene electrochemistry: Fabricating amperometric biosensors. *Analyst*, 136(10):2084–2089, 2011. doi: 10.1039/c0an00875c.

[72] J. Xu, C. H. Liu, and Z. F. Wu. Direct electrochemistry and enhanced electrocatalytic activity of hemoglobin entrapped in graphene and ZnO nanosphere composite film. *Microchim. Acta*, 172(3-4):425–430, 2011. doi: 10.1007/s00604-010-0515-x.

[73] X. Chen, C. L. Fu, and W. S. Yang. Graphite nanosheet-based composites for mediator-free H2O2 biosensor. *Analyst*, 134(10):2135–2140, 2009. doi: 10.1039/b910754a.

[74] Y. L. Cui, B. Zhang, B. Q. Liu, H. F. Chen, G. N. Chen, and D. P. Tang. Sensitive detection of hydrogen peroxide in foodstuff using an organic-inorganic hybrid multilayer-functionalized graphene biosensing platform. *Microchim. Acta*, 174(1-2):137–144, 2011. doi: 10.1007/s00604-011-0608-1.

[75] M. G. Li, S. D. Xu, M. Tang, L. Liu, F. Gao, and Y. L. Wang. Direct electrochemistry of horseradish peroxidase on graphene-modified electrode for electrocatalytic reduction towards H2O2. *Electrochim. Acta*, 56(3):1144–1149, 2011. doi: 10.1016/j.electacta.2010.10.034.

[76] Q. O. Zeng, J. S. Cheng, L. H. Tang, X. F. Liu, Y. Z. Liu, J. H. Li, and J. H. Jiang. Self-Assembled Graphene-Enzyme Hierarchical Nanostructures for Electrochemical Biosensing. *Adv. Funct. Mater.*, 20(19):3366–3372, 2010. doi: 10.1002/adfm.201000540.

[77] K. J. Huang, D. J. Niu, X. Liu, Z. W. Wu, Y. Fan, Y. F. Chang, and Y. Y. Wu. Direct electrochemistry of catalase at amine-functionalized graphene/gold nanoparticles composite film for hydrogen peroxide sensor. *Electrochim. Acta*, 56(7):2947–2953, 2011. doi: 10.1016/j.electacta.2010.12.094.

[78] Y. X. Fang, S. J. Guo, C. Z. Zhu, Y. M. Zhai, and E. K. Wang. Self-Assembly of Cationic Polyelectrolyte-Functionalized Graphene Nanosheets and Gold Nanoparticles: A Two-Dimensional Heterostructure for Hydrogen Peroxide Sensing. *Langmuir*, 26(13):11277–11282, 2010. doi: 10.1021/la100575g.

[79] K. F. Zhou, Y. H. Zhu, X. L. Yang, J. Luo, C. Z. Li, and S. R. Luan. A novel hydrogen peroxide biosensor based on Au-graphene-HRP-chitosan biocomposites. *Electrochim. Acta*, 55 (9):3055–3060, 2010. doi: 10.1016/j.electacta.2010.01.035.

[80] Y. P. He, Q. L. Sheng, J. B. Zheng, M. Z. Wang, and B. Liu. Magnetite-graphene for the direct electrochemistry of hemoglobin and its biosensing application. *Electrochim. Acta*, 56(5): 2471–2476, 2011. doi: 10.1016/j.electacta.2010.11.020.

[81] K. Zhou, Y. Zhu, X. Yang, and C. Li. Preparation and Application of Mediator-Free H2O2 Biosensors of Graphene-Fe3O4 Composites. *Electroanalysis*, 23(4):862–869, 2011. doi: 10.1002/elan.201000629.

[82] S. Liu, J. Q. Tian, L. Wang, and X. P. Sun. A method for the production of reduced graphene oxide using benzylamine as a reducing and stabilizing agent and its subsequent decoration with Ag nanoparticles for enzymeless hydrogen peroxide detection. *Carbon*, 49(10):3158–3164, 2011. doi: 10.1016/j.carbon.2011.03.036.

[83] W. B. Lu, G. H. Chang, Y. L. Luo, F. Liao, and X. P. Sun. Method for effective immobilization of Ag nanoparticles/graphene oxide composites on single-stranded DNA modified gold electrode for enzymeless H2O2 detection. *J. Mater. Sci.*, 46(15):5260–5266, 2011. doi: 10.1007/s10853-011-5464-1.

[84] L. M. Li, Z. F. Du, S. A. Liu, Q. Y. Hao, Y. G. Wang, Q. H. Li, and T. H. Wang. A novel nonenzymatic hydrogen peroxide sensor based on MnO2/graphene oxide nanocomposite. *Talanta*, 82(5):1637–1641, 2010. doi: 10.1016/j.talanta.2010.07.020.

[85] W. Lv, M. Guo, M. H. Liang, F. M. Jin, L. Cui, L. J. Zhi, and Q. H. Yang. Graphene-DNA hybrids: self-assembly and electrochemical detection performance. *J. Mater. Chem.*, 20(32): 6668–6673, 2010. doi: 10.1039/c0jm01066a.

[86] X. X. Xu, J. X. Zhang, F. Guo, W. Zheng, H. M. Zhou, B. L. Wang, Y. F. Zheng, Y. B. Wang, Y. Cheng, X. Lou, and B. Z. Jang. A novel amperometric hydrogen peroxide biosensor based on immobilized Hb in Pluronic P123-nanographene platelets composite. *Colloids Surf., B*, 84 (2):427–432, 2011. doi: 10.1016/j.colsurfb.2011.01.037.

[87] Y. Zhou, S. Liu, H. J. Jiang, H. Yang, and H. Y. Chen. Direct Electrochemistry and Bioelectrocatalysis of Microperoxidase-11 Immobilized on Chitosan-Graphene Nanocomposite. *Electroanalysis*, 22(12):1323–1328, 2010. doi: 10.1002/elan.200900637.

[88] F. Ricci and G. Palleschi. Sensor and biosensor preparation, optimisation and applications of Prussian Blue modified electrodes. *Biosens. Bioelectron.*, 21(3):389–407, September 2005. doi: 10.1016/j.bios.2004.12.001.

[89] L. Y. Cao, Y. L. Liu, B. H. Zhang, and L. H. Lu. In situ Controllable Growth of Prussian Blue Nanocubes on Reduced Graphene Oxide: Facile Synthesis and Their Application as Enhanced Nanoelectrocatalyst for H2O2 Reduction. *ACS Appl. Mater. Interfaces*, 2(8):2339–2346, 2010. doi: 10.1021/am100372m.

[90] E. Jin, X. F. Lu, L. L. Cui, D. M. Chao, and C. Wang. Fabrication of graphene/prussian blue composite nanosheets and their electrocatalytic reduction of H2O2. *Electrochim. Acta*, 55(24): 7230–7234, 2010. doi: 10.1016/j.electacta.2010.07.029.

[91] Y. Zhang, X. M. Sun, L. Z. Zhu, H. B. Shen, and N. Q. Jia. Electrochemical sensing based on graphene oxide/Prussian blue hybrid film modified electrode. *Electrochim. Acta*, 56(3): 1239–1245, 2011. doi: 10.1016/j.electacta.2010.11.011.

[92] C. X. Guo, X. T. Zheng, Z. S. Lu, X. W. Lou, and C. M. Li. Biointerface by Cell Growth on Layered Graphene-Artificial Peroxidase-Protein Nanostructure for In Situ Quantitative Molecular Detection. *Adv. Mater.*, 22(45):5164–+, 2010. doi: 10.1002/adma.201001699.

[93] X. H. Kang, J. Wang, H. Wu, I. A. Aksay, J. Liu, and Y. H. Lin. Glucose Oxidase-graphene-chitosan modified electrode for direct electrochemistry and glucose sensing. *Biosens. Bioelectron.*, 25(4):901–905, 2009. doi: 10.1016/j.bios.2009.09.004.

[94] G. H. Zeng, Y. B. Xing, J. A. Gao, Z. Q. Wang, and X. Zhang. Unconventional Layer-by-Layer Assembly of Graphene Multilayer Films for Enzyme-Based Glucose and Maltose Biosensing. *Langmuir*, 26(18):15022–15026, 2010. doi: 10.1021/la102806v.

[95] P. Wu, Q. A. Shao, Y. J. Hu, J. A. Jin, Y. J. Yin, H. Zhang, and C. X. Cai. Direct electrochemistry of glucose oxidase assembled on graphene and application to glucose detection. *Electrochim. Acta*, 55(28):8606–8614, 2010. doi: 10.1016/j.electacta.2010.07.079.

[96] Y. Chen, Y. Li, D. Sun, D. B. Tian, J. R. Zhang, and J. J. Zhu. Fabrication of gold nanoparticles on bilayer graphene for glucose electrochemical biosensing. *J. Mater. Chem.*, 21(21):7604–7611, 2011. doi: 10.1039/c1jm10293a.

[97] T. T. Baby, S. S. J. Aravind, T. Arockiadoss, R. B. Rakhi, and S. Ramaprabhu. Metal decorated graphene nanosheets as immobilization matrix for amperometric glucose biosensor. *Sens. Actuators, B*, 145(1):71–77, 2010. doi: 10.1016/j.snb.2009.11.022.

[98] C. Shan, H. Yang, D. Han, Q. Zhang, A. Ivaska, and L. Niu. Graphene/AuNPs/chitosan nanocomposites film for glucose biosensing. *Biosens. Bioelectron.*, 25(5):1070–1074, 2010. doi: 10.1016/j.bios.2009.09.024.

[99] M. H. Yang, B. G. Choi, H. Park, T. J. Park, W. H. Hong, and S. Y. Lee. Directed Self-Assembly of Gold Nanoparticles on Graphene-Ionic Liquid Hybrid for Enhancing Electrocatalytic Activity. *Electroanalysis*, 23(4):850–857, 2011. doi: 10.1002/elan.201000645.

[100] K. F. Zhou, Y. H. Zhu, X. L. Yang, and C. Z. Li. Electrocatalytic Oxidation of Glucose by the Glucose Oxidase Immobilized in Graphene-Au-Nafion Biocomposite. *Electroanalysis*, 22(3): 259–264, 2010. doi: 10.1002/elan.200900321.

[101] M. H. Yang, B. G. Choi, H. Park, W. H. Hong, S. Y. Lee, and T. J. Park. Development of a Glucose Biosensor Using Advanced Electrode Modified by Nanohybrid Composing Chemically Modified Graphene and Ionic Liquid. *Electroanalysis*, 22(11):1223–1228, 2010. doi: 10.1002/elan.200900556.

[102] Q. Zhang, S. Wu, L. Zhang, J. Lu, F. Verproot, Y. Liu, Z. Xing, J. Li, and X.-M. Song. Fabrication of polymeric ionic liquid/graphene nanocomposite for glucose oxidase immobilization and direct electrochemistry. *Biosens. Bioelectron.*, 26(5):2632–2637, 2011. doi: 10.1016/j.bios.2010.11.024.

[103] M.-J. Song, J.-H. Kim, S.-K. Lee, D.-S. Lim, S. W. Hwang, and D. Whang. Analytical Characteristics of Electrochemical Biosensor Using Pt-Dispersed Graphene on Boron Doped Diamond Electrode. *Electroanalysis*, 23(10):2408–2414, 2011. doi: 10.1002/elan.201100265.

[104] H. Wu, J. Wang, X. H. Kang, C. M. Wang, D. H. Wang, J. Liu, I. A. Aksay, and Y. H. Lin. Glucose biosensor based on immobilization of glucose oxidase in platinum nanoparticles/graphene/chitosan nanocomposite film. *Talanta*, 80(1):403–406, 2009. doi: 10.1016/j.talanta.2009.06.054.

[105] Q. Zeng, J.-S. Cheng, X.-F. Liu, H.-T. Bai, and J.-H. Jiang. Palladium nanoparticle/chitosan-grafted graphene nanocomposites for construction of a glucose biosensor. *Biosens. Bioelectron.*, 26(8):3456–3463, 2011. doi: 10.1016/j.bios.2011.01.024.

[106] G. Zhiguo, Y. Shuping, L. Zaijun, S. Xiulan, W. Guangli, F. Yinjun, and L. Junkang. An ultrasensitive electrochemical biosensor for glucose using CdTe-CdS core-shell quantum dot as ultrafast electron transfer relay between graphene-gold nanocomposite and gold nanoparticle. *Electrochim. Acta*, 56(25):9162–9167, October 2011. doi: 10.1016/j.electacta.2011.07.117.

[107] L.-M. Lu, H.-B. Li, F. Qu, X.-B. Zhang, G.-L. Shen, and R.-Q. Yu. In situ synthesis of palladium nanoparticle-graphene nanohybrids and their application in nonenzymatic glucose biosensors. *Biosens. Bioelectron.*, 26(8):3500–3504, 2011. doi: 10.1016/j.bios.2011.01.033.

[108] H. C. Chang, X. J. Wu, C. Y. Wu, Y. Chen, H. Jiang, and X. M. Wang. Catalytic oxidation and determination of beta-NADH using self-assembly hybrid of gold nanoparticles and graphene. *Analyst*, 136(13):2735–2740, 2011. doi: 10.1039/c1an15197e.

[109] C. Shan, H. Yang, D. Han, Q. Zhang, A. Ivaska, and L. Niu. Electrochemical determination of NADH and ethanol based on ionic liquid-functionalized graphene. *Biosens. Bioelectron.*, 25 (6):1504–1508, 2010. doi: 10.1016/j.bios.2009.11.009.

[110] S. P. Kumar, R. Manjunatha, C. Nethravathi, G. S. Suresh, M. Rajamathi, and T. V. Venkatesha. Electrocatalytic Oxidation of NADH on Functionalized Graphene Modified Graphite Electrode. *Electroanalysis*, 23(4):842–849, 2011. doi: 10.1002/elan.201000552.

[111] M. Du, T. Yang, and K. Jiao. Immobilization-free direct electrochemical detection for DNA specific sequences based on electrochemically converted gold nanoparticles/graphene composite film. *J. Mater. Chem.*, 20(41):9253–9260, 2010. doi: 10.1039/c0jm01549k.

[112] M. Du, T. Yang, S. Y. Ma, C. Z. Zhao, and K. Jiao. Ionic liquid-functionalized graphene as modifier for electrochemical and electrocatalytic improvement: Comparison of different carbon electrodes. *Anal. Chim. Acta*, 690(2):169–174, 2011. doi: 10.1016/j.aca.2011.01.051.

[113] K. J. Huang, D. J. Niu, J. Y. Sun, C. H. Han, Z. W. Wu, Y. L. Li, and X. Q. Xiong. Novel electrochemical sensor based on functionalized graphene for simultaneous determination of adenine and guanine in DNA. *Colloids Surf., B*, 82(2):543–549, 2011. doi: 10.1016/j.colsurfb.2010.10.014.

[114] Y. Fan, K. J. Huang, D. J. Niu, C. P. Yang, and Q. S. Jing. TiO2-graphene nanocomposite for electrochemical sensing of adenine and guanine. *Electrochim. Acta*, 56(12):4685–4690, 2011. doi: 10.1016/j.electacta.2011.02.114.

[115] H. S. Yin, Y. L. Zhou, Q. Ma, T. Liu, S. Y. Ai, and L. S. Zhu. Electrochemical oxidation behavior of guanosine-5 '-monophosphate on a glassy carbon electrode modified with a composite film of graphene and multi-walled carbon nanotubes, and its amperometric determination. *Microchim. Acta*, 172(3-4):343–349, 2011. doi: 10.1007/s00604-010-0499-6.

[116] C. L. Scott, G. J. Zhao, and M. Pumera. Stacked graphene nanofibers doped polypyrrole nanocomposites for electrochemical sensing. *Electrochem. Commun.*, 12(12):1788–1791, 2010. doi: 10.1016/j.elecom.2010.10.025.

[117] H. S. Yin, Y. L. Zhou, Q. A. Ma, S. Y. Ai, P. Ju, L. S. Zhu, and L. N. Lu. Electrochemical oxidation behavior of guanine and adenine on graphene-Nafion composite film modified glassy carbon electrode and the simultaneous determination. *Process Biochem.*, 45(10):1707–1712, 2010. doi: 10.1016/j.procbio.2010.07.004.

[118] H. S. Yin, Y. L. Zhou, Q. A. Ma, S. Y. Ai, Q. P. Chen, and L. S. Zhu. Electrocatalytic oxidation behavior of guanosine at graphene, chitosan and Fe3O4 nanoparticles modified glassy carbon electrode and its determination. *Talanta*, 82(4):1193–1199, 2010. doi: 10.1016/j.talanta.2010.06.030.

[119] B. G. Choi, H. Park, M. H. Yang, Y. M. Jung, S. Y. Lee, W. H. Hong, and T. J. Park. Microwave-assisted synthesis of highly water-soluble graphene towards electrical DNA sensor. *Nanoscale*, 2(12):2692–2697, 2010. doi: 10.1039/c0nr00562b.

[120] A. Bonanni and M. Pumera. Graphene Platform for Hairpin-DNA-Based Impedimetric Genosensing. *ACS Nano*, 5(3):2356–2361, 2011. doi: 10.1021/nn200091p.

[121] Y. W. Hu, F. H. Li, X. X. Bai, D. Li, S. C. Hua, K. K. Wang, and L. Niu. Label-free electrochemical impedance sensing of DNA hybridization based on functionalized graphene sheets. *Chem. Commun.*, 47(6):1743–1745, 2011. doi: 10.1039/c0cc04514d.

[122] Z. J. Wang, J. Zhang, P. Chen, X. Z. Zhou, Y. L. Yang, S. X. Wu, L. Niu, Y. Han, L. H. Wang, P. Chen, F. Boey, Q. C. Zhang, B. Liedberg, and H. Zhang. Label-free, electrochemical detection of methicillin-resistant staphylococcus aureus DNA with reduced graphene oxide-modified electrodes. *Biosens. Bioelectron.*, 26(9):3881–3886, 2011. doi: 10.1016/j.bios.2011.03.002.

[123] Y. Bo, H. Y. Yang, Y. Hu, T. M. Yao, and S. S. Huang. A novel electrochemical DNA biosensor based on graphene and polyaniline nanowires. *Electrochim. Acta*, 56(6):2676–2681, 2011. doi: 10.1016/j.electacta.2010.12.034.

[124] E. Dubuisson, Z. Y. Yang, and K. P. Loh. Optimizing Label-Free DNA Electrical Detection on Graphene Platform. *Anal. Chem.*, 83(7):2452–2460, 2011. doi: 10.1021/ac102431d.

[125] M. Muti, S. Sharma, A. Erdem, and P. Papakonstantinou. Electrochemical Monitoring of Nucleic Acid Hybridization by Single-Use Graphene Oxide-Based Sensor. *Electroanalysis*, 23 (1):272–279, 2011. doi: 10.1002/elan.201000425.

[126] J. Wu, Y. H. Zou, X. L. Li, H. B. Liu, G. L. Shen, and R. Q. Yu. A biosensor monitoring DNA hybridization based on polyaniline intercalated graphite oxide nanocomposite. *Sens. Actuators, B*, 104(1):43–49, 2005. doi: 10.1016/j.snb.2004.04.097.

[127] Y. Bo, W. Q. Wang, J. F. Qi, and S. S. Huang. A DNA biosensor based on graphene paste electrode modified with Prussian blue and chitosan. *Analyst*, 136(9):1946–1951, 2011. doi: 10.1039/c1an15084g.

[128] Y. Du, S. Guo, S. Dong, and E. Wang. An integrated sensing system for detection of DNA using new parallel-motif DNA triplex system and graphene-mesoporous silica-gold nanoparticle hybrids. *Biomaterials*, 32(33):8584–8592, November 2011. doi: 10.1016/j.biomaterials.2011.07.091.

[129] L. H. Tang, Y. Wang, Y. Liu, and J. H. Li. DNA-Directed Self-Assembly of Graphene Oxide with Applications to Ultrasensitive Oligonucleotide Assay. *ACS Nano*, 5(5):3817–3822, 2011. doi: 10.1021/nn200147n.

[130] J. F. Liang, Z. B. Chen, L. Guo, and L. D. Li. Electrochemical sensing of L-histidine based on structure-switching DNAzymes and gold nanoparticle-graphene nanosheet composites. *Chem. Commun.*, 47(19):5476–5478, 2011. doi: 10.1039/c1cc10965k.

[131] Y. Lu, B. R. Goldsmith, N. J. Kybert, and A. T. C. Johnson. DNA-decorated graphene chemical sensors. *Appl. Phys. Lett.*, 97(8):083107, 2010. doi: 10.1063/1.3483128.

[132] X. R. Zhang, S. G. Li, X. Jin, and S. S. Zhang. A new photoelectrochemical aptasensor for the detection of thrombin based on functionalized graphene and CdSe nanoparticles multilayers. *Chem. Commun.*, 47(17):4929–4931, 2011. doi: 10.1039/c1cc10830a.

[133] L. Wang, C. Z. Zhu, L. Han, L. H. Jin, M. Zhou, and S. J. Dong. Label-free, regenerative and sensitive surface plasmon resonance and electrochemical aptasensors based on graphene. *Chem. Commun.*, 47(27):7794–7796, 2011. doi: 10.1039/c1cc11373a.

[134] K. P. Liu, J. P. Wei, and C. M. Wang. Sensitive detection of rutin based on beta-cyclodextrin@chemically reduced graphene/Nafion composite film. *Electrochim. Acta*, 56(14): 5189–5194, 2011. doi: 10.1016/j.electacta.2011.03.042.

[135] H. S. Yin, Y. L. Zhou, L. Cui, T. Liu, P. Ju, L. S. Zhu, and S. Y. Ai. Sensitive voltammetric determination of rutin in pharmaceuticals, human serum, and traditional Chinese medicines using a glassy carbon electrode coated with graphene nanosheets, chitosan, and a poly(amido amine) dendrimer. *Microchim. Acta*, 173(3-4):337–345, 2011. doi: 10.1007/s00604-011-0568-5.

[136] S. Hu, H. Zhu, S. Liu, J. Xiang, W. Sun, and L. Zhang. Electrochemical detection of rutin with a carbon ionic liquid electrode modified by Nafion, graphene oxide and ionic liquid composite. *Microchim. Acta*, pages 1–9, 2012. doi: 10.1007/s00604-012-0811-8.

[137] T. Gan, C. Hu, Z. Chen, and S. Hu. A disposable electrochemical sensor for the determination of indole-3-acetic acid based on poly(safranine T)-reduced graphene oxide nanocomposite. *Talanta*, 85(1):310–316, July 2011. doi: 10.1016/j.talanta.2011.03.070.

[138] C. X. Guo, Y. Lei, and C. M. Li. Porphyrin Functionalized Graphene for Sensitive Electrochemical Detection of Ultratrace Explosives. *Electroanalysis*, 23(4):885–893, 2011. doi: 10.1002/elan.201000522.

[139] C. X. Guo, Z. S. Lu, Y. Lei, and C. M. Li. Ionic liquid-graphene composite for ultra-trace explosive trinitrotoluene detection. *Electrochem. Commun.*, 12(9):1237–1240, 2010. doi: 10.1016/j.elecom.2010.06.028.

[140] S. Guo, D. Wen, Y. Zhai, S. Dong, and E. Wang. Ionic liquid-graphene hybrid nanosheets as an enhanced material for electrochemical determination of trinitrotoluene. *Biosens. Bioelectron.*, 26(8):3475–3481, 2011. doi: 10.1016/j.bios.2011.01.028.

[141] J. A. Li, J. H. Chen, X. L. Zhang, C. H. Lu, and H. H. Yang. A novel sensitive detection platform for antitumor herbal drug aloe-emodin based on the graphene modified electrode. *Talanta*, 83(2):553–558, 2010. doi: 10.1016/j.talanta.2010.09.058.

[142] H. S. Yin, Q. A. Ma, Y. L. Zhou, S. Y. Ai, and L. S. Zhu. Electrochemical behavior and voltammetric determination of 4-aminophenol based on graphene-chitosan composite film modified glassy carbon electrode. *Electrochim. Acta*, 55(23):7102–7108, 2010. doi: 10.1016/j.electacta.2010.06.072.

[143] J. Y. Sun, K. J. Huang, S. Y. Wei, Z. W. Wu, and F. P. Ren. A graphene-based electrochemical sensor for sensitive determination of caffeine. *Colloids Surf., B*, 84(2):421–426, 2011. doi: 10.1016/j.colsurfb.2011.01.036.

[144] K. Wang, Q. Liu, L. Dai, J. J. Yan, C. Ju, B. J. Qiu, and X. Y. Wu. A highly sensitive and rapid organophosphate biosensor based on enhancement of CdS-decorated graphene nanocomposite. *Anal. Chim. Acta*, 695(1-2):84–88, 2011. doi: 10.1016/j.aca.2011.03.042.

[145] K. Wang, H.-N. Li, J. Wu, C. Ju, J.-J. Yan, Q. Liu, and B. Qiu. TiO2-decorated graphene nanohybrids for fabricating an amperometric acetylcholinesterase biosensor. *Analyst*, 136(16): 3349–3354, 2011. doi: 10.1039/C1AN15227K.

[146] Y. Guo, S. Guo, J. Li, E. Wang, and S. Dong. Cyclodextrin-graphene hybrid nanosheets as enhanced sensing platform for ultrasensitive determination of carbendazim. *Talanta*, 84(1): 60–64, 2011. doi: 10.1016/j.talanta.2010.12.007.

[147] W. W. Tu, J. P. Lei, S. Y. Zhang, and H. X. Ju. Characterization, Direct Electrochemistry, and Amperometric Biosensing of Graphene by Noncovalent Functionalization with Picket-Fence Porphyrin. *Chem.–Eur. J.*, 16(35):10771–10777, 2010. doi: 10.1002/chem.201000620.

[148] R. S. Dey and C. R. Raj. Development of an Amperometric Cholesterol Biosensor Based on Graphene-Pt Nanoparticle Hybrid Material. *J. Phys. Chem. C*, 114(49):21427–21433, 2010. doi: 10.1021/jp105895a.

[149] C. H. Xu, X. B. Wang, J. C. Wang, H. T. Hu, and L. Wan. Synthesis and photoelectrical properties of beta-Cyclodextrin functionalized graphene materials with high bio-recognition capability. *Chem. Phys. Lett.*, 498(1-3):162–167, 2010. doi: 10.1016/j.cplett.2010.08.060.

[150] J. Zhang, J. P. Lei, R. Pan, Y. D. Xue, and H. X. Ju. Highly sensitive electrocatalytic biosensing of hypoxanthine based on functionalization of graphene sheets with water-soluble conducting graft copolymer. *Biosens. Bioelectron.*, 26(2):371–376, 2010. doi: 10.1016/j.bios.2010.07.127.

[151] T. A. Gan, C. G. Hu, Z. L. Chen, and S. S. Hu. Fabrication and application of a novel plant hormone sensor for the determination of methyl jasmonate based on self-assembling of phosphotungstic acid-graphene oxide nanohybrid on graphite electrode. *Sens. Actuators, B*, 151(1):8–14, 2010. doi: 10.1016/j.snb.2010.10.001.

[152] L. Wang, X. H. Zhang, H. Y. Xiong, and S. F. Wang. A novel nitromethane biosensor based on biocompatible conductive redox graphene-chitosan/hemoglobin/graphene/room temperature ionic liquid matrix. *Biosens. Bioelectron.*, 26(3):991–995, 2010. doi: 10.1016/j.bios.2010.08.027.

[153] S. R. Ng, C. X. Guo, and C. M. Li. Highly Sensitive Nitric Oxide Sensing Using Three-Dimensional Graphene/Ionic Liquid Nanocomposite. *Electroanalysis*, 23(2):442–448, 2011. doi: 10.1002/elan.201000344.

[154] T. Liu, M. Xu, H. Yin, S. Ai, X. Qu, and S. Zong. A glassy carbon electrode modified with graphene and tyrosinase immobilized on platinum nanoparticles for sensing organophosphorus pesticides. *Microchim. Acta*, 175:129–135, 2011. doi: 10.1007/s00604-011-0665-5.

[155] D. Du, J. Liu, X. Y. Zhang, X. L. Cui, and Y. H. Lin. One-step electrochemical deposition of a graphene-ZrO2 nanocomposite: Preparation, characterization and application for detection of organophosphorus agents. *J. Mater. Chem.*, 21(22):8032–8037, 2011. doi: 10.1039/c1jm10696a.

[156] J. Chen, L. Zhao, H. Bai, and G. Q. Shi. Electrochemical detection of dioxygen and hydrogen peroxide by hemin immobilized on chemically converted graphene. *J. Electroanal. Chem.*, 657 (1-2):34–38, 2011. doi: 10.1016/j.jelechem.2011.03.005.

[157] X. M. Wu, Y. J. Hu, J. Jin, N. L. Zhou, P. Wu, H. Zhang, and C. X. Cai. Electrochemical Approach for Detection of Extracellular Oxygen Released from Erythrocytes Based on Graphene Film Integrated with Laccase and 2,2-Azino-bis(3-ethylbenzothiazoline-6-sulfonic acid). *Anal. Chem.*, 82(9):3588–3596, 2010. doi: 10.1021/ac100621r.

[158] S. Y. Zhang, S. Tang, J. P. Lei, H. F. Dong, and H. X. Ju. Functionalization of graphene nanoribbons with porphyrin for electrocatalysis and amperometric biosensing. *J. Electroanal. Chem.*, 656(1-2):285–288, 2011. doi: 10.1016/j.jelechem.2010.10.005.

[159] Y. Fan, J. H. Liu, H. T. Lu, and Q. Zhang. Electrochemical behavior and voltammetric determination of paracetamol on Nafion/TiO2-graphene modified glassy carbon electrode. *Colloids Surf., B*, 85(2):289–292, 2011. doi: 10.1016/j.colsurfb.2011.02.041.

[160] B. G. Choi, H. Park, T. J. Park, M. H. Yang, J. S. Kim, S. Y. Jang, N. S. Heo, S. Y. Lee, J. Kong, and W. H. Hong. Solution Chemistry of Self-Assembled Graphene Nanohybrids for High-Performance Flexible Biosensors. *ACS Nano*, 4(5):2910–2918, 2010. doi: 10.1021/nn100145x.

[161] Y. Wang, S. Zhang, D. Du, Y. Y. Shao, Z. H. Li, J. Wang, M. H. Engelhard, J. H. Li, and Y. H. Lin. Self assembly of acetylcholinesterase on a gold nanoparticles-graphene nanosheet hybrid for organophosphate pesticide detection using polyelectrolyte as a linker. *J. Mater. Chem.*, 21 (14):5319–5325, 2011. doi: 10.1039/c0jm03441j.

[162] M. Myers, J. Cooper, B. Pejcic, M. Baker, B. Raguse, and L. Wieczorek. Functionalized graphene as an aqueous phase chemiresistor sensing material. *Sens. Actuators, B*, 155(1): 154–158, 2011. doi: 10.1016/j.snb.2010.11.040.

[163] L. Feng, Y. Chen, J. Ren, and X. Qu. A graphene functionalized electrochemical aptasensor for selective label-free detection of cancer cells. *Biomaterials*, 32(11):2930–2937, 2011. doi: 10.1016/j.biomaterials.2011.01.002.

[164] Y. J. Song, Y. Chen, L. Y. Feng, J. S. Ren, and X. G. Qu. Selective and quantitative cancer cell detection using target-directed functionalized graphene and its synergetic peroxidase-like activity. *Chem. Commun.*, 47(15):4436–4438, 2011. doi: 10.1039/c0cc05533f.

[165] G. F. Wang, H. Huang, G. Zhang, X. J. Zhang, B. Fang, and L. Wang. Gold nanoparticles/L-cysteine/graphene composite based immobilization strategy for an electrochemical immunosensor. *Anal. Methods*, 2(11):1692–1697, 2010. doi: 10.1039/c0ay00389a.

[166] S. Mao, G. H. Lu, K. H. Yu, Z. Bo, and J. H. Chen. Specific Protein Detection Using Thermally Reduced Graphene Oxide Sheet Decorated with Gold Nanoparticle-Antibody Conjugates. *Adv. Mater.*, 22(32):3521–+, 2010. doi: 10.1002/adma.201000520.

[167] K. Liu, J.-J. Zhang, C. Wang, and J.-J. Zhu. Graphene-assisted dual amplification strategy for the fabrication of sensitive amperometric immunosensor. *Biosens. Bioelectron.*, 26(8):3627–3632, 2011. doi: 10.1016/j.bios.2011.02.018.

[168] B. Q. Liu, D. P. Tang, J. Tang, B. L. Su, Q. F. Li, and G. N. Chen. A graphene-based Au(111) platform for electrochemical biosensing based catalytic recycling of products on gold nanoflowers. *Analyst*, 136(11):2218–2220, 2011. doi: 10.1039/c0an00921k.

[169] D. Du, Z. X. Zou, Y. S. Shin, J. Wang, H. Wu, M. H. Engelhard, J. Liu, I. A. Aksay, and Y. H. Lin. Sensitive Immunosensor for Cancer Biomarker Based on Dual Signal Amplification Strategy of Graphene Sheets and Multienzyme Functionalized Carbon Nanospheres. *Anal. Chem.*, 82(7):2989–2995, 2010. doi: 10.1021/ac100036p.

[170] K. J. Huang, D. J. Niu, J. Y. Sun, and J. J. Zhu. An electrochemical amperometric immunobiosensor for label-free detection of alpha-fetoprotein based on amine-functionalized graphene and gold nanoparticles modified carbon ionic liquid electrode. *J. Electroanal. Chem.*, 656(1-2):72–77, 2011. doi: 10.1016/j.jelechem.2011.01.007.

[171] B. Su, D. Tang, Q. Li, J. Tang, and G. Chen. Gold-silver-graphene hybrid nanosheets-based sensors for sensitive amperometric immunoassay of alpha-fetoprotein using nanogold-enclosed titania nanoparticles as labels. *Anal. Chim. Acta*, 692(1-2):116–124, 2011. doi: 10.1016/j.aca.2011.02.061.

[172] B. L. Su, J. A. Tang, J. X. Huang, H. H. Yang, B. Qiu, G. N. Chen, and D. P. Tang. Graphene and Nanogold-Functionalized Immunosensing Interface with Enhanced Sensitivity for One-Step Electrochemical Immunoassay of Alpha-Fetoprotein in Human Serum. *Electroanalysis*, 22(22):2720–2728, 2010. doi: 10.1002/elan.201000324.

[173] J. Tang, D. P. Tang, B. L. Su, Q. F. Li, B. Qiu, and G. N. Chen. Nanosilver-penetrated polyion graphene complex membrane for mediator-free amperometric immunoassay of alpha-fetoprotein using nanosilver-coated silica nanoparticles. *Electrochim. Acta*, 56(11):3773–3780, 2011. doi: 10.1016/j.electacta.2011.02.059.

[174] J. Tang, D. P. Tang, R. Niessner, G. N. Chen, and D. Knopp. Magneto-Controlled Graphene Immunosensing Platform for Simultaneous Multiplexed Electrochemical Immunoassay Using Distinguishable Signal Tags. *Anal. Chem.*, 83(13):5407–5414, 2011. doi: 10.1021/ac200969w.

[175] Q. Wei, K. X. Mao, D. Wu, Y. X. Dai, J. A. Yang, B. Du, M. H. Yang, and H. Li. A novel label-free electrochemical immunosensor based on graphene and thionine nanocomposite. *Sens. Actuators, B*, 149(1):314–318, 2010. doi: 10.1016/j.snb.2010.06.008.

[176] Y. Cai, H. Li, B. Du, M. Yang, Y. Li, D. Wu, Y. Zhao, Y. Dai, and Q. Wei. Ultrasensitive electrochemical immunoassay for BRCA1 using BMIM center dot BF4-coated SBA-15 as labels and functionalized graphene as enhancer. *Biomaterials*, 32(8):2117–2123, 2011. doi: 10.1016/j.biomaterials.2010.11.058.

[177] T. Li, M. H. Yang, and H. Li. Label-free electrochemical detection of cancer marker based on graphene-cobalt hexacyanoferrate nanocomposite. *J. Electroanal. Chem.*, 655(1):50–55, 2011. doi: 10.1016/j.jelechem.2011.02.009.

[178] F. L. Qu, T. Li, and M. H. Yang. Colorimetric platform for visual detection of cancer biomarker based on intrinsic peroxidase activity of graphene oxide. *Biosens. Bioelectron.*, 26(9):3927–3931, 2011. doi: 10.1016/j.bios.2011.03.013.

[179] M. H. Yang and S. Q. Gong. Immunosensor for the detection of cancer biomarker based on percolated graphene thin film. *Chem. Commun.*, 46(31):5796–5798, 2010. doi: 10.1039/c0cc00675k.

[180] M. H. Yang, A. Javadi, and S. Q. Gong. Sensitive electrochemical immunosensor for the detection of cancer biomarker using quantum dot functionalized graphene sheets as labels. *Sens. Actuators, B*, 155(1):357–360, 2011. doi: 10.1016/j.snb.2010.11.055.

[181] M. H. Yang, A. Javadi, H. Li, and S. Q. Gong. Ultrasensitive immunosensor for the detection of cancer biomarker based on graphene sheet. *Biosens. Bioelectron.*, 26(2):560–565, 2010. doi: 10.1016/j.bios.2010.07.040.

[182] S. J. Xu, Y. Liu, T. H. Wang, and J. H. Li. Positive Potential Operation of a Cathodic Electrogenerated Chemiluminescence Immunosensor Based on Luminol and Graphene for Cancer Biomarker Detection. *Anal. Chem.*, 83(10):3817–3823, 2011. doi: 10.1021/ac200237j.

[183] B. Zhang and T. H. Cui. An ultrasensitive and low-cost graphene sensor based on layer-by-layer nano self-assembly. *Appl. Phys. Lett.*, 98(7):073116, 2011. doi: 10.1063/1.3557504.

[184] B. Su, J. Tang, H. Yang, G. Chen, J. Huang, and D. Tang. A Graphene Platform for Sensitive Electrochemical Immunoassay of Carcinoembryoninc Antigen Based on Gold-Nanoflower Biolabels. *Electroanalysis*, 23(4):832–841, 2011. doi: 10.1002/elan.201000635.

[185] Z. Y. Zhong, W. Wu, D. Wang, D. Wang, J. L. Shan, Y. Qing, and Z. M. Zhang. Nanogold-enwrapped graphene nanocomposites as trace labels for sensitivity enhancement of electrochemical immunosensors in clinical immunoassays: Carcinoembryonic antigen as a model. *Biosens. Bioelectron.*, 25(10):2379–2383, 2010. doi: 10.1016/j.bios.2010.03.009.

[186] S. Myung, A. Solanki, C. Kim, J. Park, K. S. Kim, and K. B. Lee. Graphene-Encapsulated Nanoparticle-Based Biosensor for the Selective Detection of Cancer Biomarkers. *Adv. Mater.*, 23(19):2221–+, 2011. doi: 10.1002/adma.201100014.

[187] Y. F. Zhao, Q. Wei, C. X. Xu, H. Li, D. Wu, Y. Y. Cai, K. X. Mao, Z. T. Cui, and B. Du. Label-free electrochemical immunosensor for sensitive detection of kanamycin. *Sens. Actuators, B*, 155(2):618–625, 2011. doi: 10.1016/j.snb.2011.01.019.

[188] Q. Wei, X. D. Xin, B. Du, D. Wu, Y. Y. Han, Y. F. Zhao, Y. Y. Cai, R. Li, M. H. Yang, and H. Li. Electrochemical immunosensor for norethisterone based on signal amplification strategy of graphene sheets and multienzyme functionalized mesoporous silica nanoparticles. *Biosens. Bioelectron.*, 26(2):723–729, 2010. doi: 10.1016/j.bios.2010.06.052.

[189] J. D. Huang, Q. Lin, X. M. Zhang, X. R. He, X. R. Xing, W. J. Lian, M. M. Zuo, and Q. Q. Zhang. Electrochemical immunosensor based on polyaniline/poly (acrylic acid) and Au-hybrid graphene nanocomposite for sensitivity enhanced detection of salbutamol. *Food Res. Int.*, 44 (1):92–97, 2011. doi: 10.1016/j.foodres.2010.11.006.

[190] D. Du, L. M. Wang, Y. Y. Shao, J. Wang, M. H. Engelhard, and Y. H. Lin. Functionalized Graphene Oxide as a Nanocarrier in a Multienzyme Labeling Amplification Strategy for Ultrasensitive Electrochemical Immunoassay of Phosphorylated p53 (S392). *Anal. Chem.*, 83(3): 746–752, 2011. doi: 10.1021/ac101715s.

[191] R. Li, D. Wu, H. Li, C. X. Xu, H. Wang, Y. F. Zhao, Y. Y. Cai, Q. Wei, and B. Du. Label-free amperometric immunosensor for the detection of human serum chorionic gonadotropin based on nanoporous gold and graphene. *Anal. Biochem.*, 414(2):196–201, 2011. doi: 10.1016/j.ab.2011.03.019.

[192] J. H. Jung, D. S. Cheon, F. Liu, K. B. Lee, and T. S. Seo. A Graphene Oxide Based Immunobiosensor for Pathogen Detection. *Angew. Chem., Int. Ed.*, 49(33):5708–5711, 2010. doi: 10.1002/anie.201001428.

[193] F. Liu, K. S. Choi, T. J. Park, S. Y. Lee, and T. S. Seo. Graphene-based electrochemical biosensor for pathogenic virus detection. *BioChip J.*, 5(2):123–128, 2011. doi: 10.1007/s13206-011-5204-2.

[194] Y. Wan, Y. Wang, J. J. Wu, and D. Zhag. Graphene Oxide Sheet-Mediated Silver Enhancement for Application to Electrochemical Biosensors. *Anal. Chem.*, 83(3):648–653, 2011. doi: 10.1021/ac103047c.

[195] Y. Wan, Z. F. Lin, D. Zhang, Y. Wang, and B. R. Hou. Impedimetric immunosensor doped with reduced graphene sheets fabricated by controllable electrodeposition for the non-labelled detection of bacteria. *Biosens. Bioelectron.*, 26(5):1959–1964, 2011. doi: 10.1016/j.bios.2010.08.008.

[196] Y. Sofue, Y. Ohno, K. Maehashi, K. Inoue, and K. Matsumoto. Highly Sensitive Electrical Detection of Sodium Ions Based on Graphene Field-Effect Transistors. *Jpn. J. Appl. Phys.*, 50 (6):06GE07, 2011. doi: 10.1143/JJAP.50.06GE07.

[197] H. G. Sudibya, Q. Y. He, H. Zhang, and P. Chen. Electrical Detection of Metal Ions Using Field-Effect Transistors Based on Micropatterned Reduced Graphene Oxide Films. *ACS Nano*, 5(3):1990–1994, 2011. doi: 10.1021/nn103043v.

[198] T. Zhang, Z. G. Cheng, Y. B. Wang, Z. J. Li, C. X. Wang, Y. B. Li, and Y. Fang. Self-Assembled 1-Octadecanethiol Monolayers on Graphene for Mercury Detection. *Nano Lett.*, 10 (11):4738–4741, 2010. doi: 10.1021/nl1032556.

[199] P. K. Ang, W. Chen, A. T. S. Wee, and K. P. Loh. Solution-Gated Epitaxial Graphene as pH Sensor. *J. Am. Chem. Soc.*, 130(44):14392–+, 2008. doi: 10.1021/ja805090z.

[200] Y. Ohno, K. Maehashi, and K. Matsumoto. Chemical and biological sensing applications based on graphene field-effect transistors. *Biosens. Bioelectron.*, 26(4):1727–1730, 2010. doi: 10.1016/j.bios.2010.08.001.

[201] Y. Ohno, K. Maehashi, Y. Yamashiro, and K. Matsumoto. Electrolyte-Gated Graphene Field-Effect Transistors for Detecting pH Protein Adsorption. *Nano Lett.*, 9(9):3318–3322, 2009. doi: 10.1021/nl901596m.

[202] H. Vedala, D. C. Sorescu, G. P. Kotchey, and A. Star. Chemical Sensitivity of Graphene Edges Decorated with Metal Nanoparticles. *Nano Lett.*, 11(6):2342–2347, 2011. doi: 10.1021/nl2006438.

[203] Y. F. Tang, G. P. Kotchey, H. Vedala, and A. Star. Electrochemical Detection with Platinum Decorated Carbon Nanomaterials. *Electroanalysis*, 23(4):870–877, 2011. doi: 10.1002/elan.201000688.

[204] N. Mohanty and V. Berry. Graphene-Based Single-Bacterium Resolution Biodevice and DNA Transistor: Interfacing Graphene Derivatives with Nanoscale and Microscale Biocomponents. *Nano Lett.*, 8(12):4469–4476, 2008. doi: 10.1021/nl802412n.

[205] S. R. Guo, J. Lin, M. Penchev, E. Yengel, M. Ghazinejad, C. S. Ozkan, and M. Ozkan. Label Free DNA Detection Using Large Area Graphene Based Field Effect Transistor Biosensors. *J. Nanosci. Nanotechnol.*, 11(6):5258–5263, 2011. doi: 10.1166/jnn.2011.3885.

[206] X. C. Dong, Y. M. Shi, W. Huang, P. Chen, and L. J. Li. Electrical Detection of DNA Hybridization with Single-Base Specificity Using Transistors Based on CVD-Grown Graphene Sheets. *Adv. Mater.*, 22(14):1649–+, 2010. doi: 10.1002/adma.200903645.

[207] R. Stine, J. T. Robinson, P. E. Sheehan, and C. R. Tamanaha. Real-Time DNA Detection Using Reduced Graphene Oxide Field Effect Transistors. *Adv. Mater.*, 22(46):5297–5300, 2010. doi: 10.1002/adma.201002121.

[208] Q. Y. He, S. X. Wu, S. Gao, X. H. Cao, Z. Y. Yin, H. Li, P. Chen, and H. Zhang. Transparent, Flexible, All-Reduced Graphene Oxide Thin Film Transistors. *ACS Nano*, 5(6):5038–5044, 2011. doi: 10.1021/nn201118c.

[209] Y. Ohno, K. Maehashi, and K. Matsumoto. Label-Free Biosensors Based on Aptamer-Modified Graphene Field-Effect Transistors. *J. Am. Chem. Soc.*, 132(51):18012–18013, 2010. doi: 10.1021/ja108127r.

[210] Y. Cui, S. N. Kim, S. E. Jones, L. L. Wissler, R. R. Naik, and M. C. McAlpine. Chemical Functionalization of Graphene Enabled by Phage Displayed Peptides. *Nano Lett.*, 10(11):4559–4565, 2010. doi: 10.1021/nl102564d.

[211] X. H. Zhao, R. M. Kong, X. B. Zhang, H. M. Meng, W. N. Liu, W. H. Tan, G. L. Shen, and R. Q. Yu. Graphene-DNAzyme Based Biosensor for Amplified Fluorescence "Turn-On" Detection of Pb2+ with a High Selectivity. *Anal. Chem.*, 83(13):5062–5066, 2011. doi: 10.1021/ac200843x.

[212] X. F. Liu, L. K. Miao, X. Jiang, Y. W. Ma, Q. L. Fan, and W. Huang. Highly Sensitive Fluorometric Hg2+ Biosensor with a Mercury(II)-Specific Oligonucleotide (MSO) Probe and Water-Soluble Graphene Oxide (WSGO). *Chin. J. Chem.*, 29(5):1031–1035, 2011. doi: 10.1002/cjoc.201190175.

[213] H. Eschnauer, L. Jakob, H. Meierer, and R. Neeb. Use and limitations of ICP-OES in wine analysis. *Microchim. Acta*, 99:291–298, 1989. doi: 10.1007/BF01244684.

[214] Y. Q. Wen, F. F. Xing, S. J. He, S. P. Song, L. H. Wang, Y. T. Long, D. Li, and C. H. Fan. A graphene-based fluorescent nanoprobe for silver(I) ions detection by using graphene oxide and a silver-specific oligonucleotide. *Chem. Commun.*, 46(15):2596–2598, 2010. doi: 10.1039/b924832c.

[215] M. Liu, H. M. Zhao, S. Chen, H. T. Yu, Y. B. Zhang, and X. Quan. Label-free fluorescent detection of Cu(II) ions based on DNA cleavage-dependent graphene-quenched DNAzymes. *Chem. Commun.*, 47(27):7749–7751, 2011. doi: 10.1039/c1cc12006a.

[216] W. T. Huang, Y. Shi, W. Y. Xie, H. Q. Luo, and N. B. Li. A reversible fluorescence nanoswitch based on bifunctional reduced graphene oxide: use for detection of Hg2+ and molecular logic gate operation. *Chem. Commun.*, 47(27):7800–7802, 2011. doi: 10.1039/c1cc11631b.

[217] Y. Q. Wen, C. Peng, D. Li, L. Zhuo, S. J. He, L. H. Wang, Q. Huang, Q. H. Xu, and C. H. Fan. Metal ion-modulated graphene-DNAzyme interactions: design of a nanoprobe for fluorescent detection of lead(II) ions with high sensitivity, selectivity and tunable dynamic range. *Chem. Commun.*, 47(22):6278–6280, 2011. doi: 10.1039/c1cc11486g.

[218] S. J. He, B. Song, D. Li, C. F. Zhu, W. P. Qi, Y. Q. Wen, L. H. Wang, S. P. Song, H. P. Fang, and C. H. Fan. A Graphene Nanoprobe for Rapid, Sensitive, and Multicolor Fluorescent DNA Analysis. *Adv. Funct. Mater.*, 20(3):453–459, 2010. doi: 10.1002/adfm.200901639.

[219] F. Li, Y. Huang, Q. Yang, Z. T. Zhong, D. Li, L. H. Wang, S. P. Song, and C. H. Fan. A graphene-enhanced molecular beacon for homogeneous DNA detection. *Nanoscale*, 2(6):1021–1026, 2010. doi: 10.1039/b9nr00401g.

[220] C. K. Wu, Y. M. Zhou, X. M. Miao, and L. S. Ling. A novel fluorescent biosensor for sequence-specific recognition of double-stranded DNA with the platform of graphene oxide. *Analyst*, 136 (10):2106–2110, 2011. doi: 10.1039/c1an15061h.

[221] M. Zhang, B. C. Yin, W. H. Tan, and B. C. Ye. A versatile graphene-based fluorescence "on/off" switch for multiplex detection of various targets. *Biosens. Bioelectron.*, 26(7):3260–3265, 2011. doi: 10.1016/j.bios.2010.12.037.

[222] H. F. Dong, W. C. Gao, F. Yan, H. X. Ji, and H. X. Ju. Fluorescence Resonance Energy Transfer between Quantum Dots and Graphene Oxide for Sensing Biomolecules. *Anal. Chem.*, 82(13):5511–5517, 2010. doi: 10.1021/ac100852z.

[223] C. H. Lu, H. H. Yang, C. L. Zhu, X. Chen, and G. N. Chen. A Graphene Platform for Sensing Biomolecules. *Angew. Chem., Int. Ed.*, 48(26):4785–4787, 2009. doi: 10.1002/anie.200901479.

[224] M. Liu, H. M. Zhao, S. Chen, H. T. Yu, Y. B. Zhang, and X. Quan. A graphene-based platform for single nucleotide polymorphism (SNP) genotyping. *Biosens. Bioelectron.*, 26(10):4213–4216, 2011. doi: 10.1016/j.bios.2011.03.023.

[225] H. X. Chang, L. H. Tang, Y. Wang, J. H. Jiang, and J. H. Li. Graphene Fluorescence Resonance Energy Transfer Aptasensor for the Thrombin Detection. *Anal. Chem.*, 82(6):2341–2346, 2010. doi: 10.1021/ac9025384.

[226] L. Sheng, J. Ren, Y. Miao, J. Wang, and E. Wang. PVP-coated graphene oxide for selective determination of ochratoxin A via quenching fluorescence of free aptamer. *Biosens. Bioelectron.*, 26(8):3494–3499, 2011. doi: 10.1016/j.bios.2011.01.032.

[227] Y. Shi, W. T. Huang, H. Q. Luo, and N. B. Li. A label-free DNA reduced graphene oxide-based fluorescent sensor for highly sensitive and selective detection of hemin. *Chem. Commun.*, 47 (16):4676–4678, 2011. doi: 10.1039/c0cc05518b.

[228] W. H. Wu, H. Y. Hu, F. Li, L. H. Wang, J. M. Gao, J. X. Lu, and C. H. Fan. A graphene oxide-based nano-beacon for DNA phosphorylation analysis. *Chem. Commun.*, 47(4):1201–1203, 2011. doi: 10.1039/c0cc04312e.

[229] C. H. Liu, Z. Wang, H. X. Jia, and Z. P. Li. Efficient fluorescence resonance energy transfer between upconversion nanophosphors and graphene oxide: a highly sensitive biosensing platform. *Chem. Commun.*, 47(16):4661–4663, 2011. doi: 10.1039/c1cc10597c.

[230] J. Li, C. H. Lu, Q. H. Yao, X. L. Zhang, J. J. Liu, H. H. Yang, and G. N. Chen. A graphene oxide platform for energy transfer-based detection of protease activity. *Biosens. Bioelectron.*, 26(9):3894–3899, 2011. doi: 10.1016/j.bios.2011.03.003.

[231] Q. Mei and Z. Zhang. Photoluminescent Graphene Oxide Ink to Print Sensors onto Microporous Membranes for Versatile Visualization Bioassays. *Angew. Chem. Int. Ed.*, 51(23):5602–5606, 2012. doi: 10.1002/anie.201201389.

[232] S. Deng, J. Lei, L. Cheng, Y. Zhang, and H. Ju. Amplified electrochemiluminescence of quantum dots by electrochemically reduced graphene oxide for nanobiosensing of acetylcholine. *Biosens. Bioelectron.*, 26(11):4552–4558, July 2011. doi: 10.1016/j.bios.2011.05.023.

[233] Y. Wang, J. Lu, L. H. Tang, H. X. Chang, and J. H. Li. Graphene Oxide Amplified Electrogenerated Chemiluminescence of Quantum Dots and Its Selective Sensing for Glutathione from Thiol-Containing Compounds. *Anal. Chem.*, 81(23):9710–9715, 2009. doi: 10.1021/ac901935a.

[234] K. Wang, Q. A. Liu, X. Y. Wu, Q. M. Guan, and H. N. Li. Graphene enhanced electrochemiluminescence of CdS nanocrystal for H2O2 sensing. *Talanta*, 82(1):372–376, 2010. doi: 10.1016/j.talanta.2010.04.054.

[235] Y. S. Guo, X. P. Jia, and S. S. Zhang. DNA cycle amplification device on magnetic microbeads for determination of thrombin based on graphene oxide enhancing signal-on electrochemiluminescence. *Chem. Commun.*, 47(2):725–727, 2011. doi: 10.1039/c0cc03266b.

[236] X. P. Chen, H. Z. Ye, W. Z. Wang, B. Qui, Z. Y. Lin, and G. N. Chen. Electrochemiluminescence Biosensor for Glucose Based on Graphene/Nafion/GOD Film Modified Glassy Carbon Electrode. *Electroanalysis*, 22(20):2347–2352, 2010. doi: 10.1002/elan.201000095.

[237] Y. J. Guo, L. Deng, J. Li, S. J. Guo, E. K. Wang, and S. J. Dong. Hemin-Graphene Hybrid Nanosheets with Intrinsic Peroxidase-like Activity for Label-free Colorimetric Detection of Single-Nucleotide Polymorphism. *ACS Nano*, 5(2):1282–1290, 2011. doi: 10.1021/nn1029586.

[238] Y. J. Song, K. G. Qu, C. Zhao, J. S. Ren, and X. G. Qu. Graphene Oxide: Intrinsic Peroxidase Catalytic Activity and Its Application to Glucose Detection. *Adv. Mater.*, 22(19):2206–2210, 2010. doi: 10.1002/adma.200903783.

3 Materials and methods

3.1 Chemicals and materials

3.1.1 Sources and safety

All chemicals, except graphite and solutions for capillary electrophoresis (CE), were purchased from Merck (Darmstadt; www.merck.de). They were of analytical grade and used without further purification. Graphite (99%) was from Thielmann Graphite GmbH (Grolsheim; www.kwthielmann.de). Only ultrapure water was used for synthesis and solutions. The used CE-standard (4-hydroxyacetophenone) and buffer solution (borat, 20 mM, pH 9.3) were purchased from Agilent Technologies (www.agilent.com).

In the following, high concentrated acids and bases (corrosive), and oxidation agents are used which require careful handling and appropriate protective equipment (glasses, coat, gloves). All solids, especially potassium permangate, have to be added to the liquid sulfuric acid instead of the reverse. Also the mixture will get very hot due to the oxidation process. Special care should be taken with sodium azide (very toxic). Azido-products may be explosive, especially if dried. The side-products of this synthesis require special disposal.

3.1.2 Graphene oxide, GO

Graphite was oxidized by a modified Hummers method to obtain water-soluble graphite oxide[1]. Briefly, graphite (100 mg) and sodium nitrate (100 mg) were added into 5 mL of fuming sulfuric acid (97-98%). Then, solid potassium permanganate (1 g) was slowly added to form the green manganate dimer (Mn_2O_7). The mixture

was stirred for 3 days, diluted with sulfuric acid (5%; warning: this has to be done with extreme caution; the process is highly exothermic) and heated for 3 h to about 100-120 °C. After slow addition of 1 mL of hydrogen peroxide (30%), the resulting solid was collected by centrifugation and washed five times with sulfuric acid (3%) and hydrogen peroxide (3%), two times with hydrochloric acid (3.7%) and two times with water. Ions remaining in the solution were removed by dialysis against ultrapure water (3 days; water was changed every day). The water was removed by lyophilization to yield ∼50 mg of water-soluble graphite oxide in the form of a light brown powder. The purity was checked by elementary analysis. The amount of sulfur, nitrogen and chloride was under wt 0.1% each. Solutions of exfoliated graphene oxide are obtained by dissolving small amounts of graphite oxide in water (e.g. 0.5 mg mL^{-1}).

3.1.3 Reduced graphene oxide, rGO

The reduction is based on the method published by *Stankovich et al.* before[2]. A clear solution of graphene oxide was prepared by sonification of 25 mg of graphite oxide in 25 mL water. After the addition of 25 µL of hydrazine solution (98%) and 50 µL of ammonia (32%), the mixture was stirred for 15 minutes and subsequently heated for 2 h to about 100-120 °C. Ions and reagents remaining in the solution were removed by dialysis against ultrapure water over 3 days. The dialysis water was changed every day. The water of the solution was then removed by lyophilization to yield ∼12 mg of reduced graphite oxide in the form of a black solid. The purity was checked by elementary analysis. The amount of nitrogen is usally under wt 3.0%. Solutions of exfoliated reduced graphene oxide are obtained by dissolving small amounts of reduced graphite oxide in water (e.g. 0.1 mg mL^{-1}).

3.1.4 Azido graphene oxide, N_3-GO

A clear solution of graphene oxide was prepared by sonification of 100 mg of graphite oxide in 35 mL water. 500 mg of sodium azide were added, and the solution was stirred for three days. Subsequently, it was heated for 2 h to about 100-120 °C. Ions

and reagents remaining in the solution were removed by dialysis against ultrapure water over 3 days. The dialysis water was changed every day.

For examination of the product by FT-IR and elementary analysis, only a small amount of the solution was lyophilized. The successful introduction of the azido group was confirmed by infrared spectroscopy (azide specific vibration at 2126 cm^{-1}). The purity was checked by elementary analysis. The amount of nitrogen is usally about wt 1.6%. For experiments with capillar electrophoresis (see Section 7.4.4) the fresh dialyzed solution was used.

3.1.5 Graphene oxide ethyl ester, GOEE

GO ethyl ester (GOEE) was prepared by adding 1-ethyl-3-(3-dimethylaminopropyl)-carbodiimide (5.0 mg), N-hydroxysuccinimide (2.8 mg) and ethanol (1 mL) to a solution of GO (5 mL; 0.5 mg mL^{-1})[3]. The solution was stirred at room temperature for 12 h. Remaining ions and agents were removed by dialysis against ultrapure water (3 days; water was changed every day). This solution was diluted (1:40) with the corresponding buffer solutions.

3.1.6 Britton-Robinson buffers

Britton Robinson buffers of varying pH values and concentrations were used for fluorescence and Raman measurements. In order to obtain these, 22.60 mL of 85% ortho-phosphoric acid, 19.07 mL of 100% acetic acid and 20.74 g of boric acid were dissolved in water and filled up to 1 liter to create a stock solution of 1 M. This stock solution was diluted and adjusted with sodium hydroxide and hydrochloric acid, respectively, controlled by a pH meter to obtain the desired solutions of 10 mM.

3.2 Instrumentation

pH measurements. A digital pH meter type *CG 842* (SI Analytics GmbH, www.si-analytics.com) was calibrated with standard buffers of pH 4.00 and pH 7.00 (Carl Roth, Karlsruhe, www.carlroth.com) at 20-60(±2) °C. It was used for pH-titrations and checking of buffer solutions.

Absorption spectroscopy. UV/Vis spectra were acquired on a *Varian Cary 50 Bio* (Agilent Technologies; www.varianinc.com) and FT-IR spectra on an *Excalibur FTS 3000 Mx* (Bio-Rad Laboratories; www.bio-rad.com).

Fluorescence spectroscopy. Luminescence spectra and excitation/emission matrices (EEMs) were acquired on a *Aminco Bowman Series 2* (Thermo Spectronic; www.thermo.com) luminescence spectrometer with *AB2 Luminescence Spectrometer V 5.30* software. Each EEM was obtained by incrementing the excitation wavelength from 300 to 500 nm in 2-nm-steps. The respective emission spectra were scanned at an offset of 20 nm from the excitation wavelength up to 600 nm in 1-nm-steps. The fluorescence intensities at various pH values strongly differ, so that the sensitivity of the detector for each pH had to be adjusted. Except for pH 10.1, the sensitivity was set in such a way that the intensity at 470/550 nm was about 85% of the maximum signal of the detector. The maximum sensitivity of the detector has been used at pH 10.1.

Raman spectroscopy. All Raman spectra except the ones in Section 5.4 were measured on a *DXR Raman-Microscope* (532 nm, Thermo Fisher Scientific; www.thermofisher.com) at 8 mW CW. The spectra in Section 5.4 were collected by *Stefanie Heydrich* (workgroup of Prof. C. Schüller, Physics Department) with an argon ion laser (at 488 nm, CW) in a self-build setup.

Resistance measurements. Resistance measurements were performed using a self-built device set up and maintained by *Alexander Zöpfl*[4]. The setup consists of a gas mixing device with three mass flow controller (Unit Instruments: 1x UFC-8160A; 1x UFC-1660), which provided a constant flow rate at 100 sccm. Simultaneously, the resistance was measured with a *Keithley 2400 sourcemeter* at a constant bias voltage

of 50 mV. The temperature of the flow cell was kept constant at 85 °C. All gases used, were purchased from Linde AG (www.linde-gas.de). Synthetic air (N_2: 80%, O_2: 20%) was used as carrier gas and was mixed with a testgas of 300 ppm NO_2 or a testgas of 3000 ppm CO_2 to obtain desired gas concentrations.

Surface plasmon resonance measurements. All measurements were done with a *Biosuplar 6 surface plasmon resonance spectrometer* (Sinzing; www.biosuplar.com). Refractive index of calibration solutions (NaCl, 100 mM and 200 mM) were determined with a *Zeiss Abbe-Refractometer* (Jena, www.zeiss.de).

Miscellaneous characterization methods. TEM pictures were acquired by *Heiko Ingo Siegmund* at the Institute of Pathology of the Universitätsklinikum Regensburg on a *LEO 912AB/ZEISS device*. SEM pictures were take on a Zeiss SEM-device at the workgroup of Prof. D. Weiss (EHT 7.00 kV, WD 6.8 mm). Auger-ESCA (XPS) was done with the help of *Matthias Sperl* (workgroup of Prof. C. Back). TGA and also some XPS-measurements were acquired by Infineon (Regensburg; www.infineon.com; collaboration with *Dr. Günther Ruhl*).

Conditioning. For dialysis, Visking hoses (type: 8/32", wall: 0.05 mm, width: 10 mm, diameter: 6.3 mm, MWCO: 14 000 Da) purchased from Carl Roth (Karlsruhe; www.carlroth.com) were used. For mass-separation, a *Universal 320-centrifuge* from Hettich-Zentrifugen (Tuttlingen; www.hettich-zentrifugen.de) was used. For all CE-experiments, a capillary electrophoresis system (with diode array detector) from Agilent Technologies (Böblingen; www.agilent.com) was used.

3.3 References

[1] W. S. Hummers and R. E. Offeman. Preparation of Graphitic Oxide. *J. Am. Chem. Soc.*, 80(6): 1339–1339, March 1958. doi: 10.1021/ja01539a017.

[2] S. Stankovich, D. A. Dikin, R. D. Piner, K. A. Kohlhaas, A. Kleinhammes, Y. Jia, Y. Wu, S. T. Nguyen, and R. S. Ruoff. Synthesis of graphene-based nanosheets via chemical reduction of exfoliated graphite oxide. *Carbon*, 45(7):1558–1565, June 2007. doi: 10.1016/j.carbon.2007.02.034.

[3] Z. Liu, J. T. Robinson, X. Sun, and H. Dai. PEGylated Nanographene Oxide for Delivery of Water-Insoluble Cancer Drugs. *J. Am. Chem. Soc.*, 130(33):10876–10877, 2008. doi: 10.1021/ja803688x.

[4] Alexander Zöpfl. Studies of Graphene and its Modifications for Sensor Applications. Master thesis, Institute of Analytical Chemistry, Chemo- and Biosensors; University of Regensburg, 2012.

4 Characterization of materials

4.1 Overview

The general aim of characterization is to confirm and improve ideas and models of the materials synthesized. Well-defined models and structures not only tell things about a specific point (here: (r)GO) in a reaction chain, but details about the precursor (graphite), possible products (modifications), and also about the reactions and procedures between them.

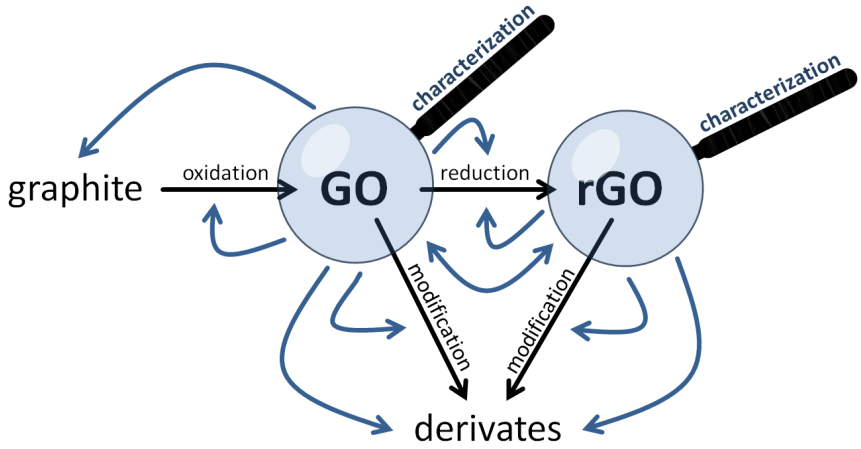

Figure 4.1. The examination and characterization of (r)GO not only provides information on the materials themselves, but also on all coupled/derived materials and processes (blue arrows).

Many optical and electrochemical methods provide easy ways of confirming or falsifing the structure of the materials created in Chapter 3. Unfortunally, these materials do not simply consist of a single defined molecular structure but of many different and complex ones. Thus, every method not just generates particular “peaks” but an average response on the optical or electrical treatment.

However, the particular results still reveal many elements about the structure, i.e. bounding, groups, defects, etc. Collectively, every response is part of a bigger picture which must be pieced together in the end to achieve an overall model.

4.2 Dispersion vs. solution

It is sometimes confusing whether a "solution of (reduced) graphene oxide" is really a *solution* or rather a *dispersion* (more exact: *suspension*). In literature, both terms are equally used[1].

The origin of the word *dispersion* is the latin verb *dispergere*, which means *to scatter*. In chemistry, *dispersion* usually refers to a heterogenous mixture of colloid particles in a liquid. Light is scattered by these particles and the mixture appears turbid. The color of the mixture depends on the wavelength(s) of the scattered light, since not all light is scattered equally (*Tyndall effect*)[2]. When the particles are very small (dimensions of molecules), the mixture becomes homogeneous and transparent. It is then called *solution*. In contrast to *dispersions*, light is not (or negligibly) scattered and the color of the *solution* depends on the absorption of light, only.

So, both of these definitions are very different cases of solid-liquid mixtures. However, (r)GO represents an intermediate case. With the aid of sonification, even large flakes can be exfoliated in water[3]. The resulting mixtures are transparent and homogeneous, and have absorption in the visible region (see UV/VIS-sections below). Therefore, the resulting mixture resembles a *solution* more than a *dispersion*. Thus, in the following, it is treated as such.

4.3 Graphene oxide

Note: This section is concerned with the characterization of graphene oxide prepared as described in Section 3.1.2. In the following "graphite oxide" refers to the solid material used directly from the synthesis whereas "graphene oxide" refers to the exfoliated material in solutions or thermally dried solutions (e.g. for TEM). The fluorescence and Raman spectroscopy results of GO are discussed in Chapter 6 and 5, respectively.

4.3.1 Properties of graphite oxide (solid)

Graphite oxide is a pilous, brown solid. Its crystal morphology is hard to describe because the major part resembles a branch-like structure but very disordered. Large flat regions also exist which, in contrast, appear organized. Although the branches "grow" isotopically, every detail of the material is actually flat and planar evolving a large surface area (see Figure 4.2).

As with most crystal structures, the macroscopic morphology reflects the micro- and nano-scopic structure. Graphene oxide is considered a 2D material. Therefore, it makes perfect sense that the bulk material, graphite oxide, forms flat structures as described above.

The branch-like isotropical growth probably is due to the strong electrostatic behavior of graphite oxide. Its surface is highly polarized because of a large fraction of oxide groups such as carboxy acids and hydroxy groups. In consequence, a electrostatic repulsion force between different planes keeps them away from each other by far.

In solution, the same repulsion allows the preparation of stable solutions in water[4]. Some of the solutions prepared during this thesis are stable for 3 years now. However, they must be kept in the dark because UV light greatly reduces solubility and leads to precipation (see Section 4.3.3 for an explanation). It is possible to solve up to 8 mg mL^{-1} of graphite oxide in water. Apart from water, graphite oxide is also soluble in some organic solvents[1].

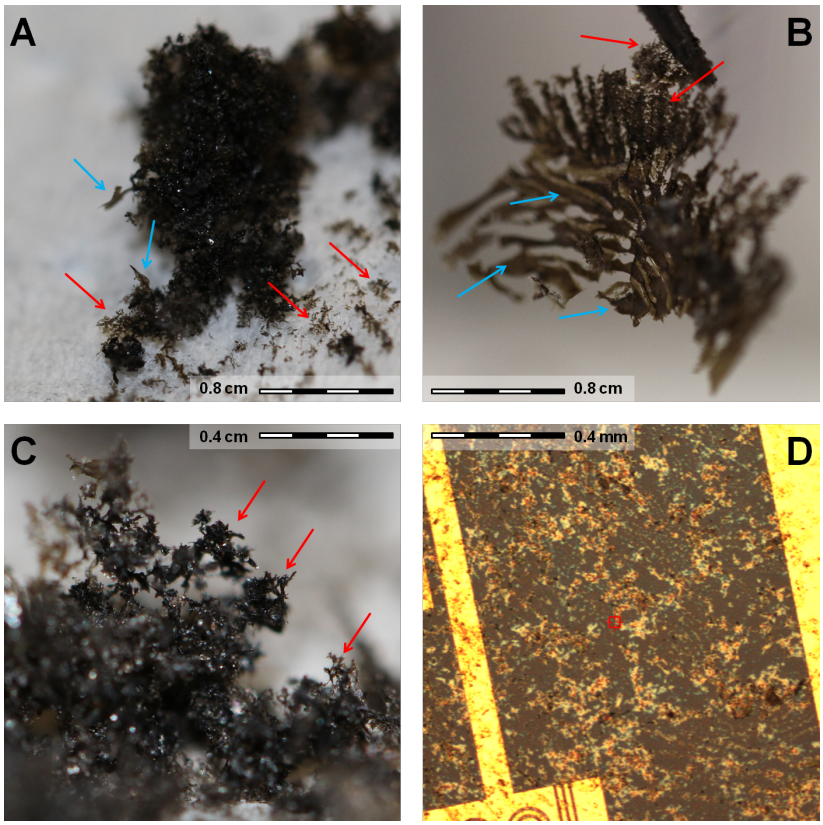

Figure 4.2. Photos (A-C) and a microscopic picture (D) of graphite oxide. Red arrows mark some of the more disordered (small branch-like) regions, whereas the blue arrows point to the more organized, flat regions. Every detail of the material is actually flat and planar (C).

Not surprisingly, graphite oxide is very hygroscopic due to its many oxide groups. Taking 60 min after lyophilization as reference point, the mass grows by ∼18-25% in the first 5 days. Most of the mass increment caused by water absorption happens in the first 24 hours.

4.3.2 Elementary analysis (CHNX)

Combustion analysis is a standard analytical method which provides an easy and fast way to get an overview over some basic elements (C,H,N plus sulfur and halogenes) in substances. The purity of any material therefore can be judged by looking at the ratio of sulfur, nitrogen and chloride.

Table 4.1 shows typical elementary results for graphite oxide prepared as described in

Section 3.1.2. The atomic ratio can be calculated from the listed mass fractions. For instance, for the first line a ratio of C:H:O of 100:74:93 is found. Taking the hygroscopy into account, up to 25% of the mass of graphite oxide is water. Therefore, it makes sense to substract water from the initial ratio. Assuming that the found hydrogen fraction completely belongs to water, 37 water units must be removed for the above example, leaving a C:O ratio of 100:56. Recalculation of the fraction mass results in 25-30% for water which is reasonable. Hence, this "water-correction" is executed for all analysis findings in this work (see Table 4.1).

Table 4.1. Combustion analysis of graphene oxide prepared as described in Section 3.1.2. Listed are the mass fractions of the particular elements. [a]Values below 0.1% are not determinable. i.e. these elements are neglected for further calculations. [b]Oxide is not directly determinable. It is the total residual. [c]Calculated without water-correction. [d]Calculated with water-correction. [e]The fraction mass of water is calculated by assigning all hydrogen to water.

#	Mass [mg]	C [%]	H [%]	S, N, Cl [%]	O[b] [%]	C:O:H[c]	C:O[d]	Water[e] [%]
1	2.544	43.42	2.66	< 0.1[a]	53.92	100:74:93	100:56	25.91
2	2.411	43.24	2.75	< 0.1[a]	54.01	100:76:94	100:56	26.76
3	2.392	43.09	2.90	< 0.1[a]	54.01	100:81:94	100:54	28.18
4	2.237	42.92	3.00	< 0.1[a]	54.08	100:84:95	100:53	29.13
5	2.042	43.30	2.60	< 0.1[a]	54.10	100:72:94	100:58	25.34
6	3.050	43.38	2.75	< 0.1[a]	53.87	100:76:93	100:55	26.76

X-ray photoelectron spectroscopy (XPS) reveals similar (uncorrected) ratios of C:O (e.g. 100:86 for batch 4). However, due to the fact that hydrogen cannot be detected with this technique, there is no criterion for the amount of absorbed water. Thermogravimetric analysis (TGA) confirmes the high water content.

Other researchers find similar proportions (2:1) of carbon and oxygen in their materials[1]. Though, they all use different synthesis and purification techniques. Additionally, it is unclear wether and how they perform similar corrections for water or gases such as carbon dioxide (see IR spectroscopy, 4.3.4). This makes it difficult to draw conclusions.

In contrast, the ratios in Table 4.1 are very comparable to each other. Actually, all batches of graphite oxide set up during this work result in the same numbers for carbon and oxygen. This is independent of small variations and of scaling. This exposes the

robustness of the synthesis.

4.3.3 UV/VIS absorption spectroscopy

The UV absorption spectrum of graphene oxide exhibits one broad band with a maximum at 228 nm and a shoulder at 300 nm which can be assigned to the π-π* transition of C=C (aromatic) and the n-π* transition of carbonyl groups, respectively (see Figure 4.3). The absorption then slowly decays but extends towards into the visible. This is causing the orange/brown color of the solution.

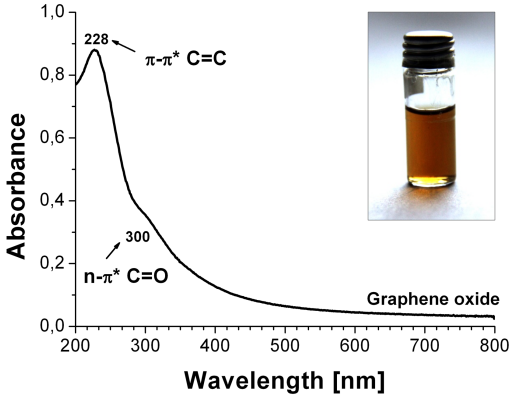

Figure 4.3. UV/Vis spectra of graphene oxide revealing a disturbed π-π-system. The inlet shows a photo of a typical orange/brown solution.

The corresponding absorption coefficients can be calculated with the Beer-Lambert law. It is displayed in Equation 4.1, where β is the concentration in $mg\ mL^{-1}$ (here: 1 mg mL^{-1}), d is the path length of the cuvette in which the sample is contained (here: 1 cm) and ϵ_m is the absorption coefficient in $mL\ mg^{-1}\ cm^{-1}$.

$$A(\lambda) = \epsilon_m(\lambda) \cdot d \cdot \beta \tag{4.1}$$

The calculated coefficients for the wavelengths 228 nm, 300 nm and 700 nm are 0.88 mL mg^{-1} cm^{-1}, 0.36 mL mg^{-1} cm^{-1} and 0.04 mL mg^{-1} cm^{-1}, respectively. That implies a 22-fold higher absorption in the UV-region than in the visible region!

Moreover, the high absorption in the UV region (228 nm and 300 nm) is responsible

for a decomposition process in graphite oxide[5]. During this process, the color of the material gets darker. Additionally, CO and CO_2 (1:3) are released. Also solutions of graphene oxide kept in daylight tend to precipate and agglomerate. In contrast, solutions kept in the dark are stable for up to 3 years (see Section 4.3.1).

The stability of solutions depends on electrostatic interactions (repulsion) which is attributed to the negative charges of carboxy acids and hydroxy groups[4]. Due to this, it can be concluded that the decomposition involves mainly these groups. The whole process partly reduces graphene oxide this way. However, it introduces irreparable holes in the lattice by eliminating carbon atoms, so the material should always kept in the dark.

4.3.4 Infrared spectroscopy

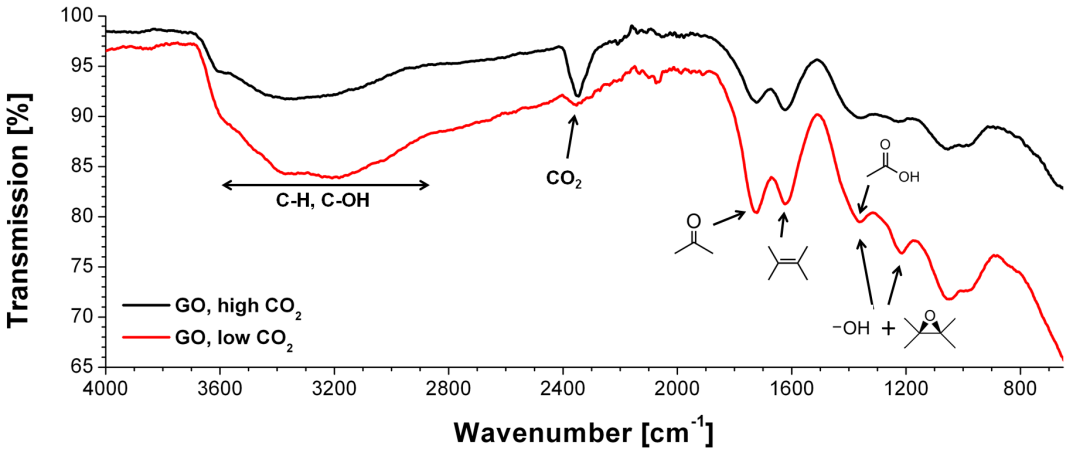

Figure 4.4. Infrared spectrum of graphene oxide revealing the presence of various oxygen functions.

The FT-IR spectrum indicates the presence of aldehydes and/or ketones (at 1728 cm^{-1}) and of aromatic C=C double bonds (at 1618 cm^{-1}). Weaker bands can be found that are assigned to hydroxy (1364 cm^{-1}) and epoxy (1225 cm^{-1}) groups. The broad band between 2866 cm^{-1} and 3607 cm^{-1} indicates the presence of aliphatic and aromatic C−H and O−H stretch vibrations[6].

The infrared spectra in Figure 4.4 show that graphene oxide absorbes and saves carbon

dioxide. In the spectra of the CO_2-rich sample a characteristic peak appears, viz. 2349.5 cm^{-1} which matches the typical CO_2-band (2349.4 cm^{-1})[7]. This peak also appears in the low-CO_2-spectra but its intensity is tiny.

The absorption of carbon dioxide is slightly examined[8,9]. At room temperature about 3 wt % are saved by (reduced) graphene oxide[9]. One CO_2 molecule corresponds to 2 wt % of the C:O ratio of 100:56 developed in Section 4.3.2, i.e. between 1 and 2 molecules are saved per 100 carbon atoms. If one CO_2-unit is subtracted from the ratio and re-normalized again to 100 carbon atoms the ratio becomes 100:55, and 100:53 for two units. The difference in both cases is negligible, so a "carbon-dioxide-correction" is omitted in this work.

The absorption of carbon dioxide depends on both temperature and on the number of layers[8]. At 195 K a monolayer saves up to 37.93 wt % of CO_2. In contrast, four layers save just 13.25 wt %. Theoretically, with surface infrared spectroscopy it should be possible to determine the number of layers of graphene oxide by measuring the intensity ratios of the CO_2-peaks and various GO-peaks. A reliable and fast optical method is in demand since Raman spectroscopy of GO does not provide similar information on the number of layers such as for pristine graphene (see Chapter 5). However, the feasibility and the reliability of this (possible) method have yet to be examined.

4.3.5 Electron microscopy

Examinations with scanning electron microscopy (SEM) and tunneling electron microscopy (TEM) clearly point to a limitation of the Hummers method. It provides easy access to (reduced) graphene oxide with only a few steps and low costs for source materials. However, the inhomogenity in shape and size of the resulting "chaotic" product with its ill-defined structure is disadvantageous (see Figure 4.5).

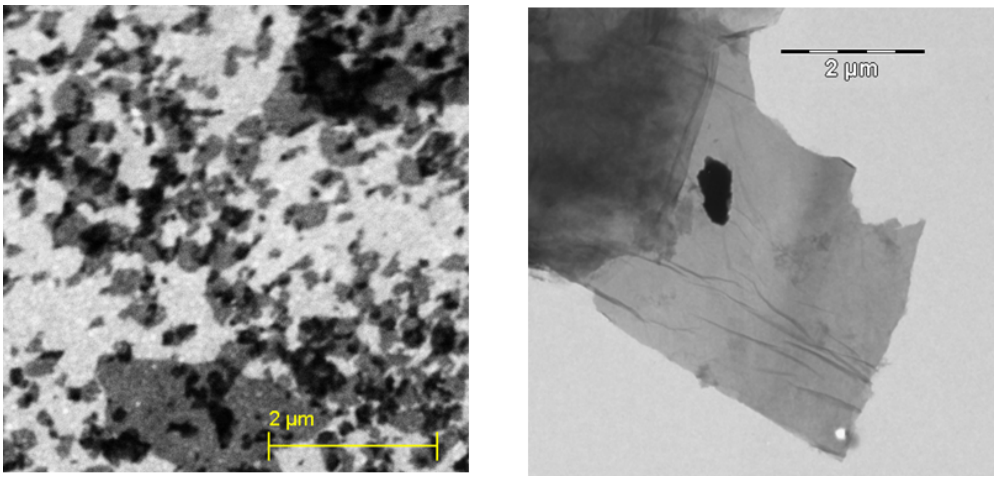

Figure 4.5. Distribution of shape and size of graphene oxide: The SEM (left) shows that flakes differ in shape and size. The TEM (right) shows a larger flake. Clearly visible are the folding lines and also some aggregates on top of the flake.

4.3.6 pH titration

The first researchers referred to graphite oxide as "graphitic acid" (see also Chapter 1) due to its properties[10]. It seems natural to explore this acidity of graphene oxide by simple pH titration but it is only done occasionally in literature[11,12]. Solutions of graphene oxide usually show pH levels between 3.5 and 4.5.

The titration plot of graphene oxide is very clear and linear at a first glance. If the titration is performed with great care, a wave-like curve between a pH of 3.9 and 9.5 is formed and two unobtrusive equivalence points appear (see Figure 4.6A). It is understood that a linear titration plot is a feature of an acid with multiple pK_a values near to each other, e.g. citric acid. Therefore, it is difficult to estimate each individual pK_a but the two at 4.7 and 6.7. From pH 9, the curve linearly increases to a pH of 11.1, which originates from the "pure" base.

The two pK_a values, 4.7 and 6.7, are believed to be average representations of various ones. No additional values are found if graphene oxide is titrated with HCl (10 mM). In accordance to the pH dependent fluorescence (see Figure 4.6B) the first one is assigned to carboxy groups.

The other one is not easy to assign. Screening of small molecules and their pK_a-values reveals both examples for carboxy and for hydroxy groups with the respective pK_a

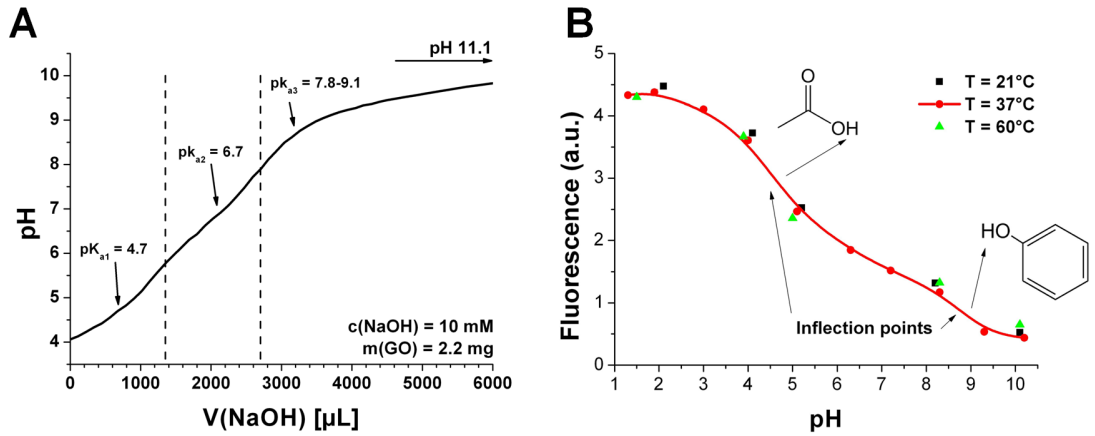

Figure 4.6. (A) Titration plot of graphene oxide (2.2 mg) using a 10 mM solution of NaOH. It shows the two unobtrusive equivalence points. Since there is no hint for the "last" point, it is not possble to assign an eventual third pK_{a3} value, clearly. (B) Fluorescence intensity of GO plotted as function of the pH value of the solution at various temperatures. The two inflection points are assigned to the dissociation of the carboxy groups (at 4.5) and the phenolic hydroxy groups (at 8.8), respectively. For more informations, see Chapter 6.

constants exist (cf. fluorescein, mellitic acid, several naphthalene derivates). Therefore, it is impossible to clearly assign. Also, there is a chance that both hydroxy and carboxy elements are responsible for this constant. Interestingly, this group does not contribute at all or only slightly to the fluorescence intensity. This fact implies that the responsible groups could be bonded to defect sites (i.e. sp^3 or isolated sp^2 regions) of graphene oxide.

A short linear region after the second equivalence point can be assigned to the hydroxy groups of graphene oxide. Unfortunately, the third equivalence point is hard to find, so the corresponding pK_a is probably a value between 7.8 and 9.1. Since the titration plot increases linearly after a pH of 9.1, it is difficult to see wether other hydroxy groups are dissociating. Considering model molecules such as naphthol or phenol or the like with pK_a values ranging from 9 to 10, more groups in graphene oxide could exist, eventually. A total pK_a of 9.0 for the hydroxy groups can be calculated if an average pK_a of 9.5 is estimated for the last region. This almost perfectly matches the results of the pH dependent fluorescence measurements. However, for good measure the titration end is considered the point at pH 9.1.

Molecules screened for comparance have structure elements that occur on graphene oxide. Some of them are sketched in Figure 4.7. By considering the various influences

on the acidity of a proton-donating group, it is clear why graphene oxide possesses multiple different pK_a values, resulting in a near-to-linear titration plot.

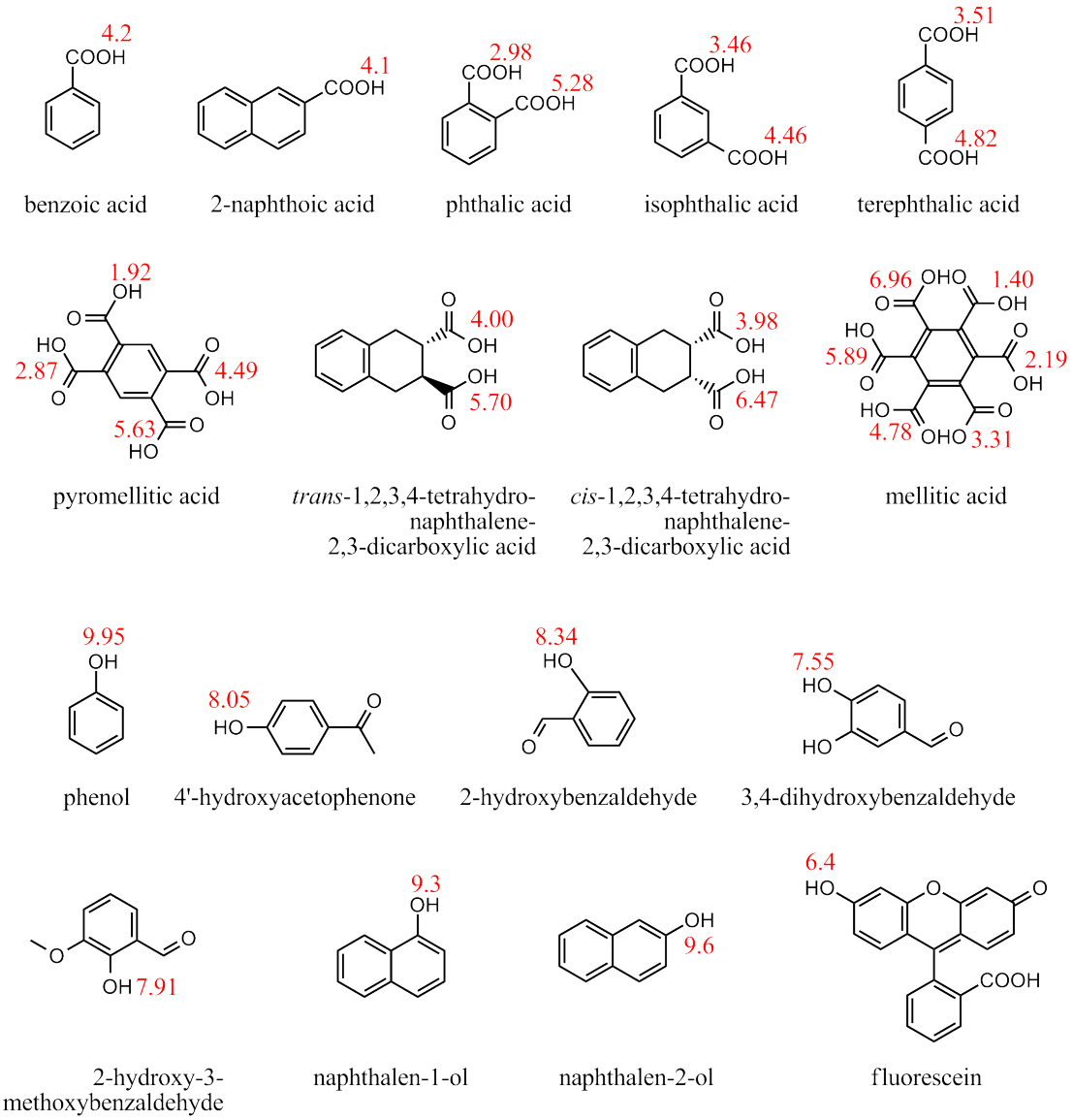

Figure 4.7. Model molecules for assignment of the pK_a of graphene oxide. The red numerals show the corresponding pK_a of the groups. For clarification not all values are listed. Values taken from ref. 13.

The end point (pH 9.1) is at 3600 µL titration volume, which is equal to 36 µmol protons per 2.2 mg of GO. If the acidic oxygen groups are considered as criterion for numbering of graphene oxide "molecules", the proton concentration can be inversed to a molar mass of about 61.11 g mol^{-1} ($\sim C_3O_{1.5}$) for graphene oxide.

Assuming that every hydrogen is bond to oxygen and, therefore, is exchangeable at appropriate pH levels, the number of total hydrogen is 18 µmol per mg of GO. This assumption is suggested by the difference in the reactivity of carbon atoms in the synthesis (see Chapter 7). In particular, the most reactive carbon atoms are at the edge and defect (e.g. sp^3) sites, i.e. they are preferentially oxidized as high as possible leaving no (direct, i.e. from carbon to hydrogen) bonds for hydrogen atoms. In contrast, non-reactive atoms stay in their orginal sp^2 state with all bonds to other carbon atoms.

36 µmol of protons correspond to 1.05 µmol of GO ($C_{100}O_{56}$, 2096 g mol^{-1}), in other words, there are 34 hydrogen atoms per GO-block, resulting in a C:O:H ratio of 100:56:34, which seems reasonable. Last, the ratio of carboxy and hydroxy groups can be estimated. For the carboxy groups all protons from 0 to 1350 µL in the titration plot are counted, and for the hydroxy groups all protons from 2700 to 3600 µL, respectively. The area in between is evenly parted for both types, so additional 675 µL each. That leads to a ratio of 9:7. If this result is included in a sum formula for the GO-block above, it can be written as $C_{81}O_3(OH)_{15}(COOH)_{19}$.

4.3.7 Piece together the puzzle

Elementary analysis provides the ratio of carbon to oxygen (100:56) for GO. This ratio is actual very high and implies that (on average) every second carbon atom carries an oxygen atom! The results of the optical methods (IR, UV/VIS, fluorescence) and pH-titration lead to the conclusion that the oxides mainly consists of carboxy acids, hydroxy groups and some epoxy groups.

However, Raman spectroscopy clearly reveals the existence of large crystalline planes in graphene oxide. Crystalline planes do not possess any oxygen at all. Due to this, other regions have to compensate this zero-oxygen zones to result in an average C:O ratio of 100:56. In other words, there have to be highly oxidized regions, which even surpass the previously mentioned ratio of 100:56!

Taking the GO-block of the pH-titration as basis ($C_{81}O_3(OH)_{15}(COOH)_{19}$) and count-

ing the three remaing oxygen as epoxy groups, the ratio of crystalline C to oxidized C is exactly 1.5 (60:40). Let us consider a zone of 200 oxidized carbon atoms. These 200 atoms "support" another 300 crystalline atoms. On average, 500 carbon atoms carry 280 oxygen atoms, altogether. However, these have to be only assigned to the oxidized carbon atoms resulting in a ratio of 200:280 (C:O)! Of course, this is one of two extremes, and very probably intermediate C:O ratios are present between the highly oxidized and non-oxidized zones.

All the data was compiled into a model for graphene oxide presented in Figure 4.8. The form and size is derived from one of the TEM pictures shown before. Since it is near to impossible to sketch a whole flake on the molecular level, this model consists of a pixelated map. The color of the pixels represent the oxidation level at the particular points to give an impression about the distribution of oxygen on the surface.

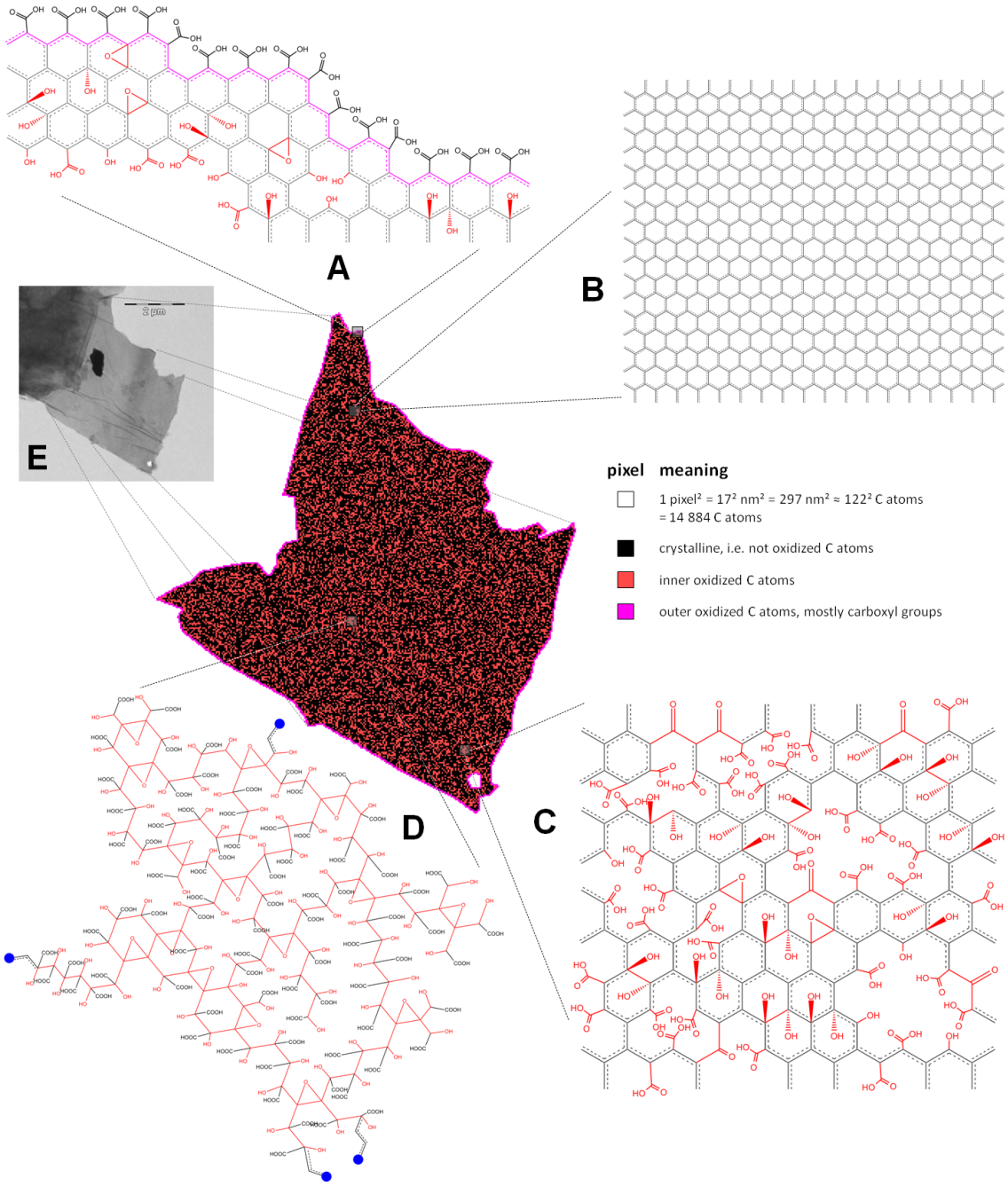

Figure 4.8. A representative flake (area: ∼13 µm^2) derived from the shown TEM picture (E). Every pixel represents an area of 17 nm by 17 nm. The color of the pixel scales the oxidation level of the corresponding region (see bottom right corner). Three different regions are detailed: The border region (A) is created by the scissor effect of the manganese oxides and, therefore, mostly possesses carboxy groups. Large crystallite zones (B) exist, i.e. non-disturbed sp^2-systems. These areas are enclosed in heavily oxidized segments (C,D). The depicted segments display (C) an average C:O ratio of 100:56 and (D) a near-to-maximum C:O ratio of 202:258. The blue dots in the latter segment emphasize the very few connections to the remaining graphene oxide system.

4.4 Reduced graphene oxide

Note: This section is concerned with the characterization of reduced graphene oxide prepared as described in Section 3.1.3. The Raman spectroscopy part of rGO is discussed in Chapter 5. Conductometry of rGO is discusses in Section 8.2.

4.4.1 Properties of reduced graphite oxide (solid)

Reduced graphite oxide is a black, crystalline powder (see Figure 4.9). It does not possess the complex crystal morphology of graphite oxide but shares a similar repulsion force at the surface.

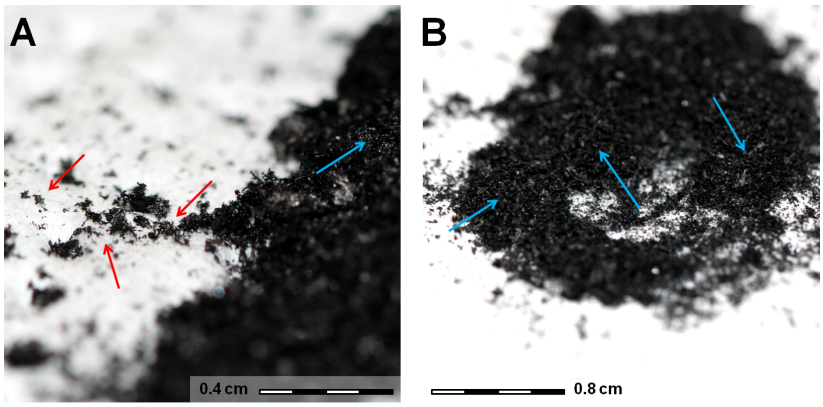

Figure 4.9. Two photos of reduced graphite oxide. It possesses a black texture and a shiny, metallic glare. The overall material is crystalline (blue arrows) but similar to graphite oxide has some small, disturbed features (red arrows).

In contrast to graphite oxide, the oxygen:carbon ratio is much lower. Since the oxygen groups are considered the source of the repulsion force, it can be concluded that this force is decreased. Combined with more interplanar forces such as π-π stacking in consequence of the reduction and recovering process, the crystalline structure of reduced graphite oxide seems reasonable. Still, the smaller repulsion force allows the preparation of stable solutions in water (up to 2 mg mL^{-1}). Some of the solutions prepared during this work are stable for 2 years now. However, the same storage conditions as for graphene oxide solutions must be maintained. Similarly, UV light reduces solubility and leads to precipation. Last, the bulk resistantivity is lowered

($\sim$ 2-5 kΩ) compared to graphite oxide ($\sim$ 150 kΩ). Electrons are considered to move more unimpeded in reduced graphite oxide due to the recovering of large parts of the π-system.

4.4.2 Elementary analysis (CHNX)

Table 4.3 shows typical elementary results for reduced graphite oxide. The materials investigated were prepared as described in Section 3.1.3. The atomic ratio can be calculated from the listed mass fractions. For instance, for the first line a ratio of C:H:O:N of 100:59:45:4 is found. Reduced graphite oxide is more hydrophobic. Therefore, only small fractions of water are found and corrected. In case of the above example, 30 water units must be removed, leaving a C:O:N ratio of 100:15:4 (see Table 4.3). This result is confirmed by XPS. TGA reveals similar mass fractions for water.

Table 4.3. Examples of combustion analysis of reduced graphite oxide prepared in Section 3.1.3. Listed are the mass fractions of the particular elements. [a]Values below 0.1% are not determinable. i.e. these elements are neglected for further calculations. [b]Oxide is not directly determinable. It is the total residual. [c]Calculated without water-correction. [d]Calculated with water-correction. [e]The fraction mass of water is calculated by assigning all hydrogen to water.

#	Mass [mg]	C [%]	H [%]	N [%]	S, Cl [%]	O[b] [%]	C:O:H:N[c]	C:O:N[d]	Water[e] [%]
1	2.421	58.93	2.91	2.83	< 0.1[a]	35.33	100:45:59:4	100:15:4	2.76
2	2.429	58.48	3.00	2.79	< 0.1[a]	35.73	100:46:62:4	100:15:4	2.73
GO	2.544	43.42	2.66	< 0.1[a]	< 0.1[a]	53.92	100:74:93:0	100:56:0	25.91

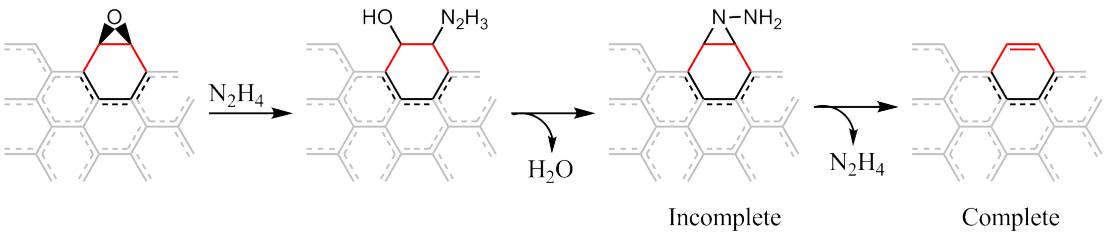

Figure 4.10. The complete and incomplete reaction of the epoxy groups with hydrazine during the reduction step (see Section 7.3 for more information). Adapted from ref. 14.

Conspicuously, there is a large incorporation of nitrogen in reduced graphite oxide which is not removed by dialysis. This nitrogen is probably due to a incomplete reaction of hydrazine with epoxy groups on the surface (see Figure 4.10) [14]. Still, the

resulting ratios are very comparable to each other. Similar to graphite oxide, this is independent of small variations and of scaling, which confirmes the robustness of the reduction step.

4.4.3 UV/VIS absorption spectroscopy

The UV absorption spectrum of reduced graphene oxide exhibits one broad band with a maximum at 260 nm. It can be assigned to the π-π^* transition of C=C bonds of the aromatic system (see Figure 4.11). The absorption then slowly decays but extends towards into the visible. This is causing the grey/black color of the solution.

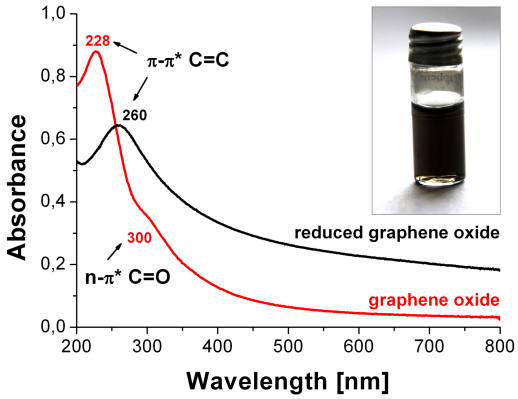

Figure 4.11. UV/Vis spectra of (reduced) graphene oxide revealing the recovery of the π-π-system. The inlet shows a photo of a typical black solution of rGO.

The calculated coefficients (1 mg mL^{-1}) for the wavelengths 260 nm and 700 nm are 0.64 mL mg^{-1} cm^{-1} and 0.20 mL mg^{-1} cm^{-1}, respectively. That implies only a 3-fold higher absorption in the UV-region than in the visible region (cf. 22-fold for GO). Still, solutions of reduced graphene oxide tend to precipate under UV-light.

4.4.4 Infrared spectroscopy

The FT-IR spectrum of reduced graphene oxide gives only limited information about functional groups. The overall transmission is very low and no distinct peaks as in the case of graphene oxide are present (see Figure 4.12). However, there are two steps

between 1533-1600 cm^{-1} and 1350-1470 cm^{-1}, respectively.

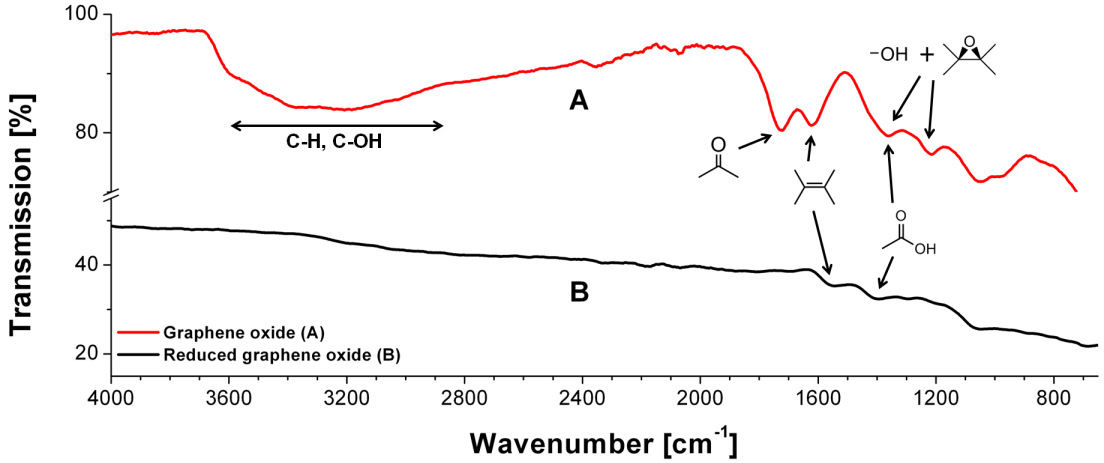

Figure 4.12. Infrared spectrum of graphene oxide and reduced graphene oxide. It reveals the presence of various oxygen functions in GO but gives only limited information for rGO, except for the two steps between 1533-1600 cm^{-1} and 1350-1470 cm^{-1}, respectively.

These steps not only fit the vibrations of the aromatic C=C double bond and the hydroxy/carboxy groups of graphene oxide. They are also congruent with the familiar G- and D-peak in the Raman spectrum (see Chapter 5).

4.4.5 Electron microscopy

The reduction of graphene oxide described in Section 7.3 does not result in any major changes of the flake size or form. Not surprisingly, the TEM of the reduced product exhibits no additional or missing features (see Figure 4.13).

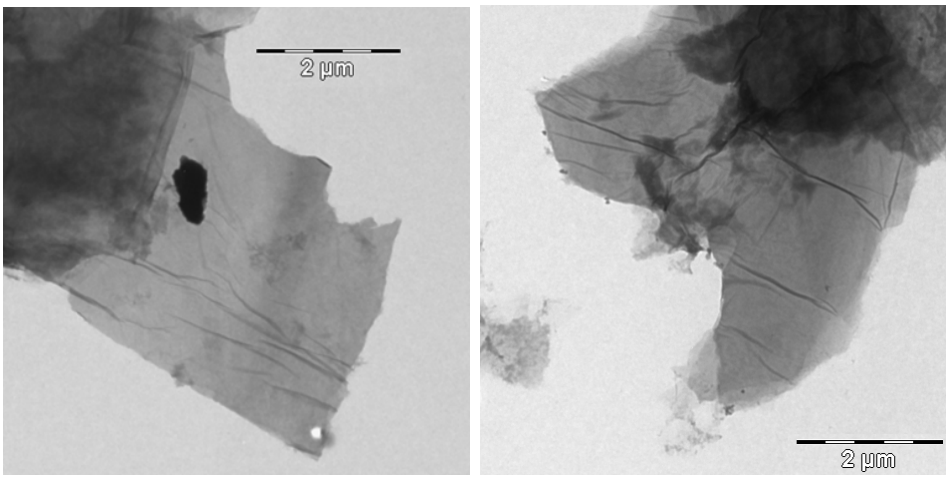

Figure 4.13. TEM pictures of graphene oxide (left) and its reduced form (right). Both show the folding lines and the chaotic shape of the flakes. Also some aggregates on top are visible.

4.4.6 pH titration

Stable solutions of reduced graphene oxide possess pH values of between 4 to 5 due to the presence of carboxy acid groups on the surface. Similar to graphene oxide, the titration plot shows a large linear region but with an increased slope (see Figure 4.14).

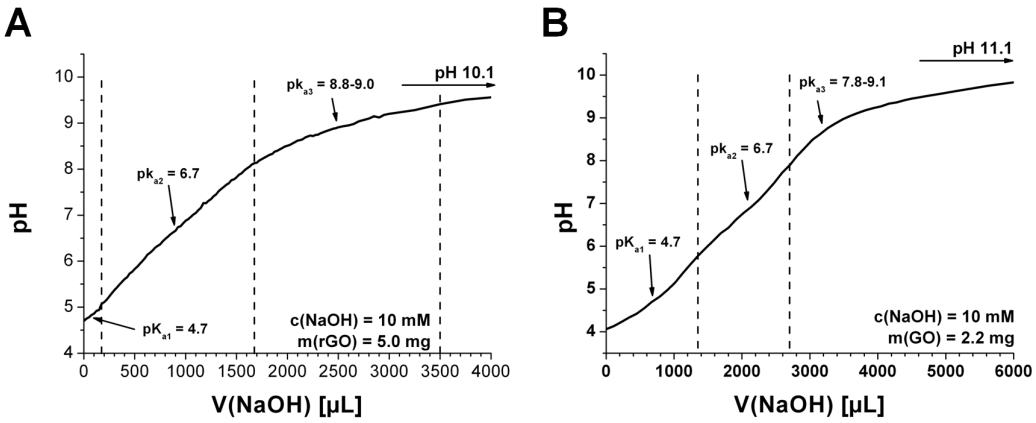

Figure 4.14. (A) Titration plot of reduced graphene oxide (5.0 mg) using a 10 mM solution of NaOH. The two first equivalence points were assigned by using the pK_a values from graphene oxide. The end point is chosen at the tiny wave at 3500 µL. (B) Titration plot of graphene oxide for comparison.

Reduced graphene oxide is derived from graphene oxide. If the reduction process is considered only as an elimination of oxide groups but not their creation, then all groups on rGO are already present on GO. Conclusively, it is natural to apply the same pK_a values to it.

Based on this, the pK_a values of 4.7 and 6.7 from GO are used to determine the first titration zones. Looking closely, a tiny wave at 3500 µL (pH 9.4) can be seen which is choosen as the end point. The pH-level of this point is similar to the one of GO. After that, the pH level increases slowly until 10.1 (at about 10 mL).

The end point is equal to 35 µmol protons per 5.0 mg of rGO. If the acidic oxygen groups are considered as criterion for numbering of rGO "molecules", the proton concentration can be inversed to a molar mass of about 142.86 g mol^{-1} ($\sim C_{9.5}O_{1.4}N_{0.4}$).

35 µmol of protons correspond to 3.3 µmol of rGO ($C_{100}O_{15}N_4$, 1496 g mol^{-1}), so there are about 10 protons per rGO-block. Equally to GO, the titration plot is divided into three zones. The first zone from 0 to 175 µL and half of the second zone (175-1675 µL), i.e. 750 µL, is assigned to carboxy groups. The remaining protons from 925 to 3500 µL are considered from hydroxy groups. That leads to a ratio of 3:7 for COOH:OH, respectively.

If this result is included in the sum formula for the rGO-block above, it is written as $C_{97}O_5N_4(OH)_7(COOH)_3$. In comparance with the sum formula of the GO-block, viz. $C_{81}O_3(OH)_{15}(COOH)_{19}$, the ratio not only inverted but increased in favor of the hydroxy groups.

This low content of carboxy groups correlate with the fluorescence behavior of both materials. In GO, these groups (with pK_a of 4.7) have the strongest impact on the fluorescence intensity. If protonated, the intensity is at a maximum and decreases by nearly 60% if completely deprotonated. After their removal in the reduction process to rGO, fluorescence no longer can be monitored. Conclusively, the electron-withdrawing-effect (negative inductive effect) is primarily responsible for the existence of a band gap in graphene oxide.

4.4.7 Piece together the puzzle

Similar to graphene oxide, all the characterization data is compiled into a pixelated map of an example flake (see Figure 4.15). Comparing both maps optically implies an increment of the crystallite zones. However, Raman spectroscopy reveals that the crystallite lattice does not grow during the reduction process. At the same time, results from other methods (absorption of UV/Vis and IR, the absence of fluorescence, the reduced bulk resistantivity) suggest an increase of the π-π-system.

This obvious contradiction is solved by examining the oxidized zones in graphene oxide. There, many inner holes exist caused by the strong oxidation process during the synthesis. The reduction process cannot heal missing carbon atoms. On the contrary, removing the carboxy groups will further reduce the number of carbon atoms and in turn widen the inner holes.

Conclusively, in rGO the same perfect crystallite zones as in GO are present. Additionally, new crystallite parts between these zones are opened up. These allow for more rapid electron movement (see Section 5.4 for details). For the model, a grey scale is introduced reflecting these different crystallite parts. The more black the more perfect is the crystal lattice this pixel represents.

Elementary analysis yields the ratio of carbon to oxygen to nitrogen (100:15:4) for rGO. The results of the optical methods (IR, UV/VIS, fluorescence) and pH-titration lead to the conclusion that the oxides mainly consists of carboxy acids and hydroxy groups. Taking the rGO-block of the pH-titration as basis ($C_{97}O_5N_4(OH)_7(COOH)_3$) and counting the five remaing oxygen atoms as single oxidized carbon atoms (e.g. for hydroxy groups having very high pK_s values), the ratio of crystalline C to oxidized C (including "nitrogenized" carbon atoms) is about $\sim$4.3 (81:19). Expectably, this ratio is much higher that for GO and consistent with the results described above.

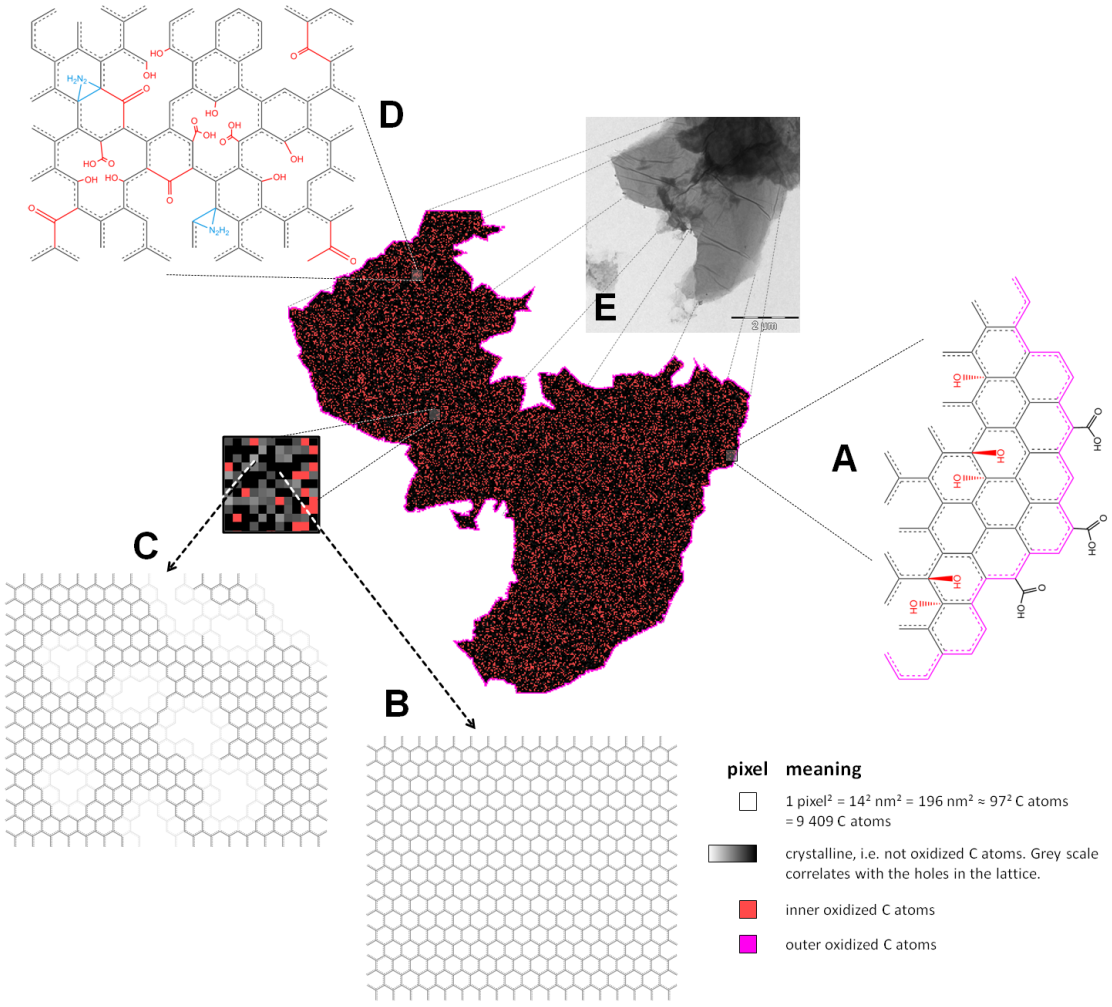

Figure 4.15. A representative flake (area: ∼13 µm^2) derived from the shown TEM picture (E). Every pixel represents an area of 14 nm by 14 nm. The color of the pixel scales the oxidation level of the corresponding region (see bottom right corner). In addition to graphene oxide, the "perfectness" of the crystal lattice is represented by a gray scale. The more white the more (and larger) holes the crystal lattice has at the corresponding pixel. Four different regions are detailed: The border region (A) has a lower amount of carboxy groups than graphene oxide. Large perfect (B) and less perfect (C) crystallite zone exist. Some regions are still significantly oxidized (D) and, moreover, possess nitrogen impurities. The depicted segment display the average C:O:N ratio of rGO.

4.5 References

[1] D. R. Dreyer, S. Park, C. W. Bielawski, and R. S. Ruoff. The chemistry of graphene oxide. *Chem. Soc. Rev.*, 39(1):228–240, 2010. doi: 10.1039/B917103G.

[2] R. J. Hirsch, V. Narurkar, and J. Carruthers. Management of injected hyaluronic acid induced Tyndall effects. *Laser. Surg. Med.*, 38(3):202–204, 2006. doi: 10.1002/lsm.20283.

[3] H. A. Becerril, J. Mao, Z. Liu, R. M. Stoltenberg, Z. Bao, and Y. Chen. Evaluation of Solution-Processed Reduced Graphene Oxide Films as Transparent Conductors. *ACS Nano*, 2(3):463–470, 2008. doi: 10.1021/nn700375n.

[4] D. Li, M. B. Muller, S. Gilje, R. B. Kaner, and G. G. Wallace. Processable aqueous dispersions of graphene nanosheets. *Nat. Nanotechnol.*, 3(2):101–105, February 2008. doi: 10.1038/nnano.2007.451.

[5] W. Scholz and H. P. Boehm. Die Ursache der Dunkelfärbung des hellen Graphitoxids. *Z. Anorg. Allg. Chem.*, 331(3-4):129–132, 1964. doi: 10.1002/zaac.19643310303.

[6] Y. Si and E. T. Samulski. Synthesis of Water Soluble Graphene. *Nano Lett.*, 8(6):1679–1682, 2008. doi: 10.1021/nl080604h.

[7] D. M. Dennison. The Infra-Red Spectra of Polyatomic Molecules. Part II. *Rev. Mod. Phys.*, 12 (3):175–214, July 1940. doi: 10.1103/RevModPhys.12.175.

[8] A. Ghosh, K. S. Subrahmanyam, K. S. Krishna, S. Datta, A. Govindaraj, S. K. Pati, and C. N. R. Rao. Uptake of H_2 and CO_2 by Graphene. *J. Phys. Chem. C*, 112(40):15704–15707, September 2008. doi: 10.1021/jp805802w.

[9] A. K. Mishra and S. Ramaprabhu. Carbon dioxide adsorption in graphene sheets. *AIP Adv.*, 1 (3):032152, 2011. doi: 10.1063/1.3638178.

[10] B. C. Brodie. On the Atomic Weight of Graphite. *Philos. Trans. R. Soc. London*, 149:249–259, January 1859. doi: 10.1098/rstl.1859.0013.

[11] Y. Gao, H.-L. Yip, K.-S. Chen, K. M. O'Malley, O. Acton, Y. Sun, G. Ting, H. Chen, and A. K.-Y. Jen. Surface Doping of Conjugated Polymers by Graphene Oxide and Its Application for Organic Electronic Devices. *Adv. Mat.*, 23(16):1903–1908, 2011. doi: 10.1002/adma.201100065.

[12] G. Zhao, J. Li, X. Ren, C. Chen, and X. Wang. Few-Layered Graphene Oxide Nanosheets As Superior Sorbents for Heavy Metal Ion Pollution Management. *Environ. Sci. Technol.*, 45(24): 10454–10462, November 2011. doi: 10.1021/es203439v.

[13] J. A. Dean, editor. *Lange's Handbook of Chemistry.* McGRAW-HILL, INC., 15th edition, 1999.

[14] S. Stankovich, D. A. Dikin, R. D. Piner, K. A. Kohlhaas, A. Kleinhammes, Y. Jia, Y. Wu, S. T. Nguyen, and R. S. Ruoff. Synthesis of graphene-based nanosheets via chemical reduction of exfoliated graphite oxide. *Carbon*, 45(7):1558–1565, June 2007. doi: 10.1016/j.carbon.2007.02.034.

[15] F. Schedin, A. K. Geim, S. V. Morozov, E. W. Hill, P. Blake, M. I. Katsnelson, and K. S. Novosëlov. Detection of individual gas molecules adsorbed on graphene. *Nat. Mater.*, 6(9): 652–655, 2007. doi: 10.1038/nmat1967.

[16] V. Dua, S. P. Surwade, S. Ammu, S. R. Agnihotra, S. Jain, K. E. Roberts, S. Park, R. S. Ruoff, and S. K. Manohar. All-Organic Vapor Sensor Using Inkjet-Printed Reduced Graphene Oxide. *Angew. Chem., Int. Ed.*, 49(12):2154–2157, 2010. doi: 10.1002/anie.200905089.

5 Raman spectroscopy of (reduced) graphene oxide

5.1 Overview

Raman spectroscopy has emerged as a standard tool for characterization and identification of carbon materials because it provides a fast, nondestructive method of examining samples[1,2]. It is therefore not surprising that graphene and related materials are routinely examined with Raman spectroscopy[3–8]. Raman spectra of graphene materials are simple, containing few peaks, but are unfortunately not so simple to interpret[2]. Further, I am only aware of one publication from 2007 that is concerned with a (deeper) investigation and interpretation of the Raman spectra of graphene oxide[8]. This is most likely because many publications discount the information in these spectra as simple "because-of-oxygen-induced"-features, without any further analysis. Although an extensive investigation of the Raman spectra is beyond the scope of this work, this chapter proposes a basic approach for spectra interpretation.

5.2 Pristine graphene

First, one should consider the vibrational modes of pristine graphene, given their simple and well-defined structure. The Raman spectrum of a monolayer graphene flake prepared by the Scotch-tape-method is given in Figure 5.1A. It shows two important features, namely the G-peak at 1584 cm^{-1} and the 2D-peak at 2676 cm^{-1}. The first order of the 2D-peak, the D-peak, is only present in samples with defects, and appears at around 1300 cm^{-1} [2].

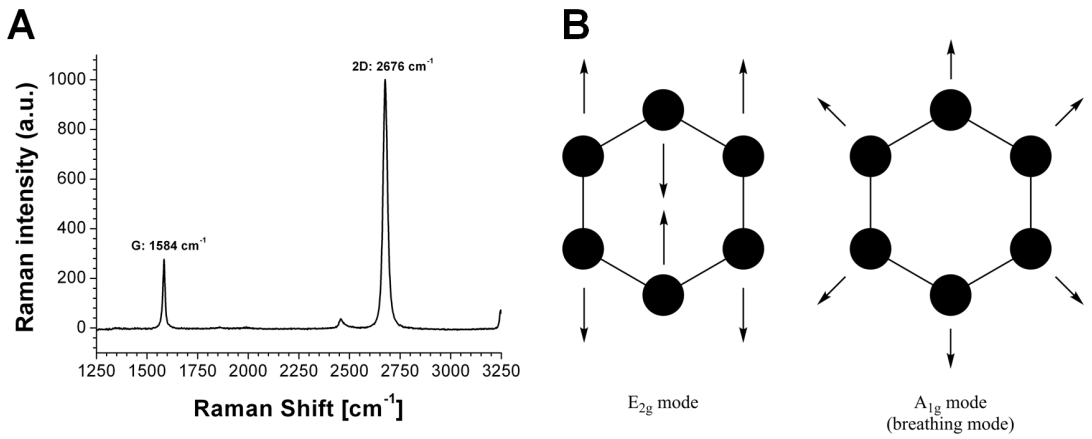

Figure 5.1. (A) Raman spectrum of a monolayer graphene flake measured in the center of the flake. Spectra adapted from ref. 9, with permission. (B) The two vibrational modes, E_{2g} and A_{1g}, are assigned to the G- and D-peak, respectively.

There are only two Raman active modes in a defect-free graphene lattice, viz. E_{2g} and A_{1g} (breathing mode)[10,11]. These modes are depicted in Figure 5.1B, and are often assigned to the G- and D-peak, respectively[11], when modeled from a molecular point of view. However, some characteristics of the D-peak cannot be explained with the latter assignment, when a macroscopic view (as in the case for graphene materials) is adapted. For instance, the D-peak and its overtone are dispersive. In some samples, the 2D-peak is present even if the D-peak is not visible (as in the example spectra in Figure 5.1A)[2]. Further investigations led to the assignment of a double resonant Raman process as the cause of the D-peak[12].

An important and interesting feature of the overtone of the D-peak, the 2D-peak (sometimes called G′-peak), is its dependence on the number of graphene layers[1]. This is attributed to the splitting of the π and π^* bands caused by the interaction of the individual layers in an AB-structure[3].

5.3 Graphene oxide

In contrast to pristine graphene, the Raman spectra of (reduced) graphene oxide possess three (four when considering the D-peak) additional peaks. The spectrum of (r)GO is similar and, from the viewpoint of pristine graphene, graphene oxide is the

contrary extreme in terms of oxidation level. Thus, only graphene oxide is discussed in the following paragraphes.

A typical spectrum of graphene oxide is given in Figure 5.2. In addition to the peaks in the Raman spectrum of the graphene flake reported in Figure 5.1A, it possesses distinct D-, 2D-, 2D′- and D+G-peaks.

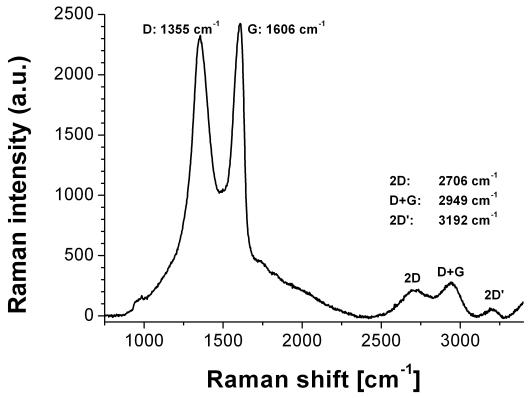

Figure 5.2. Raman spectrum of graphene oxide.

The assignment of these peaks to vibrational modes or other features in GO is not straightforward. First, it is noteworthy that both the G- and D-peak are not spectraly resolvable but indeed share the same, broad base from about 1250-1650 cm^{-1}. In contrast to the peaks of the graphene flake, they are both asymmetrical. Such broad peaks imply that these two modes each consist of the convolution of multiple components. Additionaly, there is a blue shift of the G-peak from around 1580 cm^{-1} (pristine graphene) to 1606 cm^{-1} in graphene oxide.

Kudin et al. investigated these features using DFT calculations of various carbon/oxygen configurations possibly represented in GO[8]. The segments consisted of alternating ribbon-oxygen structures. Their results explained the blue shift as an "alternating pattern of single-double carbon bonds within the sp^2 carbon ribbons". Furthermore, they presented and calculated some (basic) models, which clearly show that different arrangements of epoxy and hydroxy groups on a graphene lattice resulted in peaks between 1350 and 1600 cm^{-1}.

This result is supported by the infrared spectrum (see Section 4.3.4), which displays a distinct band at 1364 cm^{-1} that can be assigned to hydroxy groups. Since IR and

Raman are complementary, it is natural to assume that at the same wavenumber, a Raman-active process could occur. Raman investigation of smaller molecules such as benzoic acid[13] and mellitic acid[14] reveals more possible modes. For instance, the symmetrical O−C−O stretch vibration is assigned to the spectral region between 1330-1430 cm^{-1} [13,14].

As mentioned above, the shape, width and position of the 2D-peak depends on the number of graphene layers[1]. This correlation cannot be applied to the case of GO. Oxygen plasma-induced disordering on single-layer graphene reveals that the shape and intensity of the 2D-peak significantly changes during this process[15]. This correlates the large influence of oxygen to the shape of the 2D peak.

Additionally, there are strong electrostatic repulsion forces between the single GO flakes (see Section 4.3.1). Thus, the distance between two layers should be much larger as compared to pristine graphene, rendering any interaction effects between the crystallite planes negligible. For flake stacking to occur, the crystallite planes would need to be aligned in exact AB-order[3]. This is clearly not possible due to the heterogenous and random structure of GO.

This structure makes it difficult to assign the overtone peaks to a dominant cause. For instance, the 2D′-peak and the D+G-peak could be caused by water, given that GO is extremely hydrophilic and water possesses (large) Raman modes in this region[16]. Also, aliphatic and aromatic C−H and O−H stretch vibrations of organic molecules occur in this region[13,17]. However, slightly modified versions (e.g. by esterification, amidation, substitution) of GO could be compared to one other and to *realistic* models (e.g. by DFT). Indeed, substantial effort is needed to systematically screen all the influences on the Raman spectra of GO and its modifications. This, however, would provide many new insights in all GO-related structures and processes.

5.4 Size of crystallites

The size of in-plane crystallites is an important parameter for characterizing graphene-related materials. For instance, the electrical resistivity is considered to partly arise from the hopping of charge carriers between the crystallite zones[18]. Obviously, the crystallite size L_a should be somehow related to the D peak in the Raman spectrum, since it expresses disorder/defect in a system. L_a can be expressed by the following equation[18,19]:

$$L_a[nm] = 2.4 \cdot 10^{-10} \cdot \lambda^4 \cdot \frac{I_G}{I_D}, \tag{5.1}$$

where λ is the excitation wavelength and, I_G and I_D are the intensities of the G and D peak, respectively. This simplified relation allows the direct calculation of L_a from the Raman spectrum.

With this relation and a quick experiment, it is easy to examine how the precursor material influences the structure of graphene oxide. Two types of graphite are considered here, viz. flake graphite (35 mesh) and graphite powder. The Raman spectra of both are shown in Figure 5.3A. Clearly, the graphite powder has higher disorder (see D and D′ peaks) whereas the flake graphite possesses no D peak at all. The intensity ratio for the graphite powder is 12.5 (I_G/I_D) resulting in a calculated L_a of 240 nm. For flake graphite, the ratio is difficult to determine due to the absence of a D-peak. Regardless, given the intensity I_D at the same position as for the graphite powder (1363 cm^{-1}), the ratio I_G/I_D is 62.7 and L_a 1206 nm, which suggests a 5 times larger crystalline zone.

Typically, graphene oxides made from these graphite types ("flake-GO" and "powder-GO") are expected to have similar characteristics. However, Figure 5.3B reveals quite the contrary. Powder-GO possesses a higher D/G-ratio than flake-GO and, therefore, has the larger crystalline plane structure, viz. 35 nm for powder-GO and 27 nm for flake-GO.

Conceivably, the use of flake graphite in the synthesis leads to a longer preoxidation

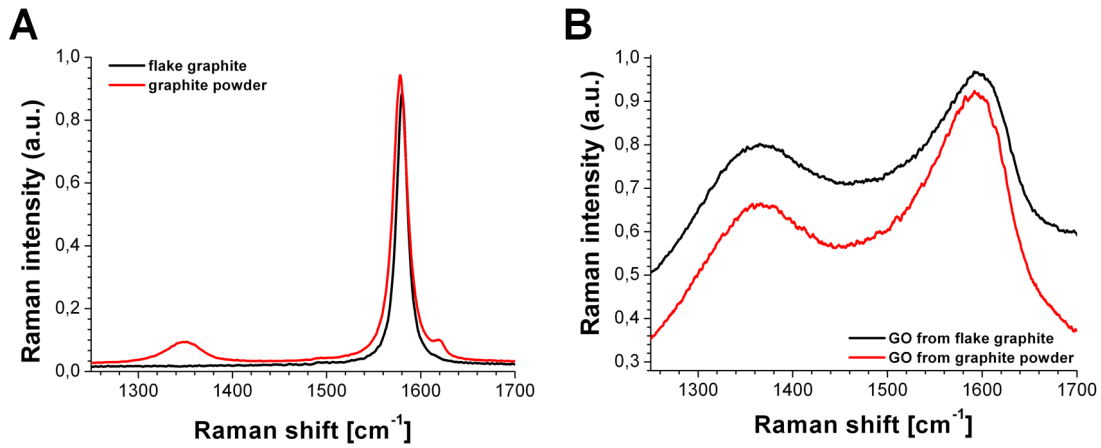

Figure 5.3. (A) Raman spectra of flake graphite and graphite powder. (B) Raman spectra of two GO types made from flake graphite and graphite powder, respectively.

step since the interplanar forces are much stronger (more π-π stacking) and the nitrogen oxide species have more time for intercalation and oxidation. As a result more oxygen is distributed over the planes compared to powder-GO. The latter promotes a faster start of the main oxidation step because of the higher number of edges, which can be accessed early by the manganese oxide species. However, one must also consider that the difference between both GO types is perhaps a natural variation of the synthesis. Nevertheless, this possibility is excluded by elementary analysis, which indicate a very robust synthesis method.

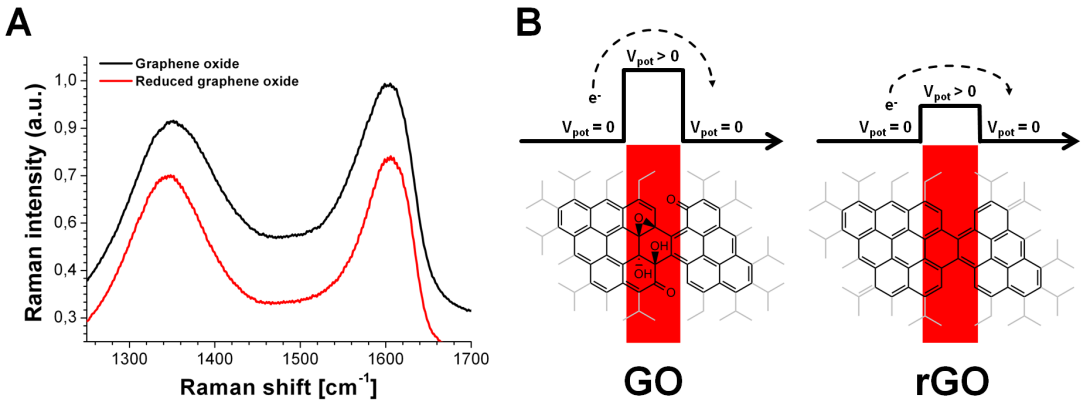

Figure 5.4. (A) Raman spectra of graphene oxide and reduced graphene oxide showing similar G/D-ratios. (B) Model of the potential barrier between two crystalline zones. The removing of oxygen and the recovery of the π-system reduce the potential of the barrier allowing the electrons to pass more easily. By looking at the structure models, it is obvious that the reduction removes the oxygen, but a bottleneck between both crystalline zones still remains, since missing carbons in the lattice cannot be healed.

Next, graphene oxide can be compared to its reduced version. By removing oxygen and recovering parts of the π-system, the crystalline zones would be expected to grow. In contrast, L_a of rGO is very similar to that of GO, indicating no change in the crystallite size (see Figure 5.4A).

The border of the crystalline zone is considered a potential barrier that electrons must pass to move from one crystalline zone to another. Although L_a does not change as a result of reduction, the conductivity still increases. This observation leads to the conclusion that the potential barrier is only lowered to a certain degree, but not completely removed. In more simple terms, the reduction does not heal the damage caused by the oxidation of graphite (see Figure 5.4B).

In general, these results are consistent with TEM examinations of the local structure of (reduced) graphene oxide, although the size of the observed crystallite zones is smaller (2-6 nm)[20,21]. This may be attributed to the following two reasons. First, it is not clear if the experimental data from these publications is (statistically) representative. Second, the exact composition of the G- and D-peak in (r)GO is also not completely resolved, thus the intensities used to determine the crystallite size could be too high. In this case, Equation 5.1 would require a correction factor or function.

5.5 pH-dependent Raman spectra

In contrast to other methods such as IR spectroscopy, Raman spectroscopy allows measurement in aqueous solutions. The Raman spectra of water possesses one large feature in the region of 3000-3600 cm^{-1} for the symmetric O−H stretch[16,22].

Given that graphene oxide is a water-soluble acid, it is interesting to study the pH-dependence of the Raman modes. The overall intensity of the G-, D- and overtone (2D, D+G, 2D′) Raman peaks is very low. Thus, a minimum of 100 Raman spectra per solution were necessary to differenciate signals in the G- and D-region. In all cases, the overtone region contained no peaks. Upon comparison of the spectral position, width and intensity of the two visible bands (G and D), it is clear that the position of the G peak depends on the pH (see Figure 5.5A).

A plot of the change in Raman shift versus pH for the G peak shows two distinct changes in slope at pH 5.0 and 8.5 (see Figure 5.5B). These two inflection points occur at a similar pH to those found in the titration plot (see section 4.3.6) and the pH dependent fluorescence measurements (see chapter 6). Given these correlations, the inflections at pH 5 and 8.5 can be assigned to the carboxy and hydroxy groups, respectively. The deprotonation of the hydroxy group has a larger effect on the shift of G than for the carboxy groups. This is in contrast with the fluorescence intensity measurements, where the carboxy group has a greater influence than the hydroxy group has.

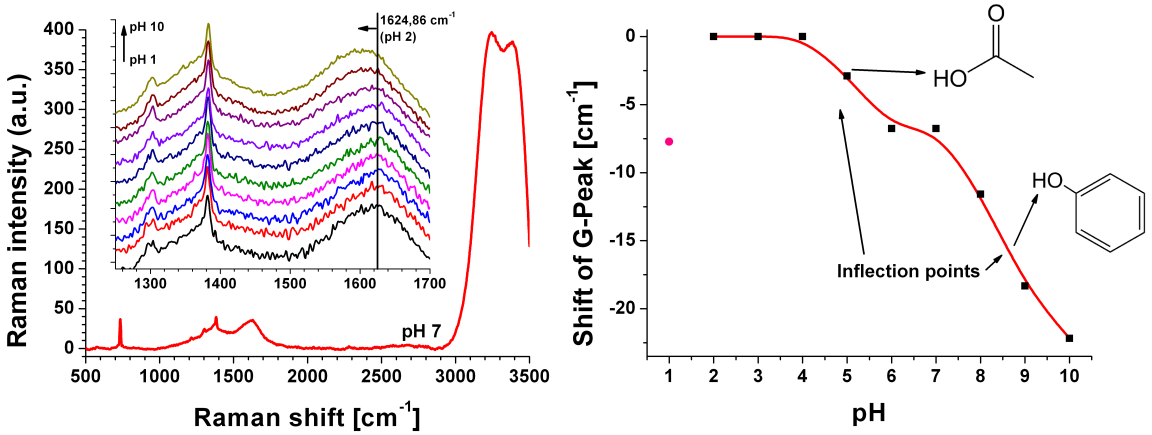

Figure 5.5. (A) Raman spectra of graphene oxide in water. The 2D region is not visible due to low overall intensity. The small features are caused by the used buffer solution. The inset shows the movement of the G peak with increasing pH level. (B) Shift of G peak as a function of pH revealing the two pK_a values of 5.0 and 8.5. The pink dot at pH 1 is considered an outlier and is attributed to the reduced solubility.

One can also observe[16] a small O−H bending mode at 1646 cm^{-1}. This mode was visible during the measurement of the blank buffer solutions. However, the intensity of this mode is much lower than the intensity of the G-peaks, and it did not show any dependence on the pH value.

As previously discussed, the G-peak represents the E_{2g}-mode for carbon (nano)materials. For graphene oxide, it is likely the sum of the actual G-peak and other modes actived by hydroxy or carboxy groups. If the E_{2g}-mode dominates the G-peak, the shift can be attributed to electronic doping of crystallite zones in GO, similar to pristine graphene[23]. This explains why the carboxy group has a smaller impact on the shift than the hydroxy group, since carboxy groups exert both a negative

inductive (-I) and a negative mesomeric (-M) effect. Even if electrons are "released" by deprotonating, they are not donated to the crystallite zones. So, a small amount of additional net charges are present in the crystallite zones. In contrast, hydroxy groups have a small negative inductive (-I) but a strong positive mesomeric (+M) effect. Here, deprotonating releases and donates the charges to the crystallite zones explaining the large shift of the G-peak of about 15 cm^{-1}.

Obviously, only aromatic carboxy and hydroxy groups are involved in this mechanism. There is no pK_a at around 6.7 in contrast to the case in the pH titration experiment. This is consistent with the pH dependent fluorescence measurement (see Chapter 6). If other bending or stretching modes (e.g. O−C−O) dominate the G-peak instead of the E_{2g}-mode, carboxy groups would have a larger impact on the shift, as compared to the hydroxy groups. This is because more carboxy groups than hydroxy groups are present in graphene oxide. Also, the effect would not be limited to aromatic groups.

5.6 References

[1] M. S. Dresselhaus, A. Jorio, and R. Saito. Characterizing Graphene, Graphite, and Carbon Nanotubes by Raman Spectroscopy. *Annu. Rev. Condens. Matter Phys.*, 1:89–108, 2010. doi: 10.1146/annurev-conmatphys-070909-103919.

[2] A. C. Ferrari. Raman spectroscopy of graphene and graphite: Disorder, electron–phonon coupling, doping and nonadiabatic effects. *Solid State Communications*, 143(1–2):47–57, July 2007. doi: 10.1016/j.ssc.2007.03.052.

[3] A. C. Ferrari, J. C. Meyer, V. Scardaci, C. Casiraghi, M. Lazzeri, F. Mauri, S. Piscanec, D. Jiang, K. S. Novoselov, S. Roth, and A. K. Geim. Raman Spectrum of Graphene and Graphene Layers. *Phys. Rev. Lett.*, 97:187401, Oct 2006. doi: 10.1103/PhysRevLett.97.187401.

[4] C. Casiraghi, A. Hartschuh, E. Lidorikis, H. Qian, H. Harutyunyan, T. Gokus, K. S. Novoselov, and A. C. Ferrari. Rayleigh Imaging of Graphene and Graphene Layers. *Nano Lett.*, 7(9): 2711–2717, 2007. doi: 10.1021/nl071168m.

[5] S. Pisana, M. Lazzeri, C. Casiraghi, K. S. Novoselov, A. K. Geim, A. C. Ferrari, and F. Mauri. Breakdown of the adiabatic Born-Oppenheimer approximation in graphene. *Nat. Mater.*, 6(3): 198–201, March 2007. doi: 10.1038/nmat1846.

[6] A. Das, S. Pisana, B. Chakraborty, S. Piscanec, S. K. Saha, U. V. Waghmare, K. S. Novoselov, K. H. R., A. K. Geim, A. C. Ferrari, and A. K. Sood. Monitoring dopants by Raman scattering in an electrochemically top-gated graphene transistor. *Nat Nano*, 3(4):210–215, April 2008. doi: 10.1038/nnano.2008.67.

[7] C. Casiraghi, S. Pisana, K. S. Novoselov, A. K. Geim, and A. C. Ferrari. Raman fingerprint of charged impurities in graphene. *Appl. Phys. Lett.*, 91(23):233108, 2007. doi: 10.1063/1.2818692.

[8] K. N. Kudin, B. Ozbas, H. C. Schniepp, R. K. Prud'homme, I. A. Aksay, and R. Car. Raman Spectra of Graphite Oxide and Functionalized Graphene Sheets. *Nano Lett.*, 8(1):36–41, December 2007. doi: 10.1021/nl071822y.

[9] Alexander Zöpfl. Studies of Graphene and its Modifications for Sensor Applications. Master thesis, Institute of Analytical Chemistry, Chemo- and Biosensors; University of Regensburg, 2012.

[10] C. Castiglioni, M. Tommasini, and G. Zerbi. Raman spectroscopy of polyconjugated molecules and materials: confinement effect in one and two dimensions. *Philos. Trans. R. Soc. Lond. A*, 362(1824):2425–2459, 2004. doi: 10.1098/rsta.2004.1448.

[11] F. Tuinstra and J. L. Koenig. Raman Spectrum of Graphite. *The Journal of Chemical Physics*, 53(3):1126–1130, 1970. doi: 10.1063/1.1674108.

[12] J. Maultzsch, S. Reich, and C. Thomsen. Double-resonant Raman scattering in graphite: Interference effects, selection rules, and phonon dispersion. *Phys. Rev. B*, 70:155403, Oct 2004. doi: 10.1103/PhysRevB.70.155403.

[13] M. Pagannone, B. Fornari, and G. Mattei. Molecular structure and orientation of chemisorbed aromatic carboxylic acids: Surface enhanced Raman spectrum of benzoic acid adsorbed on silver sol. *Spectrochim. Acta A*, 43(5):621 – 625, 1987. doi: 10.1016/0584-8539(87)80143-5.

[14] K. Osterrothová and J. Jehlička. Raman spectroscopic identification of phthalic and mellitic acids in mineral matrices. *Spectrochim. Acta A*, 77(5):1092 – 1098, 2010. doi: 10.1016/j.saa.2010.08.081.

[15] D. C. Kim, D.-Y. Jeon, H.-J. Chung, Y. Woo, J. K. Shin, and S. Seo. The structural and electrical evolution of graphene by oxygen plasma-induced disorder. *Nanotechnol.*, 20(37):375703, 2009. doi: 10.1088/0957-4484/20/37/375703.

[16] D. M. Carey and G. M. Korenowski. Measurement of the Raman spectrum of liquid water. *J. Chem. Phys.*, 108(7):2669–2675, 1998. doi: 10.1063/1.475659.

[17] J. F. Mammone, S. K. Sharma, and M. Nicol. Raman spectra of methanol and ethanol at pressures up to 100 kbar. *J. Phys. Chem.*, 84(23):3130–3134, November 1980.

[18] M. A. Pimenta, G. Dresselhaus, M. S. Dresselhaus, L. G. Cancado, A. Jorio, and R. Saito. Studying disorder in graphite-based systems by Raman spectroscopy. *Phys. Chem. Chem. Phys.*, 9(11):1276–1290, 2007. doi: 10.1039/B613962K.

[19] L. Cançado, K. Takai, T. Enoki, M. Endo, Y. Kim, H. Mizusaki, N. Speziali, A. Jorio, and M. Pimenta. Measuring the degree of stacking order in graphite by Raman spectroscopy. *Carbon*, 46(2):272–275, 2008. doi: 10.1016/j.carbon.2007.11.015.

[20] K. Erickson, R. Erni, Z. Lee, N. Alem, W. Gannett, and A. Zettl. Determination of the Local Chemical Structure of Graphene Oxide and Reduced Graphene Oxide. *Adv. Mat.*, 22(40):4467–4472, 2010. doi: 10.1002/adma.201000732.

[21] C. Gómez-Navarro, J. C. Meyer, R. S. Sundaram, A. Chuvilin, S. Kurasch, M. Burghard, K. Kern, and U. Kaiser. Atomic Structure of Reduced Graphene Oxide. *Nano Lett.*, 10(4): 1144–1148, March 2010.

[22] G. E. Walrafen and E. Pugh. Raman Combinations and Stretching Overtones from Water, Heavy Water, and NaCl in Water at Shifts to ca. 7000 cm^{-1}. *J. Solution Chem.*, 33(1):81–97, 2004. doi: 10.1023/B:JOSL.0000026646.33891.a8.

[23] M. Kalbac, A. Reina-Cecco, H. Farhat, J. Kong, L. Kavan, and M. S. Dresselhaus. The Influence of Strong Electron and Hole Doping on the Raman Intensity of Chemical Vapor-Deposition Graphene. *ACS Nano*, 4(10):6055–6063, October 2010. doi: 10.1021/nn1010914.

6 Fluorescence of graphene oxide

6.1 Overview

The oxidation level of graphene oxide introduces a band gap which enables photoluminescence to occur[1,2]. However, it has only sparsely been examined[1–3]. *Eda et al.* have photoexcited GO at 325 nm and observed a blue luminescence[4]. *Chen et al.* examined the pH-dependence of the fluorescence and the effect of the ionic strength in the visible and near-infrared spectrum[5].

Obviously, there is a gap in the visible range of the spectrum. Thus, this chapter presents a systematic study on the multiple fluorescence of GO in the near-UV and visible part. Especially, the dependence on excitation wavelength, emission wavelength and pH value are examined and discussed.

6.2 Fluorescence in the near-UV and visible range

The pH dependence of the fluorescence of GO in water solution at fixed excitation/emission wavelengths of 470/555 nm was studied first. Figure 6.1A shows that pH exerts a large effect. At pH 1.5, the intensity is about 10 times higher than that at pH 10.1. Inflection points can be identified in the titration plots at pH 4.5 and 8.8. The first one can be assigned to the dissociation of carboxy groups, and the second one to the dissociation of aromatic hydroxy groups, respectively. This is in agreement with results from pH titration (see Section 4.3.6) and other methods discussed before. Temperature exerts a minimal effect (only about 2%) on fluorescence intensity between 20 and 60 °C. Oxygen does not act as a quencher.

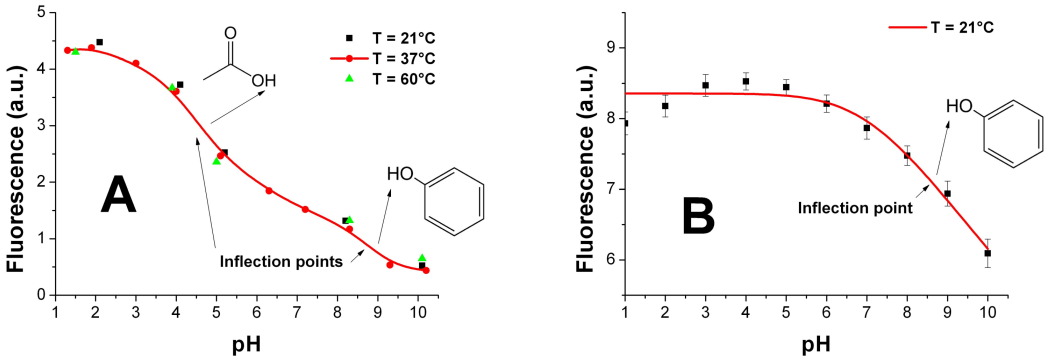

Figure 6.1. (A) Fluorescence intensity (exc/em 470/555 nm) of GO (0.1 mg mL^{-1}) plotted as function of the pH value of the solution at various temperatures. The two inflection points are assigned to the dissociation of the carboxy groups (at 4.5) and the phenolic hydroxy groups (at 8.8), respectively. (B) If GO is converted into its ethyl ester, the first inflection point disappears. The GO ethyl ester also is less soluble in water at lower pH values which results in lower total fluorescence intensity (pH 1 and 2).

In order to prove that the carboxy group is responsible for the transition at around pH 4.5 (the typical pK_a value of aromatic carboxy acids), GO was converted into its ethyl ester (GOEE) as described in the experimental part (see Section 3.1.5). Indeed, the plot for GOEE has only one inflection point at pH 8.8 (see Figure 6.1B) that can be assigned to the phenolic hydroxy groups of GO.

The absorption spectrum of GO (see Section 4.3.3) is typical for species where numerous transitions occur in parallel. The shoulder at around 300 nm is typical for the n-π^* transitions which invariably occur at about this wavelength, are rather weak in intensity, and result from the various kinds of carbonyl groups present in GO.

They easily undergo intersystem crossing to a triplet state and do not cause strong fluorescence in general. Transitions of the π-π^*-type, in contrast, are highly variable in terms of wavelength and intensities. They can occur anywhere between 220 and 600 nm and lead to S_1 states that can undergo various kind of deactivation. Aside from vibrational deactivations, these include intersystem crossing, hydrogen bond deactivation (such as diabatic photodissociation of hydroxy groups), intra- and intermolecular energy transfer, and/or quenching.

It seems that flakes of GO (or sections thereof) can quench (sections of) other flakes. It is virtually impossible to identify the π-electron system that is causing the fluorescence peaks observed, in particular the strong ones located at excitation/emission

wavelengths of 360/580 nm and 470/560 nm[6,7].

In order to obtain a complete picture of the complex luminescence of GO, the excitation-emission matrices (EEM) of GO were acquired at pH values between 1.0 and 10.1 and are shown in Figure 6.2. EEMs are a valueable tool to characterize materials with complex intrinsic fluorescence. These have been used before to characterize materials like human tissue[8], serum[9], diesel fuel[10], crude oil[11] and water samples[12,13].

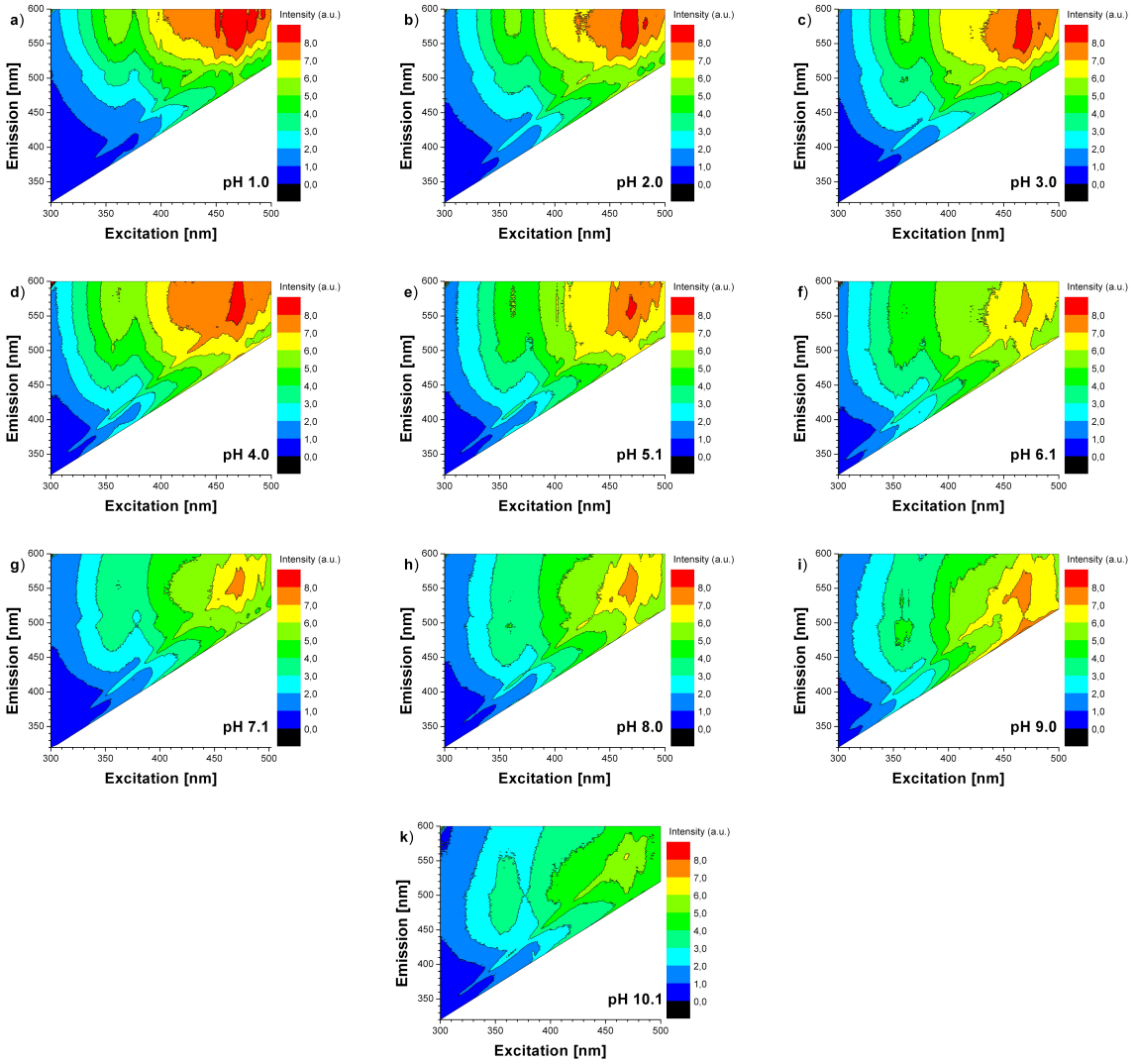

Figure 6.2. Excitation-emission matrices of graphite oxide at pH values from 1.0 to 10.1.

The EEMs of GO display a broad maximum at 470 nm excitation and 560 nm emission

at any pH value. A small peak can be observered at 360 nm excitation and 580 nm emission if the pH is lower than 4. The peak disappears at pH values above 4, and another one arises at 360 nm excitation and 500 nm emission. The EEMs also contain Raman bands shifted from the excitation wavelength by 3328 cm^{-1} and caused by water.

6.3 Discussion

It is interesting to compare the fluorescence of GO with that of other carbon nanomaterials. Carbon nanotubes excited with red light (785 nm) emit in the near infrared area[14], which was shown to enable glucose sensing[15]. Carbon nanoparticles also display strong fluorescence[3,16,17] and this may be used for purposes of bioimaging[18,19].

Fullerenes provide the best contrast to graphene oxide concerning the fluorescence. C_{70} fulleren displays a strong red emission when excited with blue light (470 nm)[20,21]. Its fluorescence is extremely efficiently quenched by oxygen, thus enabling oxygen imaging on the ppb level[21,22]. This is caused by the unusual property of thermally activated delayed fluorescence[21], which is a function of temperature, obviously.

GO is a comparatively inhomogeneous material. A comparison of absorbance and excitation spectra (see Figure 6.3) reveals that only a small fraction exhibits luminescence while the major fraction does not. It is manifest to assume that the bulk material actually suppresses this luminescence as quantum yields are quite low. Therefore, it is reasonable why GO is rather used in quenching applications[23,24].

Figure 6.1 reveals that the pH dependent fluorescence of GO has two inflection points which are assigned to the carboxy acid and the aromatic hydroxy groups. The monoprotic equilibrium of GO suggested by *Chen* et al.[5] therefore has to be extended as there are three rather than two main forms of GO at different pH values (see Figure 6.4A). GO is completely protonated at pH values < 3, and displays maximal fluorescence. From pH 3 to 6 the carboxy acid group becomes deprotonated. The fluorescence intensity decreases to 40% (at pH 6-7). At pH values > 7, the aromatic hydroxy group becomes deprotonated which results in a drop of fluorescence intensity

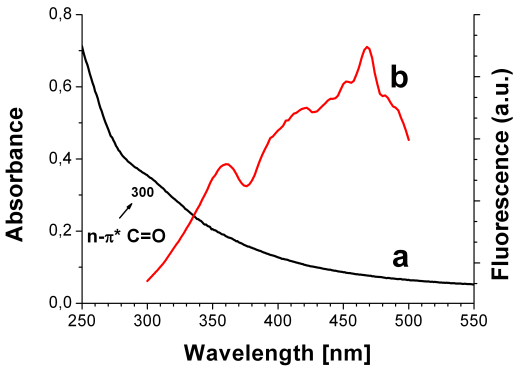

Figure 6.3. Comparison of the UV/Vis (a) and excitation spectrum (at 555 nm emission) (b) of graphene oxide revealing that only a part of GO exhibits luminescence.

to 15%. One conclusion of this observation is that GO is negatively charged at pH values of greater than 4. This is supported by the fact that esterification of the carboxy acid groups leads to only one inflection point (Figure 6.1B) and therefore to a monoprotic equilibrium (Figure 6.4B). Compared to GO, there is no decrease in fluorescence intensity of GOEE until pH 6-7 due to the missing carboxy acid functionality.

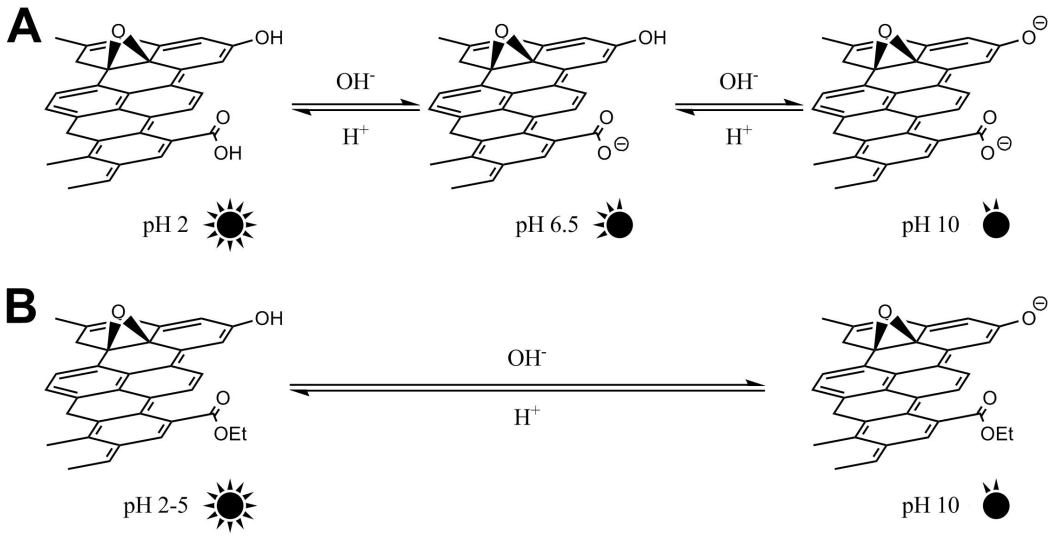

Figure 6.4. (A) Model showing the effect of the pH on the acid-base equilibria of GO. The symbols indicate the relative fluorescence intensity of the corresponding species. (B) Equilibrium after conversion of the carboxy groups into their ethyl esters.

In conclusion, it was demonstrated that the fluorescence properties of GO is highly pH dependent. Fluorescence is strongest at 470 nm excitation and 555 nm emission.

The fluorescence intensity is a function of pH but not of temperature and oxygen concentration. Conceivably, GO may be used to sense pH values in cells and related samples. The changes in fluorescence observed with changes in pH do not depend on the excitation/emission wavelength. This makes it a probe that is compatible with all (kinds of) light sources and filter combinations between 300 and 500 nm, e.g. in imaging applications with microscopes. Interference with a second label (e.g. a temperature probe) can be avoided by switching to a suitable wavelength.

6.4 References

[1] Z. Luo, P. M. Vora, E. J. Mele, A. T. C. Johnson, and J. M. Kikkawa. Photoluminescence and band gap modulation in graphene oxide. *Appl. Phys. Lett.*, 94(11):111909–3, March 2009. doi: 10.1063/1.3098358.

[2] F. Bonaccorso, Z. Sun, T. Hasan, and A. C. Ferrari. Graphene photonics and optoelectronics. *Nat. Photon.*, 4(9):611–622, September 2010. doi: 10.1038/nphoton.2010.186.

[3] D. Pan, J. Zhang, Z. Li, and M. Wu. Hydrothermal Route for Cutting Graphene Sheets into Blue-Luminescent Graphene Quantum Dots. *Adv. Mater.*, 22(6):734–738, 2010. doi: 10.1002/adma.200902825.

[4] G. Eda, Y.-Y. Lin, C. Mattevi, H. Yamaguchi, H.-A. Chen, I.-S. Chen, C.-W. Chen, and M. Chhowalla. Blue Photoluminescence from Chemically Derived Graphene Oxide. *Adv. Mater.*, 22(4):505–509, 2010. doi: 10.1002/adma.200901996.

[5] J. L. Chen and X. P. Yan. Ionic strength and pH reversible response of visible and near-infrared fluorescence of graphene oxide nanosheets for monitoring the extracellular pH. *Chem. Commun.*, 47(11):3135–3137, 2011. doi: 10.1039/c0cc03999c.

[6] G.-J. Zhao, J.-Y. Liu, L.-C. Zhou, and K.-L. Han. Site-Selective Photoinduced Electron Transfer from Alcoholic Solvents to the Chromophore Facilitated by Hydrogen Bonding: A New Fluorescence Quenching Mechanism. *J. Phys. Chem. B*, 111(30):8940–8945, 2007. doi: 10.1021/jp0734530.

[7] H. Inoue, M. Hida, N. Nakashima, and K. Yoshihara. Picosecond fluorescence lifetimes of anthraquinone derivatives. Radiationless deactivation via intra- and intermolecular hydrogen bonds. *J. Phys. Chem.*, 86(16):3184–3188, 1982. doi: 10.1021/j100213a024.

[8] A. F. Zuluaga, U. Utzinger, A. Durkin, H. Fuchs, A. Gillenwater, R. Jacob, B. Kemp, J. Fan, and R. Richards-Kortum. Fluorescence Excitation Emission Matrices of Human Tissue: A System for in Vivo Measurement and Method of Data Analysis. *Appl. Spectrosc.*, 53(3):302–311, 1999.

[9] O. S. Wolfbeis and M. Leiner. Mapping of the total fluorescence of human blood serum as a new method for its characterization. *Anal. Chim. Acta*, 167:203–215, 1985. doi: 10.1016/S0003-2670(00)84422-0.

[10] D. Patra and A. K. Mishra. Study of diesel fuel contamination by excitation emission matrix spectral subtraction fluorescence. *Anal. Chim. Acta*, 454(2):209–215, 2002. doi: 10.1016/S0003-2670(01)01568-9.

[11] J. Bugden, C. Yeung, P. Kepkay, and K. Lee. Application of ultraviolet fluorometry and excitation-emission matrix spectroscopy (EEMS) to fingerprint oil and chemically dispersed oil in seawater. *Mar. Pollut. Bull.*, 56(4):677–685, 2008. doi: 10.1016/j.marpolbul.2007.12.022.

[12] A. Baker. Fluorescence Excitation-Emission Matrix Characterization of Some Sewage-Impacted Rivers. *Environ. Sci. Technol.*, 35(5):948–953, 2001. doi: 10.1021/es000177t.

[13] P. G. Coble. Characterization of marine and terrestrial DOM in seawater using excitation-emission matrix spectroscopy. *Mar. Chem.*, 51(4):325–346, 1996. doi: 10.1016/0304-4203(95)00062-3.

[14] F. Wang, G. Dukovic, L. E. Brus, and T. F. Heinz. Time-Resolved Fluorescence of Carbon Nanotubes and Its Implication for Radiative Lifetimes. *Phys. Rev. Lett.*, 92(17):177401, 2004. doi: 10.1103/PhysRevLett.92.177401.

[15] P. W. Barone, S. Baik, D. A. Heller, and M. S. Strano. Near-infrared optical sensors based on single-walled carbon nanotubes. *Nat. Mater.*, 4(1):86–92, 2005. doi: 10.1038/nmat1276.

[16] X. Wang, L. Cao, S.-T. Yang, F. Lu, M. Meziani, L. Tian, K. Sun, M. Bloodgood, and Y.-P. Sun. Bandgap-Like Strong Fluorescence in Functionalized Carbon Nanoparticles. *Angew. Chem.*, 122 (31):5438–5442, 2010. doi: 10.1002/ange.201000982.

[17] S. N. Baker and G. A. Baker. Luminescent Carbon Nanodots: Emergent Nanolights. *Angew. Chem., Int. Ed.*, 49(38):6726–6744, 2010. doi: 10.1002/anie.200906623.

[18] L. Cao, X. Wang, M. J. Meziani, F. Lu, H. Wang, P. G. Luo, Y. Lin, B. A. Harruff, L. M. Veca, D. Murray, S.-Y. Xie, and Y.-P. Sun. Carbon Dots for Multiphoton Bioimaging. *J. Am. Chem. Soc.*, 129(37):11318–11319, 2007. doi: 10.1021/ja073527l.

[19] S. C. Ray, A. Saha, N. R. Jana, and R. Sarkar. Fluorescent Carbon Nanoparticles: Synthesis, Characterization, and Bioimaging Application. *J. Phys. Chem. C*, 113(43):18546–18551, 2009. doi: 10.1021/jp905912n.

[20] M. N. Berberan-Santos and J. M. M. Garcia. Unusually Strong Delayed Fluorescence of C70. *J. Am. Chem. Soc.*, 118(39):9391–9394, 1996. doi: 10.1021/ja961782s.

[21] S. Kochmann, C. M. Baleizão, M. N. Berberan-Santos, and O. S. Wolfbeis. Sensing and imaging of oxygen with ppb limits of detection and based on the quenching of the delayed fluorescence of $^{13}C_{70}$ fullerene in polymer hosts. *Anal. Chem.*, 85(3):1300–1304, 2013. doi: 10.1021/ac303486f.

[22] S. Nagl, C. Baleizão, S. M. Borisov, M. Schäferling, M. N. Berberan-Santos, and O. S. Wolfbeis. Optical Sensing and Imaging of Trace Oxygen with Record Response. *Angew. Chem., Int. Ed.*, 46(13):2317–2319, 2007. doi: 10.1002/anie.200603754.

[23] C.-H. Lu, H.-H. Yang, C.-L. Zhu, X. Chen, and G.-N. Chen. A Graphene Platform for Sensing Biomolecules. *Angew. Chem.*, 121(26):4879–4881, 2009. doi: 10.1002/ange.200901479.

[24] J. H. Jung, D. S. Cheon, F. Liu, K. B. Lee, and T. S. Seo. A Graphene Oxide Based Immuno-biosensor for Pathogen Detection. *Angew. Chem.*, 122(33):5844–5847, 2010. doi: 10.1002/ange.201001428.

7 Synthesis mechanisms of (reduced) graphene oxide

7.1 Overview

Graphite is an abundant and widely available mineral[1]. Due to this, top-down synthesis routes starting from graphite promise easy and scalable access to graphene materials. Graphite consists of many graphene layers held together by weak interplanar forces[2]. One must disturb and break these attractive forces to separate the material and release the individual layers. There are several mechanical and chemical methods to achieve this goal.

Mechanical exfoliation (so-called *Scotch tape method*) removes layers by repeated peeling of highly oriented pyrolytic graphite[3]. It produces the highest quality samples, but is neither a high throughput nor high-yield method[4]. Combined with the fact that the chemical modification of these samples is rather difficult and the reactivity is not well understood[5], this excludes the use of it as basis for sensor materials.

Chemical methods provide an attractive alternative. The general idea is to insert elements or molecules between the layers of graphite to simply push them apart from each other. *Viculis et al.* developed such a method using potassium and ethanol[6,7]. Potassium positions itself between the layers forming a gold-colored potassium-graphite compound KC_8. This compound reacts vigorously with water or alcohols. After adding ethanol as an exfoliating agent, it reacts with the intercalated potassium forming an alcoholate, which pushes the layers apart. The color turns from gold to black as the reaction proceeds. Figure 7.1 shows a scheme of the concept of this method. *Viculis et al.* were able to prepare platelets of 10 nm thickness (∼30 layers) and scale their

batches up to 70 g quantities of KC_8. After high-energy sonification the platelets form scrolls[7]. Unfortunately, the same disadvantage in terms of chemical modification applies to this method.

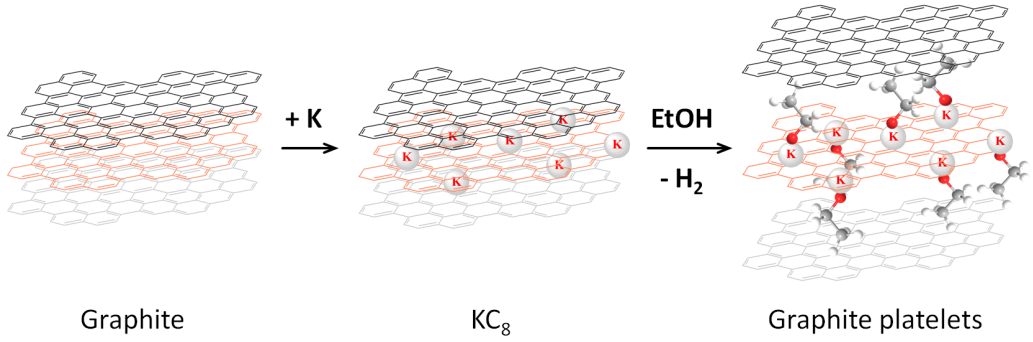

Figure 7.1. Scheme of the potassium intercalation method developed by *Viculis et al.*. Adapted from ref. 6.

Alternative methods use oxygen for the intercalation process[8–11]. Here, the surface of the graphite layers are oxidized by strong agents such as clorate[8,9] or permanganate[10,11]. The resulting product, *graphite oxide*, is very hydrophilic which allows the preparation of stable solutions in water. By repetive dilution, they can be exfoliated to eventually achieve solutions of *graphene oxide*[12]. Subsequent reduction with hydrazine or other agents/methods restores parts of the π-system and leads to *reduced graphene oxide*[12–16]. See Figure 7.2 for an overview. Unfortunately, none of the chemical methods can be termed "green".

As stated previously, this final material resembles pristine graphene in many ways[17]. Additionally, one achieves solubility and linker groups which enables a broad range of wet chemical methods[5]. For these reasons, many researchers (see Chapter 2) decided to use (reduced) graphene oxide as basis for sensor applications.

The synthesis of (reduced) graphene oxide is actually simple (see Chapter 3) as long as some common traps are avoided. In contrast, the mechanism behind is not simple and not well understood so far. Thus, in addition to the summarized version given before, a very detailed description of the synthesis and its mechanism is provided in the following sections. Last, different conditioning methods for the materials are presented and examined.

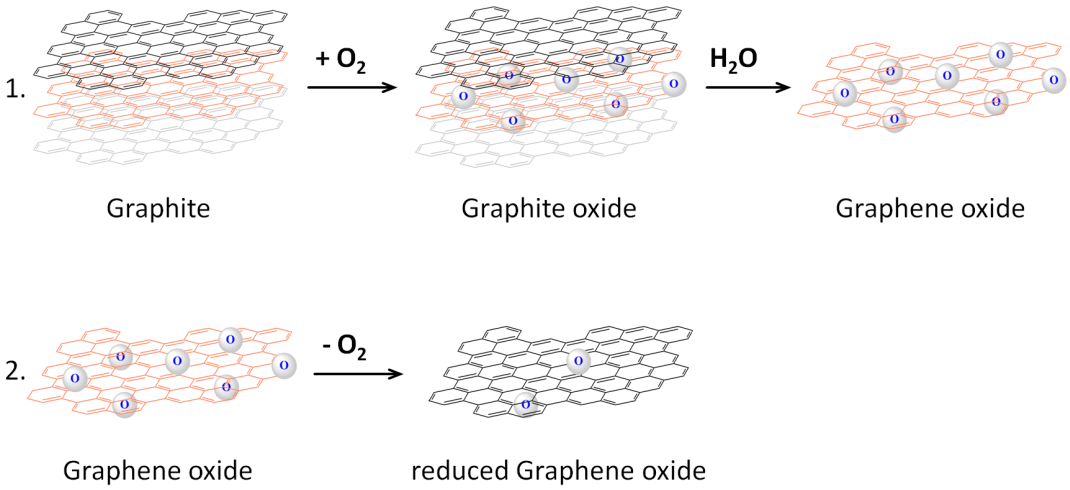

Figure 7.2. Overview of the different stages on the route to reduced graphene oxide. The detailed procedure and mechanism are explained in the following sections.

7.2 Graphene oxide

7.2.1 Detailed synthesis

In the following, high concentrated acids (corrosive) and oxidation agents are used which require careful handling and appropriate protective equipment (safety goggles, coat, gloves). All solids, especially potassium permangate, have to be added to the liquid sulfuric acid instead of the reverse. Also the mixture will get very hot due to the oxidation process. Contingently, it is very viscous after some hours or days. Only fuming sulfuric acid should be added to dilute the mixture if needed, never water. The latter one will stop the reaction immediately. Ultrapure water was used for synthesis and solutions, throughout. All reaction solutions and/or work-up solutions have to be disposed of according to (local) regulations!

A typical procedure is starting with 100 mg of graphite. For larger batches the other chemicals but sulfuric acid have only to be multiplied by the corresponding factor. Since sulfuric acid acts also as pseudo-solvent in the beginning it has to be used as much as needed so that the mixture does not become too viscous (additional factor of 2-4). In the course of this thesis, batches of up to 3 g of graphite were successfully prepared.

First, 100 mg of graphite and 100 mg sodium nitrate were added into 5 mL of fuming sulfuric acid (97-98%). 1 g of solid potassium permanganate was slowly added. The color of the mixture itself will stay dark because of the graphite but at the liquid border the formation of the green manganate dimer Mn_2O_7 can be observed (see Figure 7.3). The whole mixture was stirred for 3 days.

The initially dark-green mixture became much more viscous after 3 days of stirring. It was then slowly diluted with 5 mL of sulfuric acid (5%, i.e. 95% water) to stop the reaction. This step has to be done with extreme caution since the reaction of water with concentrated acid is highly exothermic ("*Water in acid should never be done; Acid in water rarely goes wrong.*")! The mixture itself turns reddish brown.

It was heated for 3 h to 100-120 °C. In this process the batch turned from a viscous mixture to a more fluid solution (brownish yellow/orange). The point of change was at about 1.5 h. Depending on the amount of substance in the batch the actual color can only be seen by diluting it with water (see Figure 7.3). After cooling, 1 mL of hydrogen peroxide (30%) were slowly added to remove remaining manganese oxides. As a result, the solution became more clear.

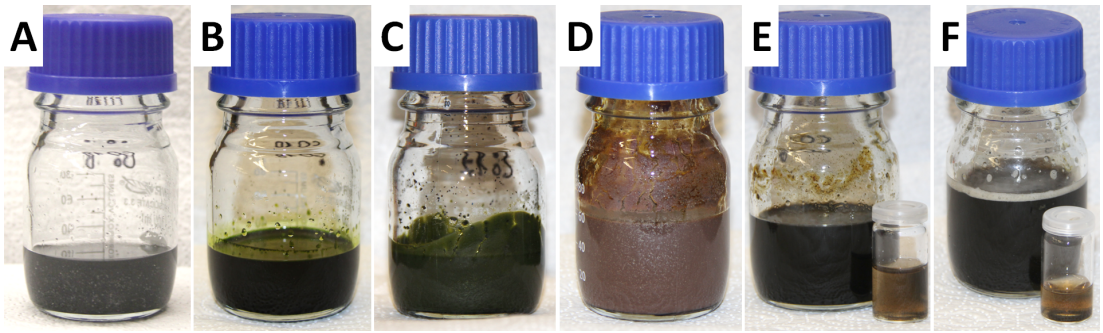

Figure 7.3. Different stages of the synthesis of graphene oxide. (A) Graphite and sodium nitrate in sulfuric acid. (B) After addition of potassium permanganate to A. The formation of the green manganate dimer is clearly visible at the liquid border. (C) After 3 days of stirring the dark-green mixture became much more viscous. (D) After careful addition of H_2SO_4 (5%) to C the mixture becomes dark brown. (E) After heating D for 3h the mixture gets fluent again. The vial shows the actual color of the mixture by diluting it with water (1:1). It is still a little turbid. (F) After the addition of H_2O_2 to F small bubbles raise. The color (after 1:1 dilution with water) gets more clear.

Finally, the product had to be worked up. Some procedures use filtering and washing of the precipated solid[18]. It should be noted that the sulfuric acid will attack and destroy cellulose (paper filters) and other materials. Another issue is the binding of graphene oxide to metal ions[19,20]. Here, manganese ions are bound which have to

be washed out. For this, large quantities of water are needed in which graphite oxide eventually also dissolve.

Hence, a two-step cleaning process is needed. First the sulfuric acid was slowly washed out by centrifugation. The resulting solid from the previous step was collected by centrifugation and washed five times with a solution of sulfuric acid (3%) and hydrogen peroxide (3%), two times with hydrochloric acid (3.7%) and two times with water. In the last step the supernatant already had a yellow color. This indicates a much higher pH level, since graphene oxide dissolves in slightly acidic, neutral as well as alkaline but not in strongly acidic solutions.

Subsequently, ions remaining in the solution were removed by dialysis against ultrapure water over 3 days. The dialysis water was changed every day. The water of the solution was then removed by lyophilization to yield ∼50 mg of graphite oxide in the form of a brown solid. The purity was checked by elementary analysis. The fraction of sulfur, nitrogen and chloride was under wt 0.1% each. Solutions of exfoliated graphene oxide are obtained by dissolving small amounts of graphite oxide in water (e.g. 0.5 mg mL^{-1}).

7.2.2 Mechanism

Since graphite is the source material, we first focus on its reactivity and chemistry. It is known that graphite does not directly react with most reagents but forms intercalation compounds[2]. However, it can be oxidized in whole or in part. The oxygen chemistry of graphite was intensively examined because of its industrial significance, because it is used in many high temperature applications and in nuclear reactors[21–24].

A common misconception is the nature of graphite and its graphene layer structure. The hybridization of carbon, viz. sp^2, suggests a superaromatic molecule. This is amplified by common Lewis formulas for reduced graphene oxide (e.g. the work of *Jahan et al.*[25]). Indeed, graphite and graphene possess a bonding system with a high metallic character[26–29]. Otherwise, both sulfonation and nitration would occur (see Figure 7.4). The non-aromatic behavior of graphite is confirmed by the absence of any nitrogen and sulfur atom in the product (see Chapter 4). Also, none of the

intermediate materials in the synthesis show explosive behavior as may be the case in the presence of many nitrogen groups.

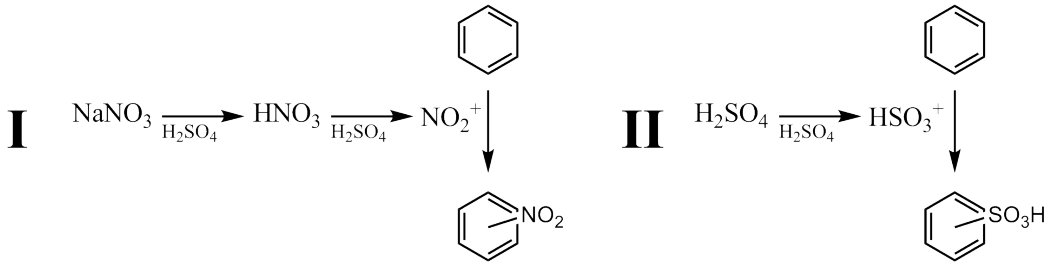

Figure 7.4. Aromatic nitration (I) and sulfonation (II). Side reactions such as *ipso*-substitution are not shown. Both reactions do not work on the metallic-like bonding system of graphite/graphene.

Next, the reaction can be divided into two main pathways. The first pathway is responsible for generating (intermediate) oxygen species which are consumed in the second pathway during the oxidation process. Altogether, there are three oxidation agents involved, namely $KMnO_4$, $NaNO_3$ and H_2SO_4. All of these are intercalated between the graphite layers[2], which promotes the oxidation effect.

Adding permanganate to fuming sulfuric acid leads to in situ generation of Mn_2O_7, a manganate dimer with a characteristic green color[30,31]. It can be observed shortly after the addition of $KMnO_4$ along the inside of the glas vial where the mixture touches the glass. Equation 7.1 explains the instability of the dimer in water. If enough water is present in the reaction the formation is reverted. The small quantity of water which is formally created in this reaction is absorbed by sulfuric acid (indicated by the "precipation"-arrow).

$$2\ KMnO_4 + H_2SO_4 \rightleftharpoons Mn_2O_7 + K_2SO_4 + H_2O\downarrow \tag{7.1}$$

Mn_2O_7 generates a large oxidative potential when reduced to a mixed oxide with Mn(II) and Mn(III) cations. Due to the anhydrous environment of the reaction, the Equation 7.2 does not involve any protons nor water. Instead, a process similar to oxidation melting is assumed to occur.

$$3\ Mn_2O_7 + 26\ e^- \rightarrow 2\ Mn_3O_4 + 13\ O^{2-} \widehat{=} 13\ \langle O \rangle \tag{7.2}$$

After three days of stirring, diluted sulfuric acid (5%, i.e. 95% water) is added to the reaction mixture. In the aqueous environment, the mixed manganese oxide spontaneously precipates as reddish brown solid. It is resolved again either by stirring for a while or by heating the mixture like it is done in the procedure described before. The last process will further reduce the mixed manganese oxide to the Mn(II)-ion species.

$$Mn_3O_4 + 2\ e^- + 8\ H^+ \rightarrow 3\ Mn^{2+} + 4\ H_2O \widehat{=} 1\ \langle O \rangle \tag{7.3}$$

This is a rather mild reduction and because of the amount of added permanganate in the beginning it is possible that not all oxides will become reduced at this point. Hydrogen peroxide is added as final step to overcome this issue. After addition, small bubbles will raise and the color of the solution gets more clear compared to the one before. It reduces the remaining manganese oxides and thus produces elementary (gaseous) oxygen as described by Equation 7.4.

$$Mn_3O_4 + H_2O_2 + \ 6\ H^+ \rightarrow \ 3\ Mn^{2+} + O_2\uparrow + 4\ H_2O \tag{7.4}$$

The generated oxygen gas of the last step leaves the reaction immediately and so it is not taken into account for the total oxygen balance. From the Equations 7.2 and 7.3 it is obvious that three Mn_2O_7 generate 15 ($13 + 2 \cdot 1$) intermediate oxygen entities ($\langle O \rangle = 2\ e^-$). For this six $KMnO_4$ units are needed, i.e. 2.5 (15 O per 6 $KMnO_4$) oxygen entities are generated per unit. So, theoretically, 62.5% of the available oxygen could be used for the oxidation of graphite. However, some of the oxygen is involed in creating nitrogen oxide species (see next paragraphs).

$NaNO_3$ in fuming sulfuric acid is converted into HNO_3 [32]. Sulfuric acid is very hy-

groscopic and dehydrates nitric acid to form the anhydride N_2O_5 [33]. Eventually, the anhydride decomposes into NO_2 and oxygen gas. NO_2 and its dimer form, N_2O_4, oxidize graphite. The following equations sum up this process. For clarification, the dimer forms of the nitrogen oxide species (N_2O_4, N_2O_2) are omitted.

$$NaNO_3 + H_2SO_4 \longrightarrow NaHSO_4 + HNO_3 \tag{7.5}$$

$$2\ HNO_3 \longrightarrow N_2O_5 + H_2O\downarrow \tag{7.6}$$

$$2\ N_2O_5 \longrightarrow 4\ NO_2 + O_2 \tag{7.7}$$

$$NO_2 + 2\ e^- \longrightarrow NO + O^{2-} \quad \widehat{=}\ 1\ \langle O \rangle \tag{7.8}$$

The resulting nitrogen monoxide is oxidized again to form nitrogen dioxide which closes the loop. It is also common to use sodium nitrite instead of sodium nitrate [34]. In this case, HNO_2 is first formed which disproportionates to HNO_3 and NO [33]. From this perspective, adding $NaNO_2$ instead of the nitrate does not make any difference.

$$3\ HNO_2 \rightleftharpoons HNO_3 + 2\ NO + H_2O\downarrow \tag{7.9}$$

The chemistry of nitrogen oxide is complex [33] and due to the oxidation potential in the present reaction all possible nitrogen oxide species (N_xO_y) are created. Their well-known toxicitiy [33] has been subject to substantial research [35]. Hence, some completely omit using any nitrate or nitrite in their synthesis [35,36].

At this point, the question arises why to use nitrate or nitrite since their oxygen output is quite low and their products are toxic. However, *Kovtyukhova et al.* mention incomplete graphite oxidization in their work which they compensate for by introducing a preoxidation step [36]. It is clear by looking in detail at their procedure that they did not use any sodium nitrate nor nitrite. The preoxidation was done with P_2O_5 in sulfuric acid [36]. Similar to this, *Marcano et al.* abandon nitrate and used H_3PO_4 in their synthesis of graphene oxide [35].

This observation leads to the following mechanistic conclusion. It indicates that the

oxidation by the nitrogen species and their heavier homologes is an important step that probably takes place before the main oxidation by potassium permanganate. Graphite is a closed material, i.e. the only active sites open for oxidation are the outer ones of the bulk solid. However, the gaseous state of the nitrogen oxide species (e.g. NO_2) and their analogous acids (e.g. HNO_3) allows graphite to intercalate them faster compared to liquid (and highly viscous) sulfuric acid or solid manganese oxide(s). The intercalated nitrogen oxides start to oxidize the graphite layers slightly. This process increases the distance between the layers so that the manganese oxides will gain better access to the inner sites ("plier effect", see Figure 7.5A). In absence of any nitrogen (or phosphorous) oxide species this process is much more slower resulting in incomplete graphite oxidization.

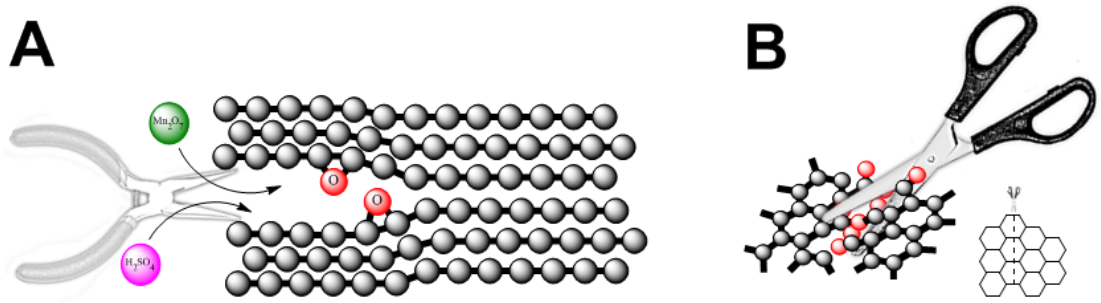

Figure 7.5. Sketches of the effects of nitrogen oxide (A) and manganese oxide (B) in the synthesis of graphite oxide. A) Nitrogen oxide opens the layers of graphite for the main oxidation ("plier effect"). B) Manganese oxide cuts through the lattice of the graphene layers ("scissor effect").

Sulfuric acid is not only a dehydration agent but also an oxidation agent. In this process, it is reduced to SO_2. The latter one is then reoxidized to SO_3 by the various manganese oxides in the mixture. Non reacted sulfur dioxide is consumed by the H_2O_2 added in the end of the whole procedure. However, in the present reaction this behavior plays only a minor role. The main task of sulfuric acid is to provide an anhydrous environment.

$$H_2SO_4 + 2\,e^- \longrightarrow SO_2 + H_2O\downarrow + O^{2-} \;\widehat{=}\; 1\,\langle O\rangle \tag{7.10}$$

In conclusion and for convenience, the net-oxygen generated in "pathway I" can be assumed to originate only from the potassium permanganate deployed in the begin-

ning. Nonetheless, both sulfuric acid and sodium nitrate play an important role in the preparation of graphene oxide. The whole pathway I is compiled in Figure 7.6.

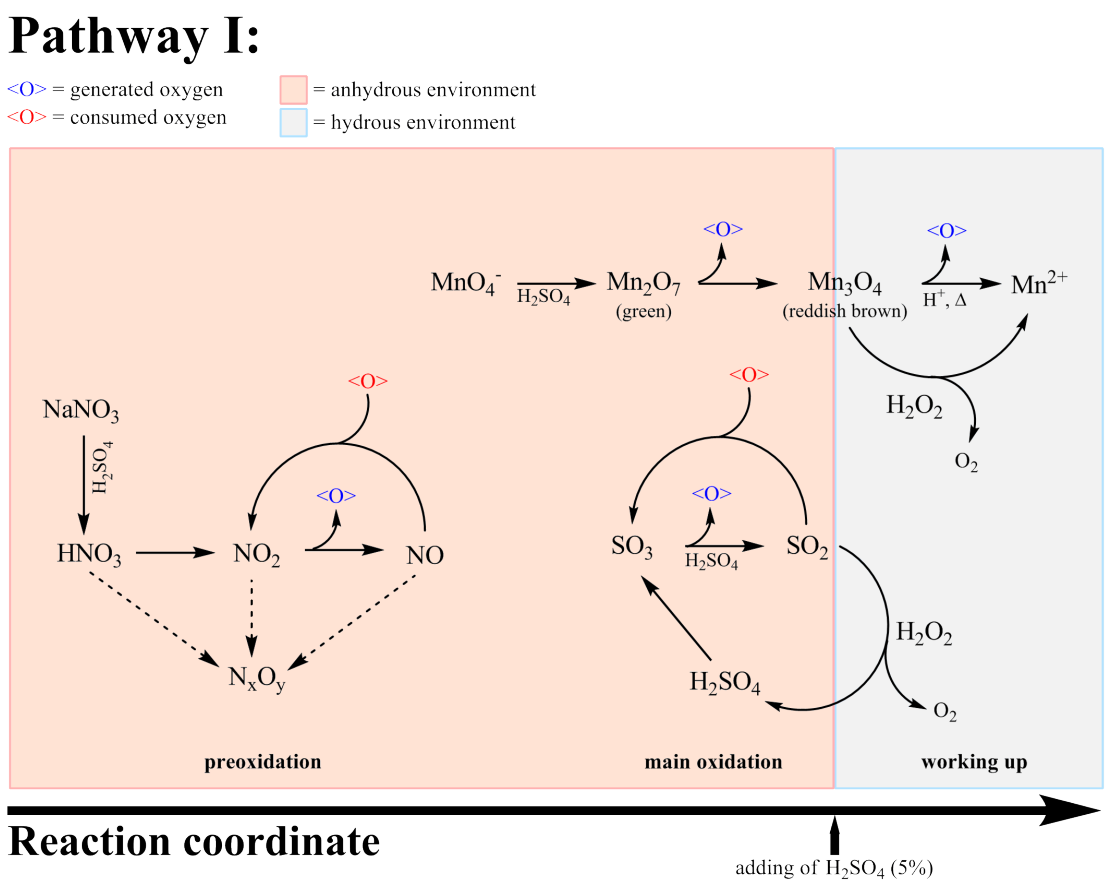

Figure 7.6. Pathway I: Intermediate oxygen species (<O>) for oxidation are generated mainly by the manganese oxide species (top). However, the nitrogen oxide circle (left) is responsible for the preoxidation step. During the reaction process the relevance of this circle decreases. The circle for sulfuric acid and sulfur oxide compounds is shown for completeness, but it is immaterial in the proposed mechanism.

In the second pathway, oxygen is consumed when creating new oxygen functions at the surface of each graphene layer. This process finalizes the breaking of the layer structure of graphite and during the reaction the metallic bulk material is stepwise transformed to an organic-like superstructure.

Breaking the bonds of graphite requires a lot of energy. Hence, high temperatures (1000-2500 °C) are needed for the full oxidation (combustion)[21]. The present reaction operates only at both room temperature (3 days) and at 120 °C (3 hours; see procedure). Obviously, here the reaction is thermodynamically controlled. All involved components are allowed to form equilibriums which favor the most stable

intermediates and products. In contrast the combustion is fast and irreversible, i.e. kinetic controlled.

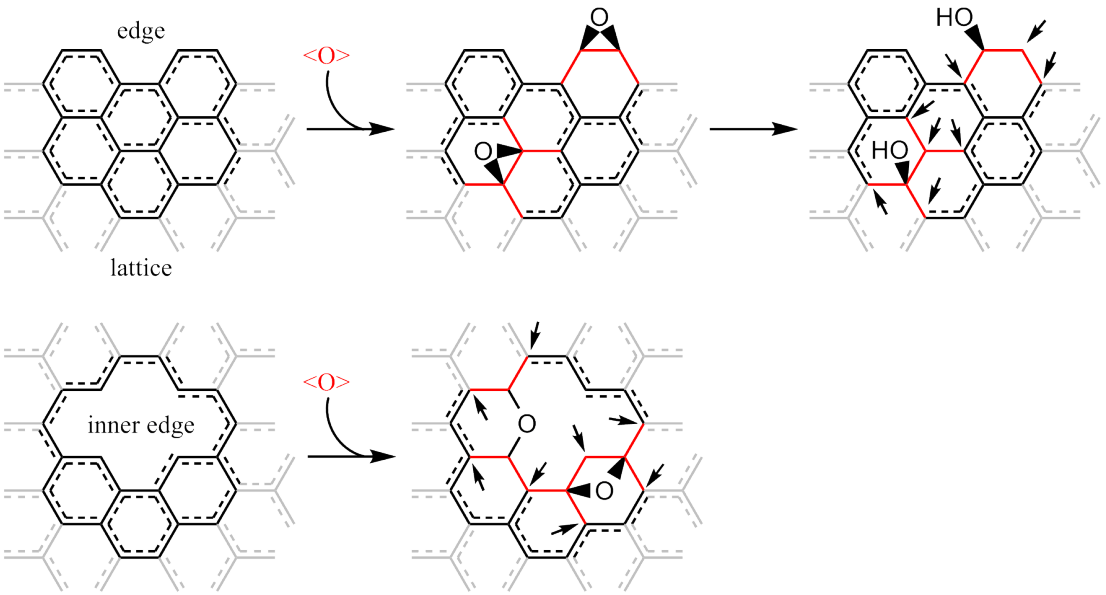

Figure 7.7. Preoxidation of graphite results in the formation of epoxides, alcoholes and ethers. The dashed lines symbolize the metallic system which is disturbed by the local oxidation (red lines). The arrows point to the new local defect sites on which (apart from the present oxide groups) further oxidation steps can take place.

A thermodynamically controlled reaction leads to the question how and where the oxidation starts. Instead of attacking directly the carbon atoms which are involved in the metal bonding system, it is more likely that oxidation starts at reactive edge and defect sites. There are many different types of defects which can occur [37,38]. Every type (e.g. vacancy and topological defects) disturbs the electronic system of the lattice (i.e. disorder) providing local targets for the oxidation agents. The ratio of disorder is determinable by Raman spectroscopy [39].

The preoxidation step performed by the nitrogen oxide species resultes only in low oxidized groups, i.e. epoxides, ethers and alcoholes. The creation of these groups result in two effects which facilitate the main oxidation afterwards. First, the opening of the layer structure (already mentioned in the description of pathway I) allows the main oxidation agents easier access to the basal plane. Second, changing the bonding order or oxidation state of a carbon atom further disturbs the electronic system (i.e. metal bonding) resulting in new local defects. Consecutively, these defect act as new

attacking sites later. The preoxidation is sketched in Figure 7.7.

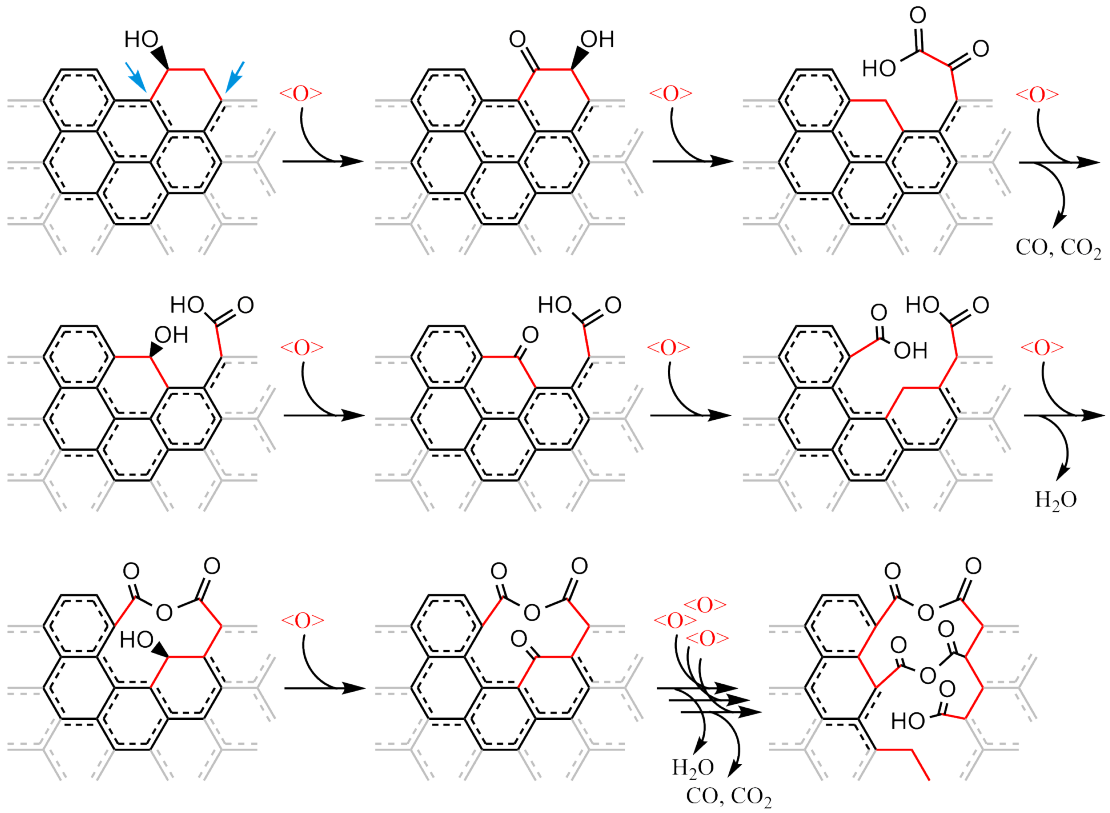

Figure 7.8. An examplary pathway for the main oxidation displaying the consumption of C atoms, the cutting into the lattice and the dehydration of carboxy acids to form anhydrides. For clarification, only a limit number of oxidation is shown here. For instance, in the very first step also the two side-positions (indicated by the blue arrows) can be oxidized. The dashed lines symbolize the metallic system which is disturbed by the local oxidation (red lines).

After preoxidation, the main oxidation is straight forward. On the one hand, manganese oxides attack the defect sites created before. There, new oxide groups and more defects are introduced. On the other hand, present oxide groups are further oxidized to their maximum state, normally carbonyl or carboxy function. Two other possible products are CO and CO_2 which leave the reaction immediately. These gases are responsible for the consumption of the carbon lattice which in turn gives (reduced) graphene oxide its inconsistent shape and size (see Section 4.3.5).

Observation of the catalytic oxidation of graphite revealed that collodial metal particles eat pathes into the graphite lattice[22]. Similarly, manganese oxides cut the layers by oxidation carbon atoms to their maximum state (+III, i.e. carboxy groups) which

eliminates bonds to other C atoms. The whole process of consuming carbon atoms at the border of and in the lattice resembles a piece of paper which is randomly cut ("scissor effect", see Figure 7.5B).

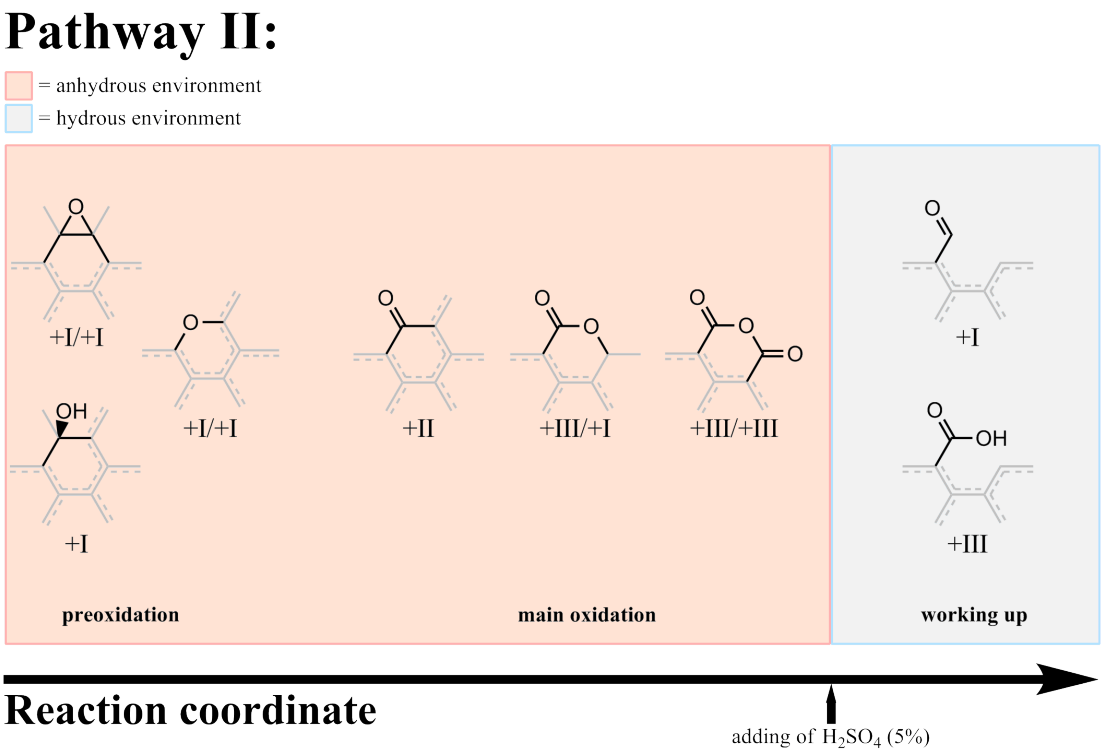

Figure 7.9. Pathway II: Possible oxide groups that occur during the synthesis of graphene oxide. From left to right, only the oxide groups are listed which supervene to the ones before, i.e. the final product also contains epoxide groups although at a low ratio. The Roman numerals depict the oxidation state of the corresponding C atoms.

The main oxidation takes place in concentrated sulfuric acid when hydrolysis is minimal. On the contrary, sulfuric acid absorbs and withdraws water resulting in dehydration of several oxide groups. For instance, anhydrides and esters are easily formed. These and other groups decompose again in the aqueous environment of the last part of the procedure. This assumption is supported by the observation of the product color. During the pre- and main-oxidation, the color of the product stays black which suggests large flake clusters (linked together by anhydrides and esters). It is not until after 1.5 hours of heating in aqueous solution that the color suddenly changes to brownish yellow/orange. This point of change indicates the breaking of the linker groups by hydrolysis. Figure 7.8 sketches an examplary pathway of the main oxidation involving the consumption, cutting and dehydration processes.

In conclusion, the mechanism of the second pathway presented here is very complex. Therefore, it is not possible to compile every detail in a single figure similar to the first one. Thus, Figure 7.9 displays only the possible oxide groups which probably occur at the different steps in the synthesis.

7.3 Reduced graphene oxide

7.3.1 Detailed synthesis

In contrast to graphene oxide, the procedure for the reduction is rather short and simple. First, a clear solution of graphene oxide was prepared by sonification of 25 mg of graphite oxide in 25 mL water. After the addition of 25 µL of 98% hydrazine solution and 50 µL of ammonia (32%), the mixture was stirred for 15 minutes and subsequently heated for 2 h to about 100-120 °C. During the heating, the solution turned from brown/orange to black (see Figure 7.10).

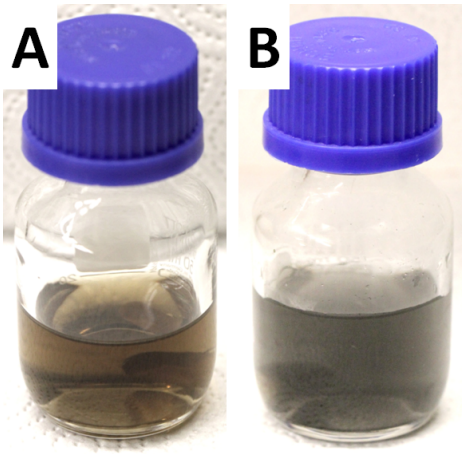

Figure 7.10. Colors before and after the reduction of graphene oxide. (A) A clear graphene oxide solution (1 mg mL^{-1}) is the starting point for the reduction. (B) After the addition of hydrazin (98%) and ammonia (32%), and subseqent heating the solution turns black.

Analogously to graphite oxide, ions and reagents remaining in the solution were removed by dialysis against ultrapure water over 3 days. The dialysis water was changed every day. The water of the solution was then removed by lyophilization to yield ∼12 mg of reduced graphite oxide in the form of a black solid. The purity was

checked by elementary analysis. The fraction of nitrogen usually is below wt 3.0% (see Section 4.4.2 for an explanation of this impurities). Solutions of exfoliated reduced graphene oxide are obtained by solving small amounts of reduced graphite oxide in water (e.g. 0.1 mg mL^{-1}).

7.3.2 Mechanism

The above procedure is short and simple. However the mechanism is not entirely clear[17]. Apart from graphene oxide, there are only two other components involved, viz. ammonia and hydrazine.

Both, hydrazine and a base first suggest a typical *Wolff-Kishner reduction* that converts aldehydes and ketones to alkanes[40–42]. This reaction would further increase defect concentrations. However, the recovery of large parts of the aromatic system can be deduced from the data of the characterization (see Chapter 4).

Hydrazine is a mild reducing agent and known not to interact with all oxygen groups. A mechanism for the elimination of epoxy groups is proposed[11]. First, a substitution reaction with hydrazine opens the ring. The hydroxy and the hydrazine groups thus formed are eliminated, next. There are also other versions with slightly different mechanisms published[43]. Probably, carboxy groups are mostly removed by thermal elimination (see Figure 7.11).

By looking at the product, it is clear that some of hydroxy groups are reduced, too. This does not happen in absence of hydrazine or other reducing agents. However, the detailed mechanisms are unclear up to now.

Aromatic hydroxy groups may exhibit some kind of local electron shortage due to the large conjugated systems. The ends of these conjugated systems carry electron-withdrawing groups, which promote the electron shortage. This could allow nucleophilic aromatic substitution by hydrazine similar to halide anions[44]. Subsequently, the attached hydrazine groups decompose by deprotonation and heating to nitrogen and water. The aromatic system at this position is recovered (see Figure 7.11). Obviously, due to thermal elimination, the promotors (carboxy groups) are consumed and

Elimination of epoxy and aliphatic hydroxyl groups:

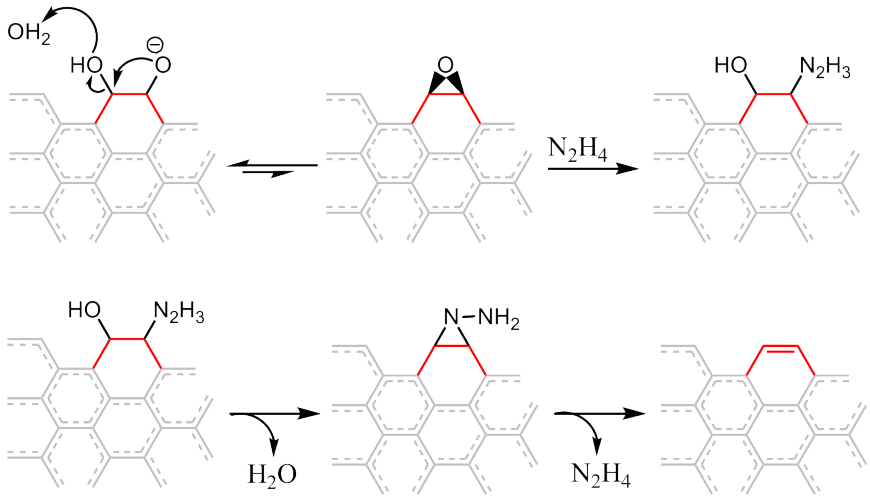

Elimination of carboxyl groups:

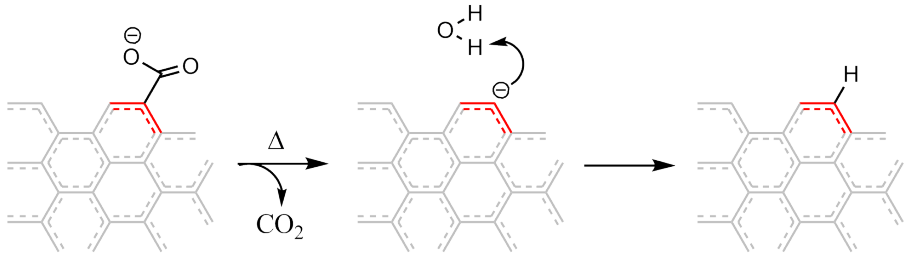

Elimination of aromatic hydroxyl groups:

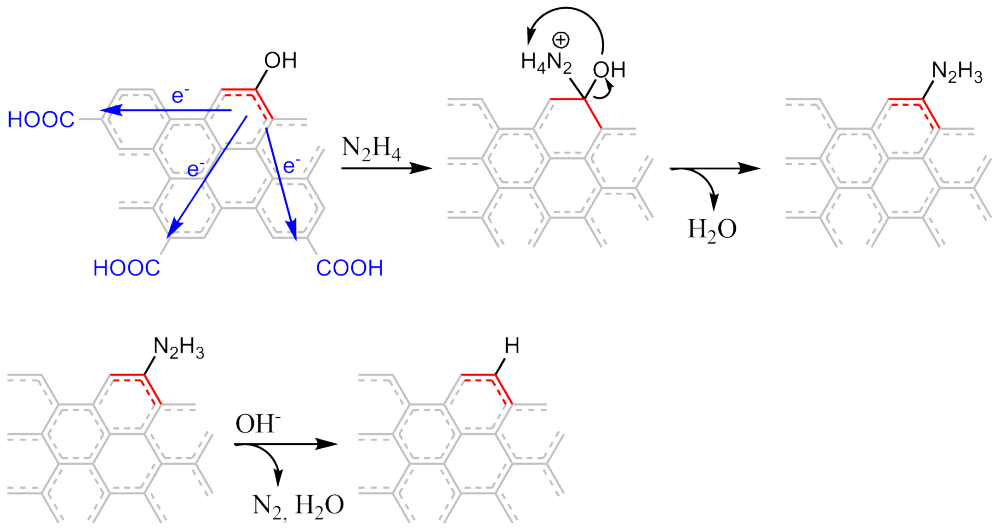

Figure 7.11. The reduction and elimination of various oxide groups by hydrazine and heat.

the reaction eventually stops. This is in conformity with the observation of "incomplete" reduction even if graphene oxide is exposed to hydrazine for up to 24 h[11].

Two vicinal, aliphatic hydroxy groups may undergo a reaction similar to the elimination of the epoxy groups. One of the hydroxy groups is deprotonated and the oxygen substitutes the other hydroxy group, forming an epoxide. From then, the path is the same as described above (see Figure 7.11). Indeed, the forming of a epoxide is reversible and the equilibrium is on the side of the two hydroxy groups. But, the elimination process is not reversible and, due to this, consumes the epoxides when formed. By contrast, one solitary, aliphatic hydroxy group is likely not removed by hydrazine, because there is no effect, which promotes the substitution reaction.

Other reduction agents such as $NaBH_4$[45], ascorbic acid[46], aluminium powder[47] or hydrohalic acids[44] have been reported. These lead to more or less reduced versions of rGO. With these, the oxidation level of the product can be directly controlled. It should be noted, though, that removing of too many of the oxygen groups by harsh reduction eliminates some beneficial properties such as solubility. These features have then to be introduced again by introducing other agents (e.g. sulfonation by sulfanilic acid)[45].

Also, not all damage done to the graphite lattice during the oxidation process can be healed by simple reduction (see Section 5.4). There are attempts to fill in the missing carbon atoms by CVD[48]. However, its extreme conditions (800 °C) render this method useless since modifications and oxygen groups are destroyed during the process.

The second component in the reaction is the base. Basic conditions are needed for two reasons. First, hydrazine must be fully depronated in order to perform any kind of reaction. Otherwise the free electron pair on each nitrogen is bonded and, therefore, cannot be donated (= reduction). Second, reduced graphene oxide seems to agglomerate during the reduction process if the pH is to low[49]. Apart from ammonia, the reduction works also with carbonates or hydroxides.

7.4 Conditioning methods

Attributable to the non-selective and harsh synthesis conditions, especially for the oxidation of graphite, both graphene oxide and its reduced form are a very "chaotic" product. First, the shape and size of the individual flakes are inconsistent (see Section 4.3.5). Some properties such as conductivity rely on a large, non-disturbed π-system which in turn is dependent on the size of a flake. Other properties such as luminescence require more disturbed systems, i.e. smaller flakes, because of the higher band gap. Therefore, it may be reasonable to separate different flake sizes if the application calls for it.

Second, it is not trivial to separate products from educts. Modifications made to (reduced) graphene oxide only slightly change flake size, form and mass, which are suitable properties for separation. Commonly used methods such as dialysis can only separate small molecules (e.g. coupling reagents) from much larger materials but fails at separating unreacted material (e.g. GO) from reacted material (e.g. GO with coupled dye) due to similar sizes.

Common techniques are presented and discussed in this section. These potentially lead to more consistent products and enable the separation of educt and product. Dialysis, chromatography, fractional centrifugation and capillar electrophoresis are examined in particular.

7.4.1 Dialysis

Dialysis is a technique which allows the separation of small molecules from larger ones by diffusion and filtration. An aqueous solution of the material to be purified is insert into a dialysis hose. The hose is put into another large volume of water (usually 100-150 times of the inner volume).

The dialysis hose has small pores which prevent molecules over a certain size to pass. Large molecules or flakes such as from (reduced) graphene oxide remain inside the hose while small reagents (H_2SO_4, NH_3, ...) can leave (= filtration effect). For the

smaller molecules the inner and outer environment is one big solution and, therefore, an equilibrium is established with a constant concentration over the whole volume. Hence, the concentration in the hose starts to decrease. By exchanging the water, this process is repeated several times until the concentration is negligibly small (= diffusion effect).

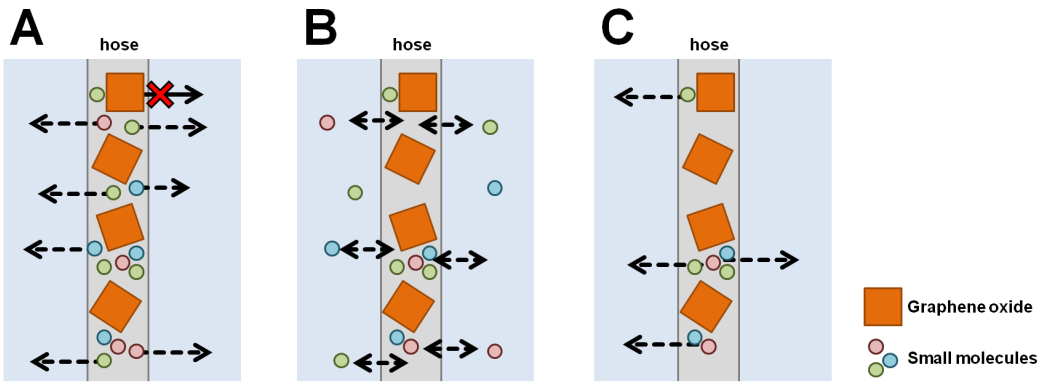

Figure 7.12. Scheme of dialysis. (A) In contrast to (reduced) graphene oxide, small molecules diffuse through the membran of the dialysis hose to the outer solution. (B) An equilibrium between the molecules inside and outside of the hose is emerged. (C) After the changing of the outer water the process starts again. The concentration of small molecules is much lower now compared to the beginning (A).

There are three important parameter which control the success of this method, namely the molecular weight cut-off, the diameter of the hose and the time of changing the water. If the water is changed to early, the equilibrium is not fully emerged which results in incomplete purification. Longer times will unnecessarily lengthen the process.

The molecular weight cut-off must be large enough to allow all small, unwanted reagents to leave the hose. At the same time, it must be small enough to keep even the smallest (r)GO-flakes inside. The diameter is responsible for the diffusion process. The molecules not only need to diffuse through the water but also through the (reduced) graphene oxide. Obviously, the diffusion in (r)GO is much lower than in water. A large diameter allows only few, slow diffusion processes. By choosing a smaller diameter, more parallel diffusion processes occur, which, collectively, lead to an overall faster diffusion.

Hoses with a diameter of 6.3 mm and a molecular weight cut-off of 14 000 Da were chosen. The water was changed every day and the whole process lasted for 3 days. The success of this method was checked by elementary analysis. For instance, graphene

oxide contains wt 20% of sulfur prior to purification which are reduced by dialysis to under 0.1%. This makes dialysis a valuable and mandatory tool in the cleaning process of (reduced) graphene oxide. The principle of dialysis are sketched in Figure 7.12.

7.4.2 Size-exclusion chromatography

Chromatography is a common technique for separation and purification in organic chemistry. A mixture of molecules in solution (mobile phase) is allowed to move through an solid phase. If the diffusion of the components in the mobile phase is different enough they get separated.

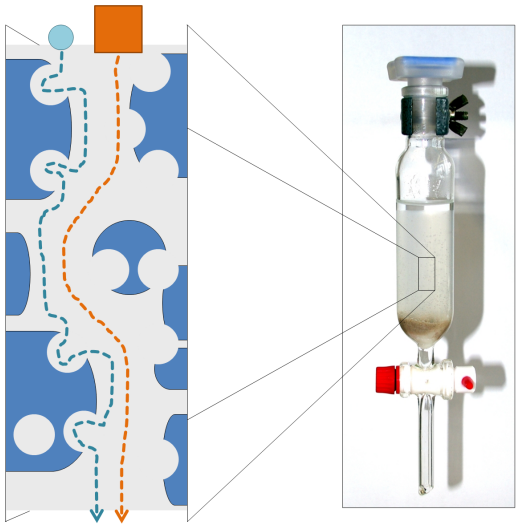

Figure 7.13. Scheme of size exclusion chromatography. Small particles or molecules (blue circle) move slowly through the porous column material because of the many pockets they can diffuse into. In contrast, larger particles or molecules (orange square) simply pass by. Clearly, the way of the orange particle is shorter and, therefore, the particles is faster passing the whole column than the small one (blue way).

Size-exclusion chromatography is a special type. The principle of this method is to separate different particles or molecules by size. They have to move through a very porous material with many small pockets. Small particles or molecules easily diffuse into this pockets and, therefore, need a longer time for passing the column than larger ones (see Figure 7.13). This technique is used for other nano- and biomaterials [50–52]. Very recently, a procedure for onsurfactant-stabilised graphene was published [53]. So, it seems natural to use it for (reduced) graphene oxide.

Unfortunately, a problem emerged during chromatographic experiments in that (reduced) graphene oxide spontanously precipated on the column. Different combinations of column material (various cross-linked dextrans, silica gels and controlled pore glasses) and solvents (water, acetonitrile, acetone) were tried, but led to the same result. On the rare successful executions, the material was hardly separated. Both, the unreliable precipitation and the partial separation have to be solved before size-exclusion chromatography becomes a viable tool for purifying (reduced) graphene oxide. At the moment, this technique clearly fails for this purpose.

7.4.3 Centrifugation

It is obvious that different flake sizes of (reduced) graphene oxide should have a different number of atoms and, therefore, different mass. This allows for separation by fractional centrifugation. The bulk material was centrifuged at 500 rpm for 15 minutes. The supernatant is then transfered to another vial and centrifuged at 1000 rpm for another 15 minutes while the residue is washed with water at 500 rpm in order to remove possibly adsorbed smaller fractions. This procedure is repeated several times up to 15,000 rpm. Every fraction has a narrow size distribution. A scheme of this method and a TEM of one fraction is shown in Figure 7.14. The total size for all fractions ranges from 2500 nm^2 (above 15,000 rpm) up to 400 μm^2 (below 500 rpm).

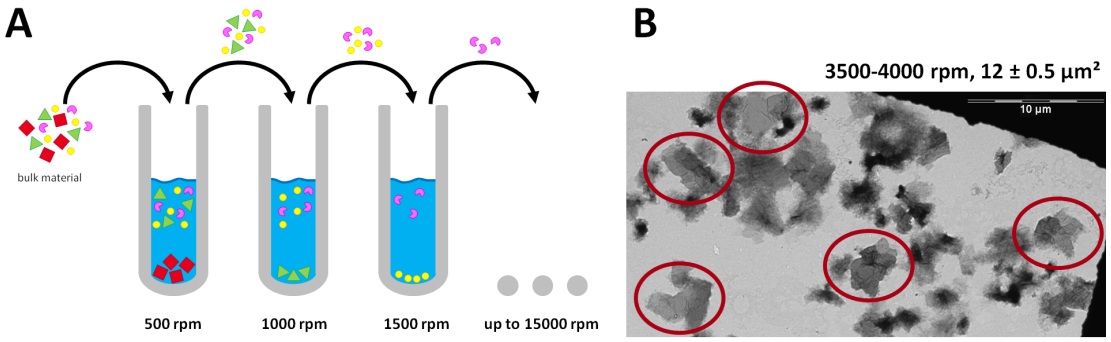

Figure 7.14. Scheme of fractional centrifugation. (A) The stepwise centrifugation of the bulk material achieves fractions of decreasing mass and, therefore, flake size. (B) TEM of an examplary fraction (3500-4000 rpm) revealing the narrow size distribution (here: 12 ± 0.5 μm^2) of the flakes.

It should be noted that the whole process consumes a lot of time (days), because of the subsequent centrifugation and washing of each individual fraction. Also, the

volume rapidly increases with increasing fraction number. A method to overcome these issues is density gradient ultracentrifugal rate separation, which takes advantage of the differences in sedimentation rate between various sized flakes[54].

In this case a density gradient (sucrose solutions of wt 20-60%) is prepared and filled into the tubes, before a sample of the bulk material is placed on top. During centrifugation the bulk material gets driven through the liquid density gradient. Thus, the individual flakes are separated by sedimentation rates. Larger flakes move to the high density areas at the bottom of the tube whereas smaller flakes stay in low density areas at the top[54]. The sucrose is then removed by dialysis or centrifugation. The results resemble the standard fractional centrifugation.

In conclusion, fractional centrifugation is a valuable tool for the preparation of monodisperse (reduced) graphene oxide fractions.

7.4.4 Capillary electropheresis

In this technique, molecules are separated by their electrophoretic mobility (charge and mass). Capillary electrophoresis also enables separation of the materials by layer and by size[55].

The substitution of epoxy groups with an azido ($-N_3$) group (see Section 3.1.4) is a simple modification of graphene oxide. For this, solid sodium azide is added to an aqueous solution of graphene oxide and stirred for several days (with subsequent heating). The product is purified by dialysis and the introduction of the azido group is confirmed by infrared spectroscopy which shows the azide-specific vibration at 2126 cm^{-1} (see Figure 7.15B).

The reaction can be performed at room temperature on air. There is another (more complex) procedure published[56]. No additional reagents are used. These reaction conditions promote a quasi-byproduct-free product. From experience, however, it is known that hardly any reaction proceeds completely. Therefore, this simple modification is a good candidate for testing CE to separate educt (unreacted GO) and product (N_3-GO).

Solutions of GO and of N_3-GO (purified by dialysis) were examined by CE. The resulting electropherograms are plotted in Figure 7.15C. The major fraction of GO elutes at 2.8 min followed by a long tailing section. The corresponding UV/Vis-spectrum at this peak is similar to the one of a "free" solution (see Figure 7.15A). The electropherogram for the N_3-GO solution also includes this major peak at the same elution time. Another peak appears at 11.5 min. Here, the corresponding UV/Vis-spectra is more similar to the N_3-GO-solution than to GO. The differences at the lower UV-region (200-250 nm) are attributed to the different detector systems used.

Solutions not only can be analysed this way by CE, but also fractions of defined time periods can be collected. Thus, CE is able to separate product from educt. However, since the typically used volumines for CE are small ($\sim$200 µL), this technique has only limited value at the moment for large scale applications.

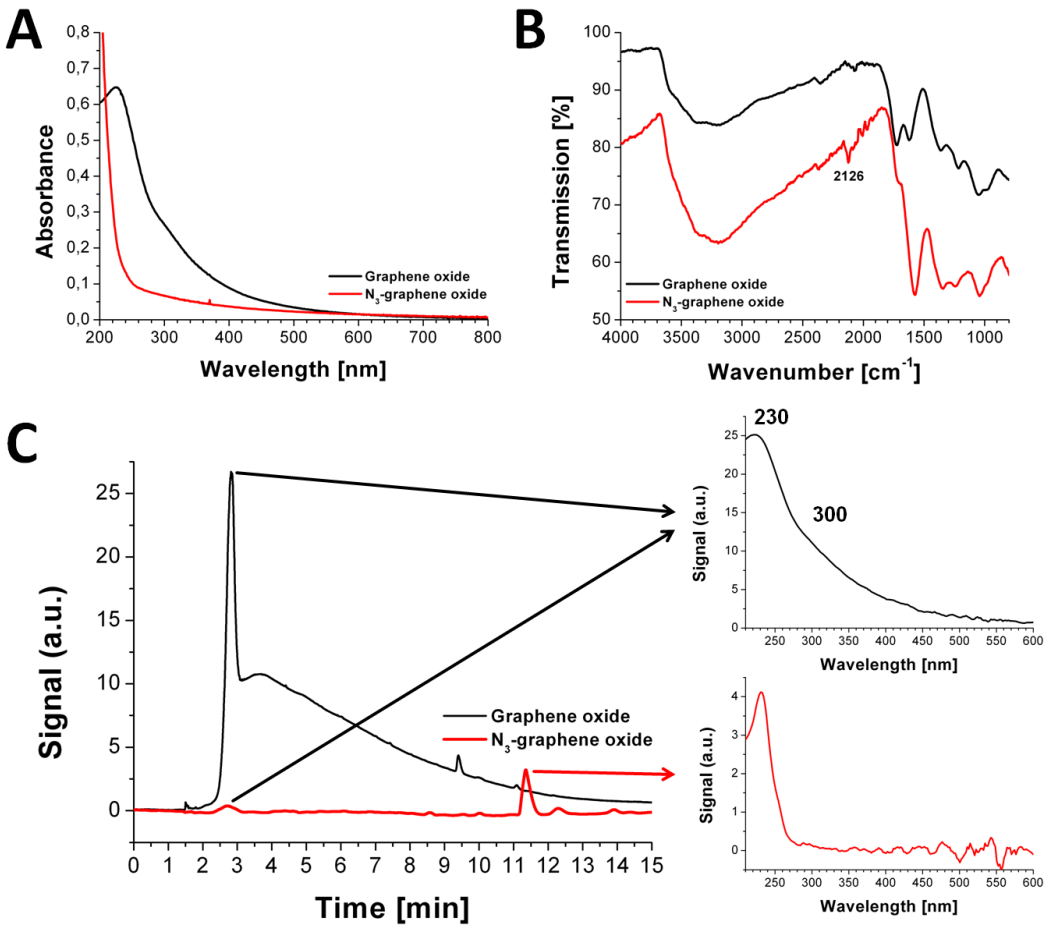

Figure 7.15. Results of capillary electrophoresis. (A) UV/Vis spectra of GO and N_3-GO. (B) IR-spectra of GO and N_3-GO. The specific N_3-stretch-vibration is clearly visible at 2126 cm^{-1}. (C) Electropherogramms (left) of a GO and N_3-GO solution and the UV/VIS spectras (right) of the peaks at 2.8 min and 11.5 min which correspond to GO and N_3-GO, respectively.

7.5 References

[1] D. W. Olson. Graphite (Natural) - Annual report. *U.S. Geological Survey*, 1:68–69, 2012.

[2] D. Chung. Review Graphite. *J. Mater. Sci.*, 37(8):1475–1489, 2002. doi: 10.1023/A:1014915307738.

[3] K. S. Novosëlov, A. K. Geim, S. V. Morozov, D. Jiang, Y. Zhang, S. V. Dubonos, I. V. Grigorieva, and A. A. Firsov. Electric Field Effect in Atomically Thin Carbon Films. *Science*, 306(5696): 666–669, 2004. doi: 10.1126/science.1102896.

[4] M. J. Allen, V. C. Tung, and R. B. Kaner. Honeycomb Carbon: A Review of Graphene. *Chem. Rev.*, 110(1):132–145, 2010. doi: 10.1021/cr900070d.

[5] K. P. Loh, Q. Bao, P. K. Ang, and J. Yang. The chemistry of graphene. *J. Mater. Chem.*, 20 (12):2277–2289, 2010. doi: 10.1039/B920539J.

[6] L. M. Viculis, J. J. Mack, O. M. Mayer, H. T. Hahn, and R. B. Kaner. Intercalation and exfoliation routes to graphite nanoplatelets. *J. Mater. Chem.*, 15(9):974–978, 2005. doi: 10.1039/B413029D.

[7] L. M. Viculis, J. J. Mack, and R. B. Kaner. A Chemical Route to Carbon Nanoscrolls. *Science*, 299(5611):1361–1361, February 2003. doi: 10.1126/science.1078842.

[8] B. C. Brodie. On the Atomic Weight of Graphite. *Philos. Trans. R. Soc. London*, 149:249–259, January 1859. doi: 10.1098/rstl.1859.0013.

[9] L. Staudenmaier. Verfahren zur Darstellung der Graphitsäure. *Ber. Dtsch. Chem. Ges.*, 31(2): 1481–1487, 1898. doi: 10.1002/cber.18980310237.

[10] W. S. Hummers and R. E. Offeman. Preparation of Graphitic Oxide. *J. Am. Chem. Soc.*, 80 (6):1339–1339, March 1958. doi: 10.1021/ja01539a017.

[11] S. Stankovich, D. A. Dikin, R. D. Piner, K. A. Kohlhaas, A. Kleinhammes, Y. Jia, Y. Wu, S. T. Nguyen, and R. S. Ruoff. Synthesis of graphene-based nanosheets via chemical reduction of exfoliated graphite oxide. *Carbon*, 45(7):1558–1565, June 2007. doi: 10.1016/j.carbon.2007.02.034.

[12] S. Park and R. S. Ruoff. Chemical methods for the production of graphenes. *Nat. Nano.*, 4(4): 217–224, April 2009. doi: 10.1038/nnano.2009.58.

[13] M. J. McAllister, J.-L. Li, D. H. Adamson, H. C. Schniepp, A. A. Abdala, J. Liu, M. Herrera-Alonso, D. L. Milius, R. Car, R. K. Prud'homme, and I. A. Aksay. Single Sheet Functionalized Graphene by Oxidation and Thermal Expansion of Graphite. *Chem. Mater.*, 19(18):4396–4404, May 2007. doi: 10.1021/cm0630800.

[14] L. J. Cote, R. Cruz-Silva, and J. Huang. Flash Reduction and Patterning of Graphite Oxide and Its Polymer Composite. *J. Am. Chem. Soc.*, 131(31):11027–11032, July 2009. doi: 10.1021/ja902348k.

[15] E. C. Salas, Z. Sun, A. Luettge, and J. M. Tour. Reduction of Graphene Oxide via Bacterial Respiration. *ACS Nano*, 4(8):4852–4856, July 2010. doi: 10.1021/nn101081t.

[16] M. Hilder, B. Winther-Jensen, D. Li, M. Forsyth, and D. R. MacFarlane. Direct electrodeposition of graphene from aqueous suspensions. *Phys. Chem. Chem. Phys.*, 13(20):9187–9193, 2011. doi: 10.1039/C1CP20173E.

[17] D. R. Dreyer, S. Park, C. W. Bielawski, and R. S. Ruoff. The chemistry of graphene oxide. *Chem. Soc. Rev.*, 39(1):228–240, 2010. doi: 10.1039/B917103G.

[18] H. Chen, M. B. Müller, K. J. Gilmore, G. G. Wallace, and D. Li. Mechanically Strong, Electrically Conductive, and Biocompatible Graphene Paper. *Adv. Mater.*, 20(18):3557–3561, 2008. doi: 10.1002/adma.200800757.

[19] B. Wang, Y. H. Chang, and L. J. Zhi. High yield production of graphene and its improved property in detecting heavy metal ions. *New Carbon Mater.*, 26(1):31–35, 2011. doi: 10.1016/S1872-5805(11)60064-4.

[20] G. Zhao, J. Li, X. Ren, C. Chen, and X. Wang. Few-Layered Graphene Oxide Nanosheets As Superior Sorbents for Heavy Metal Ion Pollution Management. *Environ. Sci. Technol.*, 45(24): 10454–10462, November 2011. doi: 10.1021/es203439v.

[21] R. Backreedy, J. M. Jones, M. Pourkashanian, and A. Williams. A study of the reaction of oxygen with graphite: Model chemistry. *Faraday Discuss.*, 119:385–394, 2002. doi: 10.1039/B102063N.

[22] G. Hennig. Catalytic oxidation of graphite. *Journal of Inorganic and Nuclear Chemistry*, 24(9): 1129–1137, December 1962. doi: 10.1016/0022-1902(62)80258-9.

[23] R. Larciprete, P. Lacovig, S. Gardonio, A. Baraldi, and S. Lizzit. Atomic Oxygen on Graphite: Chemical Characterization and Thermal Reduction. *J. Phys. Chem. C*, 116(18):9900–9908, April 2012. doi: 10.1021/jp2098153.

[24] S. M. Lee, Y. H. Lee, Y. G. Hwang, J. R. Hahn, and H. Kang. Defect-Induced Oxidation of Graphite. *Phys. Rev. Lett.*, 82(1):217–220, January 1999. doi: 10.1103/PhysRevLett.82.217.

[25] M. Jahan, Q. Bao, J.-X. Yang, and K. P. Loh. Structure-Directing Role of Graphene in the Synthesis of Metal-Organic Framework Nanowire. *J. Am. Chem. Soc.*, 132(41):14487–14495, September 2010. doi: 10.1021/ja105089w.

[26] S. Jenkins, P. Ayers, S. Kirk, P. Mori-Sánchez, and A. Martín Pendás. Bond metallicity of materials from real space charge density distributions. *Chemical Physics Letters*, 471(1–3):174–177, March 2009.

[27] G. Venugopal and S.-J. Kim. Investigation of electrical transport characteristics of nanoscale stacks fabricated on thin graphite layer. *Thin Solid Films*, 519(20):7095–7099, August 2011. doi: 10.1016/j.tsf.2011.04.082.

[28] P. R. Wallace. The Band Theory of Graphite. *Phys. Rev.*, 71(9):622–634, May 1947. doi: 10.1103/PhysRev.71.622.

[29] A. K. Geim and K. S. Novosëlov. The rise of graphene. *Nat. Mater.*, 6(3):183–191, March 2007. doi: 10.1038/nmat1849.

[30] T. S. Dzhabiev, N. N. Denisov, D. N. Moiseev, and A. E. Shilov. Formation of ozone during the reduction of potassium permanganate in sulfuric acid solutions. *Russ. J. Phys. Chem. A*, 79 (11):1755–1760, 2005.

[31] W. Levason, J. S. Ogden, and J. W. Turff. Infrared and ultraviolet-visible spectroscopic studies on manganese heptoxide (Mn2O7). *J. Chem. Soc., Dalton Trans.*, 12:2699–2702, 1983. doi: 10.1039/DT9830002699.

[32] C. W. Volney. On the Decomposition of Sodium Nitrate by Sulphuric Acid, II. *J. Am. Chem. Soc.*, 23(7):489–492, July 1901. doi: 10.1021/ja02033a013.

[33] M. Thiemann, E. Scheibler, and K. W. Wiegand. *Nitric Acid, Nitrous Acid, and Nitrogen Oxides*, volume 24, pages 177–225. Wiley-VCH Verlag GmbH & Co. KGaA, 2000. ISBN 9783527306732. doi: 10.1002/14356007.a17_293.

[34] A. Satti, P. Larpent, and Y. Gun'ko. Improvement of mechanical properties of graphene oxide/poly(allylamine) composites by chemical crosslinking. *Carbon*, 48(12):3376–3381, October 2010. doi: 10.1016/j.carbon.2010.05.030.

[35] D. C. Marcano, D. V. Kosynkin, J. M. Berlin, A. Sinitskii, Z. Sun, A. Slesarev, L. B. Alemany, W. Lu, and J. M. Tour. Improved Synthesis of Graphene Oxide. *ACS Nano*, 4(8):4806–4814, July 2010. doi: 10.1021/nn1006368.

[36] N. I. Kovtyukhova, P. J. Ollivier, B. R. Martin, T. E. Mallouk, S. A. Chizhik, E. V. Buzaneva, and A. D. Gorchinskiy. Layer-by-Layer Assembly of Ultrathin Composite Films from Micron-Sized Graphite Oxide Sheets and Polycations. *Chem. Mater.*, 11(3):771–778, January 1999. doi: 10.1021/cm981085u.

[37] F. Banhart, J. Kotakoski, and A. V. Krasheninnikov. Structural Defects in Graphene. *ACS Nano*, 5(1):26–41, November 2010. doi: 10.1021/nn102598m.

[38] O. V. Yazyev and S. G. Louie. Topological defects in graphene: Dislocations and grain boundaries. *Phys. Rev. B*, 81(19):195420, May 2010. doi: 10.1103/PhysRevB.81.195420.

[39] A. C. Ferrari. Raman spectroscopy of graphene and graphite: Disorder, electron–phonon coupling, doping and nonadiabatic effects. *Solid State Communications*, 143(1–2):47–57, July 2007. doi: 10.1016/j.ssc.2007.03.052.

[40] L. Wolff. Chemischen Institut der Universität Jena: Methode zum Ersatz des Sauerstoffatoms der Ketone und Aldehyde durch Wasserstoff. *Justus Liebigs Annalen der Chemie*, 394(1):86–108, 1912. doi: 10.1002/jlac.19123940107.

[41] Huang-Minlon. Reduction of Steroid Ketones and other Carbonyl Compounds by Modified Wolff–Kishner Method. *J. Am. Chem. Soc.*, 71(10):3301–3303, October 1949. doi: 10.1021/ja01178a008.

[42] H. H. Szmant. The Mechanism of the Wolff–Kishner Reduction, Elimination, and Isomerization Reactions. *Angew. Chem., Int. Ed.*, 7(2):120–128, 1968. doi: 10.1002/anie.196801201.

[43] X. Gao, J. Jang, and S. Nagase. Hydrazine and Thermal Reduction of Graphene Oxide: Reaction Mechanisms, Product Structures, and Reaction Design. *J. Phys. Chem. C*, 114(2):832–842, December 2009. doi: 10.1021/jp909284g.

[44] S. Pei, J. Zhao, J. Du, W. Ren, and H.-M. Cheng. Direct reduction of graphene oxide films into highly conductive and flexible graphene films by hydrohalic acids. *Carbon*, 48(15):4466–4474, December 2010. doi: 10.1016/j.carbon.2010.08.006.

[45] Y. Si and E. T. Samulski. Synthesis of Water Soluble Graphene. *Nano Lett.*, 8(6):1679–1682, 2008. doi: 10.1021/nl080604h.

[46] M. J. Fernandez-Merino, L. Guardia, J. I. Paredes, S. Villar-Rodil, P. Solis-Fernandez, A. Martinez-Alonso, and J. M. D. Tascon. Vitamin C Is an Ideal Substitute for Hydrazine in the Reduction of Graphene Oxide Suspensions. *J. Phys. Chem. C*, 114(14):6426–6432, March 2010. doi: 10.1021/jp100603h.

[47] Z. Fan, K. Wang, T. Wei, J. Yan, L. Song, and B. Shao. An environmentally friendly and efficient route for the reduction of graphene oxide by aluminum powder. *Carbon*, 48(5):1686–1689, April 2010. doi: 10.1016/j.carbon.2009.12.063.

[48] V. Lopez, R. S. Sundaram, C. Gomez-Navarro, D. Olea, M. Burghard, J. Gomez-Herrero, F. Zamora, and K. Kern. Chemical Vapor Deposition Repair of Graphene Oxide: A Route to Highly-Conductive Graphene Monolayers. *Adv. Mat.*, 21(46):4683–4686, 2009. doi: 10.1002/adma.200901582.

[49] D. Li, M. B. Muller, S. Gilje, R. B. Kaner, and G. G. Wallace. Processable aqueous dispersions of graphene nanosheets. *Nat. Nanotechnol.*, 3(2):101–105, February 2008. doi: 10.1038/nnano.2007.451.

[50] F.-K. Liu and Y.-C. Chang. Using Size-Exclusion Chromatography to Evaluate Changes in the Sizes of Au and Au/Pd Core/Shell Nanoparticles Under Thermal Treatment. *Chromatographia*, 74:767–775, 2011. doi: 10.1007/s10337-011-2139-7.

[51] M. Gaborieau and P. Castignolles. Size-exclusion chromatography (SEC) of branched polymers and polysaccharides. *Anal. Bioanal. Chem.*, 399:1413–1423, 2011. doi: 10.1007/s00216-010-4221-7.

[52] M. Terenghi, L. Elviri, M. Careri, A. Mangia, and R. Lobinski. Multiplexed Determination of Protein Biomarkers Using Metal-Tagged Antibodies and Size Exclusion Chromatography–Inductively Coupled Plasma Mass Spectrometry. *Anal. Chem.*, 81(22):9440–9448, October 2009. doi: 10.1021/ac901853g.

[53] R. J. Smith, P. J. King, C. Wirtz, G. S. Duesberg, and J. N. Coleman. Lateral size selection of surfactant-stabilised graphene flakes using size exclusion chromatography. *Chem. Phys. Lett.*, 531(0):169–172, April 2012. doi: 10.1016/j.cplett.2012.02.027.

[54] X. Sun, D. Luo, J. Liu, and D. G. Evans. Monodisperse Chemically Modified Graphene Obtained by Density Gradient Ultracentrifugal Rate Separation. *ACS Nano*, 4(6):3381–3389, June 2010. doi: 10.1021/nn1000386.

[55] M. B. Müller, J. P. Quirino, P. N. Nesterenko, P. R. Haddad, S. Gambhir, D. Li, and G. G. Wallace. Capillary zone electrophoresis of graphene oxide and chemically converted graphene. *J. Chromatogr., A*, 1217(48):7593–7597, November 2010. doi: 10.1016/j.chroma.2010.09.069.

[56] R. Salvio, S. Krabbenborg, W. J. M. Naber, A. H. Velders, D. N. Reinhoudt, and W. G. van der Wiel. The Formation of Large-Area Conducting Graphene-Like Platelets. *Chem.–Eur. J.*, 15 (33):8235–8240, 2009. doi: 10.1002/chem.200900661.

8 Sensor applications

8.1 Overview

Reduced graphene oxide and graphene oxide have many attractive features such as solution processing, higher sensitivies for particular analytes, and attraction and discrimination effects (see Section 2.4). After a detailed discussion of synthesis and characterization, the next logical step is to utilize these beneficial features for sensor applications.

Table 8.1 lists the sensor concepts developed during this work. These concepts range from very simple methods (resistance measurements), to techniques rarely used in graphene research (surface plasmon resonance), to more complex variants (N_3−GO modification with coupled alkyne-modified glucose oxidase).

Table 8.1. Overview of the sensor concepts started within the scope of this work.

Material(s)	Method	Goal, analytes
rGO	Resistance measurement	Gas sensors for NO_2, CO_2, H_2, and alkanes
(r)GO	Surface plasmon resonance	DNA sensor; sensor for ammonia and amines
N_3−GO, (alkyne-)GOx	Cyclic voltammetry; amperometry	Glucose biosensor

This section presents the basic principles behind two of them, namely, a gas sensor for NO_2 and an affinity sensor based on surface plasmon resonance for amines. Further improvements, solving various experimental issues, and completion of the sensor will be a task for future work.

8.2 Gas sensor for NO_2

Reduced graphene oxide is known for its high affinity to gases and vapors[1]. These adsorbed molecules influence the (electronic) properties by interacting with the surface. A electron-donating gas, e.g. NH_3, reduces the number of charge carriers and in turn decreases conductivity. In contrast, an electron-acceptor gas, such as NO_2, greatly reduces the bulk resistivity of rGO[1]. This effect depends on the concentration of the gas and can be utilized to sense these gases. It should be noted that this behavior in general is not selective[1] and rGO can only distinguish between electron-accepting and electron-donating molecules[2].

However, sensing of NO_2 is a good starting point for developing a gas sensor based on rGO, given its simple preparation. After drop casting of rGO on an electrode and subsequent heating of the modified electrode, it is ready to use for gas sensing. An exemplary measurement is shown in Figure 8.1. The electron-accepting effect of NO_2 results in an increase in the conductivity, which is consistent with an increase in the number of charge carriers.

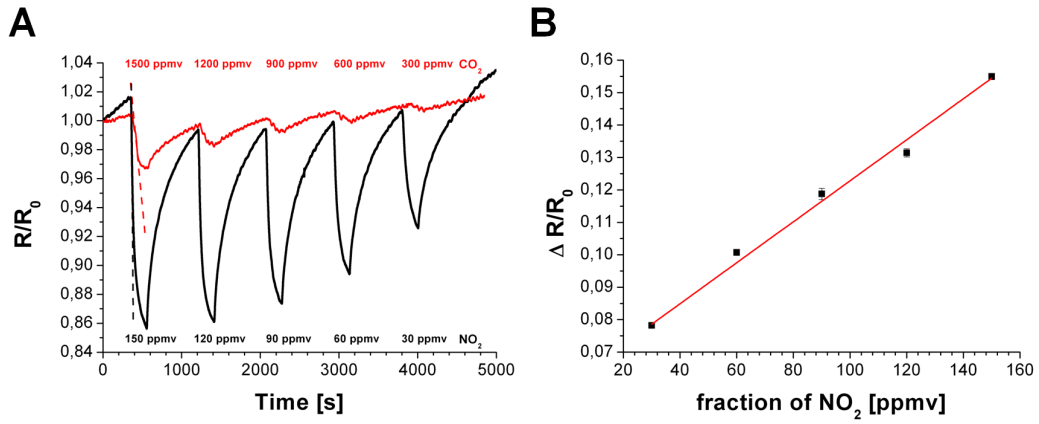

Figure 8.1. (A) Example of a resistance measurement showing the response of rGO to NO_2 (black) and CO_2 (red), both in synthetic air at various concentrations. The dashed lines indicate the different kinetics. The measurements were done at 85 °C to avoid effects caused by humidity and to allow fast regeneration of the signal after switching from test gas to synthetic air. (B) The change of the resistance varies linearly with the fraction of NO_2 in synthetic air.

These electrodes do not respond to treatment with either 0.5% H_2 or short alkanes in the ppmv range, but do respond to CO_2. The latter increases the conductivity similar to NO_2, but the change is 5 times lower. Furthermore, the plot in Figure 8.1A reveals

that the response to both NO_2 and CO_2 have different kinetics. These kinetics may be used to distinguish between the gases. In general, there are two possible measurement protocols to achieve this. First, the exposure time of the test gas can be halved. This will reduce the sensitivity for both gases, but with a much greater impact on the sensitivity of CO_2. In this case, the response to CO_2 will be negligible, whereas the response to NO_2 is still detectable in the low ppmv range. Another method would use the drastically different slopes to determine which gas is measured. However, in a mixture only NO_2 will be recognized since the sensitivity for it is much higher.

Obviously, for continuous gas measurements the test gas (or real sample) should be periodically swapped with a "recovery gas" (here: synthetic air) in both protocols. Unfortunately, this increases the complexity (and cost) of such a method. Hence, selectivity for individual (or a group of) gases must be introduced by the modification of rGO or by rGO-nanocomposites with the desired features. Sensitivity may be improved by preparing single- or few-layer rGO, since the sensitivity also depends on the number of accessible binding sites on the surface.

8.3 Surface plasmon resonance affinity sensor for amines

Surface plasmon resonance (SPR) is an optical phenomenon which can be used to measure the refractive index of a thin layer adsorbate on a metal surface[3]. The refractive index will change in response to treatment of the adsorbate (=transducer) with analytes. Selectivity, sensitivity, stability, and response time are controlled by choosing a convenient adsorbate.

Little has been reported on the use of graphene materials in combination with this technique[4–7]. Changes in the SPR signal become more sensitive the closer the absorbate is to the gold surface[3]. Therefore, a thin and homogeneous layer of (reduced) graphene oxide deposited on a metal surface for sensor applications should not reduce the SPR signal significantly. Furthermore, (reduced) graphene oxide itself can act as a receptor due to its ability to interact with aromatic systems via π-stacking.

This well known interaction was examined in initial experiments with rGO (on gold substrates). First, a thin, homogeneous, and reproducible layer of (reduced) graphene oxide on gold was required. "Physical" techniques such as spin coating and drop casting provided a fast way to prepare sensor chips with thin layers of (reduced) graphene oxide. An exemplary measurement of an artificial nucleoside is given in Figure 8.2A. The substrate used was prepared by spin coating of a solution of reduced graphene oxide on gold. Although the plot indicates binding of a small amount of nucleoside to rGO (indicated by the base line shift), the prepared layer was inhomogeneous, and the results were not reproducible.

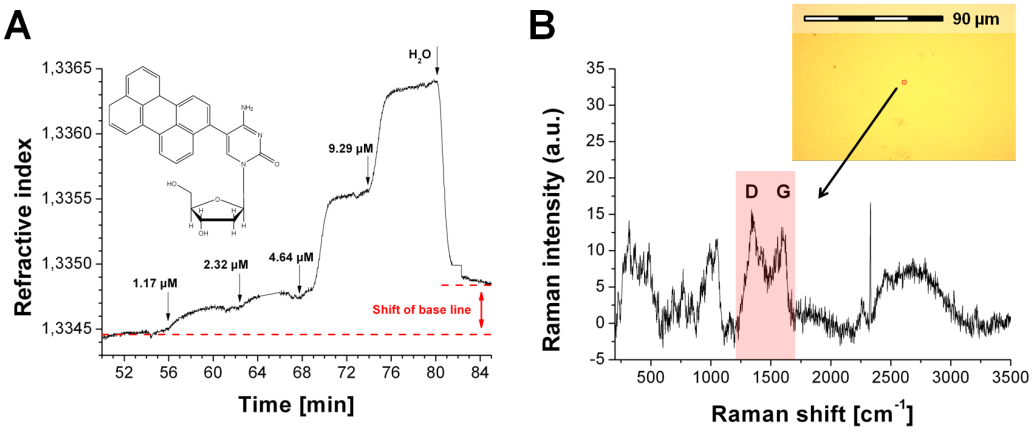

Figure 8.2. (A) Example of a SPR measurement showing the response of spin coated rGO to an artificial nucleoside (3-perylenyl-desoxyuridine) with a large π-system. The shift of the base line indicates binding of small amount of the nucleoside. (B) Example Raman spectrum of an gold chip with immobilized graphene oxide on it. The spectrum was taken at the shown position of the microscopic picture (red cross in the middle). The layer of graphene oxide cannot be seen with the naked-eye but is present all over the chip.

(Reduced) graphene oxide was chemically immobilized on gold to achieve a much more homogenous and reproducible layer. The gold substrates were coated with a monolayer of 4-aminothiol, which both binds to the gold (strong Au-S bond) and provides an amino group for amide coupling with (reduced) graphene oxide. Formation of the amide bond was achieved by soaking the coated gold substrate in a solution of graphene oxide, 1-ethyl-3-(3-dimethylaminopropyl)carbodiimide (EDC) and N-hydroxysuccinimide (NHS). The successful coupling was confirmed by microscopic Raman studies (see Figure 8.2B). Reduced graphene oxide can be seen all over the gold substrate and the layers were homogenous.

The bound graphene oxide can be reduced by hydrazine. However, both GO and rGO show a similar response to the nucleoside. The primary interaction between (reduced) graphene oxide and the nucleoside is likely due to π-stacking. Therefore, it is reasonable that the responses are similar due to the similar size of a crystallite of GO and rGO (see Section 5.4). Further measurements revealed that the coupling agents (especially EDC) are adsorbed by (r)GO. The (strongly) adsorbed agents block some of the binding sites and thus, less sites are available for analytes. In future developments, this could be overcome with other coupling techniques. For instance, graphene oxide acyl chloride prepared with thionyl chloride may be used to bind to the amino groups of the thiol. Thionyl chloride is the only reagent needed and can be easily and completely removed by vacuum distillation before the actual coupling reaction.

In addition to the nucleoside experiment, these chips were able to bind to ammonia and some amines. Preliminary results for this experiment are given in Figure 8.3A. The plot reveals, however, that the sensitivity for aliphatic molecules is much lower (millimolar range) than for aromatic molecules (micromolar range). The nature of the binding and possible ways to improve the sensitivity and selectivity have yet to be examined. Still, these results indicate a possible SPR sensor for amines using SPR.

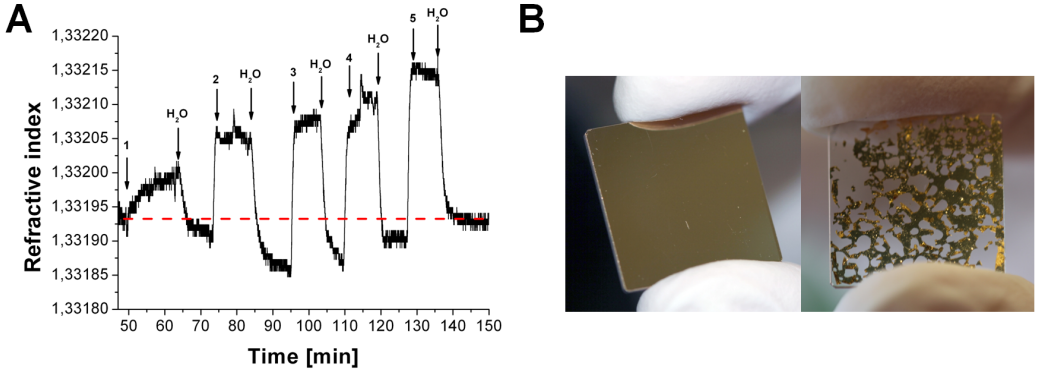

Figure 8.3. (A) SPR measurement showing the response of immobilized GO to 10 mM of ammonia (1) and different amines (2: methylamine; 3: ethylamine; 4: dimethylamine; 5: diethylamine; 10 mM each). (B) Sometimes reagents (hydrazine, ammonia, EDC, NHS) intercalate between the gold and the chromium layer of the SPR chip. This intercalation peels of the gold surface.

Finally, there are other technical issues that remain unsolved. The gold layer on the SPR chips is very thin (50 nm). There is a thin chromium layer used as an adhesive

between the gold layer and the support material (glass). During a reaction, reagents (hydrazine, ammonia, EDC, NHS) sometimes intercalate between the gold and the chromium layer. In some cases, however, this results in the release of the gold layer from the glass (see Figure 8.3B), rendering the substrate useless.

8.4 References

[1] F. Schedin, A. K. Geim, S. V. Morozov, E. W. Hill, P. Blake, M. I. Katsnelson, and K. S. Novosëlov. Detection of individual gas molecules adsorbed on graphene. *Nat. Mater.*, 6(9):652–655, 2007. doi: 10.1038/nmat1967.

[2] V. Dua, S. P. Surwade, S. Ammu, S. R. Agnihotra, S. Jain, K. E. Roberts, S. Park, R. S. Ruoff, and S. K. Manohar. All-Organic Vapor Sensor Using Inkjet-Printed Reduced Graphene Oxide. *Angew. Chem., Int. Ed.*, 49(12):2154–2157, 2010. doi: 10.1002/anie.200905089.

[3] J. Homola, S. S. Yee, and G. Gauglitz. Surface plasmon resonance sensors: review. *Sens. Actuators, B*, 54(1–2):3–15, 1999. doi: 10.1016/S0925-4005(98)00321-9.

[4] S. H. Choi, Y. L. Kim, and K. M. Byun. Graphene-on-silver substrates for sensitive surface plasmon resonance imaging biosensors. *Opt. Express*, 19(2):458–466, 2011. doi: 10.1364/OE.19.000458.

[5] L. Wang, C. Z. Zhu, L. Han, L. H. Jin, M. Zhou, and S. J. Dong. Label-free, regenerative and sensitive surface plasmon resonance and electrochemical aptasensors based on graphene. *Chem. Commun.*, 47(27):7794–7796, 2011. doi: 10.1039/c1cc11373a.

[6] T. Wu, S. Liu, Y. Luo, W. Lu, L. Wang, and X. Sun. Surface plasmon resonance-induced visible light photocatalytic reduction of graphene oxide: Using Ag nanoparticles as a plasmonic photocatalyst. *Nanoscale*, 3(5):2142–2144, 2011. doi: 10.1039/C1NR10128E.

[7] L. Wu, H. S. Chu, W. S. Koh, and E. P. Li. Highly sensitive graphene biosensors based on surface plasmon resonance. *Opt. Express*, 18(14):14395–14400, 2010. doi: 10.1364/OE.18.014395.

9 Conclusion and outlook

The syntheses and characterization of graphene oxide and reduced graphene oxide were closely examined. On the basis of the results, realistic models and schemes were developed and discussed. Also, the advantages and effects of (reduced) graphene oxide to be exploited for sensor applications were presented. In summary, these materials clearly lack the often mentioned high-end properties of pristine graphene. For instance, the high electron transfer rate is a result of the unmodified and undisturbed crystal lattice of pristine graphene. However, (reduced) graphene oxide benefits from the presence of oxygen groups, which allow solution processing and cause several other convenient effects. It should be emphasized that these features are more important for *sensor applications*, while the high-end properties are not needed for this area. Moreover, these features can be customized by varying the oxidation level.

Chapter 2 presents analytical and sensorial approaches and principles to use (r)GO or to replace materials by (r)GO in already existing concepts. *Novosëlov et al.* mentioned in one of their last reviews about graphene that "its full power will only be realized in novel applications"[1]. Of course, this is also true for (reduced) graphene oxide! For novel applications, (r)GO must be purposefully modified and furthermore characterized to completely understand these materials. Only then, features are revealed that can be utilized for sensor applications.

For instance, the (little-known) pH dependence of the position of the G-peak in the Raman spectrum of graphene oxide (see Section 5.5) may form the basis for an easy-to-use pH-test strip. For the following *exemplary scenario*, it is assumed that the influence on the position of the G-peak is simple and *completely known*. The strip itself is made of graphene oxide paper. A drop of a solution is brought onto this paper and the Raman spectrum at this position is collected by a small hand-held device (see Ref. 2 for an example device). The pH can be calculated by the position of the G-peak. Since

an energy level (the position of G-peak) is determined, this method is independent of the concentration of GO and, with this, it is independent of the homogeneity and the thickness of the paper strip. Thus, no reference dye as in similar fluorescence methods is needed. Also, it does not need any calibration step and the excitation wavelength is switchable to avoid absorption interference. It is easy to expand this concept with new layers (e.g. hydrogel with enzymes, which change the pH level) to sense other analytes. Moreover, a modification of GO with an attached receptor could allow a similar "peak-shift" in response to another analyte such as glucose. Unfortunately, the deconvolution of the whole Raman spectrum (not only the G-peak) of (r)GO is complex and not-well understood up to now. Thus, a more detailed investigation of GO and its modifications is still in demand. The purpose of the *exemplary scenario* is to descriptively depict the importance of characterization as a first step on the way to novel sensor concepts.

Very recently, *Dimiev et al.* have published an article about a "dynamic structure model" for GO[3]. In summary, they did not only examine the structure of graphene oxide but also investigated changes in this structure due to the interaction with water, acids, bases and NaCl. They revealed that the structure of GO is not a steady state but, indeed, a dynamic one, which reacts to even (normally) unreactive species such as NaCl. These results should also emphasize that there are still things to discover, examine and discuss about the structure of (r)GO.

In conclusion, both graphene oxide and its reduced version are promising materials with some excellent and advantageous features for sensor applications. These include solution processing, higher sensitivies for particular analytes, and attraction and discrimination effects (see Section 2.4). Not only will existing sensor concepts benefit from their properties. Prospectively, also novel concepts based on these materials will be developed. But, certain issues still have to be discussed and solved. As previously mentioned, the characterization ("knowing your material") is not completed yet. Another issue is concerned with separating educt from product in a large scale application. Last, for some applications it might be convenient to use a very small number of layers (down to 1 or 2), since some properties (electronic transport) depend on this number. Therefore, a method is in demand to prepare large, thin areas of (r)GO (or modifications) preferably directly from the solutions.

References

[1] K. S. Novosëlov, V. I. Fal'ko, L. Colombo, P. R. Gellert, M. G. Schwab, and K. Kim. A roadmap for graphene. *Nature*, 490(7419):192–200, October 2012.

[2] RamanSystems. Portable-PinPointer™. http://www.ramansystems.com/raman%20new%20web/english/pinpointer.htm, February 2013.

[3] A. M. Dimiev, L. B. Alemany, and J. M. Tour. Graphene Oxide. Origin of Acidity, Its Instability in Water, and a New Dynamic Structural Model. *ACS Nano*, 7(1):576–588, December 2012. doi: 10.1021/nn3047378.

10 Summary

This thesis is concerned with the synthesis, characterization and utilization of (reduced) graphene oxide (chemically derived graphene) for sensor applications. The first chapter describes the history of graphene, classifies all members of the graphene family by convenient definitions, and outlines the motivation and aim of this work.

Chapter 2 discusses several proof of principle and analytical concepts based on different graphene materials. These concepts point out the chemically derived variants, i.e. *(reduced) graphene oxide*, as extremely valuable materials for sensor applications due to their excellent features. These include solution processing, higher sensitivies for particular analytes, and attraction and discrimination effects.

Since the materials themselves and their syntheses were only superficially examined, the following chapters (4-6) provide a detailed investigation of graphene oxide and reduced graphene oxide. In particular, fluorescence and Raman spectroscopy are discussed in Chapters 6 and 5, respectively. The results reveal that both materials are indeed very complex, heterogenous entities. Also, the potential for novel sensor concepts is exhibited. Synthesis mechanisms derived from these investigations are developed in Chapter 7, which expose the similarly complex chemistry behind the simple preparation presented in Chapter 3. The mechanisms consist of several convoluted pathways and reactions.

The last chapter lists and presents sensor concepts developed during this work. In particular, the basic principles behind a gas sensor for NO_2, and an affinity sensor based on surface plasmon resonance for amines are described.

11 Curriculum vitae

Personal Data

Name:	Sven Kochmann
Address:	Hadamarstraße 28a
	93051 Regensburg
Date of birth:	January 7th, 1985
Place of birth:	Koethen (ST), Germany
Nationality:	German
Marital status:	unmarried

Education

09/1991	-	12/1992	Grundschule Radegast (ST)
01/1992	-	07/1995	Grundschule Dietfurt (BY)
09/1995	-	06/2004	Gymnasium Parsberg (BY)
		06/2004	Graduation (Abitur)

Studies and Ph.D.

10/2004	-	01/2009	Diploma, Chemistry, University of Regensburg
02/2009	-	09/2009	Diploma thesis, "*Optical pH Sensors for Dermatology*" Prof. Dr. Otto S. Wolfbeis Institute of Analytical Chemistry, Chemo- and Biosensors, University of Regensburg

Studies and Ph.D.

10/2009	-	03/2013	Ph.D. thesis, "*Graphene as a sensor material*" Prof. Dr. Otto S. Wolfbeis Institute of Analytical Chemistry, Chemo- and Biosensors, University of Regensburg

First Author Publications

S. Kochmann, T. Hirsch, O. S. Wolfbeis, *The pH Dependence of the Total Fluorescence of Graphite Oxide*, Journal of Fluorescence, Volume 22 (2012), 849–855, DOI: 10.1007/s10895-011-1019-8.

S. Kochmann, T. Hirsch, O. S. Wolfbeis, *Graphenes in chemical sensors and biosensors*, Trends in Analytical Chemistry, Volume 39 (2012), 87–113, DOI: 10.1016/j.trac.2012.06.004

S. Kochmann, C. M. Baleizão, M. N. Berberan-Santos, O. S. Wolfbeis, *Sensing and imaging of oxygen with ppb limits of detection and based on the quenching of the delayed fluorescence of $^{13}C_{70}$ fullerene in polymer hosts*, Analytical Chemistry, Volume 85 (2013), 1300–1304, DOI: 10.1021/ac303486f

Career Progression

08/2003	-	08/2005	Holiday work, Regens-Wagner (Holnstein, BY), Caring for people with mental and physical handicaps
02/2006	-	09/2012	Student assistant, University of Regensburg: Repeated supervision of lab courses for students of chemistry and medicine
2008	-	present	Tutoring of students of chemistry, medicine and biology

Career Progression

		2008	Co-author and programmer of the website of the Faculty of Chemistry and Pharmacy
2010	-	2011	Co-author and programmer of the Chebana website (*http://www.chebana.eu*)
2012	-	present	Co-author and programmer of the MagneticFun website (*http://www.magneticfun.eu*)
2009	-	present	Co-webmaster and programmer of the intranet of the Institute of Analytical Chemistry

Personal Skills and Competencies

Languages:	German, Latin, English, Spanish
Computer Skills:	Advanced knowledge, e.g., in Windows, Linux, office, LaTex, programming, web design
Hobbies:	Photography, drawing/sketching, sports, blood donations
Others:	Author of Beryllium[10], a program for safety data sheets (*http://beryllium.keksecks.de*)

01/2008	-	03/2009	Active member of the student council: Member of commission “Studiengebühren”, design and programming of the website, IT-support
09/2009	-	present	Founder, active member, and chairman of the Alumni Club of Chemistry, University of Regensburg

12 Eidesstattliche Erklärung

Ich erkläre hiermit an Eides statt, dass ich die vorliegende Arbeit ohne unzulässige Hilfe Dritter und ohne Benutzung anderer als der angegebenen Hilfsmittel angefertigt habe; die aus anderen Quellen direkt oder indirekt übernommenen Daten und Konzepte sind unter Angabe des Literaturzitats gekennzeichnet. Weitere Personen waren an der inhaltlich materiellen Herstellung der vorliegenden Arbeit nicht beteiligt. Insbesondere habe ich hierfür nicht die entgeltliche Hilfe eines Promotionsberaters oder anderer Personen in Anspruch genommen. Niemand hat von mir weder unmittelbar noch mittelbar geldwerte Leistungen für Arbeiten erhalten, die im Zusammenhang mit dem Inhalt der vorgelegten Dissertation stehen. Diese Arbeit wurde bisher weder im In- noch im Ausland in gleicher oder ähnlicher Form einer anderen Prüfungsbehörde vorgelegt.

Ort, Datum Unterschrift

Acknowledgments

Thanks above all to my advisor, **Prof. Dr. Otto S. Wolfbeis**, for providing me an interesting and challenging topic, for the excellent working conditions at his chair and also the freedom I had.

Thanks to **Dr. Thomas Hirsch** for his advices, support, sharing his experience, and developing of our workgroup in the 4^{th} floor.

I appreciate very much all the help and support of my lab mates **Alexander Zöpfl**, **Wendy Patterson**, **Christoph Fenzl**, **Stefan Wilhelm**, **Josef Heiland** and **Michael Lemberger**. Also thanks to **all present and former colleagues at the institute** for the good atmosphere and lots of help during this work.

Also, I am obliged to the secretary **Sabine Rudloff** and to the present and former technicians **Rosmarie Walter**, **Angela Haberkern**, **Manfred Muschiol**, **Thomas Schottenhammer**, **Joachim Rewitzer** and **Angelika Stoiber** for their help, support and an extra boost of *Vitamin B*.

I'm also indebted to my mother **Verena Scheinert**, and my grandparents **Inge** and **Klaus Kochmann** for their emotional and financial support.

Special thanks to: **Stefanie Heydrich** for the regular chocolate sessions (Let's write a chocolate paper!) and for sharing and extending my world view. **Wendy Patterson** for improving my English skills (Vielen Dank!), providing me an outsider's view of Germany, and bearing with me the last months in our office! **Manuela Stirner** for our funny everyday-talks, which distracted us both from some boring tasks, and, of course, for saving tons of wood by not writing me any postcards in the last years! **Katharina Limm** for the "spring-fresh" air (and the cakes!) she brought to our lab. My research student **Justus Back** for the work he contributed to this thesis. **Katrin Schweiger** for her songs on SoundCloud (esp. "Wenn Du gehst"), which were a great source of inspiration during my writing sessions! **Christina Lotz** and **Florian Kochmann** for their hospitality and some

nice days at Vienna!

Additional thanks to my fellow students and friends **Hubert Scheubeck**, **Florian Heiligtag**, **Michael Dobmeier**, **Sebastian Heinl**, **Claudia Heindl**, **Natascha Kuzmanovic**, **Stefanie Stöckl**, **Patrick Schwarz**, **Nadja Leibl**, **Judith Mayr**, **Frauke Antoni**, **Thomas Merz**, **Michael Seidl**, **Katie Unger**, **Sonja Rosenlehner**, **Johannes Schmidkonz**, **Ines Schmid**, **Isi Huber** for all the parties, beer, booze, barbecues, card circles, table soccer sessions, movie nights, cooking session, board game parties, and other fun we had in the last years!

Thanks to the **spider pig** for whatever the **spider pig** did!

Finally, additional greetings to all of **my former students** who had to bear with me the last years! Hope you learned a thing or two; I wish all of you success in your studies!